Polymeric Prodrugs for Infectious Disease and Immune Therapies

Ciana Luisa López

A dissertation
submitted in partial fulfillment of the
requirements for the degree of

Doctor of Philosophy

University of Washington
2024

Reading Committee:
Patrick Stayton, Chair
Suzie Pun
Shawn Skerrett

Program Authorized to Offer Degree:
Bioengineering

University of Washington

Abstract

Polymeric Prodrugs for Infectious Disease and Immune Therapies

Ciana Luisa López

Chair of the Supervisory Committee:

Patrick Stayton

Department of Bioengineering

Small molecule drugs are a mainstay of modern medicine, however their suboptimal delivery to a therapeutic target can undermine their value and utility. In this body of work, we explore the adoption of polymer prodrugs ("drugamers") to facilitate the delivery and controlled release of small molecule drugs to multiple important therapeutic settings. First, we explain why drugamers synthesized by Reversible Addition Fragmentation-chain Transfer (RAFT) are ideal small molecule drug delivery vehicles (**Chapter 1**). We then show that antibiotic drugamers, originally designed to treat intracellular pulmonary infections, significantly improve survival against extracellular *Klebsiella pneumoniae* infections due to enhanced targeting to local alveolar macrophage reservoirs (**Chapter 2**).

A major innovation of the work described herein is the demonstration that drugamers can be combined with and can enhance protein and cellular immune therapeutics. A radiant star

drugamer adjuvant was designed for effective loading within self-assembling protein nanoparticles as an alternative approach to vaccination (**Chapter 3**). Sustained release of the TLR7/8 agonist from the encapsulated drugamer facilitated potent immunization in vivo while mitigating toxicity associated with parent adjuvant. In **Chapter 4**, we demonstrate arming of immune cell therapeutics with drugamers. Fluorescein-tagged drugamers containing phosphoinositide-3-kinase (PI3K) inhibitors direct stable noncovalent binding to Genetically Engineered Macrophages (GEMs) via a bioorthogonal anti-fluorescein surface receptor. We conclude with an outlook of future directions to build upon drugamer therapeutics, specifically highlighting the potential for combination with biologic-secreting GEMs (**Chapter 5**).

TABLE OF CONTENTS

LIST OF FIGURES

LIST OF TABLES

ACKNOWLEDGEMENTS

All acknowledgements to individuals and funding sources are included following their respective chapters.

Thank you to my advisor, **Pat Stayton**, for training me to think globally and translationally. Thank you for your scientific excitement and candid advice. You have fostered an invigorating scientific community, and it is an honor to be a part of it. I look forward to staying in touch for years to come.

Thank you to my co-advisor, **Courtney Crane**, for introducing me to the burgeoning fields of immunotherapy and immune cell therapeutics. The time I spent in your lab was incredibly fulfilling and instrumental in helping me decide what I want to pursue moving forward. I also want to thank **Katherine Brempelis**; I could not have asked for a better example of how to conduct thoughtful and detailed research as I started graduate school.

Thank you to my collaborators, **Eoin West** and **Shawn Skerrett**, for taking me into your labs as one of your own. It has been a privilege to receive your clinical expertise and feedback. Working with you through the trials and tribulations of GEMs has been an invaluable experience. I am so thankful for your patience and mentorship.

Thank you to my other supervisory committee members, including **Suzie Pun**, **Alshakim Nelson**, and **Wayne Gombotz**. Your insight and feedback have been important and encouraging.

To my brilliant synthetic monomer and polymer chemist mentors, **Selvi Srinivasan**, **Debasish Roy**, and **Anthony Convertine**, thank you for your discussion and support.

To my dear mentor, **Azadeh Yazdan**, you have instilled in me so much hope and excitement for the future.

Ayumi Pottenger, you inspire me, and it was an honor to do grad school with you. **Guilhem Rerolle,** we've been through a lot together! Thank you for making lab feel like home. We are young, spontaneous, awake, and athletic.

To **Sarah Snyder**, **Ben Nguyen, Abdullah Bashmail, Giovany Gonzalez, Sally Baker, Simbarashe Jokonye, Naomi Hamelmann**, **and Shelton Wright**, thank you for all the banter (scientific and otherwise) and for the memes (especially Ben).

To my friends, **Veronica Porubsky**, **Trey Pichon**, **Casey Kiyohara**, **Molly Mollica**, **Lesley Martinez Rodriguez**, **Christopher Nyambura**, and **Ian Hull**. We did it! We're doing it! You are the community I want and need. You've been an incredible support to me.

To my dad, **Gabriel López**. I did not anticipate the pride I would feel being able to present my science to you. I am incredibly blessed to share many key memories and scientific discussions with you during this time. I will never forget or take for granted that you have been with me through it all.

To my tío, **José A López**, who has also helped me through many major milestones. Thank you for your training as a scientist and for feeding me with the best brain food. To my tía, **Funda**, for your histopathology lessons.

To my tío and tía, **Jerry and Susan James**, who have watched me grow in so many ways from a freshman to now, and who have provided me on multiple occasions a place to stay and a solid family squad to celebrate life with.

To my mama, **Kaori López**. There is no one who understands how my brain works better than you. Thank you for gifting me your speaking chops and enthusiasm, for being a facetime away, for traveling across the country to watch your "daughter's daughter". I hope to be as attentive and loving with Lluvia as you are with me.

To my little brother, **Jóse C López**, I am the luckiest sister, and it is what it is.

To my grandmama (GG), **Peggy James**, thank you for asking me about my science. Also, thank you for all the potatoes and tomato aspic. Spending this time with you has been irreplaceable. To my grandpa, **Phil James**, your attention to detail and doing things perfectly makes me smile.

Thank you, **Cheech** and **Osa**, for the walks.

To my partner, **Jason Martinez**, thank you for being my piece of home. I'm lucky to have you by my side. To my daughter, **Lluvia Beatriz Martinez**, te amo muchisimo.

DEDICATION

To mi'jita, la más viva,
¡a guay ti wi, a guay ti wi!

Chapter 1. SMALL MOLECULE DRUG DELIVERY VIA RAFT-BASED POLYMER PRODRUGS ('DRUGAMERS')

Ciana L López

ABSTRACT

Small molecule (SM) drugs have had major impact on humanity's ability to fight disease. However, the lack of targeted delivery reduces their therapeutic efficacy and contributes to off-target toxicities. Synthetic nanomaterials can reformulate SM drugs by incorporation into macromolecules that improve their circulation, targeting, and prevent premature metabolism. Biological materials also have potential to deliver small molecule drugs not only to improve their targeting, but to synergize with emerging biologic therapeutic mechanisms. Unfortunately, multi-step synthetic procedures and batch-to-batch variability has prevented widespread adoption and translation. We present the case for using polymer prodrugs ("drugamers") synthesized by RAFT polymerization to improve SM drug solubility, targeting, circulation, and coordination with biologics. Prodrug monomers are co-polymerized with other functional monomers at pre-determined ratios to yield drugamers with statistical and reproducible monomer incorporation yielding polymer products with dispersities, Đ, less than 1.1. RAFT drugamers are ideal for clinical translation due their synthetic versatility and simplicity using one-pot polymerization schemes that are scalable. Furthermore, precisely tuned release of SM drug cargos can be designed to optimize a drug's mechanism of action for a particular disease application and to maximize their use in combination with emerging biologic therapeutics.

1.1 THE GLOBAL IMPACT OF SMALL MOLECULE DRUGS

Small molecule (SM) drugs are a mainstay of modern medicine. Characterized as synthetic low molecular weight organic compounds (< 1000 Da) and typically comprised of 20 – 100 atoms, small molecule drugs hold the greatest portion of clinically approved drugs globally.[1] One of the first examples is acetylsalicylic acid, commonly known as aspirin (Figure 1.1A). First available in 1899, it is a synthetic derivative of a well-known and ancient herbal remedy derived from the bark of a willow tree.[2] To this day, it is used worldwide to provide pain and fever relief. Penicillin is an antibiotic naturally produced by fungi. Following its isolation from mold it was able to heal wound infections during World War II. Since then, it and other antibiotics have saved millions of people from infectious death and extended the human life span by 23 years.[3] Another significant SM drug is hormonal birth control pills (e.g., Enovid), which have allowed women to control their fertility reliably and reversibly since the 1960s, and today are used by more than 150 million women globally.[4, 5]

SM drugs are derived from natural products or rationally designed based on knowledge of a biological target. Due to their small size, they can act against both intracellular and extracellular drug targets. Compared to macromolecules, they diffuse more readily through tissues (a property referred to as a high volume of distribution, V_D). The most common targets are proteins (e.g., enzymes, receptors, ion channels, transcription factors, etc.), some lipids, and increasingly nucleic acids.[6] In the last decade, the top therapy area for U.S. drug approval was oncology (25%), infection (15%), and central nervous system disorders (11%), but the breadth of disease applications for SM drugs is extensive and continuously expanding with advances in genomics and proteomics.[7-9] Drugs act as inhibitors, activators, agonists, and by allosteric binding, and have predictable and titratable mechanisms, which enable their use as chemical probes to

understand disease biology. [4, 10] Further, in recent years drug development has shifted from broad spectrum mechanisms (e.g., cytotoxic chemotherapeutics like doxorubicin) to highly pathway specific (e.g., PARP kinase inhibitors like olaparib to treat *BRCA*-mutated cancers) (Figure 1.1A).[11, 12]

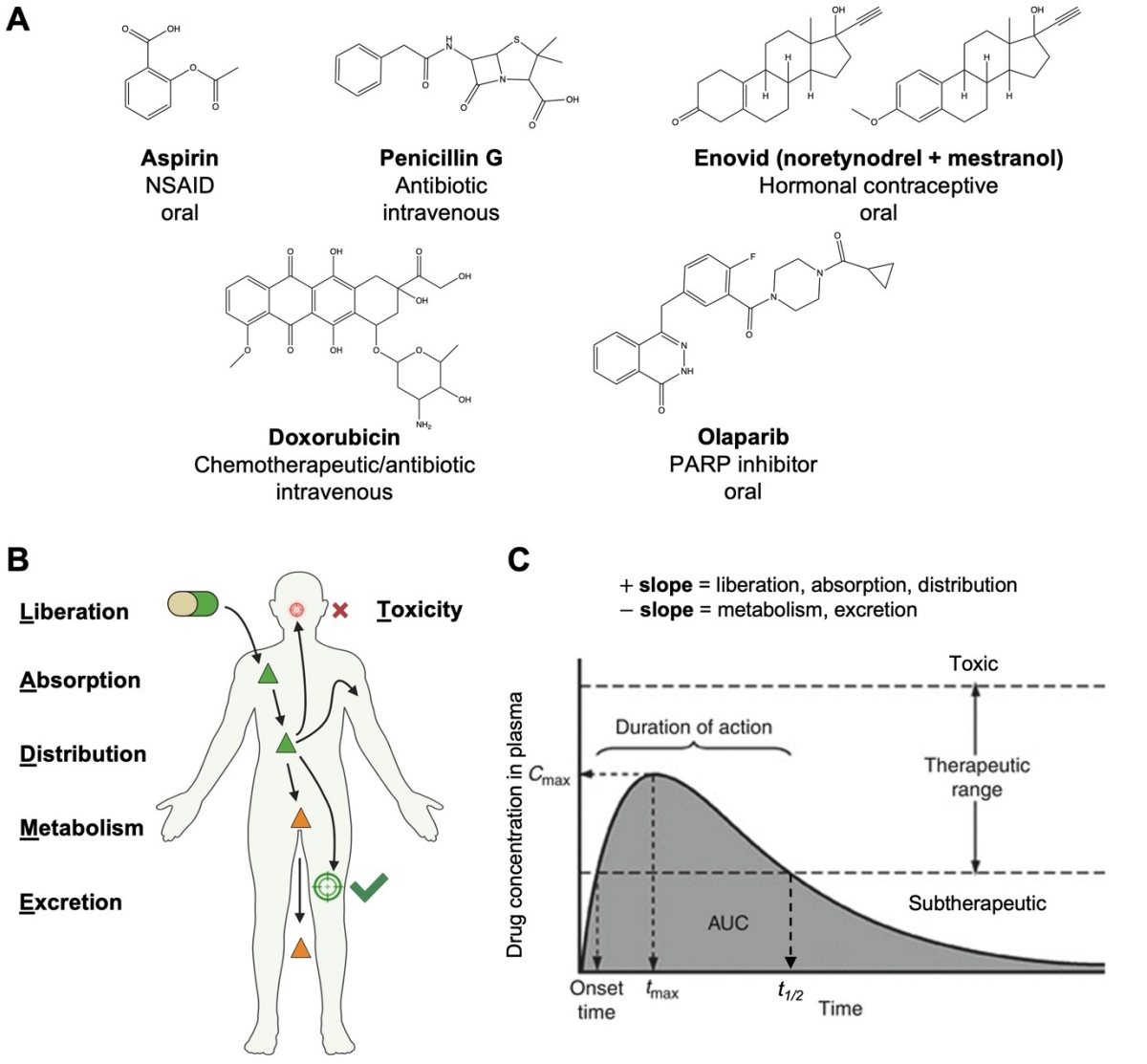

Figure 1.1 Small molecule drugs in the body (A) Chemical structures of prominent small-molecule drugs and most common route of administration (B) the pharmacological parameters that impact their therapeutic efficacy, and (C) typical pharmacokinetic curve from a single oral drug dose. Figure B was adapted from Thomas Fester [13] under the terms of the Creative Commons Attribution (CC BY 4.0) License and created with BioRender.com; Figure C was adapted from Wolff 2015 [14] with permission from the publisher, Springer Nature).

SM drugs are widely accessible and relatively affordable. SM drug production is well-established and involves large scale, continuous chemical synthesis following good manufacturing practice (GMP) and with generally low Cost of Goods Sold (COGS).[7] Their relatively simple chemical composition allows for high reproducibility and straightforward characterization.[15] SM drugs are generally available as off-the-shelf products with good stability at a range of environmental temperatures and humidities without degradation compared to biologics which required cold-chain storage.[16, 17]

SM drugs are undeniably impactful to human existence and have several therapeutic advantages that continue to reinforce their value and use as standard of care therapeutics.[15] However, there are a few key shortcomings of SM drugs that prevent achievement of their full potential for impact and translation which will be discussed in section 1.2. Astonishingly, it is estimated that 60% of SM drugs that reach phase II trials fail to meet clinical approval due to poor clinical safety and efficacy.[18] While optimization of SM physiochemical properties has been investigated to improve such SM drug attrition, addressing these shortcomings likely requires adoption of drug delivery vehicles that can modulate the dynamic complexities of biological transport to improve options and outcomes for patients. Such an endeavor will also open avenues to use SM drugs in new ways (e.g., by modulating and/or synergizing with emerging biological therapeutics).[19, 20]

1.2 SHORTCOMINGS OF SMALL MOLECULES THAT PREVENT TRANSLATION AND GREATER IMPACT

The major shortcoming of SMs is that their delivery (or pharmacokinetics) is directly tied to their chemical composition, which impacts bioavailability and ultimate pharmacological activity. A SM drug's physiochemical properties affect its absorption, distribution, metabolism, and excretion (ADME; Figure 1.1B). For one, SM drugs commonly have poor solubility and must be formulated with excipients. If delivered orally, SM drugs must navigate the harsh acidic stomach pH as well as enzymatic digestion in the stomach and small intestine before absorption into the bloodstream by enterocytes.[21] Once absorbed, SM drugs pass through the liver where redox enzymes metabolize the drug (the "first pass effect"), which may dramatically decrease the bioavailability of a SM drug before it even reaches systemic circulation or a disease target. Absorption through topical, pulmonary, nasal, sublingual, or other routes can be convenient as more localized delivery strategies but also have their own physical and metabolic barriers.[22-25]

While the small size of SMs improves absorption and distribution, it also results in a short plasma half-life ($t_{1/2}$) with rapid clearance from circulation by metabolism and excretion (Figure 1.1C). The disadvantage of a short $t_{1/2}$ is that a patient must take drugs more frequently to achieve an effective area under the concentration curve (AUC), a pharmacokinetic parameter that indicates the amount of drug exposure needed to produce a desired therapeutic effect. Unfortunately, these aspects and lack of precision targeting to diseases niches can lead to off-site toxicities. Accordingly, many FDA-approved drugs receive a black box warning, which indicates serious or life-threatening side effects. For drugs approved between 2010 and 2019, 30% of oncology, 14% of infection, and 28% of central nervous system drugs came with black box warnings.[7]

1.3 OVERCOMING BARRIERS TO EXPAND TRANSLATION AND THERAPEUTIC IMPACT OF SMALL MOLECULES

The main barriers to maximizing the therapeutic efficacy and impact of SM drugs are their 1) solubility, 2) poor targeting, and 3) suboptimal pharmacokinetic properties. Towards improving these measures, the following section will provide an overview of some of the key advances in synthetic and biological drug delivery vehicles, which provide solutions to these shortcomings. We will discuss the ways in which such materials have incorporated SMs and describe their potential for functional SM combination yet to be realized. We have limited the scope of materials covered here to organic materials, and specifically those that have shown success in or promise for clinical translation. For more extensive reviews of organic and inorganic nanomaterials and biologics, we direct you to other excellent resources.[26-29]

1.3.1 Synthetic nanomaterials

Synthetic nanomaterials for drug delivery have been a major technological advance in the last 50 years. They are characterized by a size between 10 - 999 nm, though most are less than 200 nm, which is the width of microcapillaries.[30] They are used to improve circulation, prevent systemic toxicity, and enhance therapeutic efficacy by targeted and controlled release of SM drugs. We will introduce prominent nanomaterials in development today, the majority of which are for cancer applications and describe how SM drugs are incorporated, the benefits, and some areas for improvement.

Polymer-drug conjugates

The idea of conjugating water-soluble polymers to drugs to improve their circulation and avoid premature metabolism has an extensive history.[31-33] Perhaps the most well-known and

clinically successful examples, “PEGylation”, involves conjugation of polyethylene glycol (PEG, Figure S1.1) to drugs to increase their size and prevent premature excretion (e.g., >10 nm for kidney filtration).[34, 35] Due to its neutral hydrophilic and flexible nature, PEG also endows “stealth” properties to prevent recognition and drug clearance by the immune system.[36] Initially described in 1977, Abuchowski et al. demonstrated that covalent attachment of PEG macromolecular chains (PEG1900 and PEG5000) to amino groups of bovine liver catalase provided a 4-fold extension in circulation time compared to unconjugated catalase while maintaining enzymatic activity.[37] Since then, PEGylation has been applied to both SM drugs and other therapeutics and resulted in over 30 clinical products.[35]

Around the same time, Kopeček et al. showed demonstrated incorporation of doxorubicin into hydrophilic N-(2-Hydroxypropyl)methacrylamide (HPMA, Figure S1.1) polymers, resulting in a 28-fold improvement in plasma $t_{1/2}$ compared to parent drug.[38, 39] The polymer-drug conjugate design allowed for release of the active form of the SM drug by a lysosomally degradable peptide linker constituting a first example of a polymer prodrug. It was shown that the enhanced circulation of such polymer-drug conjugates allowed for passive delivery to tumors via leaky tumor vasculature based on what is called the enhanced permeability and retention (EPR) effect and resulting in tumor growth inhibition.[40] Since then, many polymer drug conjugates have been investigated to improve targeting and pharmacokinetic properties of SM drugs.

Post-polymerization pendant conjugation of hydrophobic drugs the hydrophilic polymer backbones is a common approach that can be achieved by amine conjugation, carbodiimide coupling, maleimide coupling, click chemistry, and more.[41, 42] However, such approaches require multi-step syntheses that suffer from low and variable conjugation efficiency, providing limited control over the site and degree of drug loading and expensive reaction materials are

wasted. Discussed in more detail in section 1.4, the use of polymerizable drug monomers is a superior and straightforward approach to achieve polymers with predetermined drug incorporation ratios using one-pot synthetic schemes with greater amenability to clinical translation and scale-up.[43]

Degradable polymer matrices

The use of degradable polymeric matrices has been explored to enable the sustained release of SM drug cargos with improved pharmacokinetic properties. Hydrophobic poly(esters) such as poly(lactic acid) (PLA), poly(glycolic acid) (PGA), poly-ϵ-caprolactone (PCL), and combinations thereof (e.g., PLGA) can be formulated into continuous polymeric networks that physically entrap SM drugs (Figure S1.1).[44, 45] SM drug release occurs by 1) surface or bulk matrix cleavage of polymer bonds, 2) surface erosion of the polymer matrix, and 3) diffusion of the drug from the matrix.[46]

Such materials are attractive for translation due to their ability to be eliminated following delivery of cargo and have been incorporated into many FDA-approved materials. However, a weakness of such materials is their limited functionality for chemical conjugation with SM drugs or targeting molecules.[47] Their clinical translation for SM drug delivery is limited by physicochemical heterogeneity, variable drug loading and leakage, and polydisperse products. While degradable polymeric materials alone are not sufficient to improve targeted delivery of SM drugs, there are important opportunities for their incorporation into future generations of SM delivery materials to allow for soluble, backbone degradable macromolecules with enhanced clearance properties.

Lipid-based nanoparticles

Colloidal drug delivery systems (CDDS) have also been widely explored to extend the circulation of drugs. The spherical shape of many nanoparticles allows for drugs to be packed within a core surrounded by a hydrated corona. A prominent class of CDDS, liposomes are artificial vesicles composed of one or more lipid bilayers and surrounding an internal aqueous compartment.[26] Their structures allow for loading with SM drugs of various lipophilicities within the aqueous or lipid compartments to improve drug formulation and alter biodistribution. Doxil®, a PEG-functionalized liposomal formulation of doxorubicin, was the first nanoparticle to be FDA approved in 1995 for the treatment of ovarian cancer based on its decreased cardiotoxicity and improved injectability.[48] Unfortunately, its therapeutic impact has been limited over the standard of care parent formulation due to its low drug loading capacity, leaky drug release properties, and difficult to reproduce synthetic schemes with low shelf stability.

Polymeric Micelles

Polymeric micelles are another CDDS which are self-assembled from synthetic amphiphilic block copolymers. Compared to lipid-based nanoparticles, they have improved control over particle characteristics and improved ease of surface modification.[26] Hydrophobic drugs can physically entrapped in micellar cores or conjugated to water-soluble polymers such as PEG.[49-51] Micelle assembly is based on a critical micelle concentration (CMC) below which they will be a dispersion of linear polymers and above with they will form self-assembled

micelles.[52] Pioneered in parallel by Kataoka et al. and Kabanov et al., modification of polymer chemistries allows modulation of the CMC, which can be influenced by other environmental factors (e.g., pH, temperature, ionic strength) and enables the design of "smart" and stimuli responsive materials with site-specific drug release properties.[53-56] Despite the incredible functional and dynamic nature of these materials, their multistep and variable synthesis has prevented wide clinical adoption.

Dendrimers

Dendrimers are water-soluble highly ordered polymers characterized by their number of branched generations and typically with size on the order of 1-10 nm. Poly(amidoamine) (PAMAM) dendrimers are well-known for their ability penetrate cell barriers due to their positive charge and have been explored for drug delivery by end-group conjugation with drugs, by physical encapsulation within micelles, or by complexation with genes based on electrostatic interactions.[57] In one example, Han et al. showed that end-group conjugation of hyaluronic acid to PAMAM dendrimers could be used to target CD44 receptors overexpressed on tumor and cancer stem cells.[58] Dendrimers can theoretically achieve multivalent targeting by conjugation of targeting moieties to abundant functional end-groups. However, conjugation efficiency is typically low, limiting their full potential for enhanced targeting.

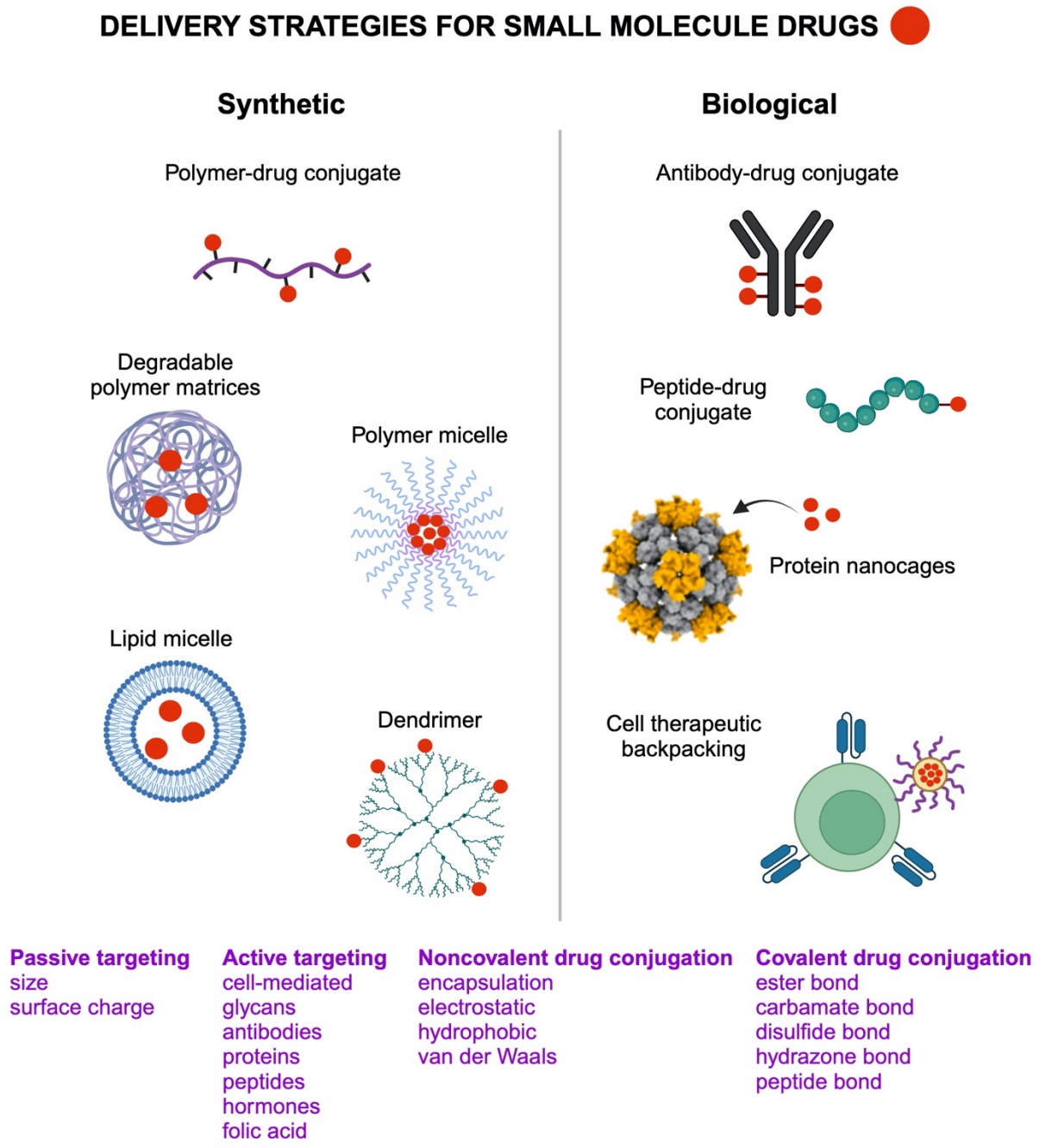

Figure 1.2 Small molecule drug delivery strategies to improve solubility, targeting, and pharmacokinetic properties by both noncovalent and covalent drug conjugation to synthetic nanomaterials and biologics. Created with BioRender.com.

1.3.2 Biologics

Biological ("Biologic") drugs are therapeutics composed of proteins, carbohydrates, nucleic acids, cells, and combinations thereof. In some cases, cell-based therapeutics are considered their own pilar of medicine, but for the purpose of this review, they are included.[59] Biologics have hit the pharmaceutical industry by storm in recent years due to their high efficacy and targeting specificity and for the first time ever in 2022, FDA approval of biologics surpassed that of SM drugs.[60] They have ushered in the era of immunoengineering, whereby therapeutic materials are design to elicit a desired host immune response, rather than be inert.[7, 61, 62]

Biologics are commonly used concurrently with small molecule drugs for a few important reasons. For one, biologics are commonly delivered via parenteral routes because of bioavailability, stability, and diffusion barriers that SM drugs do not possess.[63] Additionally, because of their complex compositions, biologics are typically grown and purified from large-scale batches of bacteria, yeast, plant, or animal cell cultures, making production and scale-up slow and expensive (though an active area of progress).[17, 64-66] Further, because of their complex composition, complete characterization of biologics is difficult and regulatory agencies have established special guidelines for generic versions, including "biosimilars", which unfortunately can have decrease therapeutic efficacy, and represents a major equity issue.[67]

There are ongoing efforts to improve these barriers, and we foresee that significant progress will be made to harmonize production methodologies and improve accessibility in the coming years. Because of their incredible specificity, in some cases, biologics will surpass SM drugs to become the standard of care (e.g., for chronic inflammatory and autoimmune disease, cancer). In other settings there is likely more rationale for SM drugs (e.g., for acute infectious disease). Importantly, many have explored opportunities to combine these therapeutic modalities to increase precision and targeting, which will be discussed in this section.

Antibody-drug and peptide-drug conjugates

While the idea of immunoengineering was limited to vaccines until the 2000s, the use of biologics to improve targeting of toxic SM drugs has been around for a while. In 1958, Mathé et al. conjugated the chemotherapeutic methotrexate to immunoglobins to treat hamsters with leukemia.[68] Since then, antibody-drug conjugates (ADCs) have enabled site-specific delivery of SM cargos, while improving drug circulation and preventing systemic toxicity.[69] As of June 2023, eleven ADCs have been FDA approved for the treatment of hematological and solid tumor cancers.[70] Shorter peptide targeting moieties are also being explored ("peptide-drug conjugates", PDCs) in clinical trials currently.

Importantly, sophisticated drug linker chemistries for ADC/PDCs have been (and continue to be) developed for stability in circulation with efficient payload release at target sites by acid-, protease-, hydrolysis-, or endolysosomal- cleavage mechanisms.[71-73] One remaining challenge is achievement of reproducible and high drug conjugation efficiency.[74] Because of their relatively simple design (antibody/peptide + linker + drug), the conjugation of drug is limited to sites that do not interfere with binding activity which limits the amount of drug that may be conjugated. Conjugation processes are inefficient and 2 – 8 drugs per antibody is typical for ADCs.[73]

Synthetic protein nanocages

Protein nanocages are a budding class of biologic materials with great potential to efficiently localize to a target tissue, engage with target cells, and deliver therapeutic cargos. Inspired by endogenous viral and protein-capsids, nanocages can be designed from protein subunits to stably self-assemble into their lowest free energy state.[75, 76] Technologies such as machine learning and *in vivo* library selection have enabled rapid and precise design of protein cages with atomic level control.[77, 78] These materials are ideal for delivery of multiple classes of materials, especially those like nucleic acids that need protection from degradation.[79] They have also been investigated for delivery of SM drugs, especially to avoid off-target toxicity.[80, 81] Cargo loading is commonly achieved by passive diffusion through nanocage pores and absorption to inner lumenal surface. New strategies are needed to direct reproducible loading and controlled release.

Cell-based therapies

Adoptive cell immunotherapy (ACT) is rapidly emerging as a highly effective treatment modality that has been primarily studied in the cancer field. For example, FDA-approved chimeric antigen receptor (CAR) T cell products have been developed to cure 25-50% of previously incurable patients with B-cell malignancies by engineering cells with antigen-specific receptors that when engages activate cancer cell killing.[82, 83] ACT involves isolation and then reinfusion of a patient's own immune cells after genetic engineering (to enhance disease-fighting capabilities), activation, and expansion. A coordinated and progressive scientific effort since the 1980s has vastly improved the effective design and diversity of ACT products, with more on the horizon (e.g., natural killer cells, tumor-infiltrating lymphocytes, macrophages).[84-88]

While CAR T cells have been the star prodigy of ACT, their limitations have been recognized upon application to solid tumors, where they face stromal delivery, trafficking (e.g., caused by "cold" tumors), and persistence (e.g., caused by T cell exhaustion) barriers.[89-91] Towards improving their viability post-transfusion, Irvine et al. showed that T cells could be decorated with SM drug loaded liposomes by endogenous cell receptors.[92, 93] Alternatively, macrophages have been engineered to express CARs and therapeutic proteins, given their unique ability to traffic to solid tumors and other disease niches where they become tissue resident.[87, 94, 95] Efforts to load macrophages with SM drugs via phagocytosis or degradable "backpacks" have enabled co-delivery of SM drugs, especially to modulate a pro- or anti- inflammatory macrophage phenotype.[96-98] An exciting direction, 'user-operated' circuits utilizing SM drugs to activate or deactivate transgene expression or cell therapeutic activity are being developed with advanced precision.[19, 99] A challenge remains in improving co-delivery of SM drugs with controlled release profiles to realize such technologies.

1.4 DRUGAMERS: PULLING FROM PREVIOUS ADVANCES TO DELIVER SMALL MOLECULES

An effective nanocarrier for SM drug delivery should be (1) targeted, (2) have controlled release of the active SM drug cargo, (3) be eliminated from the body, have (4) uniform size, and (5) scalable synthesis.[52] Reversible Addition Fragmentation-chain Transfer (RAFT)-based polymer prodrugs "drugamers" are a versatile synthetic platform to achieve these requirements with superior control using one-pot reaction schemes and exciting potential for translation. [100]

The idea of polymerizable prodrugs has grown over the last twenty years alongside advancements in controlled polymerization techniques to enable controlled release of covalently

attached SM drugs.[101-107]. An early example, Smith et al. demonstrated the synthetic versatility of RAFT-based drugamers by independently and reproducibly controlling polymer degree of polymerization (DP) and drug loading to identify a lead drugamer for improved cell uptake and antiviral activity.[108] Since then, RAFT-based drugamers have been studied in multiple preclinical disease contexts to deliver a variety of small molecule drug classes with incredible versatility and modularity. Given their therapeutic impact in diverse preclinical disease models and their empirical design centered on clinical impact, we foresee their prompt translation.

Drugamers are commonly synthesized by RAFT due to the high degree of control over macromolecular structure including molecular weight, dispersity, chemical composition, and architecture. RAFT is a living radical polymerization technique that was developed in 1998 by Chiefari et al.[109, 110] It is "radical" because chains are initiated by formation of radicals that allow for chain propagation by sequential addition of monomers until termination occurs by combination or disproportionation. It is "living" because chains are initiated at the beginning, grow at the same rate, and do not have premature termination. To achieve "living"-ness, reversible deactivation radical polymerization (RDRP) ensures that the majority of chains are maintained in a dormant form to prevent premature and irreversible termination. Rapid equilibration between active and dormant chains ensures that all chains have equal probability of growth at any given time. What makes RAFT special is the use of a thiocarbonylthio chain transfer agent (CTA, (ZC(=S)SR)), which is responsible for the rapid reversible deactivation (full RAFT mechanism shown in Figure 1.3A). The result is that all chains grow at a similar linear rate and when compared to conventional polymerization reactions (i.e., step-growth), living radical polymerizations like RAFT are characterized by narrow size dispersities, Đ, less than or equal to 1.1 (Figure 1.3B). The degree of polymerization (and thus the molecular weight) can be easily modulated by tuning the

ratio of monomer to CTA, as shown in Figure 1.3C with a poly(methyl methyacryate) (PMMA) RAFT polymerization.

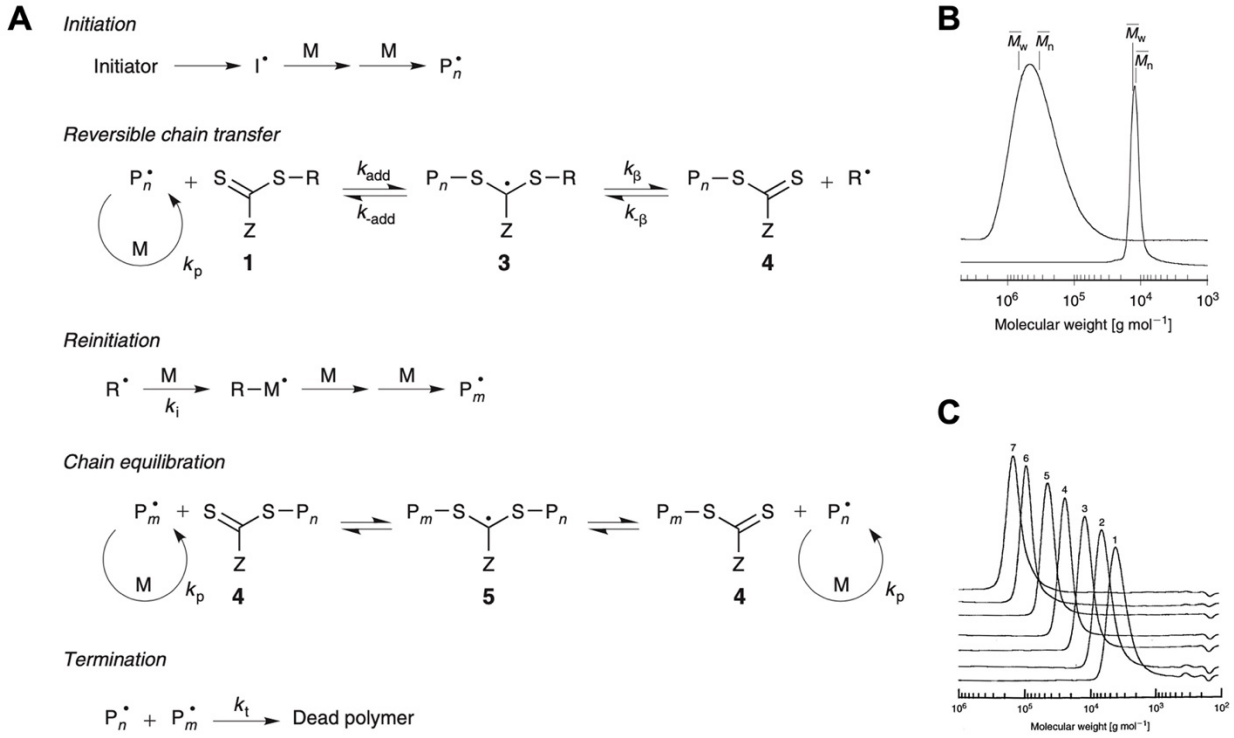

Figure 1.3 RAFT polymerization reactions yield uniform size polymer products with precise control over chain length (A) RAFT polymerization mechanism (B) Dispersity improvements using RAFT reaction of styrene (right peak) compared to conventional polymerization as shown by gel permeation chromatography traces. (C) (PMMA) chain length is precisely dictated by amount of RAFT CTA added to the reaction holding all else the same. Figures reprinted from Moad et al [109] under the terms of the Creative Commons Attribution (CC BY-NC-ND) License.

Other than RAFT, other living radical polymerization techniques exist, including atom transfer radical polymerization (ATRP) and nitroxide-mediated polymerization (NMP).[111, 112] However, the range of compatible monomer classes and solvents available limits their versatility and RAFT remains the gold standard for controlled living polymerization.[113] The polymerization reaction is relatively simple and inexpensive to implement and can be applied to a wide variety of monomers, including (meth)acrylates, (meth)acrylamides, stryrenes, butadienes,

pyridines, acetates and more and for monomers with a wide variety of functional groups (e.g., OH, COOH, NR_2, $CONR_2$).[109] The reaction can be conducted in both organic to aqueous solvents, though if there are hydrolytic esters in the monomers organic solvent is preferrable to prevent premature degradation.[114] Chapman et al. showed that reactions could be conducted without nitrogen purging, representing a major innovation for reducing cost of production.[115] RAFT reactions can be initiated by temperature, light, redox, electrochemically, mechanically, and sonochemically and in diverse conditions (solution, emulsion, suspension).[116-118] Importantly, RAFT polymers can be manufactured at large scales in continuous flow reactors without sacrificing product quality.[119, 120] All of these factors make it a viable and impactful approach to clinical translation of drugamers with versatile applications in multiple disease contexts.

1.4.1 Tunability

Drugamers are made from multiple functional monomers that represent building blocks that can be mixed and matched into copolymers (Figure 1.4). Each monomer unit serves a distinct functionality and precisely tuned release of small molecule cargos can be designed to optimize a drug's mechanism of action after targeted delivery to a particular disease niche. By RAFT polymerization, monomers are incorporated in a statistical manner allowing for optimized ratios of hydrophobic drugs and soluble components with improved targeting, detection, and additional physiochemical properties. The longer the polymer chains, the more drug can be incorporated, while maintaining solubility.

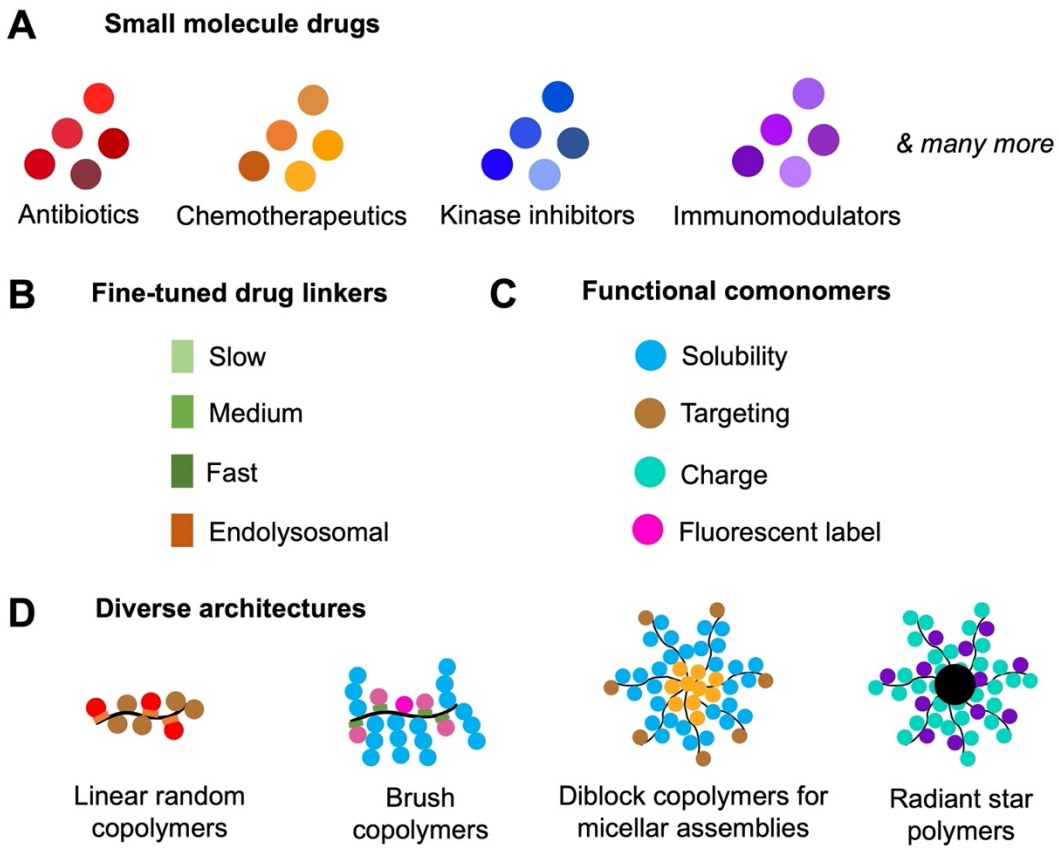

Figure 1.4 Reformulation of small molecules into designable drugamers is possible using a functional monomer library. (A) Small molecule drugs are functionalized with (B) fine-tuned drug linkers to polymerizeable monomer backbones and copolymerized with (C) functional comonomers to yield functional drugamers with (D) diverse architectures.

Inspired by ADCs and polymer-drug conjugates, drugamers are made from monomers linked to SM drugs with varied lability (e.g., hydrolytic esters, acidic hydrazones, enzyme-cleavable amides, and combinations thereof (e.g., endolysosomal) (Figure 1.4B, Figure S1.1). Sustained SM drug release profiles can be achieved from a single drugamer macromolecules by incorporation and subsequent release of multiple SM drug units. SM drug release from the polymeric backbone can be fine-tuned over days or months, depending on the disease application and is influenced by the macromolecular architecture and steric effects (properties that can be tuned as well).[121]

Enhanced targeting of drugamers has been achieved by incorporation of glycosylated monomers.[122-126] Glycan targeting has been explored extensively for multiple synthetic delivery vehicles prior to drugamers due to the facile functionalization of the small molecule.[127, 128] Mannose is widely used to target macrophages and dendritic cells by engagement of mannose receptor (Figure S1.1).[123, 129, 130] *N*-acetylgalactosamine (GalNAc) is used to target liver hepatocytes.[125, 131, 132] Glycans are ideal for drugamer incorporation due to their ease of conjugation to methacrylate backbones and similar activity ratios to other functional monomers. Such glycan strategies be enhanced by multivalent presentation which mimics innate biological mechanism for glycosylated proteins and microorganisms engagement with cellular receptors based on avidity interactions. While glycans have proved incredibly successful targeting moieties for drugamers, there are opportunities to explore other types of targeting moieties including hyaluronic acid (targeting to CD44), folic acid (targeting to folate receptors overexpressed on tumor cells), and hormones.[28] Huang et al. even showed that polymerizable protein monomers could be incorporated into RAFT polymers, indicating the possibility of enhancing drugamer targeting with antibodies, peptides, or single chain variable fragments.[133]

Lastly, an exciting opportunity to expand the impact of RAFT drugamers involves the synthesis of diverse architectures - a design component that can be modulated for a given disease application or to enable combination with biologic therapeutics. Not only does RAFT allow of precise control over chain length, but the versatility of the platform allows for synthesis of macro(CTA)s which can enable the synthesis of block copolymers with pre-determined compositions, enabling micelle formation.[109, 121] Brush polymers and co-polymers can be synthesized as well as radiant start polymers grown from hyperbranched cores.[134]

1.4.2 Success with drugamers

Drugamers allow for spatial and temporal control over drug delivery through functional monomer moieties that target and tune drug release kinetics.[121, 129] These synthetic polymers optimize drug pharmacokinetic and biodistribution profiles and are available for a host of small molecules, including antimalarials, antibiotics, chemotherapeutics, HIV antiretrovirals, and kinase inhibitors. [100, 121, 123, 125, 135-138]

Srinivasan et al. showed that antimalarial drugamers containing primaquine and tafenoquine were as efficacious as the parent drug in the *P. berghei* causal prophylaxis model and with decreased hemolytic anemia which is critical for patients with G6PD deficiency. GalNAc-containing drugamers displayed increased targeting to liver hepatocytes where endolysosomal uptake and cleavage enabled intracellular release of drug.[125]. In a cancer context, Son et al showed that drugamers containing multiple drug classes including the chemotherapeutic camptothecin and the kinase inhibitor dasatinib could be synthesized with brush architectures (enabled by copolymerization with PEG methycrylates) with independent and sustained release profiles.[43] In an HIV prophylaxis setting, Ho et al. showed that injectable drugamer depots containing the antiretroviral drug tenofovir alafenamide connected by faster or slower degrading hydroxybenzyloxycarbonyl (benzyl) and ethyloxycarbonyl (alkyl) linkers achieved sustained drug release resulting in 10-fold higher than protective concentrations over 50 days in a murine model.[138]

A significant direction for drugamer development has been for the prevention of intracellular pulmonary infections caused by the stealth and biothreat pathogens *Francisella novicida* (Fn) and *Burkholderia pseudomallei* (Bp).[100, 123, 126] Alveolar macrophage-targeted drugamers containing the fluoroquinolone antibiotic ciprofloxacin (cipro) were developed for

direct lung administration via aerosolization. Mannose and an endolysosomal valine-citrulline (VC)-linked cipro comonomers were incorporated into a random linear copolymer with improved solubility, targeting, and efficacy compared to the parent drug. Pharmacokinetic analysis showed that drugamer treatment led to a two order of magnitude improvement in alveolar macrophage AUC and an improved $t_{1/2}$ (Figure 1.5A). Further, whole lung antibiotic concentrations (Figure 1.5B) were also enhanced. Astonishingly, in highly lethal murine models of Fn and Bp intracellular infections drugamer treatment led to 100% rescue of survival (Figure 1.5 C, D) In the Chapter 2 we will expand on how antibiotic drugamers can be used to treat primarily extracellular *Klebsiella pneumoniae* infections by targeting alveolar macrophages (Figure 1.6A).

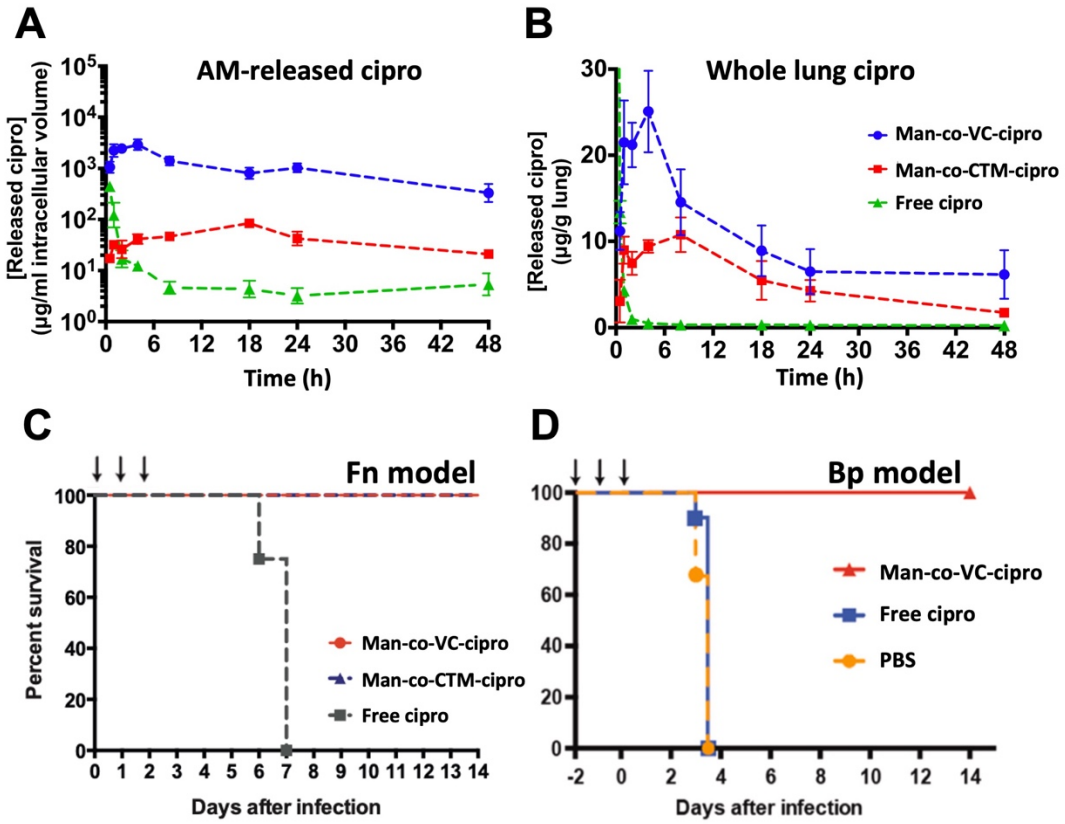

Figure 1.5 Ciprofloxacin antibiotic drugamers provide total protection in lethal murine models of intracellular infections due to optimized pharmacokinetic parameters of drugamer. Total protection of drugamer in (A) *Fransicella novicida* and (B)

Burkholderia psudomallei. The mannose-co-VC-ciprofloxacin drugamer (Man-co-VC-cipro) was compared to hydrolytic ester ciprofloxacin drugamer equivalent (Man-co-CTM-cipro) and free drug. Pharmacokinetic studies in healthy mice showed achievement of high and sustained (C) ciprofloxacin within alveolar macrophages and (D) increased whole lung ciprofloxacin compared to free drug and Man-co-CTM controls, MIC_{Fn} = 0.065 μg/g. *Fransicella novicida,* Fn; *Burkholderia psudomallei*, Bp; alveolar macrophage, AM; ciprofloxacin, cipro. Figure adapted from Su et al. and Chavas et al. with permission.[123, 126]

1.4.3 Combining drugamers with biologics

There are many opportunities to leverage drugamers in new and exciting ways beyond what is capable with parent SM drugs due to their tunable physiochemical nature, ligand targeting, and controlled release properties.[7, 139-141] In addition to discussing drugamers alone in Chapter 2, we will also discuss how drugamers can be leveraged in combination with emerging classes of biologic therapeutics (Figure 1.6 B and C). In Chapter 3 we will discuss their use as adjuvants for co-delivery within protein-based vaccines. Then, in Chapter 4, we will present a biorthogonal mechanism for noncovalent loading of drugamers on macrophage and T cell therapeutics for cancer applications.

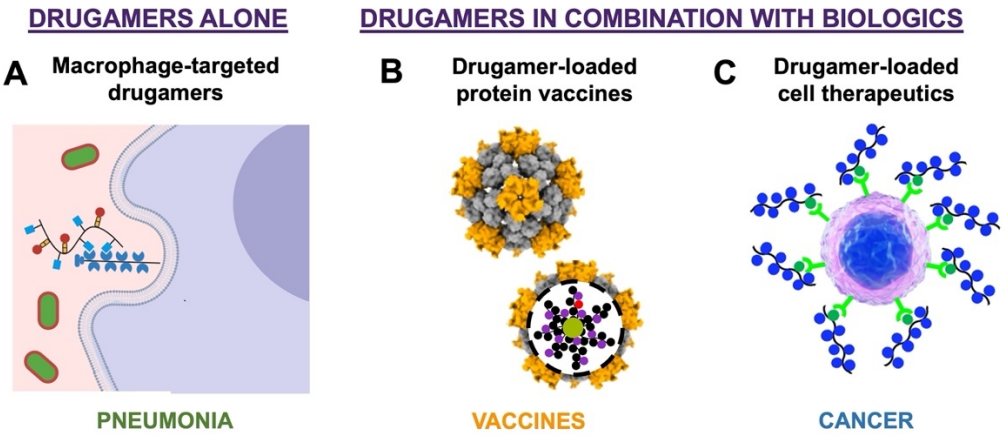

Figure 1.6 Leveraging drugamers alone or in combination with biologics for pulmonary infection and immune therapies.

REFERENCES

[1] P. Agarwal, J. Huckle, J. Newman, D.L. Reid, Trends in small molecule drug properties: A developability molecule assessment perspective, Drug Discovery Today, 27 (2022) 103366.
[2] M.J. Desborough, D.M. Keeling, The aspirin story–from willow to wonder drug, British journal of haematology, 177 (2017) 674-683.
[3] M.I. Hutchings, A.W. Truman, B. Wilkinson, Antibiotics: past, present and future, Current Opinion in Microbiology, 51 (2019) 72-80.
[4] H. Beck, M. Härter, B. Haß, C. Schmeck, L. Baerfacker, Small molecules and their impact in drug discovery: A perspective on the occasion of the 125th anniversary of the Bayer Chemical Research Laboratory, Drug Discovery Today, 27 (2022) 1560-1574.
[5] U.P. Division, Contraceptive use by method 2019 : data booklet, 2019.
[6] R. Santos, O. Ursu, A. Gaulton, A.P. Bento, R.S. Donadi, C.G. Bologa, A. Karlsson, B. Al-Lazikani, A. Hersey, T.I. Oprea, J.P. Overington, A comprehensive map of molecular drug targets, Nature Reviews Drug Discovery, 16 (2017) 19-34.
[7] D.G. Brown, H.J. Wobst, A decade of FDA-approved drugs (2010–2019): trends and future directions, Journal of medicinal chemistry, 64 (2021) 2312-2338.
[8] U. Rix, G. Superti-Furga, Target profiling of small molecules by chemical proteomics, Nature Chemical Biology, 5 (2009) 616-624.
[9] L.N. Makley, J.E. Gestwicki, Expanding the Number of 'Druggable' Targets: Non-Enzymes and Protein–Protein Interactions, Chemical Biology & Drug Design, 81 (2013) 22-32.
[10] R. Roskoski, Jr., A historical overview of protein kinases and their targeted small molecule inhibitors, Pharmacol Res, 100 (2015) 1-23.
[11] D. Kim, H.J. Nam, PARP Inhibitors: Clinical Limitations and Recent Attempts to Overcome Them, Int J Mol Sci, 23 (2022).
[12] S. Hoelder, P.A. Clarke, P. Workman, Discovery of small molecule cancer drugs: Successes, challenges and opportunities, Molecular Oncology, 6 (2012) 155-176.
[13] T. Fester, Processes in pharmacokinetics, 2020.
[14] K. Wolff, Pharmacokinetics, in: I.P. Stolerman, L.H. Price (Eds.) Encyclopedia of Psychopharmacology, Springer Berlin Heidelberg, Berlin, Heidelberg, 2015, pp. 1280-1291.
[15] F.D. Makurvet, Biologics vs. small molecules: Drug costs and patient access, Medicine in Drug Discovery, 9 (2021) 100075.
[16] K.C. Waterman, Understanding and Predicting Pharmaceutical Product Shelf-Life, in: K. Huynh-Ba (Ed.) Handbook of Stability Testing in Pharmaceutical Development: Regulations, Methodologies, and Best Practices, Springer New York, New York, NY, 2009, pp. 115-135.
[17] B.K. Muralidhara, M. Wong, Critical considerations in the formulation development of parenteral biologic drugs, Drug Discovery Today, 25 (2020) 574-581.
[18] M.J. Waring, J. Arrowsmith, A.R. Leach, P.D. Leeson, S. Mandrell, R.M. Owen, G. Pairaudeau, W.D. Pennie, S.D. Pickett, J. Wang, O. Wallace, A. Weir, An analysis of the attrition of drug candidates from four major pharmaceutical companies, Nature Reviews Drug Discovery, 14 (2015) 475-486.
[19] C.J. Bashor, I.B. Hilton, H. Bandukwala, D.M. Smith, O. Veiseh, Engineering the next generation of cell-based therapeutics, Nature Reviews Drug Discovery, 21 (2022) 655-675.
[20] Y. Zeng, W. Shi, Z. Liu, H. Xu, L. Liu, J. Hang, Y. Wang, M. Lu, W. Zhou, W. Huang, F. Tang, C-terminal modification and functionalization of proteins via a self-cleavage tag triggered by a small molecule, Nature Communications, 14 (2023) 7169.

[21] J. Reinholz, K. Landfester, V. Mailänder, The challenges of oral drug delivery via nanocarriers, Drug Delivery, 25 (2018) 1694-1705.
[22] A.Z. Alkilani, M.T. McCrudden, R.F. Donnelly, Transdermal Drug Delivery: Innovative Pharmaceutical Developments Based on Disruption of the Barrier Properties of the stratum corneum, Pharmaceutics, 7 (2015) 438-470.
[23] L.-A. Keller, O. Merkel, A. Popp, Intranasal drug delivery: opportunities and toxicologic challenges during drug development, Drug Delivery and Translational Research, 12 (2022) 735-757.
[24] S. Hua, Advances in Nanoparticulate Drug Delivery Approaches for Sublingual and Buccal Administration, Front Pharmacol, 10 (2019) 1328.
[25] J.S. Patton, P.R. Byron, Inhaling medicines: delivering drugs to the body through the lungs, Nature reviews Drug discovery, 6 (2007) 67-74.
[26] M.J. Mitchell, M.M. Billingsley, R.M. Haley, M.E. Wechsler, N.A. Peppas, R. Langer, Engineering precision nanoparticles for drug delivery, Nature Reviews Drug Discovery, 20 (2021) 101-124.
[27] A. Zielińska, F. Carreiró, A.M. Oliveira, A. Neves, B. Pires, D.N. Venkatesh, A. Durazzo, M. Lucarini, P. Eder, A.M. Silva, A. Santini, E.B. Souto, Polymeric Nanoparticles: Production, Characterization, Toxicology and Ecotoxicology, Molecules, 25 (2020).
[28] K. Ulbrich, K. Hola, V. Subr, A. Bakandritsos, J. Tucek, R. Zboril, Targeted drug delivery with polymers and magnetic nanoparticles: covalent and noncovalent approaches, release control, and clinical studies, Chemical reviews, 116 (2016) 5338-5431.
[29] A.C. Martins, M.Y. Oshiro, F. Albericio, B.G. de la Torre, G.J.V. Pereira, R.V. Gonzaga, Trends and Perspectives of Biological Drug Approvals by the FDA: A Review from 2015 to 2021, Biomedicines, 10 (2022) 2325.
[30] R. Singh, J.W. Lillard, Jr., Nanoparticle-based targeted drug delivery, Exp Mol Pathol, 86 (2009) 215-223.
[31] R. Duncan, The dawning era of polymer therapeutics, Nature Reviews Drug Discovery, 2 (2003) 347-360.
[32] J. Kopecek, P. Kopecková, HPMA copolymers: origins, early developments, present, and future, Adv Drug Deliv Rev, 62 (2010) 122-149.
[33] H. Ringsdorf, Structure and properties of pharmacologically active polymers, Journal of polymer science. Polymer symposia, 51 (1975) 135-153.
[34] J.M. Harris, R.B. Chess, Effect of pegylation on pharmaceuticals, Nature Reviews Drug Discovery, 2 (2003) 214+.
[35] Y. Gao, M. Joshi, Z. Zhao, S. Mitragotri, PEGylated therapeutics in the clinic, Bioengineering & Translational Medicine, n/a (2023).
[36] J.S. Suk, Q. Xu, N. Kim, J. Hanes, L.M. Ensign, PEGylation as a strategy for improving nanoparticle-based drug and gene delivery, Adv Drug Deliv Rev, 99 (2016) 28-51.
[37] A. Abuchowski, J.R. McCoy, N.C. Palczuk, T. van Es, F.F. Davis, Effect of covalent attachment of polyethylene glycol on immunogenicity and circulating life of bovine liver catalase, J Biol Chem, 252 (1977) 3582-3586.
[38] J. Kopeček, P. Kopečková, HPMA copolymers: Origins, early developments, present, and future, Adv Drug Deliv Rev, 62 (2010) 122-149.
[39] J.G. Shiah, M. Dvořák, P. Kopečková, Y. Sun, C.M. Peterson, J. Kopeček, Biodistribution and antitumour efficacy of long-circulating N-(2-hydroxypropyl)methacrylamide copolymer–doxorubicin conjugates in nude mice, European Journal of Cancer, 37 (2001) 131-139.

[40] Y. Matsumura, H. Maeda, A New Concept for Macromolecular Therapeutics in Cancer Chemotherapy: Mechanism of Tumoritropic Accumulation of Proteins and the Antitumor Agent Smancs, Cancer Research, 46 (1986) 6387.
[41] N.J. Agard, J.A. Prescher, C.R. Bertozzi, A Strain-Promoted [3 + 2] Azide−Alkyne Cycloaddition for Covalent Modification of Biomolecules in Living Systems, Journal of the American Chemical Society, 126 (2004) 15046-15047.
[42] M.L. Girase, P.G. Patil, P.P. Ige, Polymer-drug conjugates as nanomedicine: A review, International Journal of Polymeric Materials and Polymeric Biomaterials, 69 (2020) 990-1014.
[43] H.N. Son, S. Srinivasan, J.Y. Yhee, D. Das, B.K. Daugherty, G.Y. Berguig, V.G. Oehle, S.H. Kim, K. Kim, I.C. Kwon, P.S. Stayton, A.J. Convertine, Chemotherapeutic copolymers prepared via the RAFT polymerization of prodrug monomers, Polymer Chemistry, 7 (2016) 4494-4505.
[44] R. Gref, Y. Minamitake, M.T. Peracchia, V. Trubetskoy, V. Torchilin, R. Langer, Biodegradable long-circulating polymeric nanospheres, Science, 263 (1994) 1600-1603.
[45] Y. Lu, G.W. Coates, Pairing-Enhanced Regioselectivity: Synthesis of Alternating Poly(lactic-co-glycolic acid) from Racemic Methyl-Glycolide, Journal of the American Chemical Society, 145 (2023) 22425-22432.
[46] N. Kamaly, B. Yameen, J. Wu, O.C. Farokhzad, Degradable Controlled-Release Polymers and Polymeric Nanoparticles: Mechanisms of Controlling Drug Release, Chemical Reviews, 116 (2016) 2602-2663.
[47] I. Ekladious, Y.L. Colson, M.W. Grinstaff, Polymer-drug conjugate therapeutics: advances, insights and prospects, Nature reviews. Drug discovery, 18 (2019) 273-294.
[48] Y. Barenholz, Doxil® — The first FDA-approved nano-drug: Lessons learned, Journal of Controlled Release, 160 (2012) 117-134.
[49] J. Andrew MacKay, M. Chen, J.R. McDaniel, W. Liu, A.J. Simnick, A. Chilkoti, Self-assembling chimeric polypeptide–doxorubicin conjugate nanoparticles that abolish tumours after a single injection, Nature Materials, 8 (2009) 993-999.
[50] K. Kataoka, A. Harada, Y. Nagasaki, Block copolymer micelles for drug delivery: design, characterization and biological significance, Adv Drug Deliv Rev, 47 (2012) 113-131.
[51] G.S. Kwon, K. Kataoka, Block copolymer micelles as long-circulating drug vehicles, Adv Drug Deliv Rev, 16 (2012) 295-309.
[52] S. Hassan, G. Prakash, A. Bal Ozturk, S. Saghazadeh, M. Farhan Sohail, J. Seo, M. Remzi Dokmeci, Y.S. Zhang, A. Khademhosseini, Evolution and clinical translation of drug delivery nanomaterials, Nano Today, 15 (2017) 91-106.
[53] K. Kataoka, A. Harada, Y. Nagasaki, Block copolymer micelles for drug delivery: Design, characterization and biological significance, Adv Drug Deliv Rev, 64 (2012) 37-48.
[54] M. Murakami, H. Cabral, Y. Matsumoto, S. Wu, M.R. Kano, T. Yamori, N. Nishiyama, K. Kataoka, Improving drug potency and efficacy by nanocarrier-mediated subcellular targeting, Science translational medicine, 3 (2011) 64ra62-64ra62.
[55] A.V. Kabanov, E.V. Batrakova, V.Y. Alakhov, Pluronic® block copolymers as novel polymer therapeutics for drug and gene delivery, Journal of Controlled Release, 82 (2002) 189-212.
[56] E.V. Batrakova, A.V. Kabanov, Pluronic block copolymers: evolution of drug delivery concept from inert nanocarriers to biological response modifiers, J Control Release, 130 (2008) 98-106.

[57] Y.E. Kurtoglu, M.K. Mishra, S. Kannan, R.M. Kannan, Drug release characteristics of PAMAM dendrimer-drug conjugates with different linkers, Int J Pharm, 384 (2010) 189-194.
[58] M. Han, M.Y. Huang-Fu, W.W. Guo, N.N. Guo, J. Chen, H.N. Liu, Z.Q. Xie, M.T. Lin, Q.C. Wei, J.Q. Gao, MMP-2-Sensitive HA End-Conjugated Poly(amidoamine) Dendrimers via Click Reaction To Enhance Drug Penetration into Solid Tumor, ACS Appl Mater Interfaces, 9 (2017) 42459-42470.
[59] M.A. Fischbach, J.A. Bluestone, W.A. Lim, Cell-based therapeutics: the next pillar of medicine, Science translational medicine, 5 (2013) 179ps177-179ps177.
[60] M. Senior, Fresh from the biotech pipeline: fewer approvals, but biologics gain share, Nature Biotechnology, 41 (2023) 174-182.
[61] P. Rein, R.B. Mueller, Treatment with Biologicals in Rheumatoid Arthritis: An Overview, Rheumatology and Therapy, 4 (2017) 247-261.
[62] C. Robert, A decade of immune-checkpoint inhibitors in cancer therapy, Nature Communications, 11 (2020) 3801.
[63] A.C. Anselmo, Y. Gokarn, S. Mitragotri, Non-invasive delivery strategies for biologics, Nature Reviews Drug Discovery, 18 (2019) 19-40.
[64] K. Sampathkumar, B.A. Kerwin, Roadmap for Drug Product Development and Manufacturing of Biologics, Journal of Pharmaceutical Sciences, (2023).
[65] S. Morin, G. Segafredo, M. Piccolis, A. Das, M. Das, N. Loffredi, A. Larbi, K. Mwamelo, E. Villanueva, S. Nobre, E. Burrone, Expanding access to biotherapeutics in low-income and middle-income countries through public health non-exclusive voluntary intellectual property licensing: considerations, requirements, and opportunities, The Lancet Global Health, 11 (2023) e145-e154.
[66] S.R. Madabhushi, J. Gavin, S. Xu, C. Cutler, R. Chmielowski, W. Rayfield, N. Tugcu, H. Chen, Quantitative assessment of environmental impact of biologics manufacturing using process mass intensity analysis, Biotechnology Progress, 34 (2018) 1566-1573.
[67] V. Halimi, A. Daci, K. Ancevska Netkovska, L. Suturkova, Z.U. Babar, A. Grozdanova, Clinical and Regulatory Concerns of Biosimilars: A Review of Literature, Int J Environ Res Public Health, 17 (2020).
[68] G. Mathe, L.O. Tran Ba, J. Bernard, Effect on mouse leukemia 1210 of a combination by diazo-reaction of amethopterin and gamma-globulins from hamsters inoculated with such leukemia by heterografts, C R Hebd Seances Acad Sci, 246 (1958) 1626-1628.
[69] P.D. Senter, Potent antibody drug conjugates for cancer therapy, Current Opinion in Chemical Biology, 13 (2009) 235-244.
[70] P. Gogia, H. Ashraf, S. Bhasin, Y. Xu, Antibody-Drug Conjugates: A Review of Approved Drugs and Their Clinical Level of Evidence, Cancers (Basel), 15 (2023).
[71] C.H. Chau, P.S. Steeg, W.D. Figg, Antibody–drug conjugates for cancer, The Lancet, 394 (2019) 793-804.
[72] M.J. Birrer, K.N. Moore, I. Betella, R.C. Bates, Antibody-Drug Conjugate-Based Therapeutics: State of the Science, JNCI: Journal of the National Cancer Institute, 111 (2019) 538-549.
[73] K. Tsuchikama, Z. An, Antibody-drug conjugates: recent advances in conjugation and linker chemistries, Protein & Cell, 9 (2016) 33-46.
[74] M. Alas, A. Saghaeidehkordi, K. Kaur, Peptide–Drug Conjugates with Different Linkers for Cancer Therapy, Journal of Medicinal Chemistry, 64 (2021) 216-232.

[75] N.P. King, W. Sheffler, M.R. Sawaya, B.S. Vollmar, J.P. Sumida, I. André, T. Gonen, T.O. Yeates, D. Baker, Computational design of self-assembling protein nanomaterials with atomic level accuracy, Science, 336 (2012) 1171-1174.
[76] J.B. Bale, S. Gonen, Y. Liu, W. Sheffler, D. Ellis, C. Thomas, D. Cascio, T.O. Yeates, T. Gonen, N.P. King, Accurate design of megadalton-scale two-component icosahedral protein complexes, Science, 353 (2016) 389-394.
[77] I.D. Lutz, S. Wang, C. Norn, A. Courbet, A.J. Borst, Y.T. Zhao, A. Dosey, L. Cao, J. Xu, E.M. Leaf, C. Treichel, P. Litvicov, Z. Li, A.D. Goodson, P. Rivera-Sánchez, A.-M. Bratovianu, M. Baek, N.P. King, H. Ruohola-Baker, D. Baker, Top-down design of protein architectures with reinforcement learning, Science, 380 (2023) 266-273.
[78] A. Olshefsky, H. Benasutti, M. Sylvestre, G.L. Butterfield, G.J. Rocklin, C. Richardson, D.R. Hicks, M.J. Lajoie, K. Song, E. Leaf, C. Treichel, J. Decarreau, S. Ke, G. Kher, L. Carter, J.S. Chamberlain, D. Baker, N.P. King, S.H. Pun, In vivo selection of synthetic nucleocapsids for tissue targeting, Proceedings of the National Academy of Sciences, 120 (2023) e2306129120.
[79] G.L. Butterfield, M.J. Lajoie, H.H. Gustafson, D.L. Sellers, U. Nattermann, D. Ellis, J.B. Bale, S. Ke, G.H. Lenz, A. Yehdego, R. Ravichandran, S.H. Pun, N.P. King, D. Baker, Evolution of a designed protein assembly encapsulating its own RNA genome, Nature, 552 (2017) 415-420.
[80] Z. Wang, S. Zhang, R. Zhang, X. Chen, G. Sun, M. Zhou, Q. Han, B. Zhang, Y. Zhao, B. Jiang, Bioengineered Dual-Targeting Protein Nanocage for Stereoscopical Loading of Synergistic Hydrophilic/Hydrophobic Drugs to Enhance Anticancer Efficacy, Advanced Functional Materials, 31 (2021) 2102004.
[81] M. Murata, S. Narahara, T. Kawano, N. Hamano, J.S. Piao, J.-H. Kang, K. Ohuchida, T. Murakami, M. Hashizume, Design and Function of Engineered Protein Nanocages as a Drug Delivery System for Targeting Pancreatic Cancer Cells via Neuropilin-1, Molecular Pharmaceutics, 12 (2015) 1422-1430.
[82] A. Titov, E. Zmievskaya, I. Ganeeva, A. Valiullina, A. Petukhov, A. Rakhmatullina, R. Miftakhova, M. Fainshtein, A. Rizvanov, E. Bulatov, Adoptive Immunotherapy beyond CAR T-Cells, Cancers, 13 (2021) 743.
[83] S.L. Maude, N. Frey, P.A. Shaw, R. Aplenc, D.M. Barrett, N.J. Bunin, A. Chew, V.E. Gonzalez, Z. Zheng, S.F. Lacey, Y.D. Mahnke, J.J. Melenhorst, S.R. Rheingold, A. Shen, D.T. Teachey, B.L. Levine, C.H. June, D.L. Porter, S.A. Grupp, Chimeric Antigen Receptor T Cells for Sustained Remissions in Leukemia, New England Journal of Medicine, 371 (2014) 1507-1517.
[84] M.S. Goldberg, Improving cancer immunotherapy through nanotechnology, Nature Reviews Cancer, 19 (2019) 587-602.
[85] M. Cheng, Y. Chen, W. Xiao, R. Sun, Z. Tian, NK cell-based immunotherapy for malignant diseases, Cellular & Molecular Immunology, 10 (2013) 230-252.
[86] J.S. Granhøj, A. Witness Præst Jensen, M. Presti, Ö. Met, I.M. Svane, M. Donia, Tumor-infiltrating lymphocytes for adoptive cell therapy: recent advances, challenges, and future directions, Expert Opinion on Biological Therapy, 22 (2022) 627-641.
[87] M. Klichinsky, M. Ruella, O. Shestova, X.M. Lu, A. Best, M. Zeeman, M. Schmierer, K. Gabrusiewicz, N.R. Anderson, N.E. Petty, K.D. Cummins, F. Shen, X. Shan, K. Veliz, K. Blouch, Y. Yashiro-Ohtani, S.S. Kenderian, M.Y. Kim, R.S. O'Connor, S.R. Wallace, M.S. Kozlowski, D.M. Marchione, M. Shestov, B.A. Garcia, C.H. June, S. Gill, Human chimeric antigen receptor macrophages for cancer immunotherapy, Nat Biotechnol, 38 (2020) 947-953.

[88] S. Lee, S. Kivimäe, A. Dolor, F.C. Szoka, Macrophage-based cell therapies: The long and winding road, J Control Release, 240 (2016) 527-540.
[89] N.N. Shah, T.J. Fry, Mechanisms of resistance to CAR T cell therapy, Nature Reviews Clinical Oncology, 16 (2019) 372-385.
[90] R.G. Majzner, C.L. Mackall, Clinical lessons learned from the first leg of the CAR T cell journey, Nature Medicine, 25 (2019) 1341-1355.
[91] R. Mohanty, C.R. Chowdhury, S. Arega, P. Sen, P. Ganguly, N. Ganguly, CAR T cell therapy: A new era for cancer treatment (Review), Oncol Rep, 42 (2019) 2183-2195.
[92] M.T. Stephan, J.J. Moon, S.H. Um, A. Bershteyn, D.J. Irvine, Therapeutic cell engineering with surface-conjugated synthetic nanoparticles, Nat Med, 16 (2010) 1035-1041.
[93] Y. Zheng, L. Tang, L. Mabardi, S. Kumari, D.J. Irvine, Enhancing Adoptive Cell Therapy of Cancer through Targeted Delivery of Small-Molecule Immunomodulators to Internalizing or Noninternalizing Receptors, ACS Nano, 11 (2017) 3089-3100.
[94] T. Suzuki, P. Arumugam, T. Sakagami, N. Lachmann, C. Chalk, A. Sallese, S. Abe, C. Trapnell, B. Carey, T. Moritz, P. Malik, C. Lutzko, R.E. Wood, B.C. Trapnell, Pulmonary macrophage transplantation therapy, Nature, 514 (2014) 450-454.
[95] K.J. Brempelis, C.M. Cowan, S.A. Kreuser, K.P. Labadie, B.M. Prieskorn, N.A.P. Lieberman, C.I. Ene, K.W. Moyes, H. Chinn, K.R. DeGolier, L.R. Matsumoto, S.K. Daniel, J.K. Yokoyama, A.D. Davis, V.J. Hoglund, K.S. Smythe, S.D. Balcaitis, M.C. Jensen, R.G. Ellenbogen, J.S. Campbell, R.H. Pierce, E.C. Holland, V.G. Pillarisetty, C.A. Crane, Genetically engineered macrophages persist in solid tumors and locally deliver therapeutic proteins to activate immune responses, J Immunother Cancer, 8 (2020).
[96] T. Liang, R. Zhang, X. Liu, Q. Ding, S. Wu, C. Li, Y. Lin, Y. Ye, Z. Zhong, M. Zhou, Recent Advances in Macrophage-Mediated Drug Delivery Systems, Int J Nanomedicine, 16 (2021) 2703-2714.
[97] K.L. Wofford, D.K. Cullen, K.L. Spiller, Modulation of macrophage phenotype via phagocytosis of drug-loaded microparticles, J Biomed Mater Res A, (2019).
[98] N. Kapate, M. Dunne, N. Kumbhojkar, S. Prakash, L.L.-W. Wang, A. Graveline, K.S. Park, V. Chandran Suja, J. Goyal, J.R. Clegg, S. Mitragotri, A backpack-based myeloid cell therapy for multiple sclerosis, Proceedings of the National Academy of Sciences, 120 (2023) e2221535120.
[99] G.M. Burslem, C.M. Crews, Small-Molecule Modulation of Protein Homeostasis, Chemical Reviews, 117 (2017) 11269-11301.
[100] D. Das, J. Chen, S. Srinivasan, A.M. Kelly, B. Lee, H.N. Son, F. Radella, T.E. West, D.M. Ratner, A.J. Convertine, S.J. Skerrett, P.S. Stayton, Synthetic Macromolecular Antibiotic Platform for Inhalable Therapy against Aerosolized Intracellular Alveolar Infections, Mol Pharm, 14 (2017) 1988-1997.
[101] N. Wang, Z.C. Chen, D.S. Lu, X.F. Lin, Controllable selective synthesis of a polymerizable prodrug of cytarabine by enzymatic and chemical methods, Bioorg Med Chem Lett, 15 (2005) 4064-4067.
[102] X. Li, Q. Wu, D.S. Lv, X.F. Lin, Controllable synthesis of polymerizable ester and amide prodrugs of acyclovir by enzyme in organic solvent, Bioorg Med Chem, 14 (2006) 3377-3382.
[103] Y. Ding, W. Chen, J. Hu, M. Du, D. Yang, Polymerizable disulfide paclitaxel prodrug for controlled drug delivery, Mater Sci Eng C Mater Biol Appl, 44 (2014) 386-390.

[104] X. Hu, J. Hu, J. Tian, Z. Ge, G. Zhang, K. Luo, S. Liu, Polyprodrug Amphiphiles: Hierarchical Assemblies for Shape-Regulated Cellular Internalization, Trafficking, and Drug Delivery, Journal of the American Chemical Society, 135 (2013) 17617-17629.
[105] J.A. Johnson, Y.Y. Lu, A.O. Burts, Y. Xia, A.C. Durrell, D.A. Tirrell, R.H. Grubbs, Drug-Loaded, Bivalent-Bottle-Brush Polymers by Graft-through ROMP, Macromolecules, 43 (2010) 10326-10335.
[106] A.X. Gao, L. Liao, J.A. Johnson, Synthesis of Acid-Labile PEG and PEG-Doxorubicin-Conjugate Nanoparticles via Brush-First ROMP, ACS Macro Letters, 3 (2014) 854-857.
[107] J. Liu, W. Liu, I. Weitzhandler, J. Bhattacharyya, X. Li, J. Wang, Y. Qi, S. Bhattacharjee, A. Chilkoti, Ring-opening polymerization of prodrugs: a versatile approach to prepare well-defined drug-loaded nanoparticles, Angewandte Chemie International Edition, 54 (2015) 1002-1006.
[108] A.A.A. Smith, K. Zuwala, M.B.L. Kryger, B.M. Wohl, C. Guerrero-Sanchez, M. Tolstrup, A. Postma, A.N. Zelikin, Macromolecular prodrugs of ribavirin: towards a treatment for co-infection with HIV and HCV, Chem Sci, 6 (2015) 264-269.
[109] G. Moad, E. Rizzardo, S.H. Thang, Living radical polymerization by the RAFT process, Australian journal of chemistry, 58 (2005) 379-410.
[110] J. Chiefari, Y. Chong, F. Ercole, J. Krstina, J. Jeffery, T.P. Le, R.T. Mayadunne, G.F. Meijs, C.L. Moad, G. Moad, Living free-radical polymerization by reversible addition-fragmentation chain transfer: the RAFT process, Macromolecules, 31 (1998) 5559.
[111] J.-S. Wang, K. Matyjaszewski, Controlled/" living" radical polymerization. Halogen atom transfer radical polymerization promoted by a Cu (I)/Cu (II) redox process, Macromolecules, 28 (1995) 7901-7910.
[112] G. Moad, E. Rizzardo, The history of nitroxide-mediated polymerization, Nitroxide Mediated Polymerization: From Fundamentals to Applications in Materials Science, 19 (2016) 1-44.
[113] S. Perrier, 50th Anniversary Perspective: RAFT Polymerization□ A User Guide, Macromolecules, 50 (2017) 7433-7447.
[114] S. Shanmugam, J. Xu, C. Boyer, Aqueous RAFT Photopolymerization with Oxygen Tolerance, Macromolecules, 49 (2016) 9345-9357.
[115] R. Chapman, A.J. Gormley, K.-L. Herpoldt, M.M. Stevens, Highly controlled open vessel RAFT polymerizations by enzyme degassing, Macromolecules, 47 (2014) 8541-8547.
[116] J. Collins, T.G. McKenzie, M.D. Nothling, S. Allison-Logan, M. Ashokkumar, G.G. Qiao, Sonochemically Initiated RAFT Polymerization in Organic Solvents, Macromolecules, 52 (2019) 185-195.
[117] T.G. McKenzie, Q. Fu, M. Uchiyama, K. Satoh, J. Xu, C. Boyer, M. Kamigaito, G.G. Qiao, Beyond Traditional RAFT: Alternative Activation of Thiocarbonylthio Compounds for Controlled Polymerization, Advanced Science, 3 (2016) 1500394.
[118] T.G. McKenzie, Q. Fu, E.H. Wong, D.E. Dunstan, G.G. Qiao, Visible light mediated controlled radical polymerization in the absence of exogenous radical sources or catalysts, Macromolecules, 48 (2015) 3864-3872.
[119] N. Micic, A. Young, J. Rosselgong, C.H. Hornung, Scale-up of the Reversible Addition-Fragmentation Chain Transfer (RAFT) Polymerization Using Continuous Flow Processing, Processes, 2 (2014) 58-70.

[120] N. Corrigan, D. Rosli, J.W.J. Jones, J. Xu, C. Boyer, Oxygen Tolerance in Living Radical Polymerization: Investigation of Mechanism and Implementation in Continuous Flow Polymerization, Macromolecules, 49 (2016) 6779-6789.
[121] D. Das, S. Srinivasan, A.M. Kelly, D.Y. Chiu, B.K. Daugherty, D.M. Ratner, P.S. Stayton, A.J. Convertine, RAFT polymerization of ciprofloxacin prodrug monomers for the controlled intracellular delivery of antibiotics, Polymer Chemistry, 7 (2016) 826-837.
[122] E.H. Song, M.J. Manganiello, Y.H. Chow, B. Ghosn, A.J. Convertine, P.S. Stayton, L.M. Schnapp, D.M. Ratner, In vivo targeting of alveolar macrophages via RAFT-based glycopolymers, Biomaterials, 33 (2012) 6889-6897.
[123] F.Y. Su, S. Srinivasan, B. Lee, J. Chen, A.J. Convertine, T.E. West, D.M. Ratner, S.J. Skerrett, P.S. Stayton, Macrophage-targeted drugamers with enzyme-cleavable linkers deliver high intracellular drug dosing and sustained drug pharmacokinetics against alveolar pulmonary infections, J Control Release, 287 (2018) 1-11.
[124] K. Song, D.C. Nguyen, T. Luu, O. Yazdani, D. Roy, P.S. Stayton, S.H. Pun, A mannosylated polymer with endosomal release properties for peptide antigen delivery, Journal of Controlled Release, 356 (2023) 232-241.
[125] S. Srinivasan, D. Roy, T.E.J. Chavas, V. Vlaskin, D.K. Ho, A. Pottenger, C.L.M. LeGuyader, M. Maktabi, P. Strauch, C. Jackson, S.M. Flaherty, H. Lin, J. Zhang, B. Pybus, Q. Li, H.E. Huber, P.A. Burke, D. Wesche, R. Rochford, P.S. Stayton, Liver-targeted polymeric prodrugs of 8-aminoquinolines for malaria radical cure, J Control Release, 331 (2021) 213-227.
[126] T.E.J. Chavas, F.Y. Su, S. Srinivasan, D. Roy, B. Lee, L. Lovelace-Macon, G.F. Rerolle, E. Limqueco, S.J. Skerrett, D.M. Ratner, T.E. West, P.S. Stayton, A macrophage-targeted platform for extending drug dosing with polymer prodrugs for pulmonary infection prophylaxis, J Control Release, 330 (2021) 284-292.
[127] M.J. Joralemon, K.S. Murthy, E.E. Remsen, M.L. Becker, K.L. Wooley, Synthesis, characterization, and bioavailability of mannosylated shell cross-linked nanoparticles, Biomacromolecules, 5 (2004) 903-913.
[128] D.H. Dube, C.R. Bertozzi, Glycans in cancer and inflammation — potential for therapeutics and diagnostics, Nature Reviews Drug Discovery, 4 (2005) 477-488.
[129] J. Chen, F.Y. Su, D. Das, S. Srinivasan, H.N. Son, B. Lee, F. Radella, 2nd, D. Whittington, T. Monroe-Jones, T.E. West, A.J. Convertine, S.J. Skerrett, P.S. Stayton, D.M. Ratner, Glycan targeted polymeric antibiotic prodrugs for alveolar macrophage infections, Biomaterials, 195 (2019) 38-50.
[130] E. Dalle Vedove, G. Costabile, O.M. Merkel, Mannose and Mannose-6-Phosphate Receptor–Targeted Drug Delivery Systems and Their Application in Cancer Therapy, Advanced Healthcare Materials, 7 (2018) 1701398.
[131] H.-X. Wang, M.-H. Xiong, Y.-C. Wang, J. Zhu, J. Wang, N-acetylgalactosamine functionalized mixed micellar nanoparticles for targeted delivery of siRNA to liver, Journal of Controlled Release, 166 (2013) 106-114.
[132] R.A. Petrov, S.R. Mefedova, E.Y. Yamansarov, S.Y. Maklakova, D.A. Grishin, E.V. Lopatukhina, O.Y. Burenina, A.V. Lopukhov, S.V. Kovalev, Y.V. Timchenko, E.E. Ondar, Y.A. Ivanenkov, S.A. Evteev, A.N. Vaneev, R.V. Timoshenko, N.L. Klyachko, A.S. Erofeev, P.V. Gorelkin, E.K. Beloglazkina, A.G. Majouga, New Small-Molecule Glycoconjugates of Docetaxel and GalNAc for Targeted Delivery to Hepatocellular Carcinoma, Molecular Pharmaceutics, 18 (2021) 461-468.

[133] F. Huang, J.A. Scoble, J. Chiefari, C.C. Williams, Preparation of Protein–Polymer Conjugates: Copolymerisation by RAFT, Australian Journal of Chemistry, 73 (2020) 1027-1033.
[134] D. Das, S. Srinivasan, F.D. Brown, F.Y. Su, A.L. Burrell, J.M. Kollman, A. Postma, D.M. Ratner, P.S. Stayton, A.J. Convertine, Radiant star nanoparticle prodrugs for the treatment of intracellular alveolar infections, Polymer Chemistry, 9 (2018) 2134-2146.
[135] H. Son, S. Srinivasan, J. Yhee, D. Das, B.K. Daugherty, G. Berguig, V. Oehle, S. Kim, K. Kim, I. Kwon, Chemotherapeutic copolymers prepared via the RAFT polymerization of prodrug monomers, Polymer Chemistry, 7 (2016) 4494-4505.
[136] H. Freeman, S. Srinivasan, D. Das, P. Stayton, A. Convertine, Fully synthetic macromolecular prodrug chemotherapeutics with EGFR targeting and controlled camptothecin release kinetics, Polymer Chemistry, 9 (2018) 5224-5233.
[137] C.L. López, K.J. Brempelis, J.F. Matthaei, K.S. Montgomery, S. Srinivasan, D. Roy, F. Huang, S.A. Kreuser, J.L. Gardell, I. Blumenthal, J. Chiefari, M.C. Jensen, C.A. Crane, P.S. Stayton, Arming Immune Cell Therapeutics with Polymeric Prodrugs, Advanced Healthcare Materials, n/a 2101944.
[138] D.K. Ho, C. LeGuyader, S. Srinivasan, D. Roy, V. Vlaskin, T.E.J. Chavas, C.L. Lopez, J.M. Snyder, A. Postma, J. Chiefari, P.S. Stayton, Fully synthetic injectable depots with high drug content and tunable pharmacokinetics for long-acting drug delivery, J Control Release, 329 (2020) 257-269.
[139] J.L. Adams, J. Smothers, R. Srinivasan, A. Hoos, Big opportunities for small molecules in immuno-oncology, Nature Reviews Drug Discovery, 14 (2015) 603-622.
[140] A. Beck, L. Goetsch, C. Dumontet, N. Corvaïa, Strategies and challenges for the next generation of antibody–drug conjugates, Nature Reviews Drug Discovery, 16 (2017) 315-337.
[141] M.K. Jayatunga, W. Xie, L. Ruder, U. Schulze, C. Meier, AI in small-molecule drug discovery: A coming wave, Nat. Rev. Drug Discov, 21 (2022) 175-176.

SUPPORTING INFORMATION

Supplemental Figures

Figure S1.1 Common synthetic moieties to A) extend SM drug circulation and improve solubility, B) control drug release, and C) improve targeting.

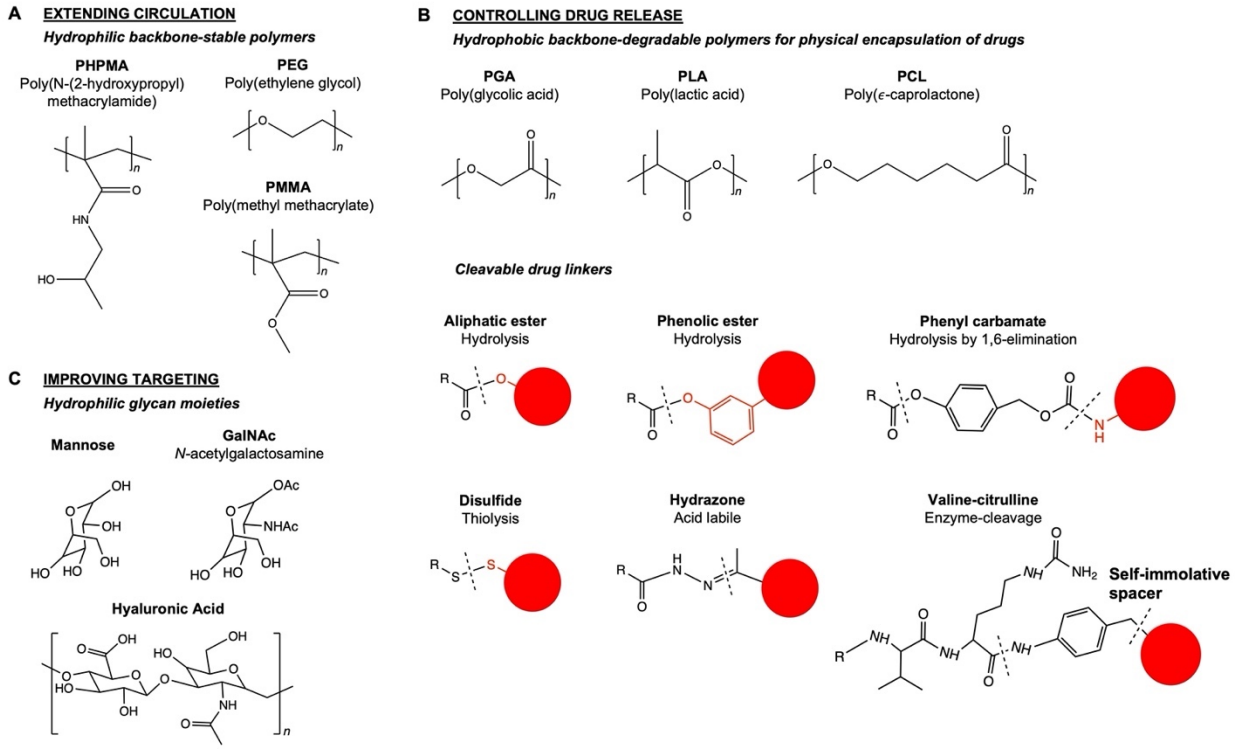

Chapter 2. AN ALVEOLAR MACROPHAGE-TARGETED DRUGAMER IMPROVES SURVIVAL AGAINST *KLEBSIELLA PNEMONIAE* PNEUMONIA[1]

Ciana L López*, Guilhem Rerolle, Sarah Snyder, Osvaldo Arias, Abdullah Bashmail, Giovany Gonzalez, Debashish Roy, Brian Lee, Jessica Snyder, Isabella Doorn, Sarah M Baker, Shelton W Wright, T Eoin West, Shawn J Skerrett, and Patrick S Stayton

[1]*Manuscript in preparation for submission*

ABSTRACT

Klebsiella pneumoniae (Kp) is a leading cause of hospital-acquired pneumonia and an emerging cause of community-acquired infections. Nanomaterials have the potential to deliver antibiotics directly to sites of infection with improved pharmacokinetics (PK) and to avoid development of antimicrobial resistance. We previously demonstrated the use of alveolar macrophage (AM)-targeted synthetic polymeric prodrugs 'drugamers' to prevent intracellular infections caused by *Francisella novicida* and *Burkholderia pseudomallei* in murine models of lower respiratory tract infections. Mannose-tagged drugamers engage with AM mannose receptors permitting uptake and triggering intracellular ciprofloxacin release. Here we show that the efficacy of the AM-targeted drugamer platform also applies to infections caused by primarily extracellular bacteria. Aerosolized ciprofloxacin drugamers significantly improved survival in a murine model of Kp pneumonia, decreased lung bacterial burden, extent of lung injury, and prevented excessive neutrophilic inflammation.

2.1 INTRODUCTION

2.1.1 Klebsiella pneumoniae incidence and background

Pneumonia is a leading cause of morbidity and mortality worldwide and is the primary cause of death by infectious agents in children under five years of age.[1] In 2019 alone, three primarily extracellular pulmonary pathogens (*Streptococcus pneumoniae*, *Staphylococcus aureus* and *Klebsiella pneumoniae* (Kp)) resulted in more than 1.5 million deaths globally.[2] Compounded by the SARS-CoV-2 pandemic, the social and economic impact of pneumonia is undeniable.[3]

Kp is a Gram-negative opportunistic pathogen and an important etiology of hospital-acquired pneumonia.[4] Its propensity for conjugative transfer of virulence factors such as multiple drug resistance (MDR) and hypervirulence has warranted its categorization by the World Health Organization as a priority 1 (critical) threat.[5] In its classical form, it commonly infects patients with comorbidities including alcohol use disorder and diabetes mellitus. In its hypervirulent form, it causes severe community-acquired syndrome in healthy individuals in the Asian Pacific Rim and increasingly worldwide.[6] Unfortunately, mortality rates are greater than 40% for resistant strains.[7]

2.1.2 Current standard of care

Treatment involves rigorous oral or intravenous (IV) antibiotics and is associated with prolonged hospitalization and high costs.[8] High systemic antibiotic dosing is necessary to overcome suboptimal lung biodistributions and poor pharmacokinetics (PK).[9, 10] For example, an oral dose of fluoroquinolone antibiotic, ciprofloxacin (cipro), has a plasma elimination half-life

($t_{1/2}$) of 4 hours. Such antibiotics are also associated with adverse side effects including neurotoxicity, ototoxicity, nephrotoxicity, and even tendon rupture.[11] Further, poor patient adherence can lead to re-emergence of antibiotic resistant strains. A stagnancy in antibiotic development in the last fifty years necessitates improved delivery of existing antibiotics to maximize antimicrobial activity and minimize the development of resistance.

2.1.3 Advancements in direct pulmonary drug delivery

Direct pulmonary drug delivery is a convenient treatment alternative to localize antibiotics to the site of bacterial persistence, avoid the liver first-pass effect, and improve patient compliance.[12] Inhalable forms of antibiotics have been approved by the U.S. Food and Drug Administration (FDA) to deliver agents effective against *Pseudomonas aeruginosa* directly to the lungs and treat infections associated with cystic fibrosis (CF). Aerosolized nanomaterial formulations, such as liposomes, have also been explored with the goal of extending antibiotic $t_{1/2}$ in the lung and increasing intracellular uptake. Arikace® is an inhalable liposomal amikacin suspension that was FDA-approved in 2018 to treat to treat Mycobacterium Avium Complex Lung Disease. Inhalable liposomal formulations of ciprofloxacin such as Lipoquin® and Pulmaquin® have received FDA orphan drug designation for treatment of bronchiectasis and CF.[13] While liposomal drug formulations have been adapted for a wide range of applications, their therapeutic impact over the standard of care parent formulation has been limited due to low drug loading, leaky drug release properties, and difficult to reproduce synthetic schemes with low shelf stability.

2.1.4 Rationale for drugamer therapeutics

Polymer prodrugs (‘drugamers’) are an attractive candidate for local, controlled antibiotic delivery.[14-16] Our group has reported that covalent incorporation of drugs using polymerizable monomers allows for 1) copolymerization with monomers that improve targeting and solubility and 2) finely tuned drug release, the combination of which optimizes drug PK and enhances therapeutic efficacy.[17-20] Inhalable cipro drugamers were able to provide total protection in lethal murine models of pulmonary tularemia and melioidosis caused by intracellular pathogens *Francisella novicida* (Fn) and *Burkholderia pseudomallei* (Bp).[21-23] Targeting of intracellular bacteria residing in alveolar macrophages (AM) was accomplished using hydrophilic mannose comonomers with high affinity for the CD206 receptor. Once drugamers were endocytosed by AMs, a protease-cleavable valine-citrulline (VC) linker facilitated intracellular release and effective clearance of AM bacterial reservoirs. The intracellular AM depot of cipro was orders of magnitude higher and sustained for the drugamer form compared to a hydrolytic-linked cipro drugamer and free cipro. Also, it was detectable for up to 7 days. Remarkably, the mannose-co-VC-cipro drugamer (referred to as ‘cipro drugamer’ moving forward) also improved the whole lung area under the concentration-time curve (AUC) of cipro by 8-fold compared to free cipro and 2-fold compared to a hydrolytic drugamer control. This is likely attributed to the membrane permeability of cipro. Importantly, a clinical Bp isolate resistant to free ciprofloxacin was effectively cleared by this drugamer formulation, indicating that its pharmacokinetic optimization improved the antibiotic potency against resistant bacteria. These findings indicate that such drugamers are also well suited for extracellular infections like Kp.

Here we propose the therapeutic use of the cipro drugamer for treatment of Kp pulmonary infections. We hypothesize that by targeting cipro release within local AM reservoirs and diffusion of lipophilic antibiotic locally, the improved whole lung cipro pharmacokinetics will extend

survival (Figure 2.1). While it is generally accepted that Kp is primarily an extracellular pathogen known to evade phagocytosis by expression of a polysaccharide capsule, there is evidence that it can also be sequestered within AMs, further validating our rationale for a macrophage-targeted approach.[24] Application of drugamers to lethal and resistant infections like Kp could provide a solution for patients with refractory illness.

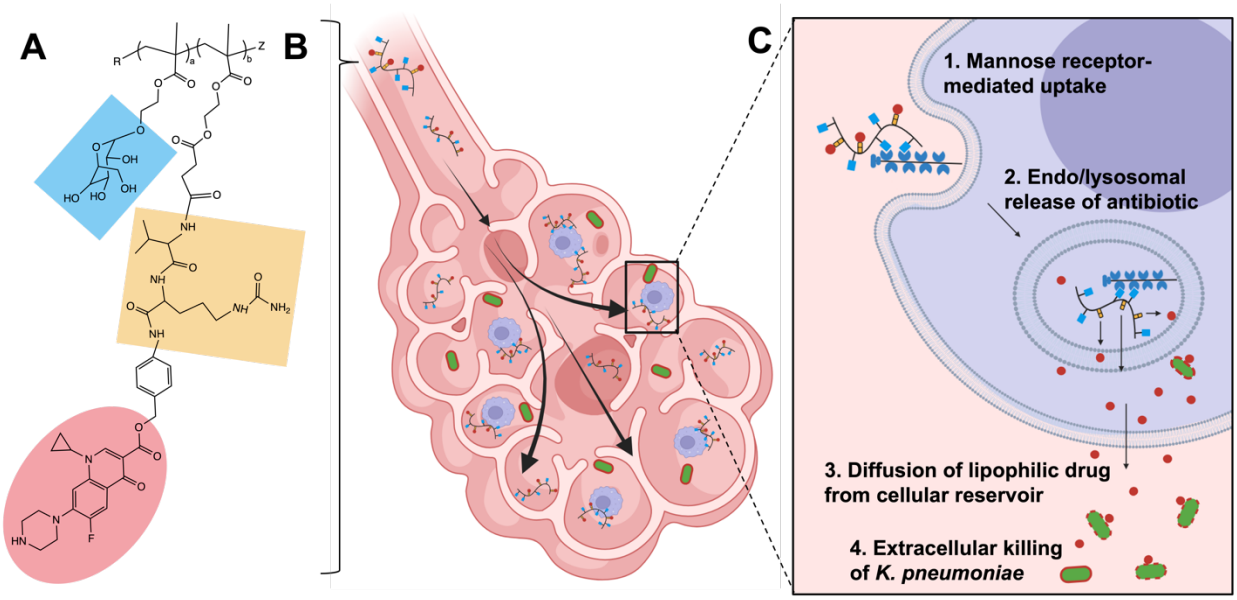

Figure 2.1 AM-targeted drugamers can be used to treat extracellular pulmonary infections like Kp. Schematic describes (A) polymeric prodrugs ('drugamers') that incorporate functional monomers that allow for targeting of AMs via mannose (blue) and intracellular protease cleavage domains (yellow) that trigger the release of antibiotic cargo (ciprofloxacin, red). (B) Drugamers can be administered directly to the lungs as an aerosol and (C) upon mannose-receptor (CD206) mediated uptake to AMs, the antibiotic is released intracellularly to form cellular drug reservoirs from which the lipophilic drug can diffuse locally to eliminate extracellular Kp infection. Alveolar macrophage (AM); *Klebsiella pneumoniae* (Kp). Image created with BioRender.com.

2.2 RESULTS AND DISCUSSION

2.2.1 Synthesis and characterization of cipro drugamer

The cipro drugamer was synthesized by reversible addition fragmentation chain-transfer (RAFT) co-polymerization of mannose-MA and VC-linked Cipro-MA as previously described.[21, 22] The purified VC-cipro polymer was characterized by ^{1}H NMR spectroscopy. The peaks corresponding to mannose and VC-cipro were observed (Figure S2.1A, Supporting Information). Monomer feed ratios are shown in Table S1. ^{1}H NMR analysis indicated 86% monomer conversion and analysis of the purified polymer with a levofloxacin standard indicated a ciprofloxacin drug weight of 9% (Figure S2.1B, Supporting Information). The number averaged molecular weight, M_n, was determined to be 24.2 kDa by size exclusion chromatography. The cipro drugamer had a narrow molecular weight distribution with dispersity, Đ = 1.1 (Figure S2.1C, Supporting Information).

2.2.2 Cipro drugamer improves survival against lethal Kp pneumonia

Preliminary experiments showed that increased frequency of aerosolized free cipro treatment (5 mg per kg dose) in a lethal Kp pneumonia murine model led to improved survival outcomes (Figure S2.2, Supporting Information), thereby indicating that a local and sustained drugamer formulation would have improved efficacy.

The therapeutic activity of the macrophage-targeted cipro drugamer was investigated in a murine model of Kp pneumonia (Figure 2.2). Mice were inoculated intratracheally (IT) with a highly lethal dose of Kp (5 – 9 x 10^3 CFU) and monitored as infection was established. 24 hours later, mice were treated with cipro drugamer (equivalent to 5 mg per kg cipro) by IT MicroSprayer® administration. Control mice received either free cipro, or phosphate buffered saline (PBS) vehicle treatment by IT MicroSprayer® administration. Survival data indicated a significant survival benefit associated with cipro drugamer treatment compared to free cipro. The

lethality of the model was evident by the PBS vehicle treatment group: no mice survived to the 14-day end point and 100% of mice (16/16) met euthanasia criteria by day 5. Most mice that received free cipro treatment also met euthanasia criteria by day 5 (56%) and only 3/16 mice survived to end of study. In comparison 75% of cipro drugamer-treated mice survived past 5 days (12/16) and 9/16 mice survived to the end of the experiment.

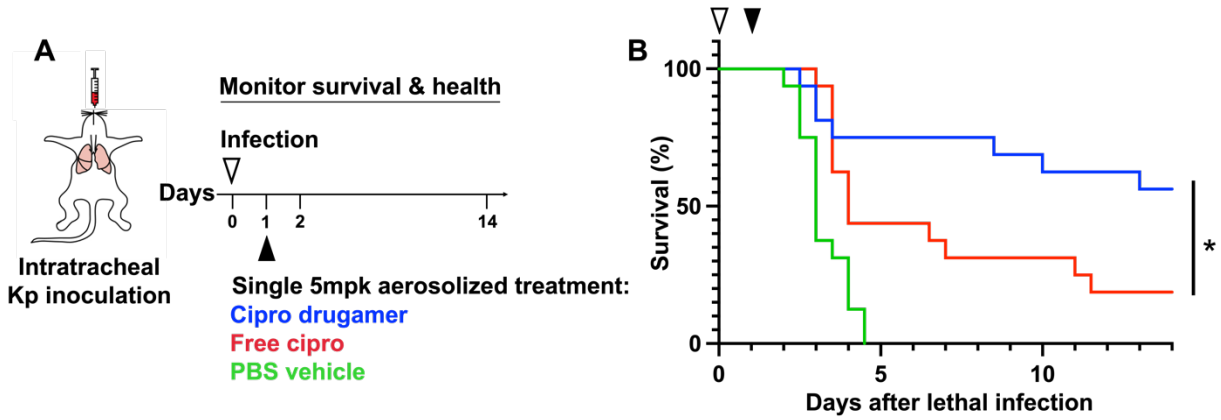

Figure 2.2 A single therapeutic dose of cipro drugamer equivalent to 5 mpk cipro significantly improves mouse survival against lethal Kp infection. (A) *In vivo* model workflow schematic. 24 hours after lethal Kp infection (5 – 9 x 10^3 CFU) free cipro, cipro drugamer, or PBS vehicle were administered (50 μL aerosolization IT) to albino C57BL/6 mice using a MicroSprayer® (n = 16 per treatment group). (B) Survival was monitored for 14 days, where * indicates a statistically significant improvement in survival using cipro drugamer compared to free cipro treatment (p-value = 0.04, as assessed by log-rank test). Ciprofloxacin (cipro); *Klebsiella pneumoniae* (Kp); intratracheally (IT); phosphate buffered saline (PBS); mg/kg (mpk). Data presented are the combination of two separate experiments with n = 8 each.

2.2.3 Cipro drugamer improves health outcomes against lethal Kp pneumonia

Morbidity parameters including body weight, ventral surface temperature, and an overall health score were measured over the course of the survival study. Weight was the most consistent indicator of morbidity and the weight of mice from all treatment groups dropped by >10% within the first 3 days, indicating that all mice developed severe infection (Figure 2.3A). By day 4, cipro

drugamer-treated mice began to regain weight, with significant improvements compared to free cipro and PBS vehicle treatment groups. Surface temperature was a less predictive, but more immanent, indicator of mortality, which can be seen by the rapid decrease for PBS vehicle-treated mice (Figure 2.3B). Free cipro treatment also led to lower surface temperatures compared to cipro drugamer. Health scores of mice were conducted based on isolation, handling, posture, coat, eyes, breathing, and activity (score out of 7, Figure 2.3C). By these measures, mice that received cipro drugamer experienced significant improvement compared to free cipro and PBS vehicle treatment, with most mice maintaining scores of 6 throughout the study. It should be noted that over the course of the experiment, the number of mice per treatment group decreased and depending on treatment, which may make morbidity differences less apparent. For clarity, a table is included with number of mice in each group surviving at each time point (Figure 2.3D).

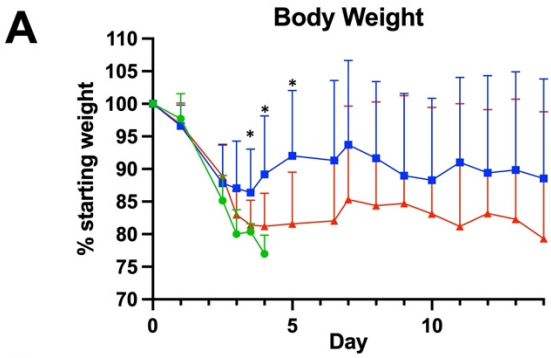

D

d	0	1	2	3	4	5	6	7	8	9	10	11	12	13	14
Cipro drugamer n	16	16	15	13	12	12	12	12	12	11	11	10	10	10	9
Free cipro n	16	16	16	15	9	7	7	5	5	5	5	4	3	3	3
PBS vehicle n	16	16	13	5	4										

Figure 2.3 Health conditions of Kp infected mice (5 – 9 x 10^3 CFU) after treatment at 24 hours with cipro drugamer (5 mpk cipro equivalent), free cipro (5 mpk), or PBS vehicle. (A) Body weight, (B) surface temperature and (C) clinical scores of mice over the course of the 14-day experiment. Clinical scores of mice based on activity, coat, breathing, posture, eyes, isolation, and resistance to handling. (D) Number of mice per group (n) by end of day (d) are indicated. Data are presented as mean and standard deviation. * = p-value <0.05, *** = p-value 0.0003 as assessed by Mann-Whitney test. *Klebsiella pneumoniae* (Kp); ciprofloxacin (cipro); phosphate buffered saline (PBS); mg/kg (mpk).

2.2.4 *Cipro drugamer decreases Kp lung bacterial burdens*

In addition to improved morbidity and mortality, bacterial burdens were compared at 72 hours post infection and after treatment at 24 hours to validate the improved antimicrobial effect of cipro drugamer (Figure 2.4A). Cipro drugamer-treated mice had a two order of magnitude decrease in lung bacterial burden (median = 2.3 x 10^4 CFU/left lung) compared to free cipro (median = 4.6 x 10^6 CFU/left lung). Cipro drugamer treatment led to a five order of magnitude improvement compared to PBS vehicle-treated mice (median = 1.1 x 10^9 CFU/left lung).

2.2.5 *Drugamer-treated mice have decreased lung injury and improved lung homeostasis*

Histopathological analysis was conducted on right lungs at 72 hours to assess the extent of lung injury associated with each treatment and compared to healthy controls (lung injury scoring criteria described in Table S2). Mice that received cipro drugamer had significantly decreased lung injury (Figure 2.4B) compared to free cipro-treated mice. This was largely attributed to decreased inflammatory cell infiltration in the bronchial lumen, as well as decreased extent of intra-alveolar and interstitial inflammation. The decreased extent of lung involvement and bacteria present was also notable. Scores for each specific criterion are shown in Figure S2.3 (Supporting Information).

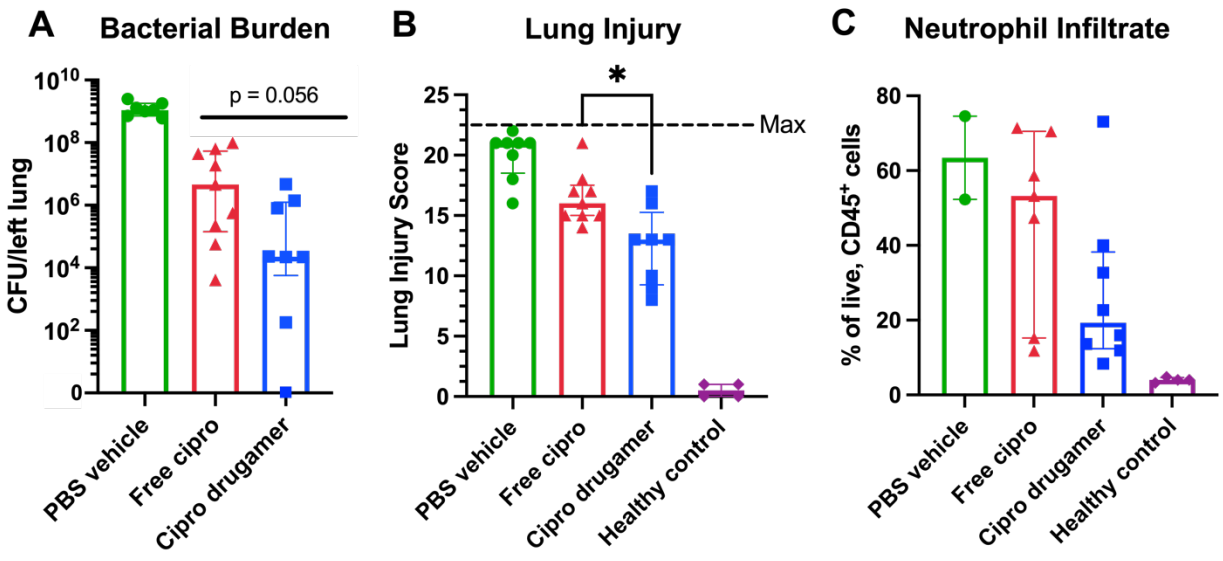

Figure 2.4 Bacterial burden, extent of lung injury, and amount of neutrophilic inflammation are decreased in mice treated with drugamer at 24 hours compared to free cipro (dose equivalence of 5 mpk) and PBS control. 72 hours after Kp infection (6 – 7 x 10^3 CFU) lung bacterial burden (A) and lung injury scores (B) were evaluated (n = 7 – 9 per treatment group). Lung injury scores were based on extent of inflammation, edema, bacteria visualized, and involvement of lung. Four days after Kp infection (650 CFU) and drugamer, free cipro, or PBS treatment (n = 2 – 6), neutrophil infiltrate populations in lung tissues (C) were compared. Data are reported as median and interquartile range. Statistical significance (*) is indicated by a *p*-value < 0.05, as assessed by Mann-Whitney test. Ciprofloxacin (cipro); mg/kg (mpk); *Klebsiella pneumoniae* (Kp); phosphate buffered saline (PBS).

Neutrophils are key players in innate host defense against Kp and are the first cell to infiltrate the lungs during infection; they phagocytose and kill Kp with antimicrobial peptides and neutrophil extracellular traps.[25] The increased inflammatory cell infiltrate noted with lung injury analysis is consistent with literature reports of both increased neutrophil recruitment during severe infection and the ability of Kp to impede efferocytic uptake and removal of apoptotic neutrophilic infiltrates by macrophages. This prevents restoration of homeostasis and instead results in necrotic and persistent inflammatory disease. Cytokine measurements at early timepoints (24, 48, and 72 hours) indicated decreased levels of tumor necrosis alpha (TNFα) and interleukin-17 (IL-17) in mice treated with both free cipro and cipro drugamer compared to PBS vehicle controls (Figure

S2.4A,B, Supporting Information). However, the possibility of diverging neutrophil activity between free cipro and cipro drugamer-treated mice was indicated by differing expression patterns of macrophage inflammatory protein-2 (MIP-2), a neutrophil chemoattractant, over time (Figure S2.4C, Supporting Information). To determine if there was decreased inflammation and improved homeostasis in cipro drugamer-treated mice at later time points following treatment, the neutrophil populations associated with each treatment were quantified at 4 days post infection and subsequent treatment and compared against healthy controls. Lungs were harvested and digested into a single cell suspension and analyzed by flow cytometry according to the gating scheme in Figure S2.5A (Supporting Information). Cipro drugamer-treated mice had decreased neutrophil infiltrate (median = 19% of live, CD45+ cells) compared to free cipro-treated mice who had neutrophil infiltrates more comparable to PBS vehicle controls (53 and 63%, respectively) (Figure 2.4C). Macrophage populations made up a smaller portion of the CD45+ cells and did not significantly differ between treatment groups (Figure S5 B). However, for individual mice with increased bacterial burden, macrophage and neutrophil populations generally trended lower and higher, respectively (Figure SC, D).

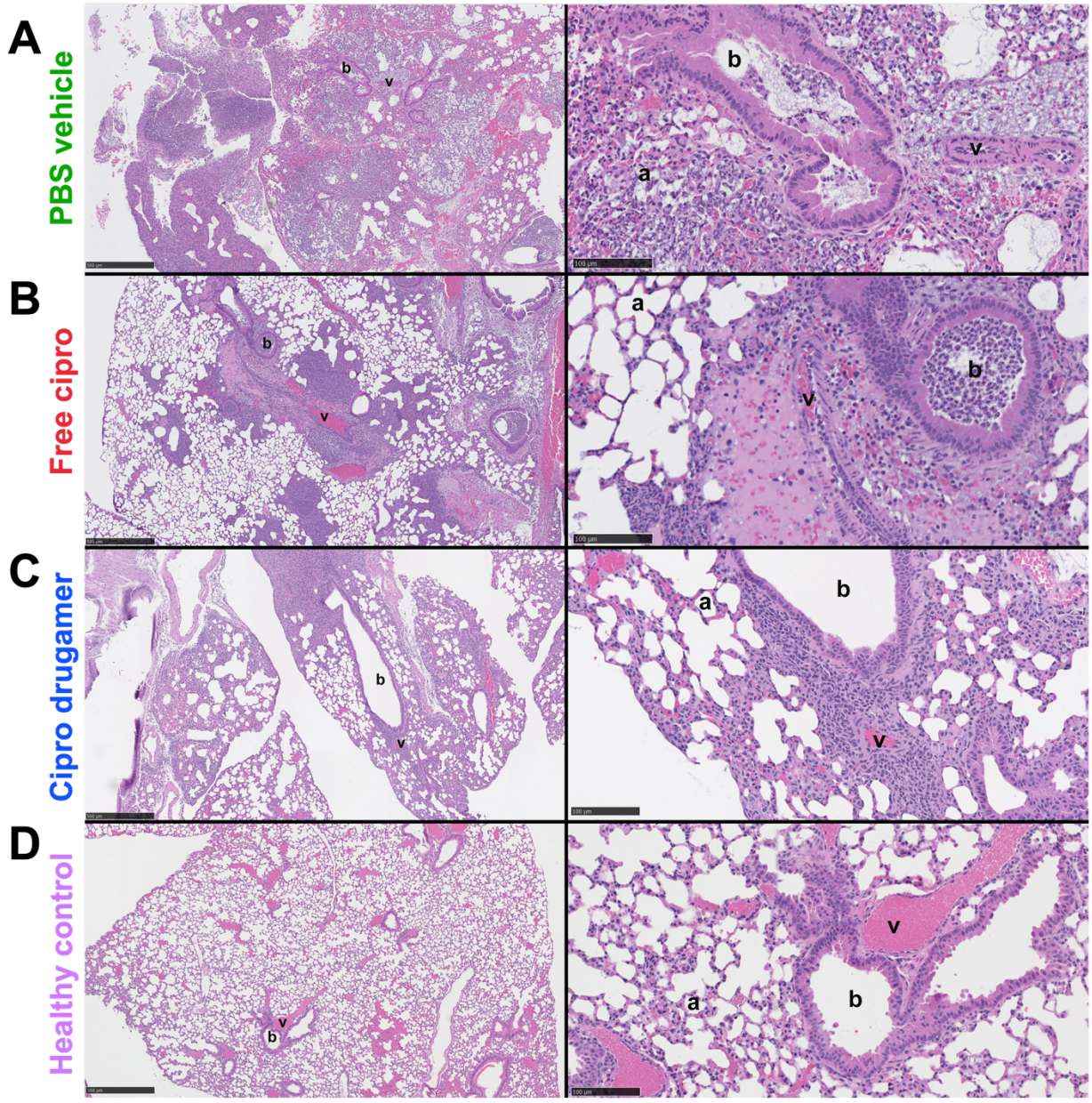

Figure 2.5 Histological images of (A) PBS vehicle, (B) free cipro, (C) cipro drugamer, or (D) healthy control mice. From left to right scale bar size = 500 μm, 100 μm. a = alveolar space, b = bronchiolar lumen, v = vessel lumen.

The capability for decreased pathogenesis with cipro drugamer treatment can be seen in histological images and compared to free cipro, PBS vehicle, and healthy controls (Figure 2.5). The cipro drugamer is designed to target the CD206 receptor on AMs, and we see improvements in the alveolar space with cipro drugamer treatment (Figure 2.5C) compared to treatment with PBS

vehicle and free cipro treatment (Figure 2.5 A and B). Abundant bacteria are visualized in the PBS vehicle-treated lung and to a lesser degree in the free cipro mice (Figure 2.5 A). A notable difference in treatment between the cipro drugamer and free cipro is also seen in the bronchiolar space (right panels of Figure 2.5 B and C) indicating that drugamer treatment prevented bronchial inflammation. While our main target was AMs, there are macrophages within the bronchus and here served as a beneficial target for antibiotic delivery.[26]

2.3 CONCLUSIONS

This study used an intratracheal MicroSprayer® to administer aerosolized drugamer treatment in our murine models of pneumonia. In a nosocomial setting, direct IT administration of drugamer might be feasible, but inhaler or nebulizer drugamer formulations should also be evaluated. This may open opportunities for effective and accessible outpatient care. Additionally, our studies showed that a single aerosolized drugamer treatment improved survival for mice with Kp pneumonia, however, it is conceivable that multiple doses would further improve survival benefits.

Overall, our study demonstrates that by incorporating the antibiotics into a targeted polymeric prodrug, we can improve treatment of primarily extracellular bacterial infections such as Kp. Cipro drugamer treatment extended survival, decreased bacterial burdens and extent of lung injury, and restored lung homeostasis. This was possible due to the improved pharmacokinetic properties of the drugamer formulation afforded by both CD206 targeting and intracellular drug cleavage with no designed mechanism for extracellular release other than the innate lipophilicity of the antibiotic.[21, 22] The use of the mannose-tagged drugamer shifts the distribution of antibiotic cargo towards resident alveolar macrophages. Our findings suggest that there is

sufficient antibiotic released from the AM to improve survival against extracellular infections. While we test our hypothesis in a Kp model, there is promise to use similar drugamer formulations against a wide range of other primarily extracellular infections that have been identified as the biggest contributors to global mortality (e.g., *Streptococcus pneumoniae*, *Staphylococcus aureus*).[2]

More effective treatments for pneumonia are urgently needed, especially with the continued emergence of antimicrobial resistance. While cipro is the small molecule drug incorporated here, the inhalable drugamer platform could provide an avenue for local delivery of other antibiotics with limited clinical utility due to high systemic toxicity (e.g., polymyxins and glycosides) despite high potency against MDR Kp infections. Further, while an antibiotic drugamer was evaluated herein, the drugamer platform allows opportunities to combine antimicrobial and host-directed drugamers (e.g., STING agonists). Drugamers may have broad applicability for lower respiratory tract infections including local drug delivery with the potential to reduce antibiotic resistance.

2.4 METHODS

RAFT synthesis of ciprofloxacin drugamer: Co-polymerization of poly(mannose-co-VC-ciprofloxacin) (referred to as cipro drugamer) was conducted from methacrylate monomers as previously described.[21, 22] Briefly, the polymerization reaction was conducted under a nitrogen atmosphere in dimethyl sulfoxide (DMSO) at 70°C using the chain transfer agent (CTA), 4-cyano-4-[(ethylsulfanylthiocarbonyl)sulfanyl]pentanoic acid (ECT), and the radical initiator 4,4′-azobis(4-cyanovaleric acid) (ABCVA). The initial monomer/CTA ratio ($[M]_0$ /$[CTA]_0$) was 40:1 and the initial CTA to initiator ratio ($[CTA]_0/[I]_0$) was 10:1. The molar ratio of mannose to VC-

Cipro-MA monomer was 85:15 (Table S1). The reaction was run for 4 hours followed by precipitation in diethyl ether and dialysis against phosphate buffer and then distilled water (6 days total; 3500 Da molecular weight cut-off). The polymer was lyophilized and passed through a PD-10 desalting column before being lyophilized into a final, purified solid product that was confirmed by ^{1}H NMR spectroscopy and size exclusion chromatography (Figure S2.2 A and C, Supporting Information). Drug weight determination by ^{1}H NMR is described in supporting information methods.

Animals and ethics statement: Female albino C57BL/6 (B6(Cg)-Tyrc-2J/J) mice, 7 – 10 weeks old, were purchased from The Jackson Laboratory and maintained at the University of Washington under specific pathogen-free conditions. All animal work was conducted in accordance with the University of Washington's Institutional Animal Care and Use Committee (Protocol #2671-06).

Bacterial growth conditions and quantification of bacterial burden: K. pneumoniae (Kp) stock 43816 was purchased from The American Type Culture Collection. Bacteria was plated on TSB agar and a single mucoid colony was isolated from which stocks were prepared in 20% glycerol in PBS and stored at -80C until use. For *in vivo* experiments an overnight culture of 0.25 mL Kp in 25 mL tryptic soy broth (TSB) was incubated in a 125 mL flask shaking at 200 rpm at 37°C with aeration and grown to stationary phase at 18 hours. Bacteria was harvested, washed three times in cold PBS (4°C) and diluted to final concentrations of 500 - 6000 CFU Kp in a 50 µL inoculation volume based on spectrophotometer measurements of the OD_{600} (OD_{600} = 0.3 was determined to be equivalent to 3.3 x 10^{8} CFU/mL). Gram stains were used to verify Kp identity. For quantification of bacterial cultures, suspensions were serially diluted and plated onto TSB

agar, incubated at 37°C for overnight after which colonies were counted. To quantify lung bacterial burdens in mice at 72 hours post infection (6 – 7 x 10^3 CFU Kp, n = 7 – 9 per treatment group), mice were euthanized, and left lungs were harvested in omnitubes containing 1 mL PBS. Lungs were homogenized using a Bead Ruptor homogenizer (Omni, Inc) for 35 seconds. Serial dilutions were plated on TSB agar in duplicate and the number of colony forming units were quantified after 16 – 18 hours incubation at 37°C. CFU/lung was calculated based on the weight of the harvested organ.

Survival Studies: Mice were inoculated intratracheally with 5 – 9 x 10^3 CFU Kp (procedure described in detail in Supporting Information). 24 hours later mice were treated with 5 mg/kg free cipro, cipro drugamer equivalent (9 wt% cipro) or PBS vehicle control (n = 16 per treatment group). Ciprofloxacin HCl (Alfa Aesar) was formulated in a 5% D-glucose (Sigma) in molecular grade water (Corning) solution. Cipro drugamer was formulated in PBS (Sigma). All treatment solutions were sterile filtered (0.22 μm, Millex C#SVG012SL, Millipore Sigma) and administered in a 50μL total volume using a MicroSprayer® aerosolizer (Model IA-1C, Penn-Century, Inc) to mice under 4% isofluorane anesthesia. Throughout the study mice were monitored 1-2 times daily based on predetermined health criteria, including temperature (ventral surface temperature > 24°C), weight (loss of ≥ 25% body weight), and a 7-point health score assessing isolation, handling, posture, coat, eyes, breathing, and activity. Upon reaching criteria in two out of three of these metrics, mice were euthanized with pentobarbital (300 mg/kg intraperitoneally), followed by exsanguination by cardiac puncture.

Histopathological analysis: Right lungs of mice were collected 72 hours after infection and submerged in 10% formalin (Sigma) at a volumetric ratio of 1:10 that was refreshed at 24 hours and replaced with 70% EtOH at 48 hours. Samples were paraffin embedded, sectioned at 4 μm, and stained with hematoxylin and eosin (H&E) by the University of Washington Histology and Imaging Core. Lung lesions were semi-quantitatively scored in a blinded fashion by a board-certified veterinary pathologist based on the degree of perivascular inflammation and edema, intrabronchiolar, intraalveolar and interstitial inflammation, extent of bacteria visualized, and extent of disease in organ. Full scoring parameters are listed in Table S2.

Analysis of neutrophil populations: Mice were inoculated with 650-750 CFU Kp and treated 24 hours later with 5 mg/kg free cipro, cipro drugamer equivalent (9 wt% cipro) or PBS vehicle control (n = 8 per treatment group). Daily health monitoring was conducted, mice were euthanized as they met criteria as described above. At the 4-day endpoint remaining mice were euthanized, the left lung was collected to determine bacterial burden. The right lung was perfused with 5mL of PBS through the right ventricle. Harvested lung tissue was minced and digested as previously described.[27, 28] Briefly, lungs were treated with 200K/mL DNase I (Roche) and 1 mg/mL liberase TM (Roche) in Roswell Park Memorial Institute (RPMI, Sigma) media at 37°C while shaking at 250 rpm for 45 minutes. Lung digest was gently mashed through a 70 μm cell strainer (Fisher) and washed with RPMI and PBS. Cells were pelleted by centrifugation, red blood cells (RBCs) were lysed (RBC lysis buffer, eBio), and remaining cells processed for flow cytometry. "Fluorescence minus one" controls were used to determine gating scheme as shown in Figure S2.3 (Supporting Information) and adapted from previous publications.[27, 28] In brief, doublets, debris, and dead cells (stained with Live/Dead Aqua BV510, Invitrogen) were excluded from

analysis and immune cells were identified using the pan-hematopoietic marker, CD45 (stained with CD45 APC-Cy7 clone 30-F11, Biolegend). Of CD45+ cells, Neutrophils were identified as Ly6G+, CD11b+ (stained with Biolegend Ly6G FITC clone 1A8 and CD11b PE-Cy7 clone M1/70). Of non-neutrophils, alveolar macrophages were identified as CD11c+ (stained with CD11c PE clone N418, Biolegend) and SiglecF+ (stained with Siglec-F PerCP eFluoro-710 clone 1RNM44N, eBioscience).

Statistical analysis: Due to the non-parametric nature of the data, unless otherwise stated, data are reported as median $\pm$ interquartile range. Significance of survival data was determined by Log-rank test. Differences between groups were determined by Kruskal-Wallis H Test. Mann-Whitney tests were used to compare individual group differences. All analyses were performed using GraphPad Prism, version 9. Investigators were not blinded to group allocation except for lung injury scoring, which was blinded. $p < 0.05$ was considered statistically significant.

2.6 ACKNOWLEDGEMENTS

This work was supported by the NIH National Institute of Allergy and Infectious Diseases Grant No. R01AI134729. C. López was supported by the NSF Graduate Research Fellowship Program Grant No. DGE-1762114.

REFERENCES

[1] G.L.R.I. Collaborators, Estimates of the global, regional, and national morbidity, mortality, and aetiologies of lower respiratory tract infections in 195 countries: a systematic analysis for the Global Burden of Disease Study 2015, The Lancet Infectious Diseases, 17 (2017) 1133-1161.
[2] G.A.R. Collaborators, Global mortality associated with 33 bacterial pathogens in 2019: a systematic analysis for the Global Burden of Disease Study 2019, The Lancet, 400 (2022) 2221-2248.
[3] C.A. Gao, N.S. Markov, T. Stoeger, A. Pawlowski, M. Kang, P. Nannapaneni, R.A. Grant, C. Pickens, J.M. Walter, J.M. Kruser, L. Rasmussen, D. Schneider, J. Starren, H.K. Donnelly, A. Donayre, Y. Luo, G.R.S. Budinger, R.G. Wunderink, A.V. Misharin, B.D. Singer, Machine learning links unresolving secondary pneumonia to mortality in patients with severe pneumonia, including COVID-19, J Clin Invest, 133 (2023).
[4] D.A. Ashurst JV, Klebsiella Pneumonia, StatPearls Publishing, 2022.
[5] W.H. Organization, Prioritization of pathogens to guide discovery, research and development of new antibiotics for drug-resistant bacterial infections, including tuberculosis, World Health Organization, Geneva, Switzerland, 2017, pp. 1-88.
[6] A. Russo Thomas, M. Marr Candace, Hypervirulent Klebsiella pneumoniae, Clinical Microbiology Reviews, 32 (2019) 10.1128/cmr.00001-00019.
[7] L. Xu, X. Sun, X. Ma, Systematic review and meta-analysis of mortality of patients infected with carbapenem-resistant Klebsiella pneumoniae, Ann Clin Microbiol Antimicrob, 16 (2017) 18.
[8] W. Huang, F. Qiao, Y. Zhang, J. Huang, Y. Deng, J. Li, Z. Zong, In-hospital Medical Costs of Infections Caused by Carbapenem-resistant Klebsiella pneumoniae, Clinical Infectious Diseases, 67 (2018) S225-S230.
[9] W. Wingender, K.H. Graefe, W. Gau, D. Förster, D. Beermann, P. Schacht, Pharmacokinetics of ciprofloxacin after oral and intravenous administration in healthy volunteers, European Journal of Clinical Microbiology, 3 (1984) 355-359.
[10] M. Brunner, O. Langer, G. Dobrozemsky, U. Müller, M. Zeitlinger, M. Mitterhauser, W. Wadsak, R. Dudczak, K. Kletter, M. Müller, [18F]Ciprofloxacin, a New Positron Emission Tomography Tracer for Noninvasive Assessment of the Tissue Distribution and Pharmacokinetics of Ciprofloxacin in Humans, Antimicrobial Agents and Chemotherapy, 48 (2004) 3850-3857.
[11] A.C. Bennett, C.L. Bennett, B.J. Witherspoon, K.B. Knopf, An evaluation of reports of ciprofloxacin, levofloxacin, and moxifloxacin-association neuropsychiatric toxicities, long-term disability, and aortic aneurysms/dissections disseminated by the Food and Drug Administration and the European Medicines Agency, Expert Opin Drug Saf, 18 (2019) 1055-1063.
[12] S. He, J. Gui, K. Xiong, M. Chen, H. Gao, Y. Fu, A roadmap to pulmonary delivery strategies for the treatment of infectious lung diseases, Journal of Nanobiotechnology, 20 (2022) 101.
[13] M. Bassetti, A. Vena, A. Russo, M. Peghin, Inhaled Liposomal Antimicrobial Delivery in Lung Infections, Drugs, 80 (2020) 1309-1318.
[14] K.E. Uhrich, S.M. Cannizzaro, R.S. Langer, K.M. Shakesheff, Polymeric Systems for Controlled Drug Release, Chemical Reviews, 99 (1999) 3181-3198.
[15] N.D. Stebbins, M.A. Ouimet, K.E. Uhrich, Antibiotic-containing polymers for localized, sustained drug delivery, Adv Drug Deliv Rev, 78 (2014) 77-87.

[16] J. Kopeček, R. Duncan, Targetable polymeric prodrugs, Journal of Controlled Release, 6 (1987) 315-327.
[17] D. Das, S. Srinivasan, A.M. Kelly, D.Y. Chiu, B.K. Daugherty, D.M. Ratner, P.S. Stayton, A.J. Convertine, RAFT polymerization of ciprofloxacin prodrug monomers for the controlled intracellular delivery of antibiotics, Polymer Chemistry, 7 (2016) 826-837.
[18] J. Chen, F.Y. Su, D. Das, S. Srinivasan, H.N. Son, B. Lee, F. Radella, 2nd, D. Whittington, T. Monroe-Jones, T.E. West, A.J. Convertine, S.J. Skerrett, P.S. Stayton, D.M. Ratner, Glycan targeted polymeric antibiotic prodrugs for alveolar macrophage infections, Biomaterials, 195 (2019) 38-50.
[19] S. Srinivasan, D. Roy, T.E.J. Chavas, V. Vlaskin, D.K. Ho, A. Pottenger, C.L.M. LeGuyader, M. Maktabi, P. Strauch, C. Jackson, S.M. Flaherty, H. Lin, J. Zhang, B. Pybus, Q. Li, H.E. Huber, P.A. Burke, D. Wesche, R. Rochford, P.S. Stayton, Liver-targeted polymeric prodrugs of 8-aminoquinolines for malaria radical cure, J Control Release, 331 (2021) 213-227.
[20] C.L. López, K.J. Brempelis, J.F. Matthaei, K.S. Montgomery, S. Srinivasan, D. Roy, F. Huang, S.A. Kreuser, J.L. Gardell, I. Blumenthal, J. Chiefari, M.C. Jensen, C.A. Crane, P.S. Stayton, Arming Immune Cell Therapeutics with Polymeric Prodrugs, Advanced Healthcare Materials, n/a 2101944.
[21] F.Y. Su, S. Srinivasan, B. Lee, J. Chen, A.J. Convertine, T.E. West, D.M. Ratner, S.J. Skerrett, P.S. Stayton, Macrophage-targeted drugamers with enzyme-cleavable linkers deliver high intracellular drug dosing and sustained drug pharmacokinetics against alveolar pulmonary infections, J Control Release, 287 (2018) 1-11.
[22] T.E.J. Chavas, F.Y. Su, S. Srinivasan, D. Roy, B. Lee, L. Lovelace-Macon, G.F. Rerolle, E. Limqueco, S.J. Skerrett, D.M. Ratner, T.E. West, P.S. Stayton, A macrophage-targeted platform for extending drug dosing with polymer prodrugs for pulmonary infection prophylaxis, J Control Release, 330 (2021) 284-292.
[23] D. Das, J. Chen, S. Srinivasan, A.M. Kelly, B. Lee, H.N. Son, F. Radella, T.E. West, D.M. Ratner, A.J. Convertine, S.J. Skerrett, P.S. Stayton, Synthetic Macromolecular Antibiotic Platform for Inhalable Therapy against Aerosolized Intracellular Alveolar Infections, Mol Pharm, 14 (2017) 1988-1997.
[24] V. Cano, C. March, J.L. Insua, N. Aguiló, E. Llobet, D. Moranta, V. Regueiro, G.P. Brennan, M.I. Millán-Lou, C. Martín, J. Garmendia, J.A. Bengoechea, Klebsiella pneumoniae survives within macrophages by avoiding delivery to lysosomes, Cell Microbiol, 17 (2015) 1537-1560.
[25] C.N. Jondle, K. Gupta, B.B. Mishra, J. Sharma, Klebsiella pneumoniae infection of murine neutrophils impairs their efferocytic clearance by modulating cell death machinery, PLOS Pathogens, 14 (2018) e1007338.
[26] C.C. Bain, A.S. MacDonald, The impact of the lung environment on macrophage development, activation and function: diversity in the face of adversity, Mucosal Immunology, 15 (2022) 223-234.
[27] A.V. Misharin, L. Morales-Nebreda, G.M. Mutlu, G.R. Budinger, H. Perlman, Flow cytometric analysis of macrophages and dendritic cell subsets in the mouse lung, Am J Respir Cell Mol Biol, 49 (2013) 503-510.
[28] M.E. Long, K.Q. Gong, W.E. Eddy, J.S. Volk, E.D. Morrell, C. Mikacenic, T.E. West, S.J. Skerrett, J. Charron, W.C. Liles, A.M. Manicone, MEK1 regulates pulmonary macrophage inflammatory responses and resolution of acute lung injury, JCI Insight, 4 (2019).

SUPPORTING INFORMATION

Supplemental Methods

Intratracheal inoculation of K. pneumoniae: Mice were anesthetized with 5% isoflurane (1 L/min O2) for 4 minutes and then positioned on an incline board, suspended by incisors. Vocal cords were visualized by laryngoscope and with an external illuminator. Mice were intubated with a 22 g catheter attached to a manometer (tuberculin syringe prepared with 100 µL of PBS) to confirm airway access. The manometer was carefully removed and replaced with a tuberculin syringe pre-loaded with 50 µL stationary-phase bacterial suspension in PBS and 150 µL air, which was slowly depressed to complete instillation. Mice were monitored for anesthesia recovery.

Cytokine measurements of left lung: Left lung homogenates were lysed in a 1:1 lysis buffer solution consisting of 15mM Tris-HCl, 1.5mM EDTA, 150mM NaCl, 1% Triton, and protease inhibitors (Complete Protease Inhibitor cocktail; Roche) on ice for 30 minutes, centrifuged at 1500 g for 15 minutes at 4°C. Supernatants were collected and stored at -80°C until analysis using the following R&D DuoSet® ELISA kits: Mouse CXCL2/MIP-2 (Catalog# DY452-05), Mouse IL-17 DuoSet ELISA Kit (Catalog# DY421-05), Mouse TNF-α (Catalog# DY410-05), and Mouse IFN-γ (Catalog# DY485-05).

^{1}H NMR determination of drug weight percentage: The ciprofloxacin drug weight percentage was analyzed by spectroscopy (Bruker AV 300) in deuterated dimethyl sulfoxide (DMSO-d6) using an internal standard, levofloxacin. Briefly, 7.2 mg drugamer was dissolved in levofloxacin solution (DMSO-d6, 1 mg/mL, 0.7 mL) and analyzed using ^{1}H NMR spectroscopy. Molar composition of

cipro drugamer was determined by comparing a single proton resonance from the internal standard at δ = 8.9 ppm against a single proton resonance from ciprofloxacin containing drugamer at δ = 8.42 ppm (Figure S2.2 B, Supporting Information).

Size exclusion chromatography (SEC): SEC was used to determine molecular weight and dispersities (Mw/Mn, Đ) of the drugamer. The purified drugamer was dissolved at 5 mg/mL in the running buffer (0.15 M sodium acetate buffered to pH 4.4 with acetic acid) for analysis by SEC. Samples were then applied to an OHpak SB-804 HQ column (Shodex) in line with a miniDAWN TREOS light scattering detector (Wyatt) and an OptiLab rEX refractive index detector (Wyatt). Absolute molecular weight average (Mn) was calculated based on dn/dc value calculated separately for the polymer using ASTRA software (Wyatt).

Supplemental Figures

Figure S2.1 Cipro drugamer synthesis. (A) Representative ^{1}H-NMR (300 MHz, dimethyl sulfonoxide-d_6 (DMSO-d6)) of synthesized polymeric ciprofloxacin prodrug with Val-Cit dipeptide linker, poly(Man-co-VC-cipro). (B) Representative ^{1}H-NMR (300 MHz, DMSO-d6) of synthesized polymeric ciprofloxacin prodrug with Val-Cit dipeptide linker, poly(Man-*co*-VC-cipro) with an internal standard, Levofloxacin, to determine the drug weight percentage. (C) Gel permeation chromatography of cipro drugamer using differential refractive index detector.

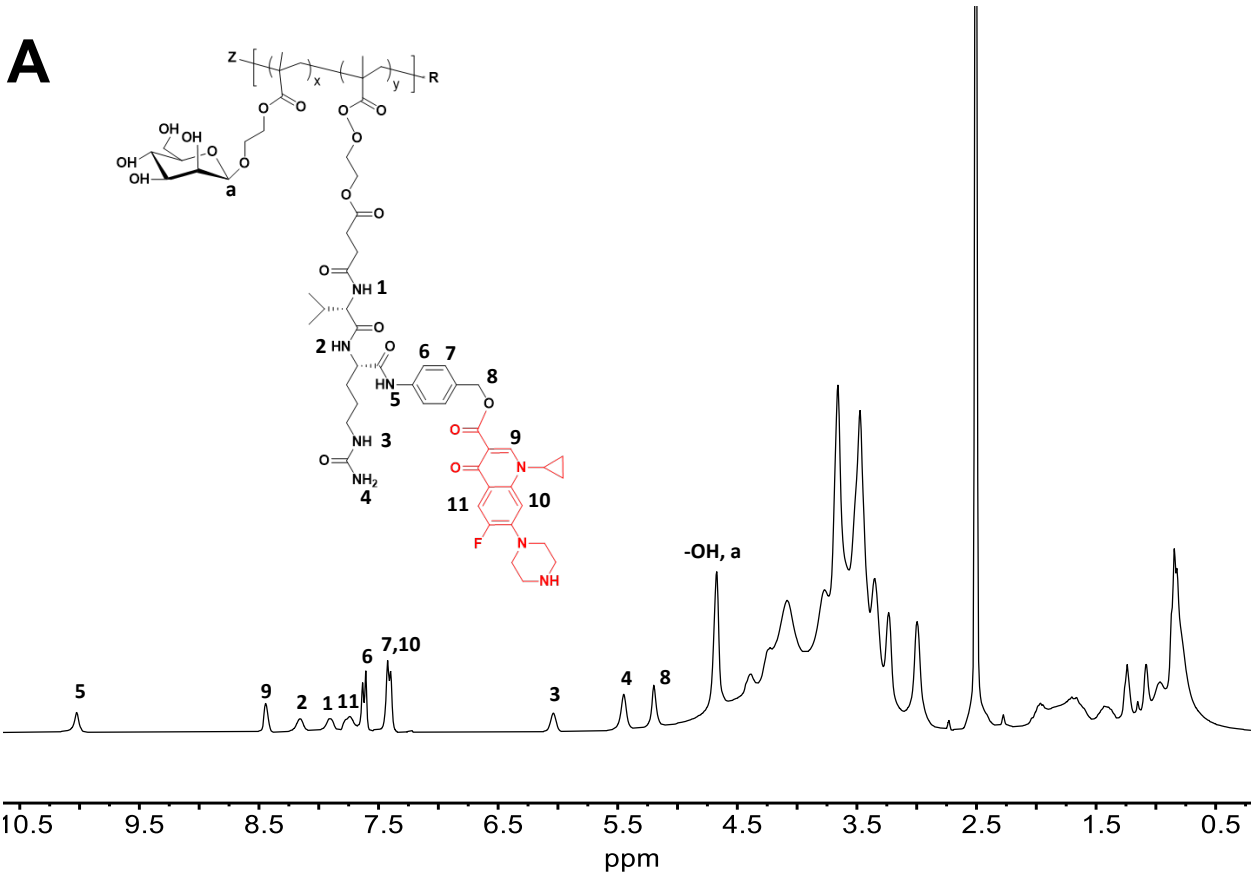

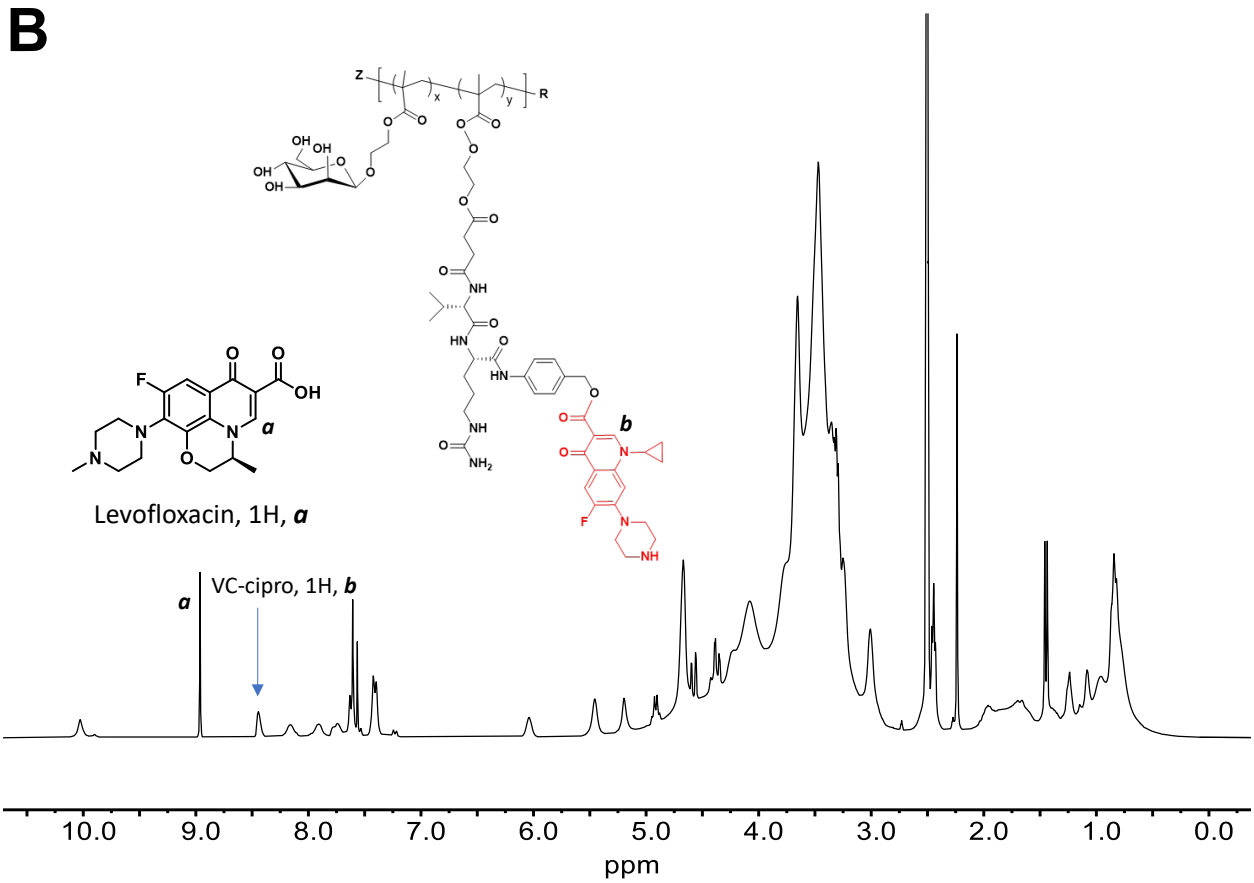
B
Levofloxacin, 1H, a
a
VC-cipro, 1H, b
b
10.0
9.0
8.0
7.0
6.0
5.0
4.0
3.0
2.0
1.0
0.0
ppm

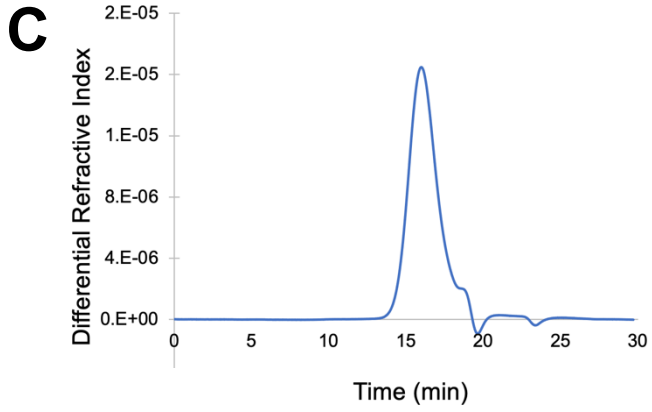
C
Differential Refractive Index
2.E-05
2.E-05
1.E-05
8.E-06
4.E-06
0.E+00
0
5
10
15
20
25
30
Time (min)

Table S2.1 Monomer feed ratios of poly(Man-co-VC-cipro), referred to as 'cipro drugamer'.

Monomer	Molecular weight (Da)	# of units/chain	Mol %	Weight %
Mannose-MA *(solubility, targeting)*	292	29	85	65
Valine-Citrulline (VC)-linked Cipro-MA *(intracellular release, antibiotic)*	905	5	15	35

Figure S2.2 Repeated treatment with free ciprofloxacin improves survival against lethal Kp infection. A) In vivo model workflow schematic. Free ciprofloxacin (5mpk) or D5W were intratracheally administered (50 μL aerosolization) to albino C57BL/6 mice at 2, 24, and 48 hours after intratracheal infection (6 x 103 CFU Kp) using a MicroSprayer® (n = 5 per treatment group). Survival (B) was monitored for 14 days. Klebsiella pneumoniae (Kp); 5% dextrose in water (D5W); mg/kg (mpk).

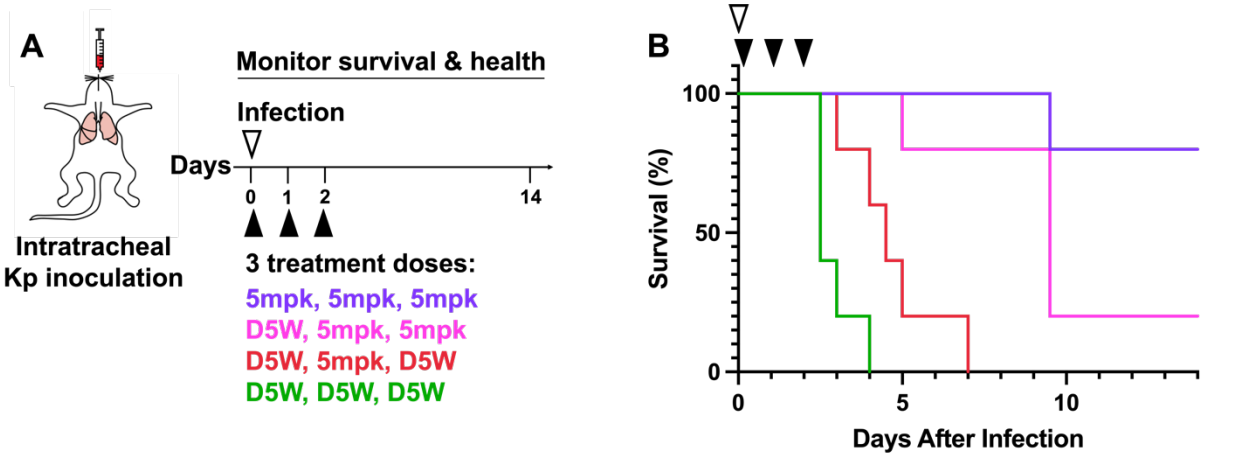

Table S2.2 Lung injury scoring criteria.

1. Extent involvement of lung*	**Scale from 0 - 4 based on estimated percentage (%)**
0	none
1	less than 5
2	5 to 20
3	21 to 40
4	greater than 40
2. Perivascular inflammation and edema	**Scale from 0 - 4**
0	normal
1	few inflammatory cells expanding the perivascular space
2	larger foci of inflammatory cells, with preservation of underlying architecture; <25% of vessels may have mild perivascular edema/hemorrhage (or moderate if only 1-2 vessels)
3	larger foci of inflammatory cells with changes of underlying vessel / alveolar wall; more severe perivascular edema / hemorrhage
4	larger foci of inflammatory cells with disruption or loss of underlying architecture including necrosis and/or hemorrhage; severe perivascular edema/hemorrhage
3. Intrabronchiolar inflammation	**Scale from 0 - 4 based on percentage of airway involved with infiltrate (%)**
0	none
1	less than 5
2	5 to 25
3	26 to 50
4	greater than 50
4. Alveolar inflammation*	**Scale from 1 - 4 based on estimated percentage (%)**
1	few inflammatory cells within alveoli - <5%
2	larger foci of inflammatory cells (<25% lung total), with preservation of underlying architecture
3	larger foci of inflammatory cells (<50% lung total) with changes of underlying alveolar wall; more severe hemorrhage (<25% affected by necrosis/hemorrhage)
4	larger foci of inflammatory cells with disruption or loss of underlying architecture including severe necrosis and/or hemorrhage (>25% lung affected by necrosis/hemorrhage)
5. Interstitial inflammation*	**Scale from 1 - 4 based on estimated percentage (%)**
1	few inflammatory cells within interstitium - <5%
2	larger foci of inflammatory cells (<25% lung total), with preservation of underlying architecture
3	larger foci of inflammatory cells (<50% lung total) with changes of underlying architecture; more severe hemorrhage (<25% affected by necrosis/hemorrhage)
4	larger foci of inflammatory cells with disruption or loss of underlying architecture including severe necrosis and/or hemorrhage (>25% lung affected by necrosis/hemorrhage)
6. Extent of bacteria visualized	**Scale from 0 - 2**
0	not seen
1	mild to moderate
2	moderate to severe

*Lungs were not inflated which can complicate measurement of extent and interstitial involvement in some cases

Figure S2.3 Lung injury scoring breakdown. Analysis of histological samples from mice 72 hours after lethal infection (6 – 7 x 10^3 CFU Kp) and treatment at +24 hours with cipro drugamer, free cipro, or PBS vehicle and compared to healthy control.

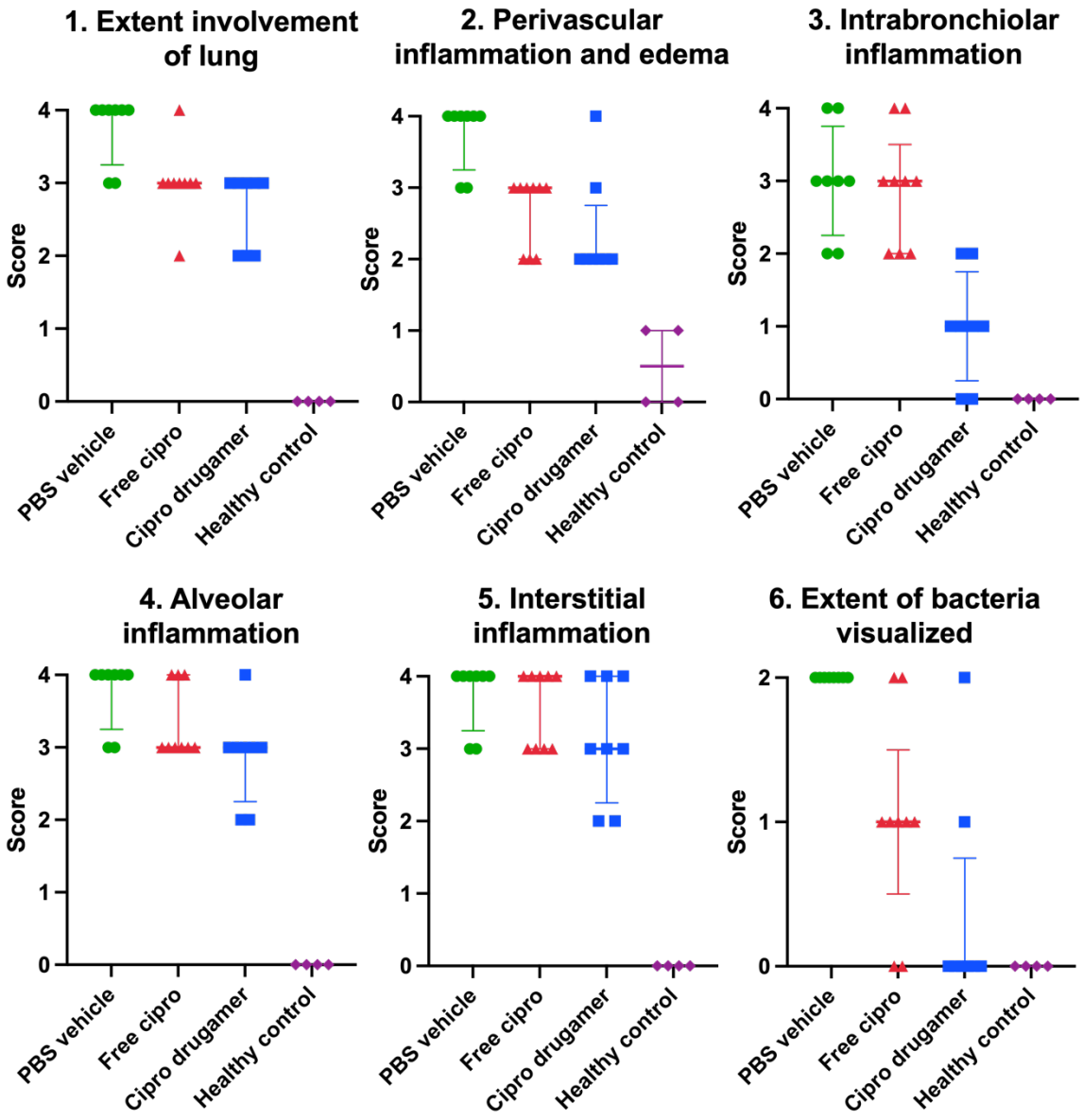

Figure S2.4 Whole lung cytokine analysis. (A) TNFα, (B) IL-17, and (C) MIP-2 were measured at 24, 48, and 72 hours after intratracheal infection of albino C57BL/6 with 6500 CFU Kp and microsprayer treatment at 24 hours with 5 mpk cipro from free drug or drugamer and compared to PBS vehicle control. Data presented as median and interquartile range (n = 3 – 4). IFNγ were also measured but were below the detection limit of the assay (31.2 pg/mL). Macrophage inflammatory protein-2 (MIP-2); tumor necrosis factor α (TNFα); interleukin-17 (IL-17); colony forming units (CFU); *Klebsiella pneumoniae* (Kp); ciprofloxacin (cipro); mg/kg (mpk); Phosphate buffered saline (PBS); Interferon gamma (IFNγ)

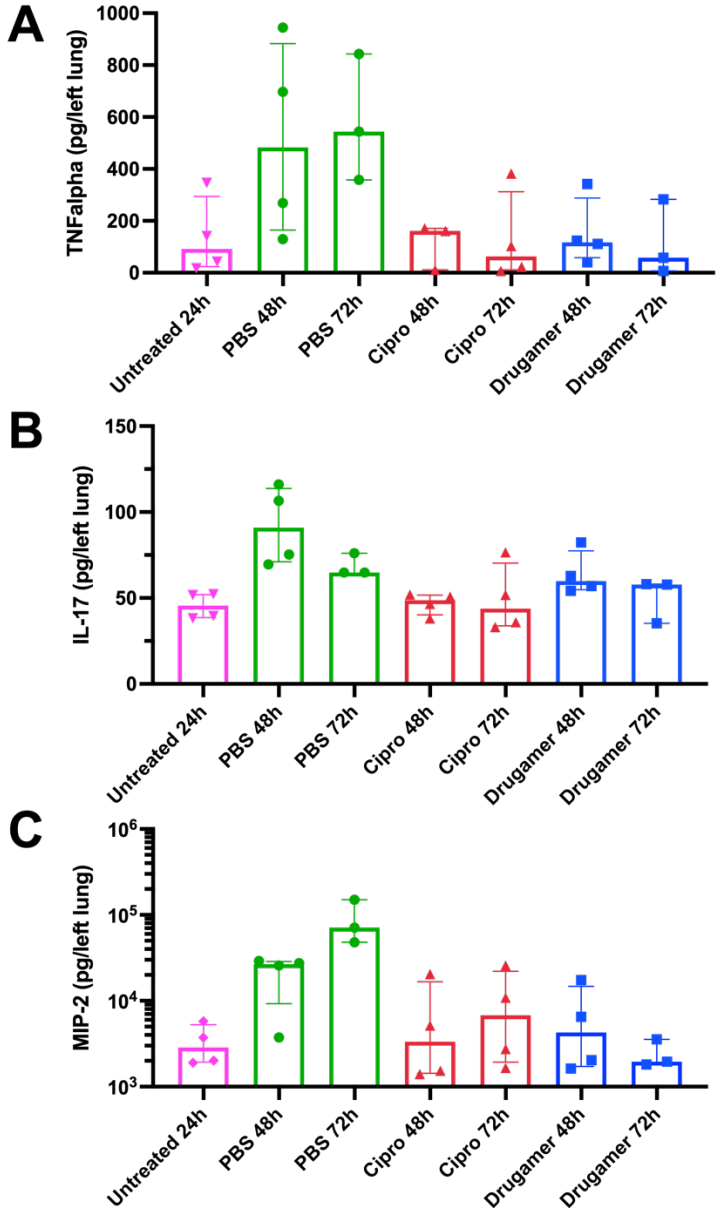

Figure S2.5 (A) Gating scheme for flow cytometry analysis of right lungs harvested from Kp-infected mice at four days post infection (650 CFU IT) and after treatment at 24 hours with 5 mpk cipro from drugamer, free cipro, or PBS vehicle. (B) Alveolar macrophages… (C) Bacterial burden was quantified in the left lung. (D) Multivariable analysis comparing for individual mice left lung bacterial burdens (x-axis), % neutrophils (y-axis; % of CD45+ cells), and % alveolar macrophages (size of symbol, % of CD45+, non-neutrophils). *Klebsiella pneumoniae* (Kp); intratracheally (IT); mg/kg (mpk); ciprofloxacin (cipro); phosphate buffered saline (PBS).

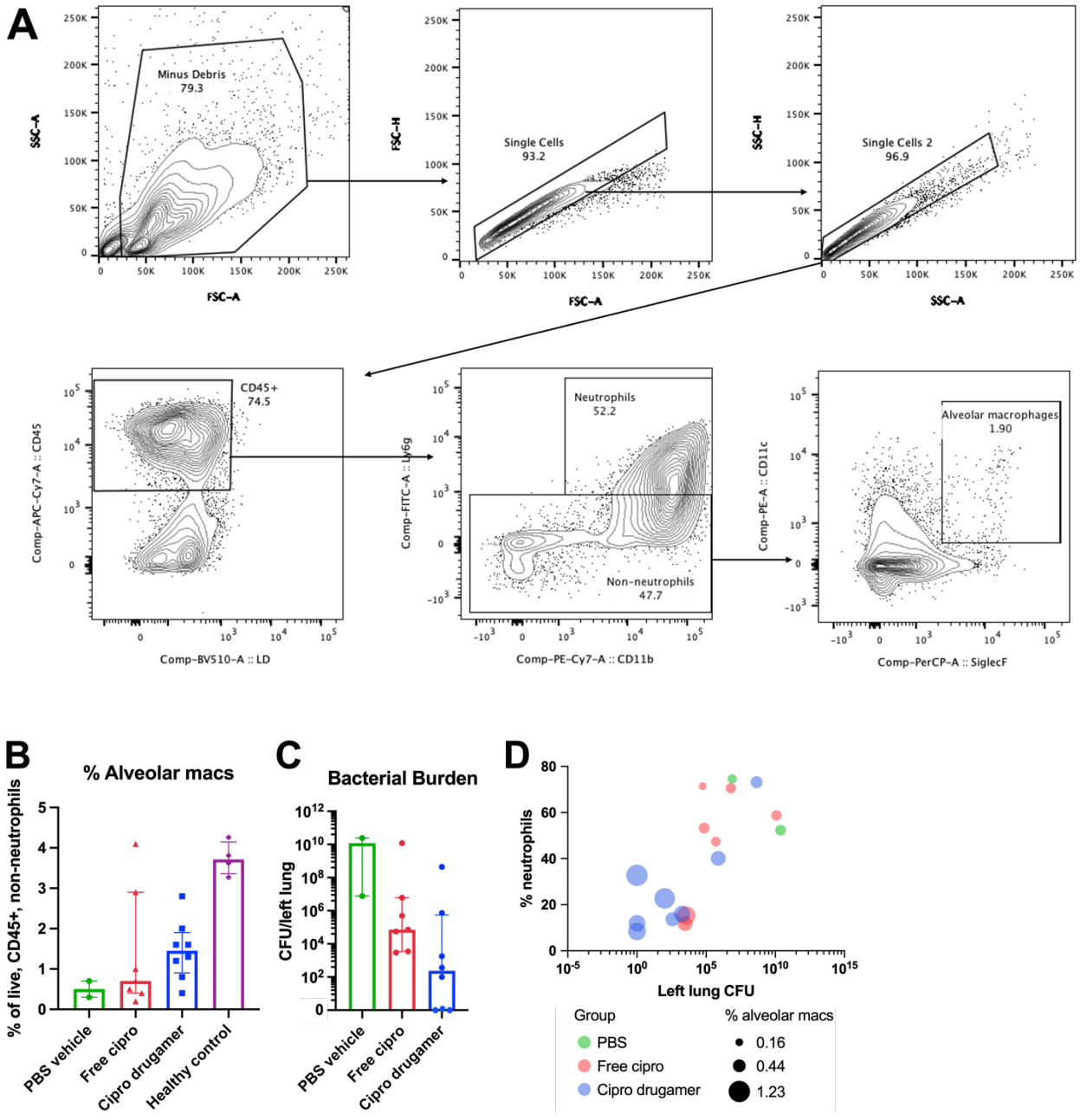

Chapter 3. DRUGAMER-LOADED PROTEIN VACCINES[1]

Karla-Luise Herpoldt*, **Ciana L López**, Isaac Sappington, Minh N. Pham, Selvi Srinivasan, Jason Netland, Katherine S. Montgomery, Debashish Roy, Alexander N. Prossnitz, Daniel Ellis, Adam J. Wargacki, Marion Pepper, Anthony J. Convertine, Patrick S. Stayton, and Neil P. King

ABSTRACT

Virus-like particles are a promising class of materials for vaccine development. They can protect cargo molecules from degradation, penetrate cells, and possess inherent immunogenicity. Cargo packaging is an important area of development because many VLP loading strategies involve passive diffusion of small cargos through the pores of the VLP. This limits the types of cargos utilized in such vaccine designs. Computational design can be used to optimize the biophysical properties of VLPs to facilitate cargo delivery, including antigens and adjuvants. Excitingly, Herpoldt et al designed a two-component protein nanoparticle, I53-50-V5 ("V5"), that could be mixed *in vitro* with a single-stranded RNA (200 - 2500 nucleotides) to achieve effective encapsulated and protection from degradation. Here we show that adjuvant-containing radiant star polymers can be encapsulated in V5 as a modular and atomically defined vaccine and small molecule drug delivery system. The polymer is synthesized by RAFT polymerization from a hydrophilic hyperbranched core allowing for compact incorporation of monomers with anionic charge and monomeric prodrugs containing the small molecule TLR7/8 agonist resiquimod. The

anionic polymer associates with positively charged inner luminal surface of V5 to achieve efficient encapsulation from which resiquimod is released in a sustained manner by hydrolysis. Co-delivery of adjuvant within the V5 resulted in efficient vaccination in mice and reduced toxicity compared to controls.

3.1 INTRODUCTION

The recent COVID-19 pandemic has galvanized the rapid development of new and effective vaccines.[2, 3] Advances in biomaterials manufacturing have enabled molecular precision in the design and synthesis of vaccine components dictated by computational biology, protein engineering, structure-based antigen design, and genetic engineering. Such progress has unlocked new avenues to investigate how our immune system works and how we can leverage it for protection against pathogens.

A functional vaccine primes the host immune system to induce an appropriate response and prevent or reduce the severity of disease upon future exposure. Historically, whole attenuated or inactivated pathogens have been incorporated into vaccines to prime an appropriate response.[4] However, the potential danger of incomplete inactivation or attenuation as well as the requirement of specialized facilities for mass production precludes their wide adoption.[5] Instead, recombinant subunit vaccines have been developed from highly purified antigens with increased safety. The subunits are purified proteins or peptide antigens themselves or are generated in situ via delivered encoding mRNA cargo. However, because subunit vaccines lack the exogenous immune activating components, including the additional nucleic, lipid, and cell membrane components associated with live and attenuated vaccines, they can suffer from poor immunogenicity and adjuvants are incorporated to improve their potency.[6, 7]

Virus-like particles (VLPs) are self-assembling proteins that mimic the structure of viral capsids but are noninfectious due to their lack viral genomes. They are am emerging class of vaccine therapeutics because (1) their size (typically 20-200 nm) allows for effective trafficking to draining lymph nodes, (2) their inherent immunogenicity and repetitive structure allows for efficient dendritic cell and B cell uptake for B cell activation and (3) they are designed to protect cargos (e.g., mRNA) from degradation before efficient delivery to a target cell.[3, 8, 9] Further, VLPs are amendable to multivalent surface functionalization for display of targeting moieties or antigens.[10-13] Their positively charged luminal surface and relatively large interior volume allows for electrostatic packaging with guest molecules such as quantum dots, proteins, nucleic acids, and synthetic polymers.[14-25]

Custom-designed self-assembling protein nanoparticles inspired by VLPs and other naturally occurring protein nanoparticles have been computationally designed as a clinically relevant platform with enhanced stability in biological circulation, functionality, and modularity with atomic-level accuracy.[13, 26-33] In a recent advancement, Herpoldt et al designed a two-component icosahedral protein nanoparticle, I53-50-V5 ("V5"), able to be synthesized from two distinct types of independently purified protein building blocks allowing for *in vitro* assembly and packaging of single-stranded RNA molecules ranging from 200 – 2500 nucleotides.[1] Compared to previous one-component ("homomeric") versions that relied on passive cargo loading and release through capsid pores associated with poor control, the two-component design allows for encapsulation of larger and diverse molecular cargos.

We hypothesized that by the same electrostatic mechanism used to load RNA, synthetic cargos such as radiant star polymeric prodrugs ("drugamers") could be packaged in V5 to effectively co-deliver small molecule drugs, such as vaccine adjuvants to improve their co-

localization with antigen and prevent systemic toxicity.[34] This recently described class of polymer nanostructures are composed of linear chains grown from a hyperbranched, hydrophilic core using reversible addition-fragmentation chain transfer (RAFT) polymerization (Figure 3.1). We reasoned that the compact, well-defined three-dimensional architectures of radiant star drugamers would enable more efficient packaging than linear polymers that would require compaction during packaging.[34] Here we present a radiant star polymer prodrug that incorporates the Toll Like Receptor (TLR) 7/8 agonist, resiquimod, that can be packaged within V5 allowing for co-formulation of adjuvant and antigen to achieve potent vaccination.

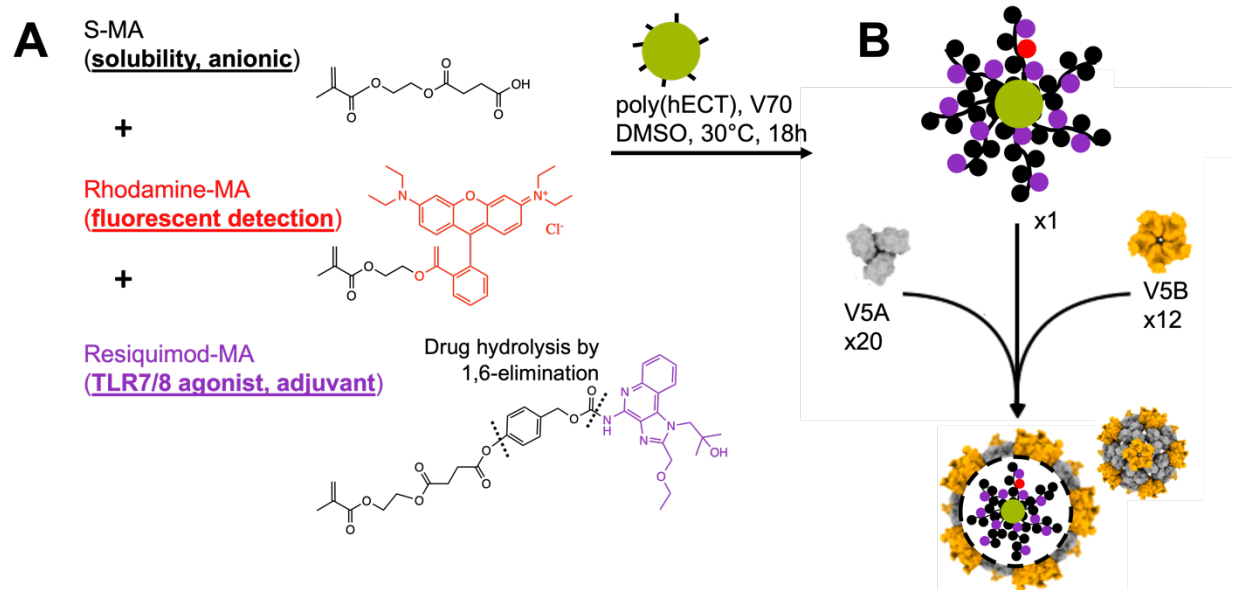

Figure 3.1 Controlled encapsulation of radiant star drugamers by *in vitro* assembly of into two-component icosahedral protein nanoparticles. (A) Radiant start polymer prodrugs are synthesized by RAFT polymerization of anionic mono-2-(methacryloyloxy)ethyl succinate (SMA), rhodamine methacrylate, and resiquimod methacrylate from a hyperbranched poly(hECT) core. (B) The anionic linear arms of the radiant star drugamer allow for electrostatic encapsulation within the positively charged luminal surface of the self-assembling protein nanoparticle composed of V5A (20 units/particles) and V5B (12 units/particle).

3.2 RESULTS AND DISCUSSION

3.2.1 Encapsulation of radiant star polymers

To enable the electrostatic encapsulation approach similar to that used for nucleic acids, the radiant star polymers incorporate an anionic monomer, mono-2-(methacryloyloxy)ethyl succinate (SMA), for the radiant arms. Each monomeric SMA subunit carried a single negative charge (Figure 3.1A). Prior to synthesis of radiant star drugamers, radiant star polymers lacking drug (denoted as RSPs) of SMA were synthesized with a range of hydrodynamic radii to determine the size range of polymers that could be encapsulated. The length of the linear chains from the hyperbranched core (and therefore the hydrodynamic radius of the polymer nanoparticle) was controlled by altering the degree of polymerization (DP) via the ratio of monomer to chain transfer agent (CTA) in the RAFT reaction. We targeted four different degrees of polymerization (DP25, DP50, DP100, and DP200) to study the ability of V5 to encapsulate synthetic polymers of varying size. A small amount of rhodamine B methacrylate (RhMA) was co-polymerized into the linear arms to enable detection of the polymers. After purification, molecular weights and hydrodynamic radii were established through aqueous gel permeation chromatography (multiple-angle light scattering coupled with size exclusion chromatography, SEC-MALS) and dynamic light scattering (DLS; Figure S3.1, Supporting Information) and indicated the RSPs ranged from 225 kDa (Rh = 10.1 nm) to 1.7 MDa (Rh = 33.9 nm).

Following the conditions previously established for nucleic acid packaging by Herpoldt et al., the four RSPs were each encapsulated at a 1:1 nanoparticle:RSP ratio.[1] Each RSP was resuspended in buffer and mixed with the V5A trimer followed by the V5B pentamer to allow assembly to proceed for an hour at 37°C. We took advantage of the rhodamine incorporated into the RSPs and their polyanionic nature deriving from the negatively charged SMA monomer to visualize encapsulation by electrophoretic mobility shift assay (EMSA; Figure 3.2A). In the

absence of V5, the RSPs migrated rapidly through agarose gels, with the smaller polymers migrating furthest. All four encapsulation reactions yielded significantly shifted fluorescent RSP bands that were also stained by Coomassie, indicating co-migration of V5 and each RSP. The reactions for the two smallest RSPs, DP25 and DP50, both yielded single sharp bands, suggesting formation of a monodisperse species. By contrast, multiple smeared bands were observed after encapsulation of the larger RSPs, DP100 and DP200, suggesting inefficient encapsulation and the formation of multiple distinct species.

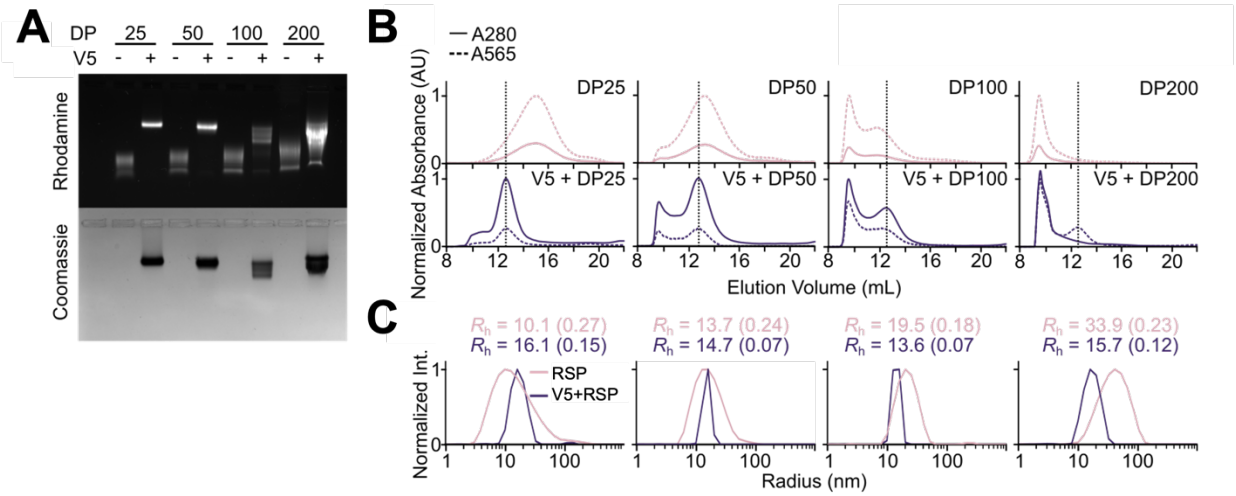

Figure 3.2 Encapsulation of synthetic polymers inside a designed protein nanoparticle. (A) Native agarose gel electrophoresis of increasing sizes of RSP present upon encapsulation. (B) SEC trace of RSP alone (top) and RSP encapsulated within V5 (bottom). Small polymers, once encapsulated, eluted at the same elution volume as empty V5 (dotted vertical line). (C) DLS size and polydispersity measurements of RSP alone or encapsulated within V5.

We further characterized RSP encapsulation by SEC, DLS, and negative stain electron microscopy (nsEM). The water-soluble nature of RSPs and their similar size to assembled V5 enabled side by side comparison of free RSPs and encapsulation reactions by SEC. Chromatograms of free RSPs or encapsulation reactions were collected at 565 nm and 280 nm to track the rhodamine in the RSP and the protein nanoparticle, respectively (Figure 3.2B). While the

two smallest RSPs are well resolved by SEC, a significant amount of DP100 and nearly all of DP200 elute at the void volume, consistent with their large size. When encapsulated within V5, the 565 nm peaks of both DP25 and DP50 shift to precisely match the elution of monodisperse V5 nanoparticles around 13 mL. Although a small amount of the DP25 encapsulation reaction, and slightly more of that of DP50, eluted at the void volume, no residual signal at 565 nm was observed at the unencapsulated elution volume, indicating that all polymer is efficiently encapsulated. Consistent with the EMSA, SEC suggested inefficient encapsulation of the two larger RSPs within V5. Although a small rhodamine peak co-eluted with V5 in the case of DP100, the majority of the RSP in both encapsulation reactions eluted at the void volume. Interestingly, most of the protein also eluted at the void volume, suggesting that the larger polymers caused protein aggregation. DLS of SEC fractions corresponding to the elution peak near 13 mL indicated that monodisperse V5 nanoparticles could be obtained after packaging each RSP, although in lower yield for the larger polymers (Figure 3.2 C). DLS of the free RSPs exhibited relatively broad size distributions that increased with the degree of polymerization as expected. Analysis of the smallest (DP25) and largest (DP200) encapsulations by nsEM confirmed the biophysical characterization. In vitro encapsulation of DP25 resulted in monodisperse particles, with 2D class averages closely resembling those seen for empty V5 (Figure 3.3 and Figure S3.2, Supporting Information). Meanwhile, we observed large aggregates and a substantial amount of unassembled protein in encapsulation reactions using DP200, consistent with the SEC and DLS data indicating that this polymer is too large to fit in the V5 lumen.

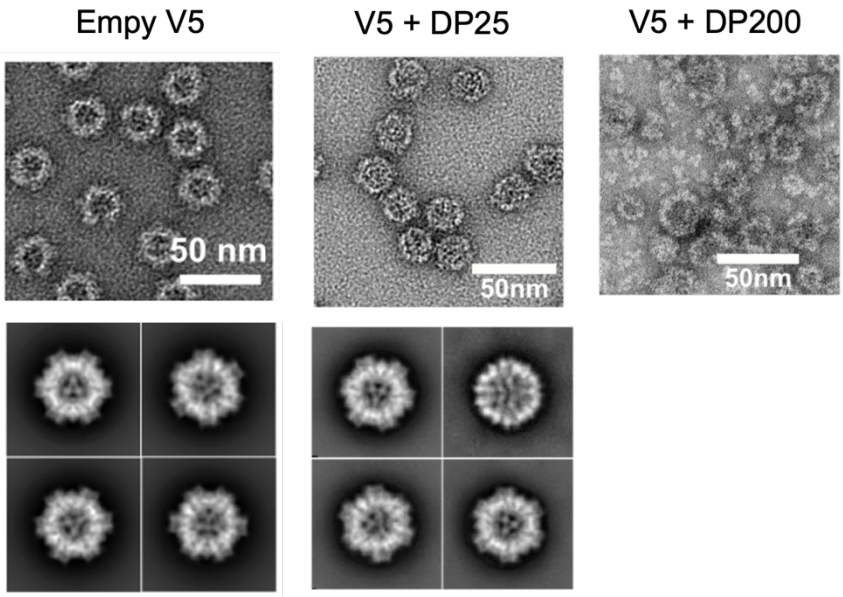

Figure 3.3 Representative negatively stained electron micrographs of V5 particles. Empty V5, and V5 encapsulated with radiant star polymer DP25 and DP200. Bottom panels of class averages for relevant groups. The data shown are from representative experiments that were performed at least twice.

3.2.2 Synthesis of a resiquimod pro-drug monomer and resiquimod-loaded RSP

Resiquimod is an antiviral imidazoquinoline that has been shown to activate the innate immune system via TLR 7 and 8.[35] While it has been approved for use in certain topical indications, it is underutilized as a vaccine adjuvant due to systemic toxicity and poor tolerability in humans.[36] Like other small molecules, it is prone to diffuse away from the injection site, and there has been substantial interest in new formulation and delivery methods for resiquimod and other imidazoquinolines.[37-41] Previous studies have suggested that an encapsulation approach to formulation could improve safety and tolerability by directly co-delivering adjuvant with antigen to antigen-presenting cells while also potentially lowering the amount required for activity.[41, 42] We incorporated resiquimod into an RSP to enable straightforward in vitro encapsulation inside V5 and subsequent release in vivo. Building polymeric pro-drug architectures using polymerizable drug monomers provides a viable approach for incorporating multiple

components such as drugs, targeting moieties, and labeling agents simultaneously without any laborious post-synthetic procedures.[34, 43-45] Additionally, by adjusting the molar ratio of the monomers, the loading of each component can be precisely controlled with a well-defined statistical distribution that allows for maintenance of the polymers negative surface charge to facilitate encapsulation within two-component protein nanoparticles.

We designed a methacrylate-based prodrug monomer carrying a para-hydroxybenzyloxycarbonyl (PHBC) spacer between the polymerizable monomer (SMA) and the resiquimod (Figure 3.1A) that can be directly polymerized by RAFT polymerization. The PHBC spacer is well known for its self-immolative nature; once the phenolic ester bond is hydrolyzed, the resulting phenolate quickly self-eliminates and triggers the spontaneous release of the intact drug.[46, 47] The monomer synthesis starting from SMA is outlined in Figure S3.3 in the Supporting Information. The successful synthesis of resiquimod methacrylate (ResMA) monomer was confirmed by ^{1}H NMR spectroscopy (Figure S3.4, Supporting Information) and ESI-MS signal at m/z value of 677.4 $[M+H]^{+}$.

Having identified an RSP size range that allows efficient encapsulation within V5, a radiant star drugamer that incorporated the resiquimod pro-drug monomer was then synthesized. The smallest RSP size (DP25) was targeted to ensure efficient encapsulation. Following co-polymerization of ResMA, RhMA, and SMA to the poly-4-Cyano-4-((ethylsulfanylthiocarbonyl)sulfanyl)pentanoic acid hydroxyethyl methacrylate (pECT HEMA) core using [2,2′-Azobis(4-methoxy-2,4-dimethylvaleronitrile)] (V70) initiator, the purified polymerized resiquimod (pResi) yielded a 96% monomer conversion and a resiquimod drug weight percent of 9.74% (Figure S3.5, Table S3.1, Supporting Information). Characterization of pResi by SEC-MALS and DLS (Figure S3.1, Supporting Information) indicated a hydrodynamic

radius of 9.8 nm and a total molecular weight of 376 kDa, matching the size of the RSP observed to efficiently encapsulate above.

3.2.3 *Encapsulation and release of pResi in vitro*

pResi was encapsulated within V5 using the same stoichiometric mixing and assembly approach described above for the RSPs. Encapsulation was confirmed by SEC, which showed a clear shift in elution volume of pResi (monitored by rhodamine absorbance at 565 nm) from 16 mL to the expected V5 elution volume of 13 mL (Figure 3.4A). Very little residual unencapsulated polymer was observed, indicating efficient encapsulation by in vitro assembly. Assuming a single polymer was encapsulated per nanoparticle and the molecular weights and drug loading above, we estimate approximately 100 molecules of resiquimod were packaged per V5 nanoparticle.

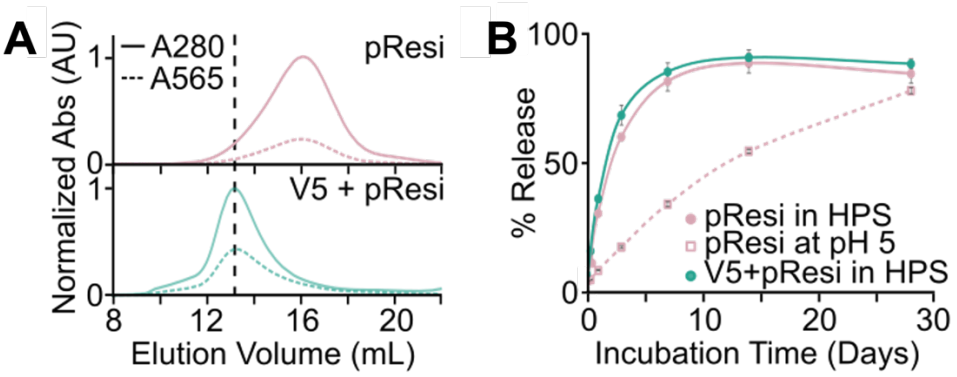

Figure 3.4 Sustained release of resiquimod adjuvant from V5-encapsulated radiant star drugamer. (A) SEC trace of pResi alone (top) and pResi encapsulated within V5 (bottom). Once encapsulated, the polymer nanoparticle elutes earlier from the column, at the same elution volume as empty I53-50-V5, indicating it is now trapped within the protein nanoparticle. (B) Release kinetics of free resiquimod from pResi alone or V5-encapsulated in human serum and pResi alone at pH 5.

We studied the rate at which resiquimod is released from pResi via cleavage of the PHBC linker. Figure 3.4B shows the amount of resiquimod released at 37°C as a function of time from

pResi alone or encapsulated in V5 when incubated in human serum or buffer at pH 5 to simulate the acidic conditions within the endosome. Encapsulated pResi could not be studied at pH 5 due to the tendency of V5 to flocculate at low pH. No difference was observed in the rate of release of resiquimod in human serum regardless of encapsulation state ($t_{1/2}$ of 1.5 d vs 1.9 d for encapsulated vs. non-encapsulated pResi), suggesting that the presence of the protein nanoparticle might not impact drug release in circulation. At low pH, the release rate of resiquimod from pResi was significantly slower ($t_{1/2}$ = 19.6 d), suggesting that drug release from the polymer architecture may slow after endocytosis of the encapsulated nanoparticle.

3.2.4 *Encapsulated pResi provides potent immune activation without systemic toxicity*

After confirming that resiquimod was released from the polymer prodrug via hydrolysis, we tested the ability of the encapsulated pResi to induce cytokine production by peripheral blood mononuclear cells (PBMCs) in vitro. Human PBMCs from three donors were incubated for 24 hours with varying concentrations of free resiquimod or pResi encapsulated within V5. Compared with dose-matched free resiquimod, encapsulated pResi appeared to elicit higher levels of secreted Interleukin-6 (IL-6) and Tumor Necrosis Factor-alpha (TNF-α) across the concentration series until saturating concentrations were reached (5 μM), although this difference did not reach statistical significance (Figure 3.5A). Empty V5 and pResi alone each resulted in much lower activation (Figure S3.6, Supporting Information), suggesting that the pResi is more readily taken up by cells when encapsulated and that empty V5 has a minimal impact on immune stimulation.

Having demonstrated the biological activity of encapsulated pResi in vitro, we then evaluated its effects in immunization studies in mice. We used V5 itself as the immunizing antigen and measured anti-V5 binding titers after three immunizations with a series of distinct

formulations. In addition to encapsulated pResi containing 0.36 μg of resiquimod, we tested pResi mixed with pre-assembled V5 (i.e., non-encapsulated), V5 formulated with 0.36 or 20 μg of free resiquimod, V5 encapsulating the DP25 RSP lacking resiquimod, V5 alone, and V5 formulated with AddaVax, a squalene-based oil-in-water emulsion we have used as an adjuvant in previous immunization studies.[13, 30, 32] The amounts of V5 and resiquimod administered were matched in all relevant groups except for the high dose of free resiquimod (20 μg), which was selected based on typical doses used in previous studies in mice.[48] Formulating V5 with free resiquimod at either dose resulted in no improvement over the encapsulated DP25 RSP or V5 alone (Figure 3.5B). In contrast, encapsulated pResi elicited serum antibody titers against V5 that were significantly higher than non-encapsulated pResi and were comparable to AddaVax. Plotting the kinetics of the serological response, which was followed for four months following the second boost, showed that encapsulated pResi elicited a durable response in which the levels of antibodies against V5 remained consistently higher than the groups receiving free resiquimod or no adjuvant (Figure 3.5C).

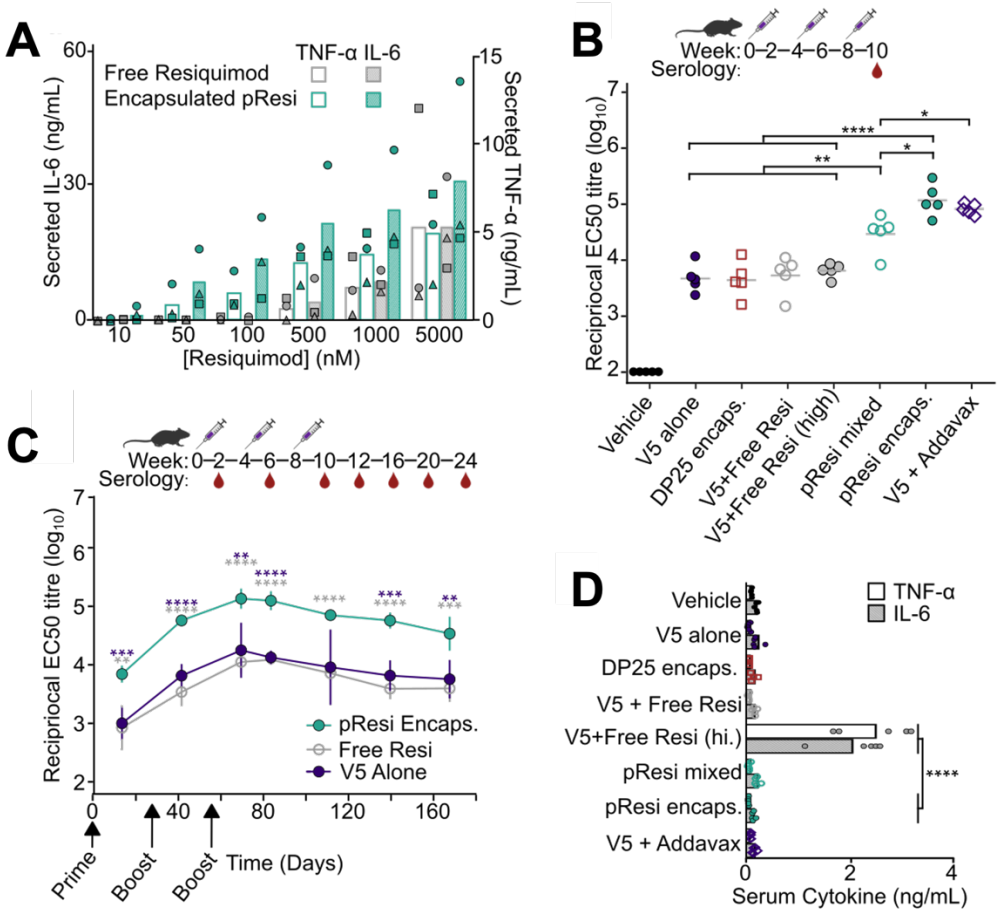

Figure 3.5 Encapsulated polymeric adjuvants improve immune responses *in vitro* and *in vivo*. (A) *In vitro* cytokine response from human PBMCs (each of three donors represented by a distinct symbol) incubated for 24 h with free resiquimod or encapsulated pResi. (B) Serum IgG responses against V5 after three immunizations of BALB/c mice (n=5), measured as EC50 titre. (C) Anti-V5 antibody titers measured over 24 weeks for groups receiving encapsulated pResi (green), free resiquimod (grey), or no adjuvant (purple). (D) *In vivo* systemic cytokine responses measured 1 hour post immunization. Only free resiquimod at a dose commonly used in the literature induced TNF-α and IL-6 levels above background. The data shown are from representative experiments that were performed at least twice. Error bars in panel f indicate standard deviation. Statistical significance was determined by an independent t-test with Bonferroni correction; ****, $p \leq 1\times10^{-4}$; ***, $p \leq 1\times10^{-3}$; **, $p \leq 1\times10^{-2}$; *, $p \leq 5\times10^{-2}$.

To determine the effect of polymerizing resiquimod and packaging it into V5 on systemic toxicity, we measured serum cytokine levels 1 hour after immunization, a commonly used timepoint to evaluate toxicity.[39] TNF-α and IL-6 were elevated when 20 µg of free resiquimod was delivered (Figure 3.5D). By contrast, levels of these cytokines were indistinguishable from

background in all other groups, including pResi encapsulated in V5, which elicited antibody levels that were significantly higher than all other formulations except AddaVax (Figure 3.5B). These data indicate that encapsulating resiquimod in V5 significantly increased immunogenicity without causing the systemic cytokine secretion that has been associated with toxicity in previous studies of this adjuvant.[37]

3.3 STUDY LIMITATIONS

While in these studies we used V5 as the antigen, such nanoparticle encapsulate materials can serve as a platform for multivalent decoration with both antigens or cell-specific targeting moieties achieved by genetic fusion, chemical conjugation, "plug-and-play" decoration, or *in vivo* library selection.[11, 12, 29, 49] Further, while we did not characterize or target delivery to specific cell types in our studies here, cell-specific targeting could be achieved by similar methods.[50]

Lastly, there is extensive rationale for utilization of imidazoquinolones like resiquimod as vaccine adjuvants because of specific receptor stimulation and immune signaling cascades of both TLR7 and TLR8 immune pathways. However, it should be noted that murine TLR8 pathways are divergent from human, which limits the full characterization and potential of our vaccine in the murine model used herein.[37]

3.4 CONCLUSIONS

We demonstrate the functional potential of cargo-bearing V5 nanoparticles *in vivo* by encapsulating and delivering a small molecule TLR7/8 agonist in immunization experiments in mice. We showed that a radiant star polymer was an ideal encapsulated material due to its statistical

incorporation of functional monomers that maintain its negative surface charge and allow for high drug loading without the need for further compaction prior to encapsulation. While fully synthetic polymer encapsulation by VLPs has been explored previously, to our knowledge, this is the first time a fully synthetic polymer prodrug has been encapsulated.[22-25] Resiquimod-packaged nanoparticles elicited more potent humoral immune responses against V5 than V5 mixed with a 55-fold higher dose of free resiquimod, while simultaneously minimizing systemic toxicity. These results support several previous studies demonstrating that chemical linkage of resiquimod to an antigen improves B and T cell responses and outcomes after challenge and are consistent with the notion that the ideal vaccine formulation links adjuvant to antigen, thereby restricting immune stimulation to relevant lymphoid tissues and enhancing both B and T cell-mediated protection.[40-42, 51, 52] Our vaccine approach has appreciable synthetic definition and control over positioning of molecular features and allows for decoupling of immunogenicity of antigen (V5 in this case) and adjuvant (radiant star polymer adjuvant), which can be used to investigate how antigen epitope and adjuvant mechanisms can be mixed and matched to fit a desired disease setting. While we describe a vaccine application here, other small molecules drugs could be delivered to disease settings and target tissues using this V5-encapsulated drugamer approach.

3.5 METHODS

Materials

Materials were purchased from Sigma Aldrich unless otherwise specified. Resiquimod was purchased from AstaTech. 4-Cyano-4-(ethylsulfanylthiocarbonyl) sulfanylpentanoic acid (ECT) was obtained from Omm Scientific. [2,2′-Azobis(4-methoxy-2,4-dimethylvaleronitrile)] (V-70) was purchased from FUJIFILM Wako Pure Chemical Corporation and used without further

purification. Spectra/Por regenerated cellulose dialysis membranes were purchased from Spectrum Laboratories.

Dynamic Light Scattering

Dynamic light scattering was performed on a DynaPro NanoStar (Wyatt Technology Corp.). Measurements were performed in triplicate in a 1 µL quartz cuvette. Each measurement collected 10 acquisitions at 5 s per acquisition.

Negative Stain Electron Microscopy

Negative stain electron micrographs were collected on a Talos model L120C electron microscope (Thermo Scientific). Protein nanoparticles were diluted to a concentration of 0.1 mg/mL in 25 mM Tris pH 8, 500 mM NaCl. Sample was applied to carbon coated 300 mesh copper grids (Ted Pella) which had been glow discharged immediately before use. The grids were washed and then stained with 0.75% (w/v) uranyl formate stain, immediately blotted, and then stained again.

Electrophoretic Mobility Shift Analysis

A 2% (w/v) agarose gel was prepared by dissolving agarose (Fisher Scientific) in TAE buffer. SYBR Gold Nucleic Acid Gel Stain (Invitrogen) was added to the gel before casting. Electrophoresis was performed at 100 V for 1 hour. After imaging nucleic acid, gels were incubated overnight in Gelcode Blue Stain Reagent (Thermo Scientific) for imaging of protein bands.

In vitro Assembly of I53-50-V5, RSP Encapsulation

Prior to assembly, trimeric and pentameric nanoparticle components were separately diluted from storage buffer to concentrations ranging from 5 to 50 μM in 20 mM Tris pH 8.0, 150 mM NaCl, 0.375% CHAPS. For encapsulation reactions, molecular cargos (i.e., RNA or polymers) were added to the solution containing the trimeric component, and the assembly reactions were initiated by mixing the trimer/cargo- and pentamer-containing solutions followed by overnight incubation at 37°C unless otherwise indicated.

Monomer Synthesis

Synthetic Scheme S1 (Supplementary Information) was followed to obtain the Resiquimod prodrug (ResMA) monomer (6). Rhodamine B methacrylate (RhMA) was synthesized and fully characterized as described previously.[53] All synthesized compounds were purified by precipitation and/or silica gel column chromatography techniques. The successful synthesis and purity of the monomers were confirmed and characterized by ^{1}H NMR spectroscopy (Bruker Avance Spectrometer 300 MHz) and Electrospray Ionization-Mass spectrometry (Bruker Esquire ion trap mass spectrometer). In brief, intermediate 4 was synthesized following previously reported methods.[77] To 4 (1.26 g, 2.93 mmol) in 10 mL dichloromethane at 0 ºC, was added methyl trifluoromethanesulfonate (0.31 mL, 2.83 mmol) in 2 mL dichloromethane dropwise over 5 min. After 10 min at 0 ºC, the reaction mixture was stirred at room temperature for 1.5 h and then concentrated to 4 mL under reduced pressure. This solution was precipitated into diethyl ether in 50 mL conical centrifuge tubes (40 mL ether/tube), vortexed and centrifuged to isolate the product as a sticky pellet. This pellet was again treated with diethyl ether (40 mL/tube), vortexed and centrifuged to get the intermediate 5. This intermediate was dissolved in 15 mL CH_2Cl_2 and added to Resiquimod (692 mg, 2.20 mmol) in 35 mL CH_2Cl_2 at room temperature. The resulting reaction

mixture was stirred for 21 h and then the solvent was rotary evaporated under reduced pressure. The crude product was purified by silica gel column chromatography using 3 % methanol in chloroform to afford resiquimod prodrug monomer ResMA (6). The reaction yielded 1.14 g, a 76.5 % conversion. ^{1}H NMR (300 MHz, DMSO-d_6) given in Supplementary Figure 5 shows expected product formation: δ 1.13 (t, J = 6.9 Hz, 3H) 1.18 (s, 6H), 1.85 (s, 3H), 2.70 (t, J = 6.3 Hz, 2H), 2.85 (t, J = 6.3 Hz, 2H), δ 3.53 (q, J = 6.9 Hz, 2H), δ 4.31 (s, 4H), δ 4.55 – 45.12 (2 s and 1 brs merged, 5H), 5.21 (s, 2H), 5.66 (s, 1H), 6.02 (s, 1H), 7.11 (d, J = 8.7 Hz, 2H), 7.45 – 7.58 (1 d and 1 t merged, 3H), 7.63 (t, J = 7.5 Hz, 1H), 7.94 (d, J = 7.8 Hz, 1H), 8.54 (d, J = 8.1 Hz, 1H), 9.94 (s, 1H). MS (ESI, m/z): calculated for $C_{35}H_{40}N_4O_{10}$ (M): 676.3, found: 677.4 $[M+H]^+$.

pResi Core Synthesis poly(HEMA-ECT) (pHECT)

Synthesis of the macro-CTA (pHECT) was described previously.[40] The RSN core was synthesized by RAFT homopolymerization of the HEMA-ECT in DMSO-d_6 under a nitrogen atmosphere using ABCVA (V501) as the radical initiator. The Degree of Polymerization (DP) of HEMA-ECT was 10 and the initiator was 10% of the HEMA-ECT. HEMA-ECT (500 mg, 1.33 mmol), ABCVA (V501) (37.3 mg, 0.133 mmol), 1,3,5-trioxane (7.4 mg), and DMSO-d_6 (1.286 g) were added in a 5 mL round bottom flask. The flask was sealed and the reaction mixture was degassed by bubbling nitrogen into the solution for 35 min and was then placed in a preheated oil bath at 70°C for 18 h. The reaction was stopped by introducing oxygen by removing the septum and cooling the solution with a mild stream of air. The crude polymer was isolated by repeated precipitations into diethyl ether (8 times). Acetone was used to dissolve the polymer in between precipitations. The purified and dried polymer was characterized by ^{1}H NMR spectroscopy. $T_{initial}$ and T_{final} ^{1}H NMR spectra of the crude solution indicated 99% monomer conversion, using an

internal standard (1,3,5-trioxane) added into the polymerization solution. After purification of unreacted monomers, the polymer was characterized by ^{1}H NMR spectroscopy in $CDCl_3$. All peaks characteristic of poly(HEMA-ECT) were observed.

RSP Synthesis

Copolymerization of SMA and RhMA was conducted in DMSO in the presence of pHECT (macro-CTA) and ABCVA (initiator, I) following a synthetic procedure outlined previously.[40]

pResi Synthesis

Copolymerization of SMA, ResMA, and RhMA was conducted in DMSO in the presence of poly(hECT) (macro-CTA) and V-70 (initiator, I). The initial molar feed percentages of each methacrylate monomer were 91.3 mol%, 7.8 mol%, and 0.9 mol%, respectively. The $[M]_0 : [CTA]_0 : [I]_0$ was 25 : 1 : 0.05 at an initial monomer concentration of 94.5 wt%. To a 5 mL round bottom flask was added SMA (200 mg, 0.869 mmol), ResMA (50 mg, 0.074 mmol), RhMA (5 mg, 0.008 mmol), poly(hECT) (14.2 mg, 0.0377 mmol), and V70 (0.581 mg, 0.002 mmol) in a 2 mL total volume of DMSO. The solution was septa sealed and purged with nitrogen for 30 minutes. It was then transferred to a preheated oil bath at 30°C and allowed to polymerize for 18 hours. After the solution cooled, the polymer was purified by ether precipitation. The polymer was added dropwise to a 50 mL conical tube containing 45 mL diethyl ether and vigorously vortexed, followed by centrifugation at 3750 rpm, 4°C for 5 minutes. The ether supernatant was decanted, and the polymer pellet was air dried and resolublized in 1 mL DMSO. This process was repeated for a total of 3 ether precipitations, followed by one ether wash.

To determine the degree of polymerization of monomer, 20 μL of the reaction mixture was taken before ($T_{initial}$) and after (T_{final}) the 18 h polymerization reaction, mixed with 700 μL DMSO-d_6, and analyzed via ^{1}H NMR spectroscopy. The total molar fraction of monomer converted to polymer was calculated by comparing the vinyl resonances (3H) between 5.0-6.5 ppm from the two spectra. Following purification, ^{1}H NMR spectra were recorded in the presence of fasudil hydrochloride (eNovation Chemicals) internal standard to determine the Resiquimod drug weight percent of the RSN (Figure S6).

Size Exclusion Chromatography (SEC-MALS)

The average molecular mass (Mn) and dispersity of the RSNs were determined using 100% mass recovery and multiangle light scattering (MALS) SEC. The running solvent was 25 mM Tris-HCl pH 8 with 150 mM NaCl (flow rate: 0.5 mL/min) and samples were prepared at 5 mg/mL. Separation was performed on a Phenomenex PolySep GFC-P 6000 and data was collected by a Wyatt miniDAWN Treos and Wyatt Optilab rex. 100% mass recovery was performed using Wyatt's protocol with the refractive index data obtained from the Optilab rex. A dn/dc value of 0.164 resulted in accurate calculations of the injected mass across all RSNs characterized by SEC-MALS. The dn/dc value was corroborated by performing a batch dn/dc determination over a range of RSN concentrations from 0.1 - 2 mg/mL. Wyatt ASTRA software was used for data analysis and determination of absolute molecular weight and dispersity.

pResi Encapsulation

Prior to encapsulation into I53-50-V5, pResi was dissolved into 25 mM Tris, pH 8 containing 0.3% CHAPS to a concentration of 10 mg/mL. Assemblies were performed as described above at a

stoichiometric ratio such that there were equimolar amounts of pResi and assembled I53-50-V5 nanoparticles in solution. The reaction mixture was incubated for 30 minutes at 37°C before purification over a Superose 6 HR column (Cytiva) with a mobile phase of 25 mM Tris pH 8, 150 mM NaCl.

Drug Release Assay

HPLC analysis of Resiquimod was performed using an Agilent 1260 HPLC equipped with Agilent ChemStation software (Palo Alto, CA, USA). The UV detector was operated at 254 nm. A Zorbax SB-C18 analytical column (2.1 x 100 mm, 3.5 µm; Agilent Technologies, CA, USA) was used at ambient temperature with mobile phases of 1% acetic acid in acetonitrile and aqueous 1% (v/v) acetic acid with 5% (v/v) acetonitrile. With a 15 µL sample injection volume, the gradient method involved an increase from 2-95 % (v/v) organic phase over the first twenty-four minutes at 0.2 mL/min, 95-100 % (v/v) organic from 24-25 minutes, and then a ramp down from 100-2% organic from 26.5-37 minutes at 0.35 mL/min.

pResi RSNs either suspended in 1:1 PBS:human serum or 10 mM sodium phosphate pH 5, 150 mM NaCl; or encapsulated in I53-50-V5 nanoparticles in 1:1 PBS:serum, were incubated at 37°C at a concentration of 100 µM resiquimod in a final volume of 100 µL for 28 days. At prescribed time points (0 h, 3 h, 8 h, 1 d, 3 d, 7 d, 14 d, 28 d), samples were transferred to -80°C until all samples could be processed together. Resiquimod was extracted from each sample by 2:1 acetonitrile extraction at 4°C and centrifugation at 18,000 rcf, 4°C for 20 minutes. Supernatants containing resiquimod were filtered through a Millex GV low protein binding PVDF filter (0.22 µm; Millipore, Burlington, MA, USA) and nitrogen evaporated (Biotage, Uppsala, Sweden) for

90 minutes at 13 psi. Samples were resuspended in 100 µL deionized water and run against a resiquimod standard curve.

Immunogen Preparation

Nanoparticles encapsulating pResi were prepared as described above. For groups receiving V5 with free resiquimod or mixed with pResi, assemblies were prepared by mixing V5A and V5B in equimolar amounts. Assembly reactions were incubated at 37°C for 30 minutes before an additional molar equivalent of V5A was added to the reaction and allowed to sit at 4°C overnight before purification on a Superose 6 10/300 HR column using a buffer of 25 mM Tris pH 8, 150 mM NaCl. This additional equivalent of V5A was added to ensure that nanoparticles were completely formed, with no missing trimeric components37. Following purification, nanoparticles were mixed with free resiquimod (prepared from a stock solution in DMSO) or pResi which had been dissolved into the same buffer.

Endotoxin Measurement and Removal

Endotoxin was removed from nanoparticle components during protein purification using a detergent wash during IMAC. Proteins were immobilized on a 5 mL HisTrap HP column (GE Healthcare) equilibrated with buffer (25 mM Tris pH 8, 500 mM NaCl, 0.75% CHAPS) and the column was washed with ~10 CV of the equilibration buffer. Elution was performed with a linear gradient of 0 to 500 mM imidazole in equilibration buffer. Fractions containing the desired protein were pooled and stored in a buffer containing detergent until assembly. Purified proteins were tested for endotoxin prior to assembly using a Charles River EndoSafe® PTS system, and measured concentrations were routinely below 100 EU/mL. Detergent was removed from

assembled nanoparticles prior to immunization by buffer exchange via SEC into 25 mM Tris pH 8, 1500 mM NaCl.

Mice

Female C57BL/6J mice were sourced at the age of 4 weeks from Jackson Laboratory, Bar Harbor, Maine (stock #000664). Animals were maintained at the Comparative Medicine Facility at the University of Washington, Seattle, WA, which is accredited by the American Association for the Accreditation of Laboratory Animal Care International (AAALAC). Animal procedures were performed with the approval and under the guidance of the Institutional Animal Care and Use Committee of the University of Washington, Seattle, WA.

Immunizations and serum collection

6-week old mice (n=5/group) were immunized with 25 μg immunogen at week 0 and subsequently boosted at weeks 4 and 8. Mice were immunized by intramuscular injection at the quadriceps muscle using a 27-gauge needle (BD, San Diego, CA) with 50 μL immunogen solution per leg (100 μL total) under isoflurane anesthesia. Blood samples were obtained via submental venipuncture using a 5 mm lancet (Braintree Scientific, Braintree, MA) two weeks after the initial immunization and every 2-4 weeks thereafter. For measurements of systemic cytokines, blood samples were obtained as above, 1 hour post immunization. At the endpoint of week 12, mice were anesthetized with isoflurane for blood collection via cardiac puncture. The in vivo study was repeated twice. For measurement of response duration, blood samples were collected from the initial cohort of mice every 4 weeks for 24 weeks, before being anesthetized with isoflurane for terminal blood collection via cardiac puncture. Blood was rested in 1.5 mL Eppendorf tubes for

30 minutes at room temperature to allow for coagulation. Serum was then isolated from cellular components and clotting factors via centrifugation at 2000 g for 10 minutes. Serum was stored at -80°C until use.

Cell Culture

Frozen human PBMCs were thawed and washed in 40 mL PBS containing 10% (w/v) heat-inactivated FBS, then 10 mL of complete RPMI 1640 (25 mM HEPES, sodium bicarbonate, 1 mM sodium pyruvate, 1 mM L-glutamine, 1% (w/v) penicillin/streptomycin and 10% (w/v) FBS.) Cells were counted and resuspended in complete RPMI 1640 at 2×106 cells/mL and 0.25 mL/well was plated in 96-well tissue culture plates. Resiquimod and its pro-drug form were dissolved in DMSO and diluted in TBS to the desired concentration, maintaining a final concentration of DMSO in each well of less than 0.1% (v/v). pResi was dissolved into TBS and diluted in each well to the desired concentration. Encapsulated pResi was prepared as above and adjusted to the correct concentration using a standard curve based on the absorbance of rhodamine at 565 nm. After 24 hours of incubation at 37°C and 8% CO2, plates were centrifuged at 1500 rpm for 5 minutes and 0.2 mL of supernatants were removed and transferred to fresh 96-well plates. Samples were stored at -80°C before being analyzed by ELISA.

Enzyme-Linked Immunosorbent Assay

Enzyme-linked immunosorbent assays (ELISA) were used to determine the levels of V5-specific antibodies in mouse sera. Maxisorp (Nunc) ELISA plates were coated overnight at 4°C with 0.08 μg/mL of V5 per well in 0.1 M sodium bicarbonate buffer, pH 9.4. Plates were then blocked with a 4% (w/v) solution of dried milk powder (BioRad) in TBS with 0.05% (v/v) Tween 20 (TBST)

for 1 hour at room temperature. Serial dilutions of sera were added to the plates and, after washing, antibody binding was measured using a hydrogen peroxidase-coupled horse anti-mouse IgG antibody. Plates were then washed thoroughly in TBST, colorimetric substrate (TMB, Thermo Fisher) was added, and absorbance was read at 450 nm. To quantify the presence of cytokines in cell culture and mouse sera, cytokine quantification kits were purchased from R&D Systems and used following the manufacturer's recommendations.

3.6 ACKNOWLEDGEMENTS

We thank Mengyu Wu and Andrew Borst in the Electron Microscopy Core Laboratory at the Institute for Protein Design for assistance with electron microscopy. We thank Rashmi Ravichandran at the Institute for Protein Design for assistance in protein production and purification. This study was supported by the Bill & Melinda Gates Foundation (OPP1156262), the Defense Threat Reduction Agency (HDTRA1-18-1-0001), the National Science Foundation (NSF CHE 1629214), and DARPA (W911NF-17-2-0020). K-L. H. was supported by an Innovation Fellowship from the Washington Research Foundation. C.L.L and A.N.P. were supported by NSF GRFP #DGE-1762114.

REFERENCES

[1] K.L. Herpoldt, C.L. López, I. Sappington, M.N. Pham, S. Srinivasan, J. Netland, K.S. Montgomery, D. Roy, A.N. Prossnitz, D. Ellis, A.J. Wargacki, M. Pepper, A.J. Convertine, P.S. Stayton, N.P. King, Macromolecular Cargo Encapsulation via In Vitro Assembly of Two-Component Protein Nanoparticles, Adv Healthc Mater, (2024) e2303910.
[2] B.S. Graham, Rapid COVID-19 vaccine development, Science, 368 (2020) 945-946.
[3] M. Li, H. Wang, L. Tian, Z. Pang, Q. Yang, T. Huang, J. Fan, L. Song, Y. Tong, H. Fan, COVID-19 vaccine development: milestones, lessons and prospects, Signal Transduction and Targeted Therapy, 7 (2022) 146.
[4] R. Noad, P. Roy, Virus-like particles as immunogens, Trends in Microbiology, 11 (2003) 438-444.
[5] A. Bouazzaoui, A.A.H. Abdellatif, F.A. Al-Allaf, N.M. Bogari, S. Al-Dehlawi, S.H. Qari, Strategies for Vaccination: Conventional Vaccine Approaches Versus New-Generation Strategies in Combination with Adjuvants, Pharmaceutics, 13 (2021) 140.
[6] E. Kuroda, C. Coban, K.J. Ishii, Particulate adjuvant and innate immunity: past achievements, present findings, and future prospects, Int Rev Immunol, 32 (2013) 209-220.
[7] L.A. Brito, P. Malyala, D.T. O'Hagan, Vaccine adjuvant formulations: a pharmaceutical perspective, Semin Immunol, 25 (2013) 130-145.
[8] M.O. Mohsen, A.C. Gomes, G. Cabral-Miranda, C.C. Krueger, F.M.S. Leoratti, J.V. Stein, M.F. Bachmann, Delivering adjuvants and antigens in separate nanoparticles eliminates the need of physical linkage for effective vaccination, Journal of Controlled Release, 251 (2017) 92-100.
[9] R. Gupta, K. Arora, S.S. Roy, A. Joseph, R. Rastogi, N.M. Arora, P.K. Kundu, Platforms, advances, and technical challenges in virus-like particles-based vaccines, Frontiers in Immunology, 14 (2023).
[10] M.J. Rohovie, M. Nagasawa, J.R. Swartz, Virus-like particles: Next-generation nanoparticles for targeted therapeutic delivery, Bioeng Transl Med, 2 (2017) 43-57.
[11] A. Marini, Y. Zhou, Y. Li, I.J. Taylor, D.B. Leneghan, J. Jin, M. Zaric, D. Mekhaiel, C.A. Long, K. Miura, S. Biswas, A Universal Plug-and-Display Vaccine Carrier Based on HBsAg VLP to Maximize Effective Antibody Response, Frontiers in Immunology, 10 (2019).
[12] K.D. Brune, M. Howarth, New Routes and Opportunities for Modular Construction of Particulate Vaccines: Stick, Click, and Glue, Frontiers in Immunology, 9 (2018).
[13] A.C. Walls, B. Fiala, A. Schäfer, S. Wrenn, M.N. Pham, M. Murphy, L.V. Tse, L. Shehata, M.A. O'Connor, C. Chen, M.J. Navarro, M.C. Miranda, D. Pettie, R. Ravichandran, J.C. Kraft, C. Ogohara, A. Palser, S. Chalk, E.C. Lee, K. Guerriero, E. Kepl, C.M. Chow, C. Sydeman, E.A. Hodge, B. Brown, J.T. Fuller, K.H. Dinnon, 3rd, L.E. Gralinski, S.R. Leist, K.L. Gully, T.B. Lewis, M. Guttman, H.Y. Chu, K.K. Lee, D.H. Fuller, R.S. Baric, P. Kellam, L. Carter, M. Pepper, T.P. Sheahan, D. Veesler, N.P. King, Elicitation of Potent Neutralizing Antibody Responses by Designed Protein Nanoparticle Vaccines for SARS-CoV-2, Cell, 183 (2020) 1367-1382.e1317.
[14] C.E. Ashley, E.C. Carnes, G.K. Phillips, P.N. Durfee, M.D. Buley, C.A. Lino, D.P. Padilla, B. Phillips, M.B. Carter, C.L. Willman, Cell-specific delivery of diverse cargos by bacteriophage MS2 virus-like particles, ACS nano, 5 (2011) 5729-5745.
[15] K.M. Choi, S.H. Choi, H. Jeon, I.S. Kim, H.J. Ahn, Chimeric capsid protein as a nanocarrier for siRNA delivery: stability and cellular uptake of encapsulated siRNA, ACS Nano, 5 (2011) 8690-8699.

[16] T. Yamada, Y. Iwasaki, H. Tada, H. Iwabuki, M.K. Chuah, T. VandenDriessche, H. Fukuda, A. Kondo, M. Ueda, M. Seno, K. Tanizawa, S. Kuroda, Nanoparticles for the delivery of genes and drugs to human hepatocytes, Nat Biotechnol, 21 (2003) 885-890.
[17] J.D. Fiedler, S.D. Brown, J.L. Lau, M.G. Finn, RNA-directed packaging of enzymes within virus-like particles, Angew Chem Int Ed Engl, 49 (2010) 9648-9651.
[18] D.P. Patterson, B. Schwarz, R.S. Waters, T. Gedeon, T. Douglas, Encapsulation of an enzyme cascade within the bacteriophage P22 virus-like particle, ACS Chem Biol, 9 (2014) 359-365.
[19] S. Jekhmane, R. de Haas, O. Paulino da Silva Filho, A.H. van Asbeck, M.E. Favretto, A. Hernandez Garcia, R. Brock, R. de Vries, Virus-Like Particles of mRNA with Artificial Minimal Coat Proteins: Particle Formation, Stability, and Transfection Efficiency, Nucleic Acid Therapeutics, 27 (2017) 159-167.
[20] S. Lilavivat, D. Sardar, S. Jana, G.C. Thomas, K.J. Woycechowsky, In Vivo Encapsulation of Nucleic Acids Using an Engineered Nonviral Protein Capsid, Journal of the American Chemical Society, 134 (2012) 13152-13155.
[21] T. Douglas, M. Young, Viruses: Making Friends with Old Foes, Science, 312 (2006) 873-875.
[22] F.D. Sikkema, M. Comellas-Aragonès, R.G. Fokkink, B.J.M. Verduin, J.J.L.M. Cornelissen, R.J.M. Nolte, Monodisperse polymer–virus hybrid nanoparticles, Organic & Biomolecular Chemistry, 5 (2007) 54-57.
[23] Y. Ma, R.J. Nolte, J.J. Cornelissen, Virus-based nanocarriers for drug delivery, Adv Drug Deliv Rev, 64 (2012) 811-825.
[24] S.J. Maassen, A.M. van der Ham, J.J.L.M. Cornelissen, Combining Protein Cages and Polymers: from Understanding Self-Assembly to Functional Materials, ACS Macro Letters, 5 (2016) 987-994.
[25] T. Douglas, M. Young, Host–guest encapsulation of materials by assembled virus protein cages, Nature, 393 (1998) 152-155.
[26] N.P. King, W. Sheffler, M.R. Sawaya, B.S. Vollmar, J.P. Sumida, I. André, T. Gonen, T.O. Yeates, D. Baker, Computational design of self-assembling protein nanomaterials with atomic level accuracy, Science, 336 (2012) 1171-1174.
[27] N.P. King, J.B. Bale, W. Sheffler, D.E. McNamara, S. Gonen, T. Gonen, T.O. Yeates, D. Baker, Accurate design of co-assembling multi-component protein nanomaterials, Nature, 510 (2014) 103-108.
[28] Y. Hsia, J.B. Bale, S. Gonen, D. Shi, W. Sheffler, K.K. Fong, U. Nattermann, C. Xu, P.-S. Huang, R. Ravichandran, S. Yi, T.N. Davis, T. Gonen, N.P. King, D. Baker, Design of a hyperstable 60-subunit protein icosahedron, Nature, 535 (2016) 136-139.
[29] G. Ueda, A. Antanasijevic, J.A. Fallas, W. Sheffler, J. Copps, D. Ellis, G.B. Hutchinson, A. Moyer, A. Yasmeen, Y. Tsybovsky, Y.J. Park, M.J. Bick, B. Sankaran, R.A. Gillespie, P.J. Brouwer, P.H. Zwart, D. Veesler, M. Kanekiyo, B.S. Graham, R.W. Sanders, J.P. Moore, P.J. Klasse, A.B. Ward, N.P. King, D. Baker, Tailored design of protein nanoparticle scaffolds for multivalent presentation of viral glycoprotein antigens, Elife, 9 (2020).
[30] J. Marcandalli, B. Fiala, S. Ols, M. Perotti, W. de van der Schueren, J. Snijder, E. Hodge, M. Benhaim, R. Ravichandran, L. Carter, W. Sheffler, L. Brunner, M. Lawrenz, P. Dubois, A. Lanzavecchia, F. Sallusto, K.K. Lee, D. Veesler, C.E. Correnti, L.J. Stewart, D. Baker, K. Loré, L. Perez, N.P. King, Induction of Potent Neutralizing Antibody Responses by a Designed Protein Nanoparticle Vaccine for Respiratory Syncytial Virus, Cell, 176 (2019) 1420-1431.e1417.

[31] S. Tetter, N. Terasaka, A. Steinauer, R.J. Bingham, S. Clark, A.J.P. Scott, N. Patel, M. Leibundgut, E. Wroblewski, N. Ban, P.G. Stockley, R. Twarock, D. Hilvert, Evolution of a virus-like architecture and packaging mechanism in a repurposed bacterial protein, Science, 372 (2021) 1220-1224.
[32] S. Boyoglu-Barnum, D. Ellis, R.A. Gillespie, G.B. Hutchinson, Y.J. Park, S.M. Moin, O.J. Acton, R. Ravichandran, M. Murphy, D. Pettie, N. Matheson, L. Carter, A. Creanga, M.J. Watson, S. Kephart, S. Ataca, J.R. Vaile, G. Ueda, M.C. Crank, L. Stewart, K.K. Lee, M. Guttman, D. Baker, J.R. Mascola, D. Veesler, B.S. Graham, N.P. King, M. Kanekiyo, Quadrivalent influenza nanoparticle vaccines induce broad protection, Nature, 592 (2021) 623-628.
[33] J.Y. Song, W.S. Choi, J.Y. Heo, J.S. Lee, D.S. Jung, S.-W. Kim, K.-H. Park, J.S. Eom, S.J. Jeong, J. Lee, K.T. Kwon, H.J. Choi, J.W. Sohn, Y.K. Kim, J.Y. Noh, W.J. Kim, F. Roman, M.A. Ceregido, F. Solmi, A. Philippot, A.C. Walls, L. Carter, D. Veesler, N.P. King, H. Kim, J.H. Ryu, S.J. Lee, Y.W. Park, H.K. Park, H.J. Cheong, Safety and immunogenicity of a SARS-CoV-2 recombinant protein nanoparticle vaccine (GBP510) adjuvanted with AS03: A randomised, placebo-controlled, observer-blinded phase 1/2 trial, eClinicalMedicine, 51 (2022).
[34] D. Das, S. Srinivasan, F.D. Brown, F.Y. Su, A.L. Burrell, J.M. Kollman, A. Postma, D.M. Ratner, P.S. Stayton, A.J. Convertine, Radiant star nanoparticle prodrugs for the treatment of intracellular alveolar infections, Polymer Chemistry, 9 (2018) 2134-2146.
[35] M. Jurk, F. Heil, J. Vollmer, C. Schetter, A.M. Krieg, H. Wagner, G. Lipford, S. Bauer, Human TLR7 or TLR8 independently confer responsiveness to the antiviral compound R-848, Nat Immunol, 3 (2002) 499-499.
[36] J.P. Vasilakos, M.A. Tomai, The use of Toll-like receptor 7/8 agonists as vaccine adjuvants, Expert Rev Vaccines, 12 (2013) 809-819.
[37] D.J. Dowling, Recent Advances in the Discovery and Delivery of TLR7/8 Agonists as Vaccine Adjuvants, ImmunoHorizons, 2 (2018) 185-197.
[38] D. Smirnov, J.J. Schmidt, J.T. Capecchi, P.D. Wightman, Vaccine adjuvant activity of 3M-052: An imidazoquinoline designed for local activity without systemic cytokine induction, Vaccine, 29 (2011) 5434-5442.
[39] S. Bhagchandani, J.A. Johnson, D.J. Irvine, Evolution of Toll-like receptor 7/8 agonist therapeutics and their delivery approaches: From antiviral formulations to vaccine adjuvants, Adv Drug Deliv Rev, 175 (2021) 113803.
[40] G.M. Lynn, R. Laga, P.A. Darrah, A.S. Ishizuka, A.J. Balaci, A.E. Dulcey, M. Pechar, R. Pola, M.Y. Gerner, A. Yamamoto, C.R. Buechler, K.M. Quinn, M.G. Smelkinson, O. Vanek, R. Cawood, T. Hills, O. Vasalatiy, K. Kastenmüller, J.R. Francica, L. Stutts, J.K. Tom, K.A. Ryu, A.P. Esser-Kahn, T. Etrych, K.D. Fisher, L.W. Seymour, R.A. Seder, In vivo characterization of the physicochemical properties of polymer-linked TLR agonists that enhance vaccine immunogenicity, Nature Biotechnology, 33 (2015) 1201-1210.
[41] D.S. Wilson, S. Hirosue, M.M. Raczy, L. Bonilla-Ramirez, L. Jeanbart, R. Wang, M. Kwissa, J.F. Franetich, M.A.S. Broggi, G. Diaceri, X. Quaglia-Thermes, D. Mazier, M.A. Swartz, J.A. Hubbell, Antigens reversibly conjugated to a polymeric glyco-adjuvant induce protective humoral and cellular immunity, Nat Mater, 18 (2019) 175-185.
[42] G.M. Lynn, C. Sedlik, F. Baharom, Y. Zhu, R.A. Ramirez-Valdez, V.L. Coble, K. Tobin, S.R. Nichols, Y. Itzkowitz, N. Zaidi, J.M. Gammon, N.J. Blobel, J. Denizeau, P. de la Rochere, B.J. Francica, B. Decker, M. Maciejewski, J. Cheung, H. Yamane, M.G. Smelkinson, J.R. Francica, R. Laga, J.D. Bernstock, L.W. Seymour, C.G. Drake, C.M. Jewell, O. Lantz, E.

Piaggio, A.S. Ishizuka, R.A. Seder, Peptide–TLR-7/8a conjugate vaccines chemically programmed for nanoparticle self-assembly enhance CD8 T-cell immunity to tumor antigens, Nature Biotechnology, 38 (2020) 320-332.
[43] F.Y. Su, S. Srinivasan, B. Lee, J. Chen, A.J. Convertine, T.E. West, D.M. Ratner, S.J. Skerrett, P.S. Stayton, Macrophage-targeted drugamers with enzyme-cleavable linkers deliver high intracellular drug dosing and sustained drug pharmacokinetics against alveolar pulmonary infections, J Control Release, 287 (2018) 1-11.
[44] C.L. López, K.J. Brempelis, J.F. Matthaei, K.S. Montgomery, S. Srinivasan, D. Roy, F. Huang, S.A. Kreuser, J.L. Gardell, I. Blumenthal, J. Chiefari, M.C. Jensen, C.A. Crane, P.S. Stayton, Arming Immune Cell Therapeutics with Polymeric Prodrugs, Advanced Healthcare Materials, n/a 2101944.
[45] S. Srinivasan, D. Roy, T.E.J. Chavas, V. Vlaskin, D.K. Ho, A. Pottenger, C.L.M. LeGuyader, M. Maktabi, P. Strauch, C. Jackson, S.M. Flaherty, H. Lin, J. Zhang, B. Pybus, Q. Li, H.E. Huber, P.A. Burke, D. Wesche, R. Rochford, P.S. Stayton, Liver-targeted polymeric prodrugs of 8-aminoquinolines for malaria radical cure, J Control Release, 331 (2021) 213-227.
[46] R.B. Greenwald, A. Pendri, C.D. Conover, H. Zhao, Y.H. Choe, A. Martinez, K. Shum, S. Guan, Drug delivery systems employing 1, 4-or 1, 6-elimination: poly (ethylene glycol) prodrugs of amine-containing compounds, Journal of medicinal chemistry, 42 (1999) 3657-3667.
[47] J. Noh, B. Kwon, E. Han, M. Park, W. Yang, W. Cho, W. Yoo, G. Khang, D. Lee, Amplification of oxidative stress by a dual stimuli-responsive hybrid drug enhances cancer cell death, Nature Communications, 6 (2015) 6907.
[48] W.W. Zhang, G. Matlashewski, Immunization with a Toll-like receptor 7 and/or 8 agonist vaccine adjuvant increases protective immunity against Leishmania major in BALB/c mice, Infect Immun, 76 (2008) 3777-3783.
[49] Y. Wu, H. Wen, Z.J. Bernstein, K.M. Hainline, T.S. Blakney, K.L. Congdon, D.J. Snyder, J.H. Sampson, L. Sanchez-Perez, J.H. Collier, Multiepitope supramolecular peptide nanofibers eliciting coordinated humoral and cellular antitumor immune responses, Science Advances, 8 (2022) eabm7833.
[50] A. Olshefsky, H. Benasutti, M. Sylvestre, G.L. Butterfield, G.J. Rocklin, C. Richardson, D.R. Hicks, M.J. Lajoie, K. Song, E. Leaf, C. Treichel, J. Decarreau, S. Ke, G. Kher, L. Carter, J.S. Chamberlain, D. Baker, N.P. King, S.H. Pun, In vivo selection of synthetic nucleocapsids for tissue targeting, Proceedings of the National Academy of Sciences, 120 (2023) e2306129120.
[51] M.M. Westcott, E.A. Clemens, B.C. Holbrook, S.B. King, M.A. Alexander-Miller, The choice of linker for conjugating R848 to inactivated influenza virus determines the stimulatory capacity for innate immune cells, Vaccine, 36 (2018) 1174-1182.
[52] C.B. Fox, R.M. Kramer, V.L. Barnes, Q.M. Dowling, T.S. Vedvick, Working together: interactions between vaccine antigens and adjuvants, Ther Adv Vaccines, 1 (2013) 7-20.

SUPPORTING INFORMATION

Supplemental Methods

Plasmid Construction

Genes sequences encoding the individual nanoparticle subunits of I53-50-V4 were amplified off of the bicistronic gene described in Butterfield et al.[1] and cloned into pET29b+ (Novagen) using the NdeI and XhoI restriction sites. The F24E mutation and additional tags such as C-terminal StrepTags were inserted through PCR and Gibson assembly. Amino acid sequences for all proteins used in this study are provided in Table S3.2.

Protein Expression and Purification

Plasmids were transformed into T7 Express E. coli (New England BioLabs) and expressed overnight at 18°C after cultures were induced with 1 mM Isopropyl β-D-1-thiogalactopyranoside (IPTG). Expression cultures were pelleted by centrifugation and resuspended in lysis buffer composed of 50 mM Tris pH 8.0, 1 M NaCl, 0.75% CHAPS, 20 mM Imidazole, 1 mM DTT, 1 mM PMSF, 0.1 mg/mL DNase, and 0.05 mg/mL RNase. The resuspended pellets were lysed by sonication and centrifuged to yield clarified supernatants containing His-tagged protein of interest. These proteins were purified by immobilized metal affinity chromatography (IMAC) with a HisTrap High Performance column (Cytiva) after binding in lysis buffer as described above and eluted in a buffer containing 50 mM Tris pH 8.0, 1 M NaCl, 0.75% CHAPS, 500 mM Imidazole, and 1 mM DTT. After molecular weight confirmation by SDS-PAGE, IMAC fractions containing the desired proteins were further purified by SEC using a Superdex S200 Increase 10/300 GL

column (Cytiva) in a buffer containing 50 mM Tris pH 8.0, 1 M NaCl, 0.75% CHAPS and stored at -20°C.

Supplemental Figures

Figure S3.1 Biophysical characterization of SMA-co-RhMA radiant star polymers. a, Aqueous SEC-MALS of RSNs, showing dispersity of synthesized polymer nanoparticles. b, Quantification of average molecular mass by SEC-MALS, dispersity (Đ), and hydrodynamic radius by DLS.

A

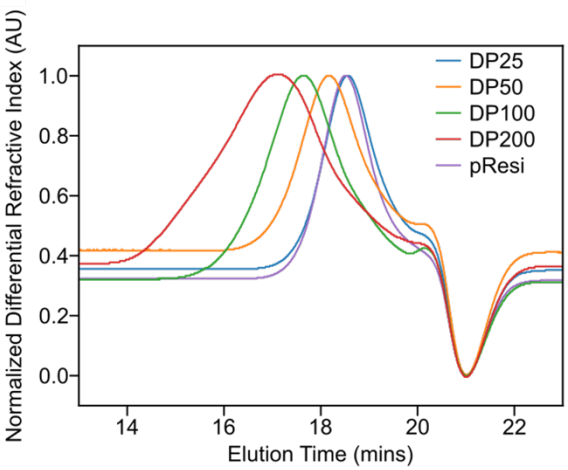

B

	Mn (Da)	Đ	Rh (nm)
DP25	225,900	1.13	10.1
DP50	348,600	1.25	13.7
DP100	670,000	1.45	19.5
DP200	1,720,000	1.72	33.9
pResi	376,000	1.11	9.8

Figure S3.2 Negative stain electron microscopy (nsEM) two-dimensional class averages of various nanoparticles. Selected 2D class averages of (a) empty V5, (b) V5 encapsulating DP25. For each the encapsulated RSP DP25, the twenty most populated classes are shown with no observed aberrant classes.

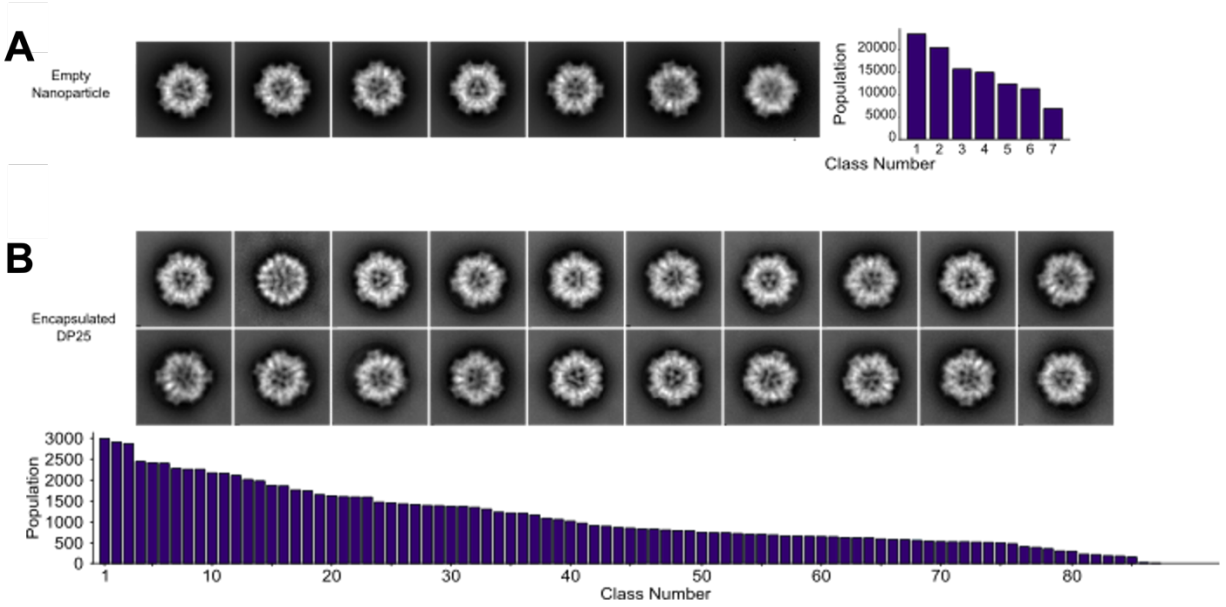

Figure S3.3 Synthesis scheme of Resiquimod prodrug (ResMA) monomer 6.

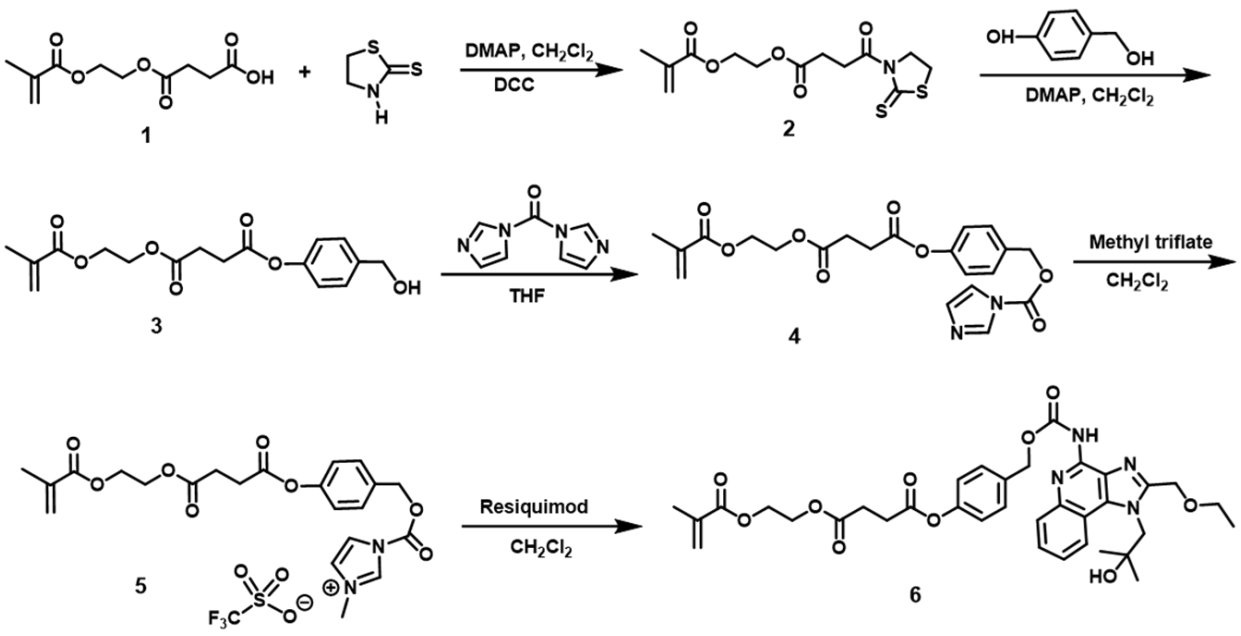

Figure S3.4 ^{1}H NMR spectrum of Resiquimod prodrug monomer ResMA (6) in DMSO-d_6.

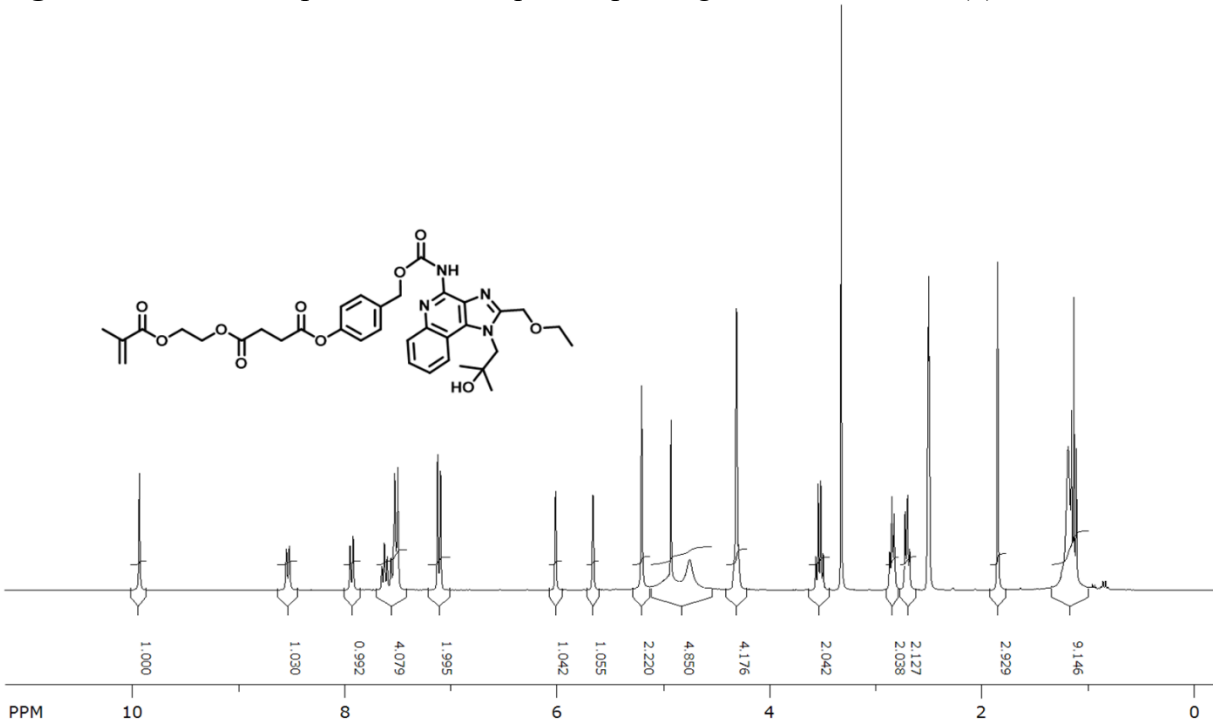

Figure S3.5 ^{1}H NMR spectrum of Resiquimod RSP with fasudil hydrochloride as internal standard in DMSO-d_6. Resiquimod drug weight % on the polymer was calculated via ^{1}H NMR spectroscopy using fasudil hydrochloride as the internal standard. NMR sample contained pResi 20 mg/mL and fasudil hydrochloride 2 mg/mL in DMSO-d_6. The ratio of integration of the resiquimod proton at 8.54 ppm to the fasudil proton at 8.72 ppm provided the resiquimod weight % as 9.72%.

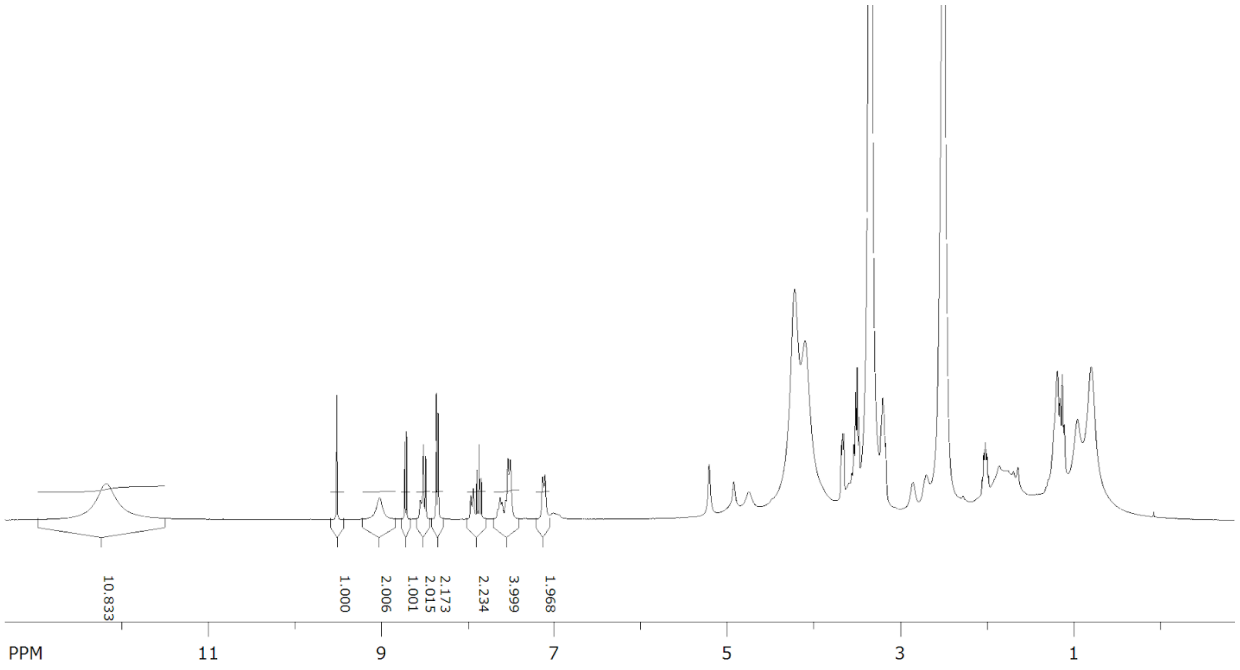

Table S3.1 pResi radiant star drugamer polymerization stoichiometry and results

Monomer	MW [Da]	Target units/chain*	Mol %	Wt %	Calculated units/chain[a]
SMA	230	22.8	91.3	78.3	21.9
ResMA	677	2.0	7.8	19.7	1.9
RhMA	591	0.2	0.9	2.0	0.2
[M]:[CTA]:[I]	Total monomer conversion[a] [%]		Total MW [Da][a]		Drug loading [%]
25:1:0.25	96		376,000		9.74

*polymer core poly(hECT) has 23 branch points (CTAs) and therefore 23 branching chains. With a target degree of polymerization (DP) of 25 for each chain, the sum theoretical DP is 575
[a]based on monomer conversion determined by ^{1}H-NMR

Figure S3.6 Cytokine levels measured from human PBMCs for empty V5 and pResi nanoparticles. Levels of secreted TNF-alpha (A) and IL-6 (B) were measured from human PBMCs incubated with varying amounts of pResi alone (concentrations matched to free resiquimod in Figure 3.5D) or V5 alone. Although no resiquimod is present in the empty V5 samples, the protein concentration used matches that from the corresponding encapsulated pResi samples in Figure 3.5D to control for any stimulation resulting from the nanoparticle itself.

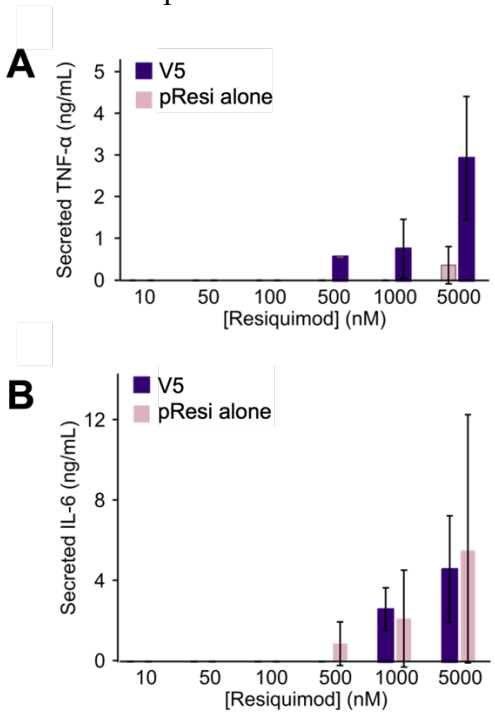

Table S3.2 Amino acid sequences of proteins used in this study.

Protein	Amino Acid Sequence*	Notes
I53-50-V0A	MKMEELFKKHKIVAVLRANSVEEAIEKAVAVFAGGVHLIEITFT VPDADTVIKALSVLKEKGAIIGAGTVTSVEQCRKAVESGAEFIV SPHLDEEISQFCKEKGVFYMPGVMTPTELVKAMKLGHTILKL FPGEVVGPQFVKAMKGPFPNVKFVPTGGVNLDNVCEWFKA GVLAVGVGSALVKGTPDEVREKAKAFVEKIRGCTEHHHHHH	Original I53-50A trimer (Bale et al., 2016)
I53-50-V1A† (I53-50-A.1PT1)	MKMEELFKKHKIVAVLRANSVEEAIEKAVAVFAGGVHLIEITFT VPDADTVIKALSVLKEKGAIIGAGTVTSVEQCRKAVESGAEFIV SPHLDEEISQFCKEKGVFYMPGVMTPTELVKAMKLGHDILKL FPGEVVGPQFVKAMKGPFPNVKFVPTGGVNLDNVCKWFKA GVLAVGVGKALVKGKPDEVREKAKKFVKKIRGCTEGSLEHH HHHH	Engineered I53-50A trimer (Bale et al., 2016)
I53-50-V5A‡ (I53-50-V4A)	MGHHHHHHGGMTMEELFKRHTIVAVLRANSVEEAIEKAVAV FAGGVHLIEITFTVPDADTVIKALSVLKEDGAIIGAGTVTSVDQ CRKAVESGAEFIVSPHLDEEISQFCKEKGVFYMPGVMTPTEL VKAMKLGHDILKLFPGEVVGPQFVKAMKGPFPNVKFVPTGG VNLDNVCKWFKAGVLAVGVGNALVKGNPDKVREKAKKFVKK IRGCTEGSWSHPQFEK	Evolved I53-50A trimer (Butterfield et al., 2017)
I53-50-V0B	MNQHSHKDYETVRIAVVRARWHAEIVDACVSAFEAAMADIG GDRFAVDVFDVPGAYEIPLHARTLAETGRYGAVLGTAFVVNG GIYRHEFVASAVIDGMMNVQLSTGVPVLSAVLTPHRYRDSDA HTLLFLALFAVKGMEAARACVEILAAREKIAAGSLEHHHHHH	Original I53-50B pentamer (Bale et al., 2016)
I53-50-V1B†	MNQHSHKDHETVRIAVVRARWHAEIVDACVSAFEAAMRDIG GDRFAVDVFDVPGAYEIPLHARTLAETGRYGAVLGTAFVVNG GIYRHEFVASAVIDGMMNVQLDTGVPVLSAVLTPHNYDKSKA HTLLFLALFAVKGMEAARACVEILAAREKIAAGSLEHHHHHH	Engineered I53-50B pentamer (Butterfield et al., 2017)
I53-50-V5B‡	MGSSHHHHHHSSGENLYFQGNQHSQKDQETVRIAVVRARW HAEIVDACVSAFEAAMRKIGGERFAVDVFDVPGAYEIPLHAR TLAKTGRYGAVLGTAFVVNGGIYRHEFVASAVIDGMMNVQLD TGVPVLSAVLTPHNYDKSNAKTLLFLALFAVKGMEAARACVEI LAAREKIAAGS	This study

*Purification tags and linkers are underlined.
†Differences in V1 constructs compared to V0 constructs are highlighted in yellow.
‡Differences in V5 constructs compared to V1 constructs are highlighted in green. The F24E mutation in I53-50-V5B relative to I53-50-V4B [1] is highlighted in orange.

[1] G.L. Butterfield, M.J. Lajoie, H.H. Gustafson, D.L. Sellers, U. Nattermann, D. Ellis, J.B. Bale, S. Ke, G.H. Lenz, A. Yehdego, R. Ravichandran, S.H. Pun, N.P. King, D. Baker, Evolution of a designed protein assembly encapsulating its own RNA genome, Nature, 552 (2017) 415-420.

Chapter 4. ARMING IMMUNE CELLS THERAPEUTICS WITH DRUGAMERS[1]

Ciana L López*, Katherine J Brempelis, James F Matthaei, Kate S Montgomery, Selvi Srinivasan, Debashish Roy, Fei Huang, Shannon A Kreuser, Jennifer L Gardell, Ian Blumenthal, John Chiefari, Michael C Jensen, Courtney A Crane, and Patrick S Stayton

[1]*Adapted with permission from López, CL, et al. "Arming Immune Cells with Polymeric Prodrugs." Adv. Healthc. Mater., 2101944 (2021).*

ABSTRACT

Engineered immune cells are an exciting therapeutic modality, which survey and attack tumors. Backpacking strategies exploit cell targeting capabilities for delivery of drugs to combat tumors and their immune-suppressive environments. Here, a new platform for arming cell therapeutics through dual receptor and polymeric prodrug engineering is developed. Macrophage and T cell therapeutics are engineered to express a bioorthogonal single chain variable fragment receptor. The receptor binds a fluorescein ligand that directs cell loading with ligand-tagged polymeric prodrugs, termed "drugamers." The fluorescein ligand facilitates stable binding of drugamer to engineered macrophages over 10 days with 80% surface retention. Drugamers also incorporate prodrug monomers of the phosphoinositide-3-kinase inhibitor, PI-103. The extended release of PI-103 from the drugamer sustains antiproliferative activity against a glioblastoma cell line compared to the parent drug. The versatility and modularity of this cell arming system is demonstrated by loading T cells with a second fluorescein-drugamer. This drugamer incorporates

a small molecule estrogen analog, CMP8, which stabilizes a degron-tagged transgene to provide temporal regulation of protein activity in engineered T cells. These results demonstrate that this bioorthogonal receptor and drugamer system can be used to arm multiple immune cell classes with both antitumor and transgene-activating small molecule prodrugs.

4.1 INTRODUCTION

4.1.1 Cell-based therapies for cancer treatment

Many malignant solid tumors remain a therapeutic challenge due to their active immune suppression, physiochemical barriers, and their metastatic dispersal.[1-3] For example, glioblastoma presents the special blood–brain barrier to therapeutic delivery and is characterized by hypoxic niches, immune downregulation, high interstitial pressure, and diffuse infiltration into the surrounding healthy brain tissue.[4] Current therapeutic strategies for activating immunosuppressive tumor microenvironments (TMEs) have shown rapidly growing impact, including checkpoint inhibitors, though resistance mechanisms have also been noted.[5, 6]

Cell-based therapies have also emerged as a powerful addition to cancer treatment and represent the first actively targeted therapeutics given the ability of immune cells to migrate to tumor cell niches. Engineered chimeric antigen receptor (CAR) T cells have cleared hematological malignancies with complete remission, but have been initially been less active in solid tumor settings due to difficulties in overcoming the immunosuppressive TME.[7-10] Macrophages have also been investigated as cell therapeutics, as they home to primary and metastatic tumors and play an active role in the immune status of the TME.[11-16] We recently showed that genetically engineered macrophages (GEMs) traffic to solid tumors and persist at least 40 days in mouse

models, where they can be engineered to sustainably secrete immunomodulatory protein drugs in that tumor environment.[17, 18] These cell-based immunotherapies can synergize with existing drugs by recruiting endogenous and engineered T cells into a renormalized and immune-stimulated TME.[19-21]

4.1.2 Combining cell therapy with other drug repertoires

Highly mutagenic cancers with unknown antigen markers likely require the combination of therapeutic mechanisms acting in parallel.[22-24] Cellular backpacking mechanisms represent a promising new approach to combining cell therapy with additional protein and small molecule drug repertoires.[25-30] Irvine and co-workers have developed a backpacking system for T cells using covalently loaded nanoparticles that deliver protein drugs that improve the persistence of cell therapeutics in hematological malignancies.[25] Mitragotri and co-workers showed that macrophages could be loaded via endogenous cell receptors with degradable polymeric backpacks containing protein drugs.[26, 29] Kabanov and co-workers showed that macrophages with backpacks could deliver enzymes to the inflamed brain.[27] These approaches merge drug delivery systems developed in the nanomedicine field with cell therapies to improve drug targeting, gain controlled release profiles, and to limit off-target toxicities.[31-35] Such strategies may help overcome reliance of the drug delivery systems on the enhanced permeation and retention mechanisms and add active cell targeting capabilities.[36]

4.1.3 Our approach: Arming immune cell therapeutics with polymeric prodrug backpacks via a single chain variable-fragment

We demonstrate here a new approach to arming immune cell therapeutics with polymeric prodrug backpacks. This platform uses protein and cell engineering to express a bioorthogonal single chain variable fragment (scFv) receptor that resembles the CAR design. This humanized scFv receptor is used to assemble polymeric prodrugs ("drugamers") through a high affinity receptor–ligand interaction (Figure 4.1). The polymeric prodrugs with designable linkers are synthesized using a functionalized monomer approach, providing a new route to incorporating a more sophisticated small molecule drug and linker repertoire, together with the high affinity ligand to direct cell arming, and water solubilizing monomers.[37-40] This cell backpacking system has been first demonstrated with phosphoinositide 3-kinase (PI3K) inhibitor drugamers to arm GEM therapeutics. The versatility of this arming system was further demonstrated by engineering T cells with the same construct. To show the additional versatility of the small molecule drug repertoire of drugamers, we armed the engineered T cells with polymeric prodrugs of CMP8. CMP8 is a small molecule estrogen analog that controls degradation domain (degron)-tagged transgene protein products. The CMP8 polymeric prodrug system was thus designed to provide temporal control of a protein activity in T cells coengineered with the antifluorescein scFv receptor and the degron-tagged transgene.[41] Taken together, these studies demonstrate the potential of this cell backpacking system to arm multiple classes of immune cell therapeutics, and with polymeric prodrugs of multiple classes and activities. The antifluorescein receptor was designed with an additional surface tag, and thus has additional functionality for future ex vivo cell selection, in vivo cell tracking, and in vivo cell ablation.[42-45]

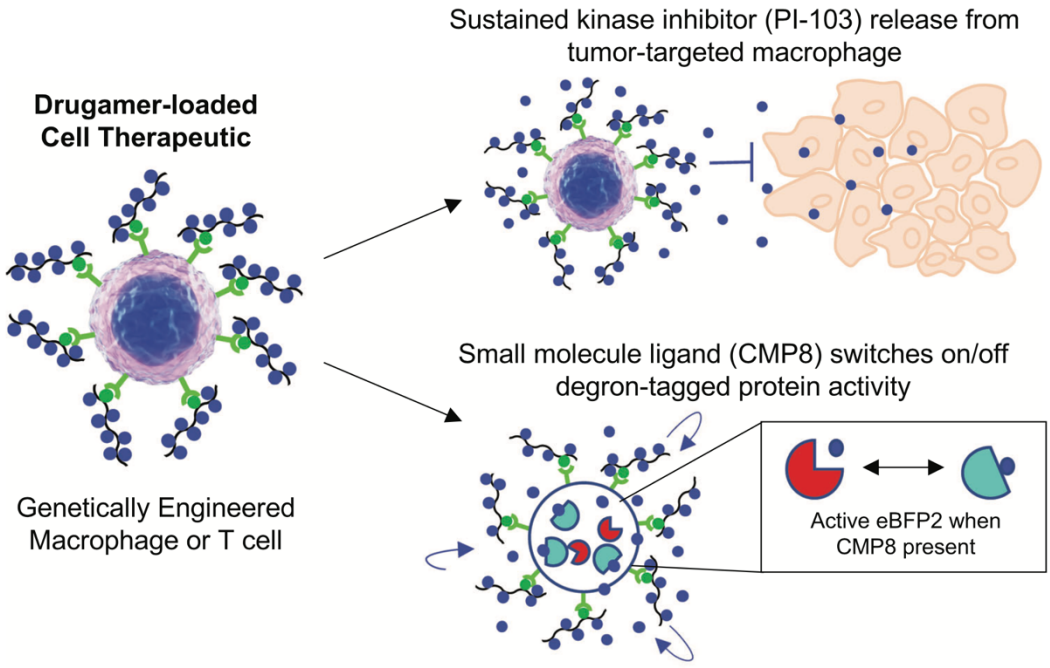

Figure 4.1 Schematic mechanism of polymeric prodrug "drugamer" loading on engineered cell therapeutics. Immune cells are engineered with a bioorthogonal and humanized scFv receptor that binds to polymeric prodrugs via a high affinity receptor–ligand binding reaction. The polymeric prodrugs sustain the release of small molecule drug cargo via tunable linker design and selection. The versatility of this platform was demonstrated by arming genetically engineered macrophage cells with polymeric prodrugs of a PI3K kinase inhibitor PI-103 (upper right), and by arming engineered T cells with a different drugamer that releases CMP8 to switch on and off the model degron-tagged eBlue fluorescent protein 2 (eBFP2) activity (lower right).

4.2 RESULTS AND DISCUSSION

4.2.1 PI3K inhibitor selection

Aberrations in the PI3K pathway are among the most frequent events in solid cancers, driving tumorigenesis by upregulating cell proliferation and migration and dysregulating apoptosis.[46] Development of kinase inhibitors has led to promising drug candidates that aim to prevent on-target, off-tumor side effects compared to conventional chemotherapies, which is important when navigating complex interactions between tumor and healthy tissues.[47, 48]

Imatinib mesylate (Gleevec), a tyrosine kinase inhibitor, is a highly effective standard of care treatment for first- line treatment of chronic myeloid leukemia, with survival at 95% over 6 years.[49] Additionally, alpelisib (Piqray) was recently the first FDA approved PI3K inhibitor for HR+/HER2− breast cancer after demonstrating significantly prolonged progression-free survival.[50] However, the broad adoption of PI3K pathway inhibitors for clinical use has been limited due to poor solubility and pharmacokinetic properties as well as dangerous inhibition of insulin signaling causing hyperglycemia.[51, 52] Drugamer therapeutics and cell-mediated delivery strategies may help overcome these solubility and pharmacokinetic property issues to open new uses for these drug candidates.

In our studies, four kinase inhibitor drug candidates were screened for eventual loading onto GEMs via drugamers: PI-103 (pan-class 1 PI3K and mTOR inhibitor), BKM-120 (pan-class 1 PI3K inhibitor), GSK-2636771 (PI3Kβ inhibitor), and dasatinib (pan-class tyrosine kinase inhibitor). Drug selection was dependent on three criteria: 1) a clinical stage kinase inhibitor that is broadly applicable in multiple types of human cancers, 2) monomer synthesis feasibility, and 3) clinical issues that might be improved by the cellular delivery method (e.g., poor solubility and pharmacokinetic properties, off-target side effects that could be improved by more targeted delivery and controlled local release kinetics from the polymeric prodrug). PI-103 had the lowest effect on macrophage viability and was selected for further studies based also on its suitability for prodrug monomer synthesis (Figure 4.2). PI-103 represents a promising drug for future studies because it inhibits both PI3K and mTOR, indicating its potential to potently inhibit mutationally distinct cancer cells at multiple pathway points.[53] PI-103 has antiproliferative effects on cancer cells, and there is also evidence that PI-103 and other PI3K inhibitors can polarize tumor associated macrophages (TAMs) toward a proinflammatory phenotype by inhibition of p110δ/λ.[54, 55]

TAMs are a key non-neoplastic tumor resident, for example, making up 30–50% of cells in glioblastoma tumors and producing stromal factors that change the local milieu facilitating neoplastic invasion.[11-14, 56] This additional drug benefit could prove useful in in vivo settings to repolarize resident TAMs or maintain the proinflammatory phenotype of the GEM carrier.

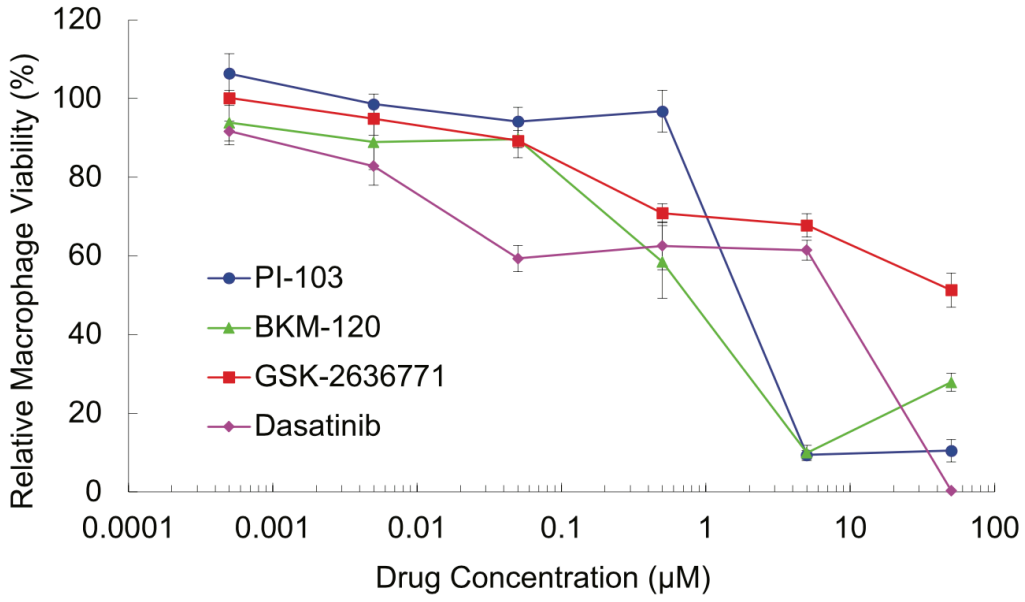

Figure 4.2 Kinase inhibitor drugs including PI-103, BKM-120, GSK-2636771, and dasatinib were screened for toxicity against human monocyte-derived macrophages and normalized to DMSO vehicle. Viability was measured as a function of relative ATP production. PI-103 (blue circle); BKM-120 (green triangle); GSK-2636771 (red square); dasatinib (pink diamond). Data are presented as mean ± SD, baseline corrected (n = 4).

4.2.2 Synthesis and characterization of PI-103 drugamer

Reversible addition–fragmentation chain-transfer (RAFT) synthesis was used to control the incorporation ratios of the sterically complex prodrug and fluorescein monomers.[39, 40, 57] The chemical structure and synthetic route for the PI-103 prodrug monomer are provided in Figure 4.3A. The PI-103 and fluorescein monomer syntheses were confirmed by ^{1}H NMR (Figures S1B and S2B, Supporting Information) and mass spectrometry analyses (Figure S1C and S2C,

Supporting Information). The RAFT copolymerization of PI-103 methacrylate with PEGMA950, fluorescein and rhodamine methacrylate yielded a final PI-103 drug weight percentage of 13.25 wt% (Table S3A and Figure S3B,C, Supporting Information). The degree of polymerization (DP) of PEGMA950, PI-103-MA, FIMA, and RhMA were 15, 6, 1.4, and 1, respectively (Table S3A, Supporting Information). The approximate molecular weight of polymer was determined to be 19 kDa based on the monomer conversion (^{1}H NMR), and GPC (refractive index) trace showed relatively unimodal molecular weight distribution of the polymer chains (Figure S3D, Supporting Information) despite the polymer consisting of four monomers with various functional groups. GPC comparison against a standard PEGMA950 polymer (MW = 20,000 Da) confirmed the ^{1}HMR molecular weight approximation despite rhodamine interference with light scattering detectors.

4.2.3 Sustained release kinetics and activity of PI-103 with the fluorescein-tagged drugamer

A key advantage of the drugamers as a cell-targeted cargo is the tunability of drug release kinetics to fit their anticancer mechanism, or with cues from the tumor microenvironment (e.g., drug cleavage by enzymes in the tumor matrix).[39, 58] PI-103 was hydrolyzed from drugamer in human serum over 15 days (Figure 4.3B). By day 1, 15 ± 3% of PI-103 was released. By day 4, 55 ± 14% had been released. By day 8, 83 ± 15% had been released and by day 18, 100 ± 3% had been released. These release kinetics could be further optimized for faster or slower release with alternative linkers or polymer architectures, depending on the therapeutic application and drug pharmacokinetic requirements.[37, 59] A phospho-blot activity assay confirmed that the activity of PI-103 was maintained after hydrolysis (Figure 4.3C). Similar to free drug treatment, the PI-103 released from the drugamer inhibited Akt phosphorylation downstream of p110 and mTOR signaling in the U87 glioblastoma cell line.

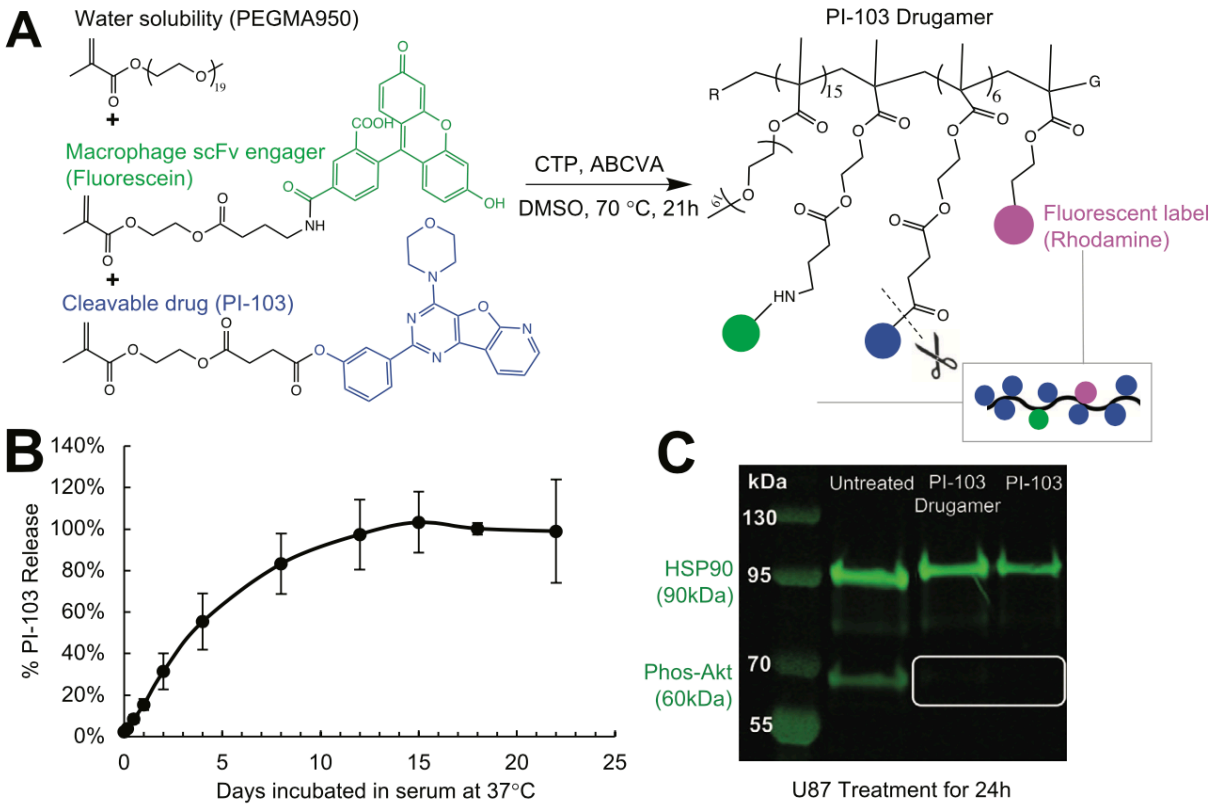

Figure 4.3 Synthesis and characterization of PI-103 drugamer. A) Drugamer synthesis by reversible addition–fragmentation chain-transfer (RAFT) polymerization with 4-cyano-4-(phenylcarbonothioylthio)-pentanoic acid (CTP) and 4,4′-azobis(4-cyanovaleric acid) (ABCVA) and by incorporation of methacrylate monomers: polyethylene glycol, molecular weight 950 (PEGMA950); PI-103 kinase inhibitor (blue); and fluorescein ligand for assembly and binding to scFv receptor (green); labeled with rhodamine (pink). B) PI-103 release kinetics from drugamer over 22 days incubated at 37 °C in 50% human serum. Experiment performed in triplicate and data expressed as mean with standard deviation bars. C) PI-103 inhibition of phospho-Akt in U87 cells was characterized following 24 h incubation with parent PI-103 and the PI-103 drugamer and compared to control untreated cells.

4.2.4 Genetically Engineered Macrophages (GEMs) express an antifluorescein receptor and direct stable surface assembly of fluorescein-labeled drugamers

Bioorthogonal cell receptors were designed by fusion of an antifluorescein scFv (FITC-E2) and truncated EGFRt, Her2tG, or CD19t membrane proteins lacking intracellular signaling domains. Flexible Gly-Gly-Gly-Ser (GGGS) linkers were investigated either alone or with an

additional IgG4 hinge to add stability to the scFv.[42-45, 60] These fusion constructs retain all the original characteristics of the surface receptors, while endowing cells with the ability to bind fluorescein-tethered molecules, thus equipping engineered cells with tags for ex vivo cell selection, in vivo cell tracking, and in vivo cell ablation.[42-45] FITC-E2 has been used in multiple CAR T cell applications and is approved for clinical trials.[61, 62] Additionally, a FITC-E2-IgG4hinge-CD28TM was also built representing a standard CAR with no signaling domains.[63] All sequences use the human granulocyte-macrophage colony stimulating factor receptor signal sequence (GMCSFRss) to direct surface expression.[42] Six constructs (AntiFl α–ζ) were built as described in Table S4C in the Supporting Information, with four of six constructs providing functional display of FITC-E2 (Figure S4A, Supporting Information).

The highest expression of FITC-E2 in GEMs was seen by AntiFl construct γ and δ, followed by β, then ζ. AntiFl-α and AntiFl-ϵ did not have detectable scFv expression, similar to control CD19t. Of the constructs tested, AntiFl-ζ had highest drugamer loading (Figure S4B, Supporting Information), and thus was selected for subsequent experiments. An optimal multiplicity of infection (MOI) for AntiFl-ζ was determined by lentiviral titration as seen in Figure 4.4B with an optimal transduction efficiency at 250 lentiviral particles (LPs) cell^{-1} with greater than 99% FITC-E2+ and with only slight improvements to 100% at 500, 750, and 1000 LPs cell^{-1}.

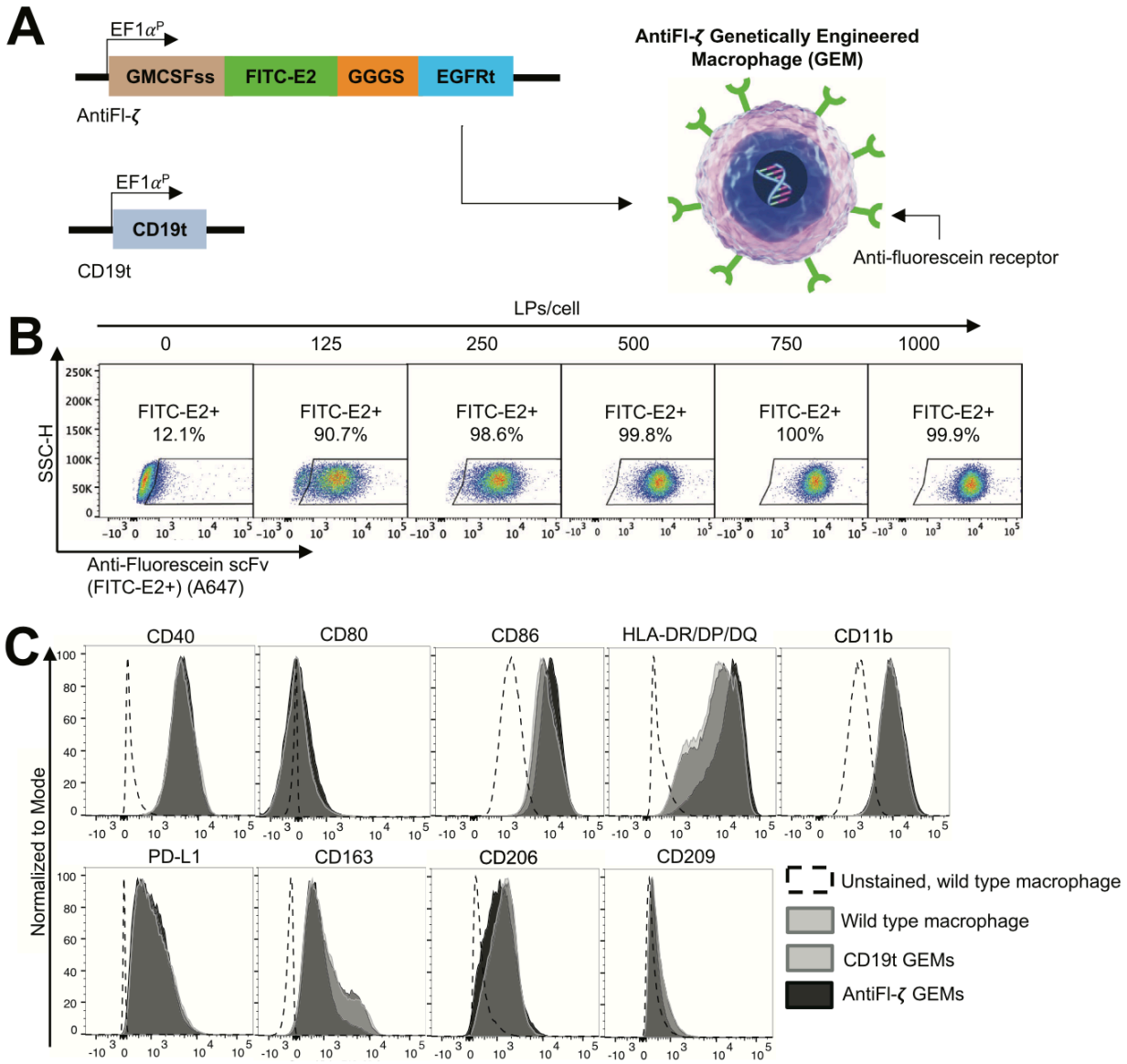

Figure 4.4 Lentiviral transduction of primary human macrophages provides high and bioorthogonal expression of AntiFl-ζ. A) The AntiFl-ζ expression construct is composed of an antiflourescein scFv (FITC-E2) linked by a glycine repeat to an EGFRt transmembrane domain and surface tag. The control construct consists of a truncated CD19 tag without FITC-E2. Constructs were cloned into an epHIV7.2 lentiviral backbone and cotransfected into 293T cells with packaging plasmids for synthesis of lentiviral particles (LPs). Transduction of patient-derived macrophages yields the AntiFl-ζ GEMs with the bioorthogonal surface receptors for drugamer assembly. B) AntiFl-ζ expression by GEMs occurs with high transduction efficiency around 250 LPs per cell (99% FITC-E2+) and increases with increasing LPs per cell. Representative plots from one donor ($n = 3$) are shown. C) Comparison of untransduced, wild type macrophages, CD19t GEMs, and AntiFl-ζ GEMs expression of characteristic macrophage phenotype markers (CD40, CD80, CD86, HLA-DR/DP/DQ, CD11b, PD-L1, CD163, CD206, and CD209) 7 days after

lentiviral transduction shows minimal changes to cell phenotype following lentiviral transduction. Representative results from one donor are shown (4 patient donor-derived macrophages were studied in total).

Expression of macrophage-characteristic (CD11b, PD- L1, and HLA-DR/DP/DQ) and proinflammatory or anti-inflammatory/TAM-like phenotypes (costimulatory molecules CD40, CD80, CD86, and scavenger receptors CD163, CD206, CD209, respectively) was similar for AntiFl-ζ GEMs, control GEMs that only expressed a CD19t surface tag (no scFv), and wildtype macrophages (GEM constructs shown in Figure 4.4A). This indicated that no significant modifications to macrophage phenotype were caused by AntiFl-ζ expression.

A dose titration of PI-103 drugamer binding to GEMs showed that AntiFl-ζ GEMs had consistently higher drugamer loading compared to CD19t control GEMs, indicating scFv-specific loading (Figure 4.5A; Figure S5A, Supporting Information). Above 200×10^{-9} M drugamer (rhodamine-tagged for detection), AntiFl-ζ and CD19t GEM populations displayed increasing fluorescent signal indicating AntiFL-ζ receptor saturation and nonspecific drugamer binding (51,120 ± 10,614 cells per treatment group). From these saturation data, it was approximated that 500,000 AntiFl-ζ GEMs were loaded with 3.8 μg PI-103 drugamer, equating to 0.5 μg PI-103. Confocal imaging confirmed the colocalization of drugamers to AntiFL-ζ GEMs as shown in Figure S5B in the Supporting Information and compared to untransduced control macrophages one day after drugamer binding. Comparison of Z-slices indicated a higher degree of drugamer surface display for AntiFL-ζ GEMs compared to control macrophages. Drugamer remained bound to AntiFl-ζ GEMs for ten days in vitro with surface fluorescence signal remaining stable near 80%, indicating that the majority of drugamer was surface bound (Figure 4.5B,C). It is possible that the slight increase in rhodamine fluorescence from our drugamer-bound GEMs is due to the inherent increase in autofluorescence of cells with time and/or because cells bind drugamer as neighboring

cells die. While the drugamer binding interaction proved stable in vitro, there are stronger affinity scFvs that can be exploited for future in vivo applications.[64]

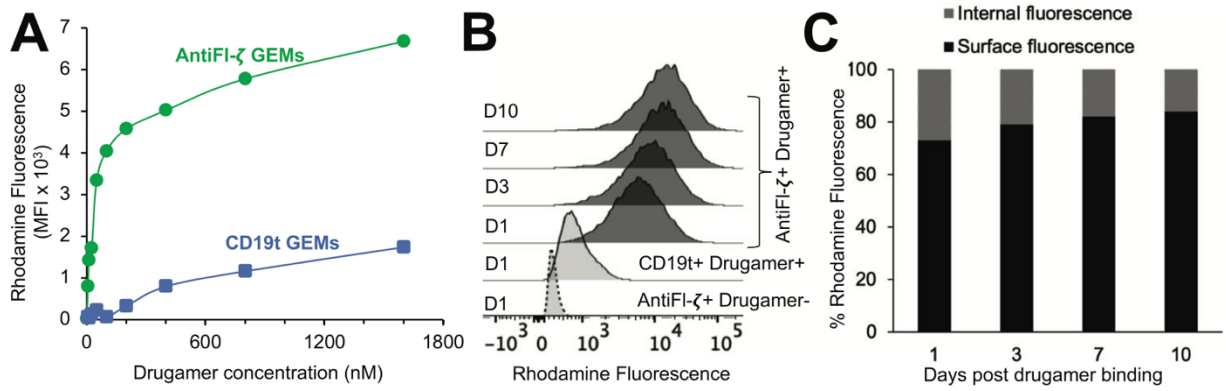

Figure 4.5 Loading and characterization of genetically engineered macrophages (GEMs) with rhodamine-labeled drugamer. A) Cell loading was measured with antifluorescein scFv (AntiFl-ζ) and control truncated CD19 (CD19t) GEMs (no scFv) as a function of drugamer concentration to determine the binding curve (AntiFl-ζ GEMs, green circle; CD19t GEMs, blue square; n = 3, representative plot corrected against baseline fluorescent levels (0.527 × 103 MFI)). B) PI-103 drugamer remains bound to GEMs for up to 10 days in cell culture as evidenced by retention of rhodamine fluorescence. Data shown are representative results from one donor (n = 3; 2nd and 3rd replicates conducted with control drugamer). C) The level of PI-103 drugamer internalization by the AntiFl-ζ GEMs was measured after acid-salt washout of surface-bound polymer and determination of rhodamine (Rh) fluorescence loss. Results determined that ≈80% of drugamer remained bound on the AntiFl-ζ GEMs over 10 days. Data shown are representative results from one donor (n = 3).

4.2.5 Sustained Release of PI-103 from Drugamer Extends Proliferative Inhibition of U87 Glioblastoma Cell Line Compared to Parent Drug

We hypothesized that the 5×10^{-6} M dose of PI-103 would be less effective than the sustained release of drug from 5×10^{-6} M drugamer (equivalent to 30×10^{-6} M PI-103 at 100% release, and with 12.4% released by 18 h, 42.8% by 72 h, 56.3% by 96 h, and 69.8% by 120 h as determined in Figure 3B). As controls, U87s were treated with 10×10^{-6} M nocodazole, a potent mitotic inhibitor that rapidly diminishes all cell activity, and 5×10^{-6} M control drugamer lacking the PI-103 monomer that should have no effect on U87 viability. Treatment with the PI-103

drugamer led to significant and sustained suppression of U87 ATP activity for up to 5 days compared to treatment with parent PI-103 drug as shown in Figure 4.6 (72 h, $^{**}p = 0.007$; 96 h, $^{**}p = 0.002$; and 120 h, $^{**}p = 0.0013$). The nocodazole positive control completely eliminated U87 activity and the control drugamer had no significant effect. Because PI-103 undergoes rapid metabolism in vivo, this prodrug approach may improve the pharmacokinetics and therapeutic efficacy.[53, 64] Furthermore, PI-103 is very poorly water soluble and our polymer formulation improves this material property.

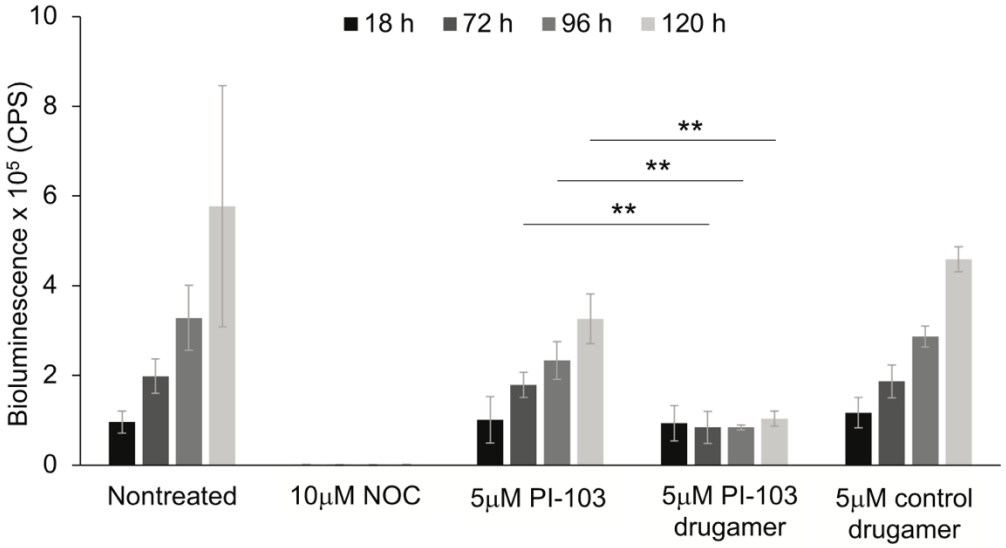

Figure 4.5 The longitudinal anti-U87 glioblastoma tumor cell activity of the PI-103 drugamer was compared to parent PI-103 drug, to control drugamer that does not contain PI-103, and to nontreated and nocodazole (NOC; a potent mitotic inhibitor drug) controls. The PI-103 drugamer was incubated at 5 × 10−6 M polymer (corresponding to 30 × 10−6 M PI-103 at 100% release), and significantly inhibited U87 ATP production for the five days characterized compared to parent PI-103. The control drugamer had no significant inhibitory effect on cells. Average bioluminescence per well was measured in counts per second (CPS) and scaled with relative ATP production for each U87 treatment group. Data are presented as mean ± SD, baseline corrected (n = 4). Welch's t-tests were used to determine statistical significance between groups at a specific time point ($^{*}p < 0.05$, $^{**}p < 0.01$, and $^{***}p < 0.001$).

4.2.6 Arming T Cells Using the scFv Receptor–Drugamer System to Deliver Transgene Activating Small Molecule Drugs as Gene Circuit and Protein Switches

The versatility and modularity of the polymeric prodrug backpacking platform was shown by engineering the T cells, H9 and Jurkat cells, with the AntiFl-ζ receptor. The AntiFl-ζ -expressing T cells were loaded with a drugamer carrying the estrogen analog, CMP8 (H9 cell loading shown in Figure 4.6A; Jurkat T cell loading shown in Figure S8 in the Supporting Information).[65] The CMP8 monomer and drugamer synthetic details are described in Figures S6 and S7 in the Supporting Information. The AntiFl-ζ Jurkat T cells were cotransduced to express the model blue fluorescent protein (eBFP2) conjugated to a degradation-domain (degron; eBFP2-ERdd). This degron is based on the human Estrogen Receptor alpha ligand binding domain (UNIPROT P03372). It has been given a suite of mutations that confers both reversible instability to conjugated transgene products in the absence of activator drug and renders the domain insensitive to endogenous human estradiol. The degron can be stabilized by estrogen analogs such as tamoxifen and the nonbiological estrogen analog, CMP8.[41] The AntiFl.eBFP2-ERdd Jurkat T cells were loaded with CMP8 drugamer and the ability of released CMP8 to activate eBFP2 was tested over the course of 24 h. The fraction of eBFP2 positive AntiFl.eBFP2-ERdd Jurkat T cells steadily increased from 9.9% to 38.4% (Figure 4.6B) demonstrating the ability of the released CMP8 to stabilize and activate intracellular eBFP2- ERdd. We envision that this type of arming of activator prodrug could be useful in switching on proteins produced from gene circuits and for controlling the duration of that activity by eventual depletion of CMP8.

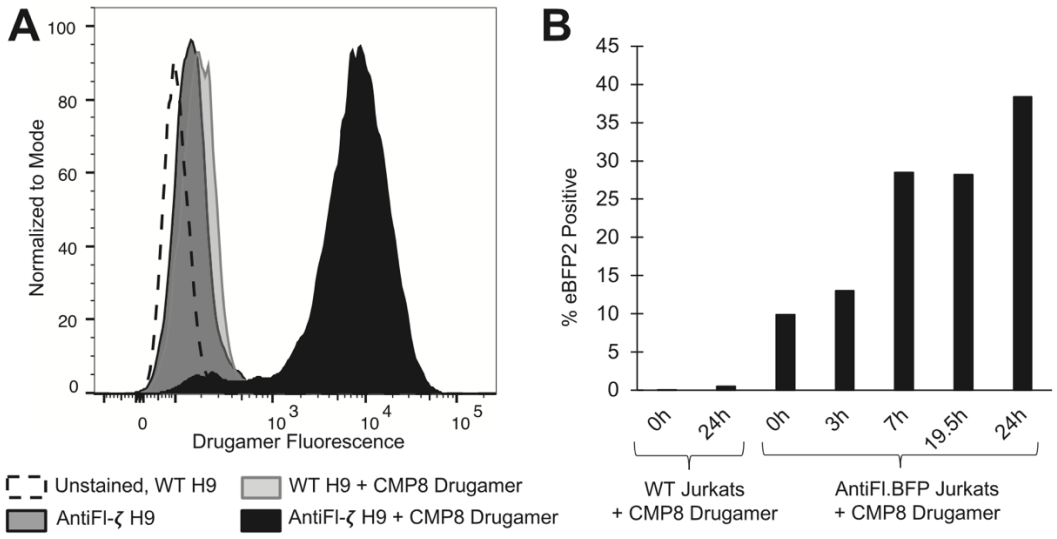

Figure 4.6 Arming engineered T cells with CMP8 drugamer activates the degron-tagged transgene, eBFP2-ERdd, and increases intracellular protein (eBFP2) fluorescence activity through sustained local drug release. A) The T cell line, H9, was first used to validate the versatility of AntiFl expression and function in different immune cell classes. AntiFl H9s were loaded with CMP8 drugamer and drugamer fluorescence was compared against drugamer-loaded wild type (WT) and AntiFl H9 controls with no drugamer loading (n = 1; 28,311 ± 12,390 cells total analyzed per group). Figure S8 in the Supporting Information shows loading of Jurkat T cells similarly. B) Jurkat T cells were cotransduced with AntiFl and a transgene encoding for a degron-tagged fluorescent protein, eBFP2 (AntiFl.BFP Jurkats). Arming of AntiFl.BFP Jurkats with CMP8 drugamer resulted in increased eBFP2 fluorescence detection induced by the gradual release of CMP8 from the drugamer when compared to a CMP8 drugamer-loaded WT Jurkat control. eBFP2 fluorescence detection from CMP8 drugamer-loaded AntiFl.BFP Jurkats increased steadily over 24 h (n = 1; 21,559 ± 10,833 cells total analyzed per group, %eBFP2 positivity gated on 0 h WT Jurkat).

4.3 CONCLUSIONS

A bioorthogonal receptor approach was shown to assemble polymeric prodrugs on GEMs and T cells as a new type of cell backpacking platform. The antifluorescein receptor was optimized and could be expressed by GEMs without altering their characteristic phenotype and polarization. The GEMs were armed with drugamers that control and sustain the release of targeted PI3K kinase inhibitors through the polymeric prodrug approach. The drugamer-based

backpacking platform was shown to be highly versatile by engineering and arming T cells via the same humanized scFv receptor. The modularity of the prodrug cargo was shown by designing drugamers with the CMP8 small molecule, which was shown to regulate a protein product from a synthetic gene circuit in degron-engineered T cells. This approach could be used to control the induction and duration of such engineered T cell or macrophage circuits through the tunability of the drug release profiles. These results are a first step to exploiting this new cell arming platform to improve cell therapy functionality through combination kinase inhibitor, chemotherapeutic, and cell regulatory drugs in a variety of cancer or infectious disease applications.

4.4 METHODS

Reagents: Reagents were purchased from Sigma-Aldrich unless otherwise specified. Rhodamine B methacrylate was prepared by following the previously published procedure.[66] Polyethylene glycol methacrylate (PEGMA950) monomer was purified using basic aluminum oxide (Brockmann l) before polymerization. Chain transfer agent (CTA), 4-cyano-4-(phenylcarbonothioylthio)pentanoic acid (CTP), and initiator, 4,4′-azobis(4-cyanovaleric acid) (ABCVA, V501), were used without further purification. Fasudil hydrochloride was purchased from eNovation Chemicals. Spectra/Por regenerated cellulose dialysis membranes were purchased from Spectrum Laboratories. Sephadex G-25 prepacked PD10 columns were obtained from GE Healthcare Life Sciences.

Synthesis of PI-103 Prodrug and FITC Monomers: Synthetic schemes in Figures S1A and S2A in the Supporting Information were followed to obtain PI-103 prodrug monomer and fluorescein monomer, respectively. PI-103 monomer was synthesized by conjugating the phenolic hydroxyl

group of PI-103 to the carboxylic end of mono-2-(methacryloyloxy)ethyl succinate (SMA) using *N*-(3-dimethylaminopropyl)-*N*′-ethylcarbodimide hydrochloride (EDCI.HCl) as the coupling agent and *N*,*N*-dimethylpyridin-4-amine (DMAP) as the base. Fluorescein monomer was synthesized by a four-step synthetic pathway starting from 4-aminobutanoic acid using carbodiimide/DMAP coupling chemistry. The amine group was first protected with Boc group, and then coupled with 2-hydroxyethyl methacrylate (HEMA). Deprotection of the Boc group yielded amine terminated methacrylate derivative which upon conjugation with NHS activated 5-carboxyfluorescein afforded the fluorescein monomer. All the synthesized monomers and intermediates were purified by precipitation and/or silica gel column chromatography techniques. The successful synthesis and purity of the monomers were confirmed and characterized by ^{1}H NMR spectroscopy (Bruker Avance spectrometers 300 MHz) and electrospray ionization-mass spectrometry (Bruker Esquire ion trap mass spectrometer) (Figures S1B,C and S2B,C, Supporting Information).

RAFT Synthesis of PI-103 Drugamer: Copolymerization of (poly (PEGMA950-*co*-PI103-*co*-FIMA-*co*-RhMA)) (referred to PI-103 drugamer) was conducted in DMSO-*d*6 under a nitrogen atmosphere using CTP as the CTA and ABCVA as the radical initiator. The initial monomer/CTA ratio ($[M]_0/[CTA]_0$) was 25:1 and the initial CTA to initiator ratio ($[CTA]_0/[I]_0$) was 10:2.5. The molar ratio of PEGMA to PI103-MA to FIMA to RhMA monomers was 16.25:6.25:1.5:1. To a 5 mL round bottom flask were added PI-103 methacrylate (53 mg, 0.1849 mmol), PEGMA950 (234 mg, 0.4667 mmol), FIMA (13 mg, 0.1969 mmol), RhMA (8.9 mg, 0.1969 mmol, CTP (4 mg, 0.0339 mmol), ABCVA (V501) (1 mg, 0.0068 mmol), and DMSO-*d*6 (2127 μL). CTP and ABCVA stock solutions were prepared at 67.62 and 16.96mg mL^{-1}, respectively, before added to

the polymerization flask. The flask was sealed, and the reaction mixture was degassed by bubbling nitrogen into the solution for 35 min and was then placed in a preheated oil bath at 70 °C for 21 h. The reaction was stopped by introducing oxygen by removing the septa and cooling the solution with a mild stream of air. All crude polymers were analyzed by ^{1}H NMR spectroscopy. The degree of polymerization (DP) and monomer conversion were obtained from $T_{initial}$ and T_{final} ^{1}H NMR spectrums of the crude solution. The crude polymer was then isolated by precipitation into diethyl ether (two times). The polymer was further washed in ether two times. Next the polymer was dissolved in DMSO (10 mL) and dialyzed against DMSO (120 h), and then cold nanopure water (4 °C, 40 h) using a regenerated cellulose dialysis membrane with a molecular weight cut-off (MWCO) of 6–8 kDa (Spectrum Labs). Following dialysis, the polymer solution was then lyophilized and was further purified with PD-10 desalting column(s) (Sephadex G-25 M). The purified polymer was characterized by ^{1}H NMR spectroscopy for monomer incorporation and its PI-103 drug wt% was determined using an internal standard (Fasudil HCl) (Figure S3B,C, Supporting Information). The drug wt% was calculated by comparing the integration between PI-103 proton at 7.2 ppm and the Fasudil HCl proton at 9.5 ppm in the 1H NMR spectrum. A gel permeation chromatography (GPC) trace was collected using a Tosoh SEC TSK-GEL α-3000 and α-e4000 columns (Tosoh Bioscience) connected in series to an Agilent 1200 Series Liquid Chromatography System and Wyatt Technology miniDAWN TREOS, 3 angle MALS light scattering instrument and Optilab TrEX, refractive index detector. As an eluent, HPLC-grade DMF containing 0.1 wt% LiBr at 60 °C was used as the mobile phase at a flow rate of 1 mL min^{-1}. A control drugamer was synthesized with similar composition, except lacking the PI-103 monomer. ^{1}H NMR confirmed synthesis and purification as shown in Figure S3G in the Supporting Information.

PI-103 Release Kinetics from Drugamer: High-performance liquid chromatography (HPLC) analysis of PI-103 was conducted using an Agilent 1260 Quaternary HPLC Pump, Agilent 1260 Infinity Standard Automatic Sampler, Agilent 1260 Infinity Programmable Absorbance Detector, and Agilent ChemStation software. The UV detector was operated at 285 nm. A Zorbax SB-C18 analytical column (Narrow Bore RR; 2.1 × 100 mm; 3.5 μm; Agilent Technologies) was used at ambient temperature with mobile phases of 1% aqueous acetic acid with 5% acetonitrile and 1% acetic acid in acetonitrile. A 40 min gradient from 15% to 90% organic phase was operated at a flow rate of 0.25 mL min^{-1} and with a 15 μL injection volume. To determine the PI-103 drugamer release kinetics, 50×10^{-6} M polymer (equivalent to 250×10^{-6} M PI-103 at 100% release, based on molar feed ratio) was incubated in 50% aqueous human pooled serum (Sigma) at 37 °C for 22 days. At 0, 0.167, 0.5, 1, 2, 4, 8, 12, 15, 18, and 22 days samples were stored at −80 °C. At the end of the study, PI-103 was recovered from the samples by 2:1 acetonitrile extraction at 4 °C and centrifugation at 18 000 rcf, 4 °C for 20 min. Supernatant containing extracted PI-103 was filtered through a Millex GV low protein binding PVDF filter (0.22 μm; Millipore). The amount of PI-103 released over time was quantified by comparing the area under the curve (AUC) against a PI-103 (Selleck Chemicals) standard curve (Figure S3F, Supporting Information). Liquid chromatography tandem mass spectrometry (LC/MS) was used to confirm peak identity (PI-103, m/z = 349.2).

CMP8-SMA Monomer and Polymer Synthesis: CMP8-SMA monomer was synthesized via HBTU coupling chemistry and described in detail in Figure S6 in the Supporting Information. CMP8 polymer was synthesized by RAFT polymerization and described in detail in Figure S7 in the Supporting Information.

Cell Culture: U87 cells (HTB-14; ATCC) were cultured in Dulbecco's Modified Eagle Medium (DMEM; Gibco) supplemented with 1% GlutaMax (Gibco), 10×10^{-3} M HEPES (Gibco) and 10% fetal bovine serum (FBS; Peak Serum) and passaged prior to formation of neurospheres. Jurkat T cells (TIB-152; ATCC) and H9 cells (HTB-176; ATCC) were cultured in RPMI 1640 (Gibco) supplemented with 2×10^{-3} M l-glutamine (Cell-gro), 25×10^{-3} M HEPES (Irvine Scientific), and 10% heat-inactivated FBS (Hyclone).

Phospho-Blot Assay: U87s were irradiated with 10,000 radians to arrest proliferation, followed by plating at 500,000 cells in 6-well plates. Following adherence, cells were treated with 5×10^{-6} M PI-103 or, to account for gradual release of drug from the polymer backbone, 136×10^{-6} M PI-103 drugamer, resulting in an approximately similar amount of PI-103 released by 24 h. After treatment, cells were lysed with RIPA buffer supplemented with 50× HALT protease/phosphatase inhibitors and EDTA (Thermo Fisher Scientific) and stored at −80 °C. After running on a NuPAGE 4–12% Bis Tris Gel (Invitrogen), proteins were transferred to a 0.2 μm nitrocellulose membrane (Invitrogen) and incubated with the following primary antibodies overnight at 4 °C and according to manufacturer's instructions: HSP90 rabbit mAb (1:1000, Cat# 48775), pan-Akt mouse mAb (1:2000, Cat# 29205), and phos-Akt rabbit mAb (Ser473, 1:2000, Cat# 40605), all from Cell Signaling Technology (CST). Membranes were incubated with Li-Cor IRDye 800CW goat anti-rabbit IgG (Cat# 925-32211) and 680RD goat antimouse IgG (Cat# 925- 68070) secondary antibodies (1:5000) and image analysis was performed using LI-COR Odyssey 9120 Imaging System and LI-COR Image studio software.

U87 Drugamer Activity Assay: U87 cells were plated at 2000 cells in a 96-well plate and rested overnight before treatment with 10×10^{-6} M nocodazole (Sigma), or 5×10^{-6} M PI-103, PI-103 drugamer, or control drugamer (FlTC-Rhodamine-PEGMA950) at 37 °C. At 18, 72, 96, and 120 h, cell viability was assessed by CellTiter-Glo Luminescent assay (Promega) in quadruplicate. The bioluminescence signal was measured by a VICTOR X3 Multilabel Plate Reader (Perkin Elmer).

Macrophage/GEM Culture: Human monocyte-derived macrophages were generated by CD14 isolation from peripheral blood mononuclear cells (PBMCs) as previously described and using healthy donor peripheral blood products (BloodWorks Northwest).[17, 18] CD14+ cells were selected using an EasySep Human CD14 Positive Selection Kits I or II (Stem- cell Technologies) and differentiated with 10 ng mL−1 human granulocyte- macrophage stimulating factor (huGM-CSF; R&D Systems). Cells were cultured in Roswell Park Memorial Institute buffer (RPMI; Gibco) supplemented with 10% FBS (RP10) for three days, before a refresh of 50% media and 100% huGM-CSF. On day 6, macrophages were lifted and replated at 60 000 cells cm^{-2}. For GEM generation, day 7 macrophages were transduced with lentivirus and harvested for subsequent assays after 5–7 days with media replacements every 3 days. For initial expression tests of antiFL constructs α–ζ, GM-CSF-differentiated macrophages were transduced with 750 LPs $macrophage^{-1}$ of α–ζ or a CD19t control. In subsequent drugamer binding experiments, TrypLE (Gibco) was used to lift drugamer-bound cells.

Macrophage Viability Assay: Macrophages were plated at 10 000 cells in a 96-well plate and left to rest overnight before treatment with 0.0005×10^{-6} M to 50×10^{-6} M of PI-103, BKM-120

(MedChemExpress, MCE), GSK-2636771 (MCE), or dasatinib (MCE) at 37 °C. At 72 h, cell viability was assessed by CellTiter-Glo assay in quadruplicate.

Lentivirus Production: Development of the CD19t fusion construct is described previously.[18, 67] Fusion proteins consisting of the FITC-E2 scFv fused via a GGGS linker to a surface marker, e.g., EGFRt, CD19t, and Her2tG, were designed to bind and retain fluorescein conjugated to a therapeutic cargo to the outside of the cell. An additional fusion protein consisting of eBFP2 (GenBank ID: EF517318) fused to a degron based on the estrogen receptor ligand binding domain (ERdd) was designed to test the release kinetics of the CMP8 drugamer.[41] GBlocks gene fragments encoding for these fusion proteins were ordered from GeneArt and inserted between NheI and NotI restriction enzyme sites of an epHIV7.2 lentiviral backbone with an EF1α promoter.[42] Plasmids were cotransfected into 293T cells along with Vpx, reverse transcriptase (Rev), gag polyprotein (Gag-pol), and vesicular stomatitis virus G glycoprotein envelope (vsv-g) as previously described.[18] Lentiviral particles (LPs) were harvested from the 293T supernatant, purified and concentrated by ultracentrifugation (90 min, 24,500 rpm, 4 °C), and titered using the QuickTiter Lentivirus Titer kit (Cell Biolabs).

T Cell Transduction: Transduced H9 and Jurkat cell lines were created by plating 1e6 cells in 0.5 mL RPMI 1640 media containing protamine sulfate (100 μg mL^{-1}; APP Pharmaceuticals). Plated cells were transduced at an MOI of 1.

Flow Cytometry: Cells were incubated with 1:10 Human BD Fc block (BD Biosciences) for 10 min at room temperature prior to primary and secondary (if applicable) antibody staining for 20

min at 4 °C and fixed with 2% paraformaldehyde. Unless otherwise noted, all cells were stained with Live/Dead (UV450/50, 1:1000, Invitrogen). Transduction efficiency of GEMs with antifluorescein receptor lentiviral constructs (α–ζ) was conducted by staining with FITC antimouse DO11.10 (1 μL per 100 μL, Mouse IgG2a, κ, BioLegend) primary antibody and A647 anti-Mouse IgG2a (0.5 μL per 100 μL, Rat IgG, BioLegend) secondary antibody and against noninfected controls. AntiFl-ζ transduction efficiency of H9s and Jurkats was assessed by staining with FITC-A647 (IgG Fraction Monoclonal Mouse Anti-Fluorescein, Jackson Immunoresearch). To stain macrophages/GEMs for endogenous phenotype markers, cells were stained with CD40-BUV395 (1×, Clone 5C3, BD Horizon), CD209-BV421 (1×, Clone DCN46, BD Horizon), CD86-BV605 (same as described previously), CD163-BV711 (1×, Clone GHI/61, BioLegend), CD11b-PerCP- Cy5.5 (1×, Clone LM2, Biolegend), CD206-PE (1×, Clone 15-2, BioLegend), PD-L1-PE-Cy7 (1×, CD274, Clone 29E.2A3, BioLegend), HLA-DR-APC (1×, Clone L243, BioLegend), and CD80-APC-H7 (1×, Clone L307.4, BD Biosciences). To study drugamer binding to AntiFl-ζ and CD19t GEMs, cells were fixed and processed directly for flow with no additional staining. Drugamer was detected by the incorporated rhodamine monomer (excitation: 532 nm; emission: 586 nm). To validate transduction efficiency of control CD19t GEMs for relevant experiments, cells were stained with CD19-PE (1×, Clone HIB19, BioLegend). All flow cytometry experiments were run on a BD LSRFortessa with the FACSDiva software and analyzed using FlowJo, V9, V.10 (BD Biosciences).

Drugamer–GEM Binding Specificity and Saturation Assay: GM-CSF-differentiated macrophages were transduced to encode for either an AntiFl-ζ or a control CD19t surface tag on day 7 (500,000 cells per group). After 7 days, cells were incubated with 0×10^{-9} to 1600×10^{-9} M PI-103 drugamer

for 15 min, followed by two washes with 1× PBS and an overnight rest to eliminate nonspecific binding. The next day, GEMs were lifted with TrypLE (Gibco) and processed for flow cytometry. The median fluorescence intensity (MFI) of the drugamer-associated rhodamine was used to assess drugamer binding to GEMs.

Drugamer Binding Longevity Assay: GEMs expressing AntiFl-ζ or ζ control CD19t were incubated with 500×10^{-9} M PI-103 drugamer for 15 min, followed by two washes with 1× PBS (Gibco) and a media refresh with RP10. The relative amount of polymer that remained bound was determined by flow cytometry using drugamer-associated rhodamine fluorescence on 1, 3, 7, and 10 days post drugamer binding. Cells underwent two media changes over the course of the drugamer incubation.

Drugamer Cell Surface Display Assay: Receptor internalization was assessed by treatment of PI-103 drugamer-bound AntiFl-ζ GEMs with 0.5 M acetic acid 150×10^{-3} M NaCl.[69] In doing so, the noncovalent surface interactions between drugamer and AntiFl-ζ GEM receptors were disrupted, leaving only internalized drugamer present in GEMs. Flow cytometry was used to quantify drugamer fluorescence associated with GEMs before and after acid treatment 1, 3, 7, and 10 days post drugamer binding.

Confocal Microscopy: AntiFl-ζ GEMs and untransduced control macrophages plated in 8-well chamber slides at 25,000 cells per well were washed and incubated with 500×10^{-9} M drugamer for 15 min at 37 °C followed by two PBS washes, RP10 media replacement and incubation overnight. Cells were stained with Wheat Germ Agglutinin, Alexa Fluor 488 Conjugate (1:200)

and DAPI nuclear stain (2 drops mL PBS^{-1} ; Thermo Fisher Scientific) and fixed. After two PBS washes, cells were mounted, covered, and dried overnight for imaging the following day on a Leica TCS-SPE laser scanning confocal microscope.

CMP8 Drugamer Binding Assay: AntiFl-*ζ* H9 cells, and appropriate controls, were incubated with 500×10^{-9} M CMP8 drugamer in PBS for 20 min at room temperature, followed by washing with PBS, staining for flow cytometry, and fixation in 1% paraformaldehyde.

CMP8 Drugamer Activation of eBFP2-ERdd Assay: AntiFl.eBFP2-ERdd Jurkat cells, and appropriate controls, were incubated with 100×10^{-9} M CMP8 drugamer in PBS for 20 min at room temperature, followed by washing with PBS, and placing into culture at 37 °C, 5% CO_2 for 24 h. Samples were taken for analysis after 0, 3, 7, 19.5, and 24 h of incubation, stained for flow cytometry, and fixed in 1% paraformaldehyde.

Statistical Analysis: Viability/toxicity data (using CellTiter Glo Assays) were expressed as mean ± standard deviation. Statistical analysis comparing two groups was conducted using two-tailed Welch's *t*-tests. All statistical analysis was conducted using GraphPad Prism 9.0 software. A statistically significant difference was evaluated at $p < 0.05$, where $*p < 0.05$, $**p < 0.01$, and $***p < 0.001$.

4.5 ACKNOWLEDGEMENTS

The authors would like to congratulate and thank Prof. Buddy Ratner for his lifetime of leadership, mentorship, and especially, friendship. He has been a wonderful inspiration to the authors and so

many others in all his fundamental science work and translational contributions that have impacted so many around the world; the authors wish him many continued years of biomaterials engineering and community! The authors thank Dr. Thomas Roberts for his consultation and discussion on the selection of kinase inhibitor drugs. The authors would also like to acknowledge the Steven Higgins Foundation, the Matthew Larsen Foundation, the Pediatric Brain Tumor Research Foundation, and the Washington Research Foun- dation for their support of this work. This material is based upon work supported by the NIH National Institute of Allergy and Infectious Diseases under Grant No. R21AI149400 and the National Science Foundation Graduate Research Fellowship Program under Grant No. DGE-1762114. Any opinions, findings, and conclusions or recommendations expressed in this material are those of the author(s) and do not necessarily reflect the views of the National Science Foundation.

REFERENCES

[1] I. Fuso Nerini, L. Morosi, M. Zucchetti, A. Ballerini, R. Giavazzi, M. D'Incalci, Intratumor heterogeneity and its impact on drug distribution and sensitivity, Clin Pharmacol Ther, 96 (2014) 224-238.
[2] A.I. Minchinton, I.F. Tannock, Drug penetration in solid tumours, Nat Rev Cancer, 6 (2006) 583-592.
[3] T.F. Gajewski, H. Schreiber, Y.-X. Fu, Innate and adaptive immune cells in the tumor microenvironment, Nat Immunol, 14 (2013) 1014-1022.
[4] G.F. Woodworth, G.P. Dunn, E.A. Nance, J. Hanes, H. Brem, Emerging insights into barriers to effective brain tumor therapeutics, Front Oncol, 4 (2014) 126.
[5] R.K. Vaddepally, P. Kharel, R. Pandey, R. Garje, A.B. Chandra, Review of Indications of FDA-Approved Immune Checkpoint Inhibitors per NCCN Guidelines with the Level of Evidence, Cancers (Basel), 12 (2020).
[6] L. Barrueto, F. Caminero, L. Cash, C. Makris, P. Lamichhane, R.R. Deshmukh, Resistance to Checkpoint Inhibition in Cancer Immunotherapy, Transl Oncol, 13 (2020) 100738-100738.
[7] S. Srivastava, S.R. Riddell, Engineering CAR-T cells: Design concepts, Trends Immunol, 36 (2015) 494-502.
[8] S.L. Maude, N. Frey, P.A. Shaw, R. Aplenc, D.M. Barrett, N.J. Bunin, A. Chew, V.E. Gonzalez, Z. Zheng, S.F. Lacey, Y.D. Mahnke, J.J. Melenhorst, S.R. Rheingold, A. Shen, D.T. Teachey, B.L. Levine, C.H. June, D.L. Porter, S.A. Grupp, Chimeric Antigen Receptor T Cells for Sustained Remissions in Leukemia, New England Journal of Medicine, 371 (2014) 1507-1517.
[9] G.L. Beatty, M. O'Hara, Chimeric antigen receptor-modified T cells for the treatment of solid tumors: Defining the challenges and next steps, Pharmacol Ther, 166 (2016) 30-39.
[10] M.M. D'Aloia, I.G. Zizzari, B. Sacchetti, L. Pierelli, M. Alimandi, CAR-T cells: the long and winding road to solid tumors, Cell Death Dis, 9 (2018) 282.
[11] D. Hambardzumyan, D.H. Gutmann, H. Kettenmann, The role of microglia and macrophages in glioma maintenance and progression, Nat Neurosci, 19 (2016) 20-27.
[12] J.Q. Xixi Zhao, Yuchen Sun, Jizhao Wang, Xu Liu, Feidi Wang, Hong, W.W. Zhang, Xingcong Ma, Xiaoyan Gao and Shuqun Zhang, Prognostic significance of tumor-associated macrophages in breast cancer: a meta-analysis of the literature, Oncotarget, 8 (2017) 30576-30586.
[13] B.C. Xiaoming Zhonga, Zhiwen Yanga, The Role of Tumor-Associated Macrophages in Colorectal Carcinoma Progression, Cell Physiol Biochem, 45 (2018) 356-365.
[14] Y. Zhu, J.M. Herndon, D.K. Sojka, K.W. Kim, B.L. Knolhoff, C. Zuo, D.R. Cullinan, J. Luo, A.R. Bearden, K.J. Lavine, W.M. Yokoyama, W.G. Hawkins, R.C. Fields, G.J. Randolph, D.G. DeNardo, Tissue-Resident Macrophages in Pancreatic Ductal Adenocarcinoma Originate from Embryonic Hematopoiesis and Promote Tumor Progression, Immunity, 47 (2017) 323-338 e326.
[15] Y. Wang, Y.-X. Lin, S.-L. Qiao, J. Wang, H. Wang, Progress in Tumor-Associated Macrophages: From Bench to Bedside, Advanced Biosystems, 3 (2019) 1800232.
[16] M. Klichinsky, M. Ruella, O. Shestova, X.M. Lu, A. Best, M. Zeeman, M. Schmierer, K. Gabrusiewicz, N.R. Anderson, N.E. Petty, K.D. Cummins, F. Shen, X. Shan, K. Veliz, K. Blouch, Y. Yashiro-Ohtani, S.S. Kenderian, M.Y. Kim, R.S. O'Connor, S.R. Wallace, M.S.

Kozlowski, D.M. Marchione, M. Shestov, B.A. Garcia, C.H. June, S. Gill, Human chimeric antigen receptor macrophages for cancer immunotherapy, Nat Biotechnol, 38 (2020) 947-953.
[17] K.J. Brempelis, C.M. Cowan, S.A. Kreuser, K.P. Labadie, B.M. Prieskorn, N.A.P. Lieberman, C.I. Ene, K.W. Moyes, H. Chinn, K.R. DeGolier, L.R. Matsumoto, S.K. Daniel, J.K. Yokoyama, A.D. Davis, V.J. Hoglund, K.S. Smythe, S.D. Balcaitis, M.C. Jensen, R.G. Ellenbogen, J.S. Campbell, R.H. Pierce, E.C. Holland, V.G. Pillarisetty, C.A. Crane, Genetically engineered macrophages persist in solid tumors and locally deliver therapeutic proteins to activate immune responses, J Immunother Cancer, 8 (2020).
[18] K.W. Moyes, N.A. Lieberman, S.A. Kreuser, H. Chinn, C. Winter, G. Deutsch, V. Hoglund, R. Watson, C.A. Crane, Genetically Engineered Macrophages: A Potential Platform for Cancer Immunotherapy, Hum Gene Ther, 28 (2017) 200-215.
[19] C.E. Brown, B. Aguilar, R. Starr, X. Yang, W.-C. Chang, L. Weng, B. Chang, A. Sarkissian, A. Brito, J.F. Sanchez, J.R. Ostberg, M. D'Apuzzo, B. Badie, M.E. Barish, S.J. Forman, Optimization of IL13Rα2-Targeted Chimeric Antigen Receptor T Cells for Improved Anti-tumor Efficacy against Glioblastoma, Molecular Therapy, 26 (2018) 31-44.
[20] J.L. Gardell, L.R. Matsumoto, H. Chinn, K.R. DeGolier, S.A. Kreuser, B. Prieskorn, S. Balcaitis, A. Davis, R.G. Ellenbogen, C.A. Crane, Human macrophages engineered to secrete a bispecific T cell engager support antigen-dependent T cell responses to glioblastoma, J Immunother Cancer, 8 (2020).
[21] S. Kaczanowska, D.W. Beury, V. Gopalan, A.K. Tycko, H. Qin, M.E. Clements, J. Drake, C. Nwanze, M. Murgai, Z. Rae, W. Ju, K.A. Alexander, J. Kline, C.F. Contreras, K.M. Wessel, S. Patel, S. Hannenhalli, M.C. Kelly, R.N. Kaplan, Genetically engineered myeloid cells rebalance the core immune suppression program in metastasis, Cell, 184 (2021) 2033-2052.e2021.
[22] J.C. Castle, M. Uduman, S. Pabla, R.B. Stein, J.S. Buell, Mutation-Derived Neoantigens for Cancer Immunotherapy, Front Immunol, 10 (2019) 1856.
[23] R.X. Zhang, H.L. Wong, H.Y. Xue, J.Y. Eoh, X.Y. Wu, Nanomedicine of synergistic drug combinations for cancer therapy – Strategies and perspectives, Journal of Controlled Release, 240 (2016) 489-503.
[24] M. Vanneman, G. Dranoff, Combining immunotherapy and targeted therapies in cancer treatment, Nat Rev Cancer, 12 (2012) 237-251.
[25] M.T. Stephan, J.J. Moon, S.H. Um, A. Bershteyn, D.J. Irvine, Therapeutic cell engineering with surface-conjugated synthetic nanoparticles, Nat Med, 16 (2010) 1035-1041.
[26] N. Doshi, A.J. Swiston, J.B. Gilbert, M.L. Alcaraz, R.E. Cohen, M.F. Rubner, S. Mitragotri, Cell-Based Drug Delivery Devices Using Phagocytosis-Resistant Backpacks, Advanced Materials, 23 (2011) H105-H109.
[27] N.L. Klyachko, R. Polak, M.J. Haney, Y. Zhao, R.J. Gomes Neto, M.C. Hill, A.V. Kabanov, R.E. Cohen, M.F. Rubner, E.V. Batrakova, Macrophages with cellular backpacks for targeted drug delivery to the brain, Biomaterials, 140 (2017) 79-87.
[28] M.J. Haney, Y. Zhao, J. Fay, H. Duhyeong, M. Wang, H. Wang, Z. Li, Y.Z. Lee, M.K. Karuppan, N. El-Hage, A.V. Kabanov, E.V. Batrakova, Genetically modified macrophages accomplish targeted gene delivery to the inflamed brain in transgenic Parkin Q311X(A) mice: importance of administration routes, Scientific Reports, 10 (2020) 11818.
[29] C.W.t. Shields, M.A. Evans, L.L. Wang, N. Baugh, S. Iyer, D. Wu, Z. Zhao, A. Pusuluri, A. Ukidve, D.C. Pan, S. Mitragotri, Cellular backpacks for macrophage immunotherapy, Sci Adv, 6 (2020) eaaz6579.

[30] B. Singh, S. Mitragotri, Harnessing cells to deliver nanoparticle drugs to treat cancer, Biotechnology Advances, 42 (2020) 107339.
[31] P. Mi, K. Miyata, K. Kataoka, H. Cabral, Clinical Translation of Self-Assembled Cancer Nanomedicines, Advanced Therapeutics, 4 (2021) 2000159.
[32] S. Quader, K. Kataoka, Nanomaterial-Enabled Cancer Therapy, Molecular Therapy, 25 (2017) 1501-1513.
[33] E.V. Batrakova, A.V. Kabanov, Pluronic block copolymers: evolution of drug delivery concept from inert nanocarriers to biological response modifiers, J Control Release, 130 (2008) 98-106.
[34] J. Kopeček, J. Yang, Polymer nanomedicines, Adv Drug Deliv Rev, 156 (2020) 40-64.
[35] R. Duncan, Polymer therapeutics at a crossroads? Finding the path for improved translation in the twenty-first century, Journal of Drug Targeting, 25 (2017) 759-780.
[36] Y. Matsumura, H. Maeda, A New Concept for Macromolecular Therapeutics in Cancer Chemotherapy: Mechanism of Tumoritropic Accumulation of Proteins and the Antitumor Agent Smancs, Cancer Research, 46 (1986) 6387.
[37] D. Das, S. Srinivasan, A.M. Kelly, D.Y. Chiu, B.K. Daugherty, D.M. Ratner, P.S. Stayton, A.J. Convertine, RAFT polymerization of ciprofloxacin prodrug monomers for the controlled intracellular delivery of antibiotics, Polymer Chemistry, 7 (2016) 826-837.
[38] D. Das, J. Chen, S. Srinivasan, A.M. Kelly, B. Lee, H.N. Son, F. Radella, T.E. West, D.M. Ratner, A.J. Convertine, S.J. Skerrett, P.S. Stayton, Synthetic Macromolecular Antibiotic Platform for Inhalable Therapy against Aerosolized Intracellular Alveolar Infections, Mol Pharm, 14 (2017) 1988-1997.
[39] F.Y. Su, S. Srinivasan, B. Lee, J. Chen, A.J. Convertine, T.E. West, D.M. Ratner, S.J. Skerrett, P.S. Stayton, Macrophage-targeted drugamers with enzyme-cleavable linkers deliver high intracellular drug dosing and sustained drug pharmacokinetics against alveolar pulmonary infections, J Control Release, 287 (2018) 1-11.
[40] S. Srinivasan, D. Roy, T.E.J. Chavas, V. Vlaskin, D.K. Ho, A. Pottenger, C.L.M. LeGuyader, M. Maktabi, P. Strauch, C. Jackson, S.M. Flaherty, H. Lin, J. Zhang, B. Pybus, Q. Li, H.E. Huber, P.A. Burke, D. Wesche, R. Rochford, P.S. Stayton, Liver-targeted polymeric prodrugs of 8-aminoquinolines for malaria radical cure, J Control Release, 331 (2021) 213-227.
[41] Y. Miyazaki, H. Imoto, L.C. Chen, T.J. Wandless, Destabilizing domains derived from the human estrogen receptor, J Am Chem Soc, 134 (2012) 3942-3945.
[42] X. Wang, W.C. Chang, C.W. Wong, D. Colcher, M. Sherman, J.R. Ostberg, S.J. Forman, S.R. Riddell, M.C. Jensen, A transgene-encoded cell surface polypeptide for selection, in vivo tracking, and ablation of engineered cells, Blood, 118 (2011) 1255-1263.
[43] L.E. Budde, C. Berger, Y. Lin, J. Wang, X. Lin, S.E. Frayo, S.A. Brouns, D.M. Spencer, B.G. Till, M.C. Jensen, S.R. Riddell, O.W. Press, Combining a CD20 chimeric antigen receptor and an inducible caspase 9 suicide switch to improve the efficacy and safety of T cell adoptive immunotherapy for lymphoma, PLoS One, 8 (2013) e82742.
[44] M.D. Antonio Di Stasi, Siok-Keen Tey, M.D., Gianpietro Dotti, M.D., Yuriko Fujita, M.D., Alana Kennedy-Nasser, M.D., Caridad Martinez, M.D., Karin Straathof, M.D., Enli Liu, M.D., April G. Durett, M.Sc., Bambi Grilley, R.Ph., Hao Liu, Ph.D., Conrad R. Cruz, M.D., Barbara Savoldo, M.D., Adrian P. Gee, Ph.D., John Schindler, Ph.D., Robert A. Krance, M.D., Helen E. Heslop, M.D., David M. Spencer, Ph.D., Cliona M. Rooney, Ph.D., and Malcolm K. Brenner, M.D., Inducible Apoptosis as a Safety Switch
for Adoptive Cell Therapy, The New England Journal of Medicine, 365 (2011) 1673-1683.

[45] A.J. Johnson, J. Wei, J.M. Rosser, A. Künkele, C.A. Chang, A.N. Reid, M.C. Jensen, Rationally Designed Transgene-Encoded Cell-Surface Polypeptide Tag for Multiplexed Programming of CAR T-cell Synthetic Outputs, Cancer Immunology Research, (2021).
[46] S.Z. Millis, S. Ikeda, S. Reddy, Z. Gatalica, R. Kurzrock, Landscape of Phosphatidylinositol-3-Kinase Pathway Alterations Across 19784 Diverse Solid Tumors, JAMA Oncol, 2 (2016) 1565-1573.
[47] Q.W. Fan, Z.A. Knight, D.D. Goldenberg, W. Yu, K.E. Mostov, D. Stokoe, K.M. Shokat, W.A. Weiss, A dual PI3 kinase/mTOR inhibitor reveals emergent efficacy in glioma, Cancer Cell, 9 (2006) 341-349.
[48] N.E. Torbett, A. Luna-Moran, Z.A. Knight, A. Houk, M. Moasser, W. Weiss, K.M. Shokat, D. Stokoe, A chemical screen in diverse breast cancer cell lines reveals genetic enhancers and suppressors of sensitivity to PI3K isoform-selective inhibition, Biochem J, 415 (2008) 97-110.
[49] A. Hochhaus, S.G. O'Brien, F. Guilhot, B.J. Druker, S. Branford, L. Foroni, J.M. Goldman, M.C. Muller, J.P. Radich, M. Rudoltz, M. Mone, I. Gathmann, T.P. Hughes, R.A. Larson, I. Investigators, Six-year follow-up of patients receiving imatinib for the first-line treatment of chronic myeloid leukemia, Leukemia, 23 (2009) 1054-1061.
[50] H.S. Rugo, F. Andre, T. Yamashita, H. Cerda, I. Toledano, S.M. Stemmer, J.C. Jurado, D. Juric, I. Mayer, E.M. Ciruelos, H. Iwata, P. Conte, M. Campone, C. Wilke, D. Mills, A. Lteif, M. Miller, F. Gaudenzi, S. Loibl, Time course and management of key adverse events during the randomized phase III SOLAR-1 study of PI3K inhibitor alpelisib plus fulvestrant in patients with HR-positive advanced breast cancer, Ann Oncol, 31 (2020) 1001-1010.
[51] B.D. Hopkins, C. Pauli, X. Du, D.G. Wang, X. Li, D. Wu, S.C. Amadiume, M.D. Goncalves, C. Hodakoski, M.R. Lundquist, R. Bareja, Y. Ma, E.M. Harris, A. Sboner, H. Beltran, M.A. Rubin, S. Mukherjee, L.C. Cantley, Suppression of insulin feedback enhances the efficacy of PI3K inhibitors, Nature, 560 (2018) 499-503.
[52] H.F. Zhao, J. Wang, W. Shao, C.P. Wu, Z.P. Chen, S.T. To, W.P. Li, Recent advances in the use of PI3K inhibitors for glioblastoma multiforme: current preclinical and clinical development, Mol Cancer, 16 (2017) 100.
[53] F.I. Raynaud, S. Eccles, P.A. Clarke, A. Hayes, B. Nutley, S. Alix, A. Henley, F. Di-Stefano, Z. Ahmad, S. Guillard, L.M. Bjerke, L. Kelland, M. Valenti, L. Patterson, S. Gowan, A. de Haven Brandon, M. Hayakawa, H. Kaizawa, T. Koizumi, T. Ohishi, S. Patel, N. Saghir, P. Parker, M. Waterfield, P. Workman, Pharmacologic characterization of a potent inhibitor of class I phosphatidylinositide 3-kinases, Cancer Res, 67 (2007) 5840-5850.
[54] L. Xenou, E.A. Papakonstanti, p110delta PI3K as a therapeutic target of solid tumours, Clin Sci (Lond), 134 (2020) 1377-1397.
[55] W. Zheng, J.W. Pollard, Inhibiting macrophage PI3Kgamma to enhance immunotherapy, Cell Res, 26 (2016) 1267-1268.
[56] A. Gieryng, D. Pszczolkowska, K.A. Walentynowicz, W.D. Rajan, B. Kaminska, Immune microenvironment of gliomas, Lab Invest, 97 (2017) 498-518.
[57] D.K. Ho, C. LeGuyader, S. Srinivasan, D. Roy, V. Vlaskin, T.E.J. Chavas, C.L. Lopez, J.M. Snyder, A. Postma, J. Chiefari, P.S. Stayton, Fully synthetic injectable depots with high drug content and tunable pharmacokinetics for long-acting drug delivery, J Control Release, 329 (2020) 257-269.
[58] M.M. Mohamed, B.F. Sloane, Cysteine cathepsins: multifunctional enzymes in cancer, Nat Rev Cancer, 6 (2006) 764-775.

[59] D. Das, S. Srinivasan, F.D. Brown, F.Y. Su, A.L. Burrell, J.M. Kollman, A. Postma, D.M. Ratner, P.S. Stayton, A.J. Convertine, Radiant star nanoparticle prodrugs for the treatment of intracellular alveolar infections, Polymer Chemistry, 9 (2018) 2134-2146.
[60] M. Hudecek, M.T. Lupo-Stanghellini, P.L. Kosasih, D. Sommermeyer, M.C. Jensen, C. Rader, S.R. Riddell, Receptor affinity and extracellular domain modifications affect tumor recognition by ROR1-specific chimeric antigen receptor T cells, Clin Cancer Res, 19 (2013) 3153-3164.
[61] A. Honegger, S. Spinelli, C. Cambillau, A. Pluckthun, A mutation designed to alter crystal packing permits structural analysis of a tight-binding fluorescein-scFv complex, Protein Sci, 14 (2005) 2537-2549.
[62] Y.J. Lu, H. Chu, L.W. Wheeler, M. Nelson, E. Westrick, J.F. Matthaei, I.I. Cardle, A. Johnson, J. Gustafson, N. Parker, M. Vetzel, L.-C. Xu, E.Z. Wang, M.C. Jensen, P.J. Klein, P.S. Low, C.P. Leamon, Preclinical Evaluation of Bispecific Adaptor Molecule Controlled Folate Receptor CAR-T Cell Therapy With Special Focus on Pediatric Malignancies, Frontiers in Oncology, 9 (2019).
[63] R.W. Daniels, A.J. Rossano, G.T. Macleod, B. Ganetzky, Expression of multiple transgenes from a single construct using viral 2A peptides in Drosophila, PLoS One, 9 (2014) e100637.
[64] L. Gao, Z. Qin, B. Zhang, Z. Yin, X. Zhang, J. Yang, An investigation of the metabolic activity, isozyme contribution, species differences and potential drug–drug interactions of PI-103, and the identification of efflux transporters for PI-103-O-glucuronide in HeLa1A9 cells, RSC Advances, 10 (2020) 9610-9622.
[65] O. Kinzel, D. Fattori, E. Muraglia, P. Gallinari, M.C. Nardi, C. Paolini, G. Roscilli, C. Toniatti, O. Gonzalez Paz, R. Laufer, A. Lahm, A. Tramontano, R. Cortese, R. De Francesco, G. Ciliberto, U. Koch, A Structure-Guided Approach to an Orthogonal Estrogen-Receptor-Based Gene Switch Activated by Ligands Suitable for in Vivo Studies, Journal of Medicinal Chemistry, 49 (2006) 5404-5407.
[66] J. Chen, H.N. Son, J.J. Hill, S. Srinivasan, F.Y. Su, P.S. Stayton, A.J. Convertine, D.M. Ratner, Nanostructured glycopolymer augmented liposomes to elucidate carbohydrate-mediated targeting, Nanomedicine, 12 (2016) 2031-2041.
[67] C. Berger, M.C. Jensen, P.M. Lansdorp, M. Gough, C. Elliott, S.R. Riddell, Adoptive transfer of effector CD8+ T cells derived from central memory cells establishes persistent T cell memory in primates, J Clin Invest, 118 (2008) 294-305.

SUPPORTING INFORMATION

Figure S4.1. Synthesis and characterization of PI-103 prodrug monomer. (A) PI-103 monomer (**3**): Mono-2-(methacryloyloxy)ethyl succinate (SMA) 759 mg (3.3 mmol), *N*-(3-dimethylaminopropyl)-*N′*-ethylcarbodimide hydrochloride (EDCI.HCl) 1.26 g (6.6 mmol) and *N,N*-dimethylpyridin-4-amine (DMAP) 403 mg (3.3 mmol) in 200 mL anhydrous CH_2Cl_2 was treated with PI103 766 mg (2.2 mmol). After 5 minutes at 0 °C, the reaction mixture was stirred at room temperature for 3 h. The reaction mixture was washed with water (2 X 100 mL), dried over anhydrous sodium sulfate and the solvent was rotary evaporated under reduced pressure. The crude product was purified by silica gel column chromatography using 20 % tetrahydrofuran in chloroform as column eluent. Column purified product was dissolved in 8 mL column eluent, precipitated into 20 % ether/hexane using two 50 mL conical centrifuge tubes (40 mL ether/hexane mixture/tube) and kept at -20 °C overnight to complete the precipitation. The precipitate was collected by centrifugation, washed with 20 % cold ether/hexane and dried under high vacuum. Yield = 962 mg (78.0 %). (B) ^{1}H-NMR spectrum of PI103-SMA monomer (**3**). ^{1}H NMR (300 MHz, DMSO-d_6) δ 1.84 (s, 3H), 2.74 (t, J = 6.3 Hz, 2H), 2.91 (t, J = 6.3 Hz, 2H), 3.83 (t, J = 4.4 Hz, 4H), 4.10 (t, J = 4.4 Hz, 4H), 4.33 (s, 4H), 5.65 (s, 1H), 6.02 (s, 1H), 7.23 (d, J = 8.2 Hz, 1H), 7.55 (t, J = 8.0 Hz, 1H), 7.61 (dd, J = 4.9 Hz, J = 7.7 Hz, 1H), 8.10 (s, 1H), 8.32 (d, J = 7.9 Hz, 1H), 8.59 – 8.71 (one doublet and one singlet merged, 2H). (C) ESI-Mass spectrum of PI103-SMA (**3**) monomer. MS (ESI, m/z): calculated for $C_{29}H_{28}N_4O_8$ (M): 560.2, found: 561.3 $[M+1]^+$ and 583.4 $[M+Na]^+$.

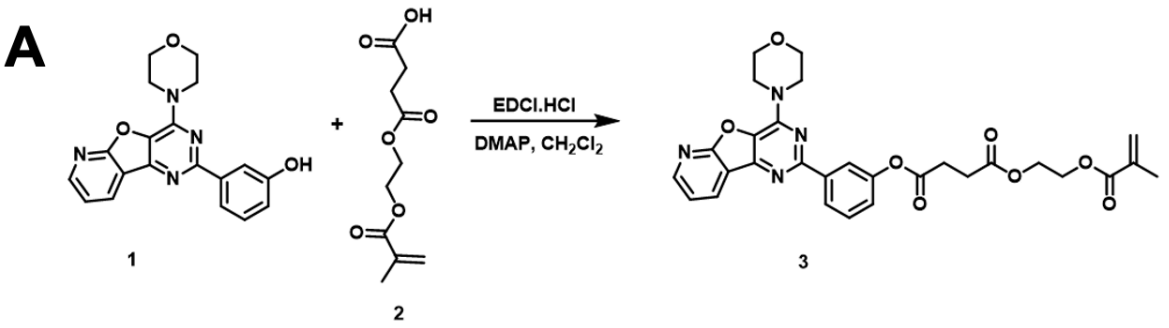
A
EDCI.HCl
DMAP, CH2Cl2
1
2
3

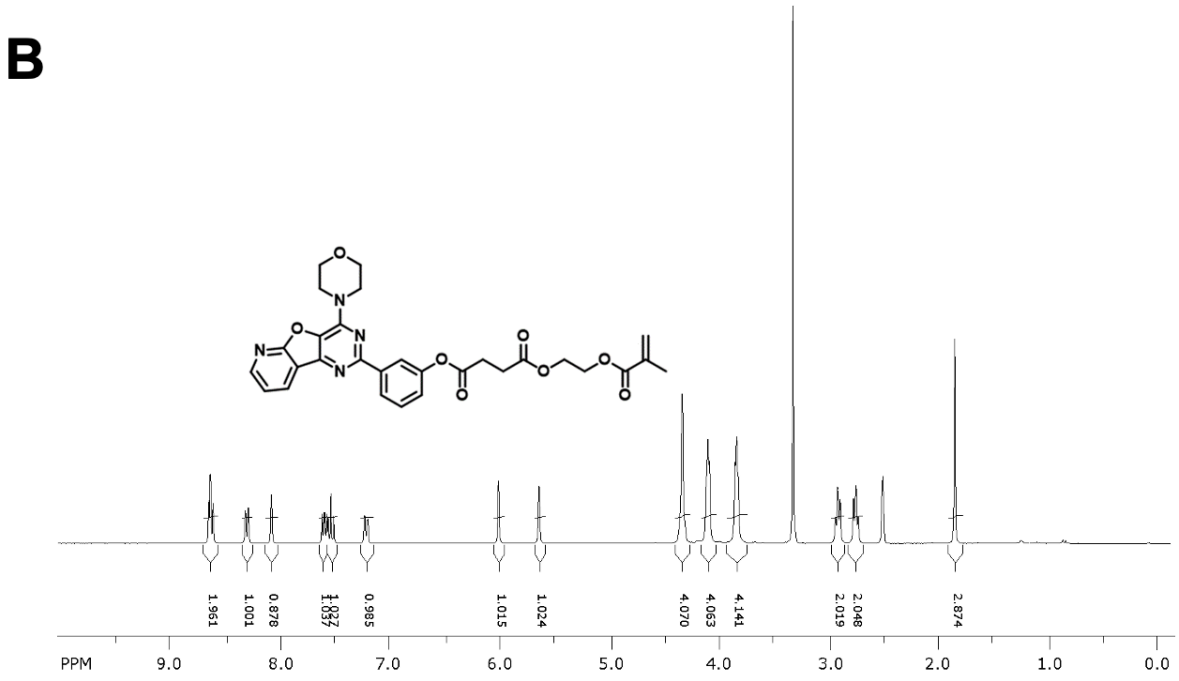
B
1.951
1.001
0.878
1.037
0.985
1.015
1.024
4.070
4.063
4.141
2.019
2.046
2.874
PPM
9.0
8.0
7.0
6.0
5.0
4.0
3.0
2.0
1.0
0.0

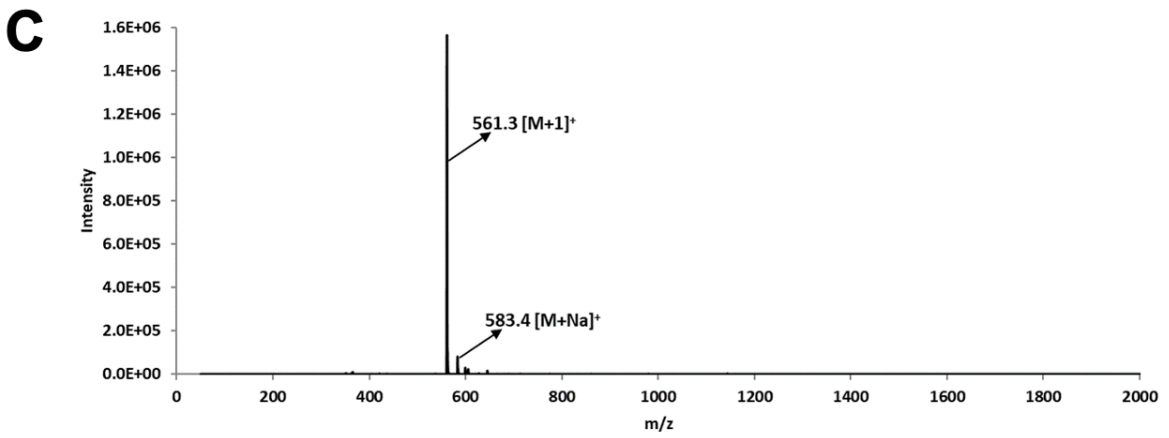
C
Intensity
m/z
561.3 [M+1]+
583.4 [M+Na]+
1.6E+06
1.4E+06
1.2E+06
1.0E+06
8.0E+05
6.0E+05
4.0E+05
2.0E+05
0.0E+00
0
200
400
600
800
1000
1200
1400
1600
1800
2000

Figure S4.2. Synthesis and characterization of FITC monomer. (A) Methacryloyloxyethyl 4-(*tert*-butoxycarbonylamino)butanoate (**6**): 4-(Tert-butoxycarbonylamino) butanoic acid **5** was prepared from 4-amino butanoic acid (**4**) following Buchini et al.[1] Compound **5** 2.03 g (10 mmol) in 60 mL CH_2Cl_2 was treated with DMAP 1.22 g (10 mmol), *N,N'*-dicyclohexylcarbodiimide 2.27 g (11 mmol) and 2-hydroxylethyl methacrylate 1.3 g (10 mmol). The reaction mixture was stirred at room temperature for 5 h. The byproduct dicyclohexylurea was filtered off, and the filtrate was rotary evaporated under reduced pressure. The crude product was purified by silica gel chromatography using 4.5 % methanol/chloroform as eluent. Yield: 3.05 g (96.8 %, contains 2-3 % DCU). MS (ESI, m/z): calculated for $C_{15}H_{25}NO_6$ (M): 315.2, found: 338.2$[M+Na]^+$. Fluorescein Monomer (**9**): Methacryloyloxyethyl 4-(tert-butoxycarbonylamino)butanoate (**6**) 3 g (9.5 mmol) in 20 mL 40 % trifluoroacetic acid indichloromethane was stirred at room temperature for 3.5 h. Solvent was rotary evaporated and the residue was precipitated in 30 % ether/hexane using two 50 mL conical tubes (40 mL/tube). This was centrifuged after keeping at -20 ^oC for 2 h. The oily product at the bottom was collected by carefully decanting the supernatant. This process was repeated two more times. The oily product (**7**) was purged with air for 6 h to remove the traces of solvents and subsequently used for the next step without any further purification. Methacryloyloxyethyl 4-aminobutanoate TFA salt (**7**) 658 mg (2 mmol) in 10 mL *N,N*-dimethylformamide (DMF) was treated with triethylamine 1.12 mL (8 mmol) under ice-cold condition. After 10 min, ice bath was removed, and the mixture was stirred at room temperature for 20 min. 5-Carboxyfluorescein succinimidyl ester (**8**) 800 mg (1.7 mmol) was added as solid and stirring was continued for 8 h protected from light. The solvent was concentrated under reduced pressure and the residue was purified by silica gel chromatography with 8 % methanol/chloroform as eluent to obtain (**9**). Yield = 810 mg (83.07 %). (B) ^{1}H-NMR spectrum of monomer methacryloyloxyethyl 4-(tert-butoxycarbonylamino)butanoate **(6)**. ^{1}H NMR (300 MHz, CDCl3) δ 1.43 (s, 9H), 1.81 (pent, J = 7.1 Hz, 2H), 1.94 (s, 3H), 2.37 (t, J = 7.3 Hz, 2H), 3.16 (q, J = 6.4 Hz, 2H), 4.35 (s, 4H), 4.66 (s, 1H), 5.59 (s, 1H), 6.12 (s, 1H). ^{1}H-NMR spectrum of Fluorescein monomer **(9)**. ^{1}H NMR (300 MHz, MeOH-d_4) δ 1.91 (s, 3H), 1.97 (t, J = 7.1 Hz, 2H), 2.48 (t, J = 7.2 Hz, 2H), 3.48 (t, J = 6.7 Hz, 2H), 4.35 (s, 4H), 5.62 (s, 1H), 6.09 (s, 1H), 6.53 (d, J = 8.6 Hz, 2H), 6.61 (d, J = 8.6 Hz, 2H), 6.69 (s, 2H), 7.30 (d, J = 8.0 Hz, 1H), 8.18 (d, J = 8.0 Hz, 1H), 8.41 (s, 1H). (C) ESI-Mass spectrum of monomer methacryloyloxyethyl 4-(tert-butoxycarbonylamino)butanoate **(6).** MS (ESI, m/z): calculated for $C_{15}H_{25}NO_6$ (M): 315.4, found: 338.2 $[M+Na]^+$. ESI-Mass spectrum of Fluorescein monomer (**9**). MS (ESI, m/z): calculated for $C_{31}H_{27}NO_{10}$ (M): 573.2, found: 575.2 $[M+2H]^{2+}$ and 596.6 $[M+Na]^+$.

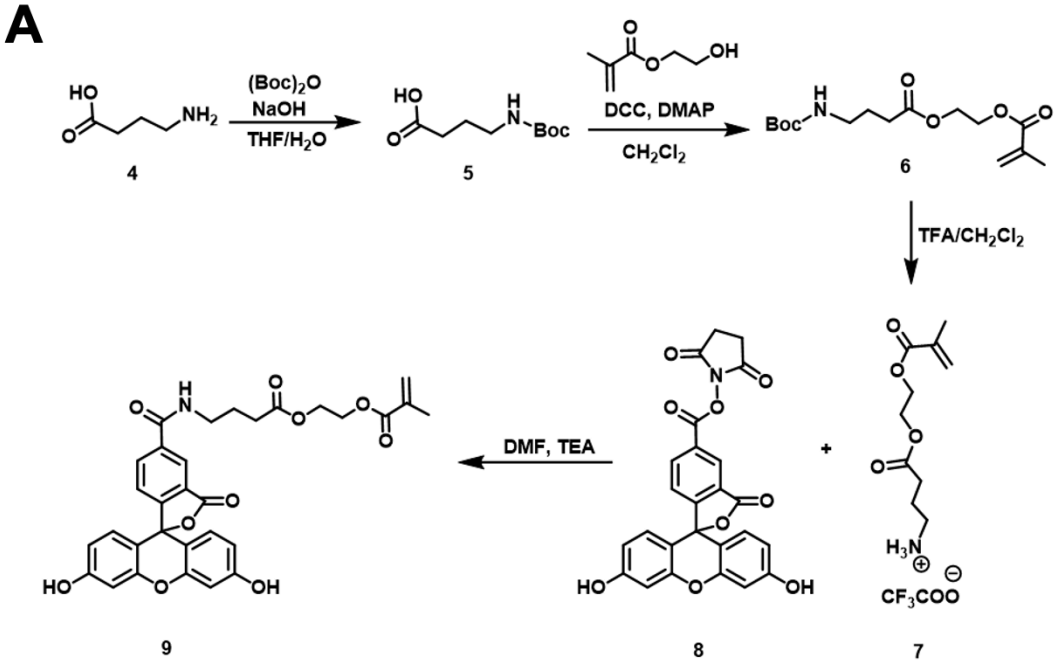
A
HO
NH2
(Boc)2O
NaOH
THF/H2O
4
HO
N
Boc
5
OH
DCC, DMAP
CH2Cl2
Boc
N
6
TFA/CH2Cl2
DMF, TEA
HO
OH
9
8
+
H3N
CF3COO
7


B
(6)
0.970
1.000
0.822
4.189
2.109
2.017
2.964
2.228
9.294
PPM
7.2
6.8
6.4
6.0
5.6
5.2
4.8
4.4
4.0
3.6
3.2
2.8
2.4
2.0
1.6
1.2
0.8
0.4
0.0

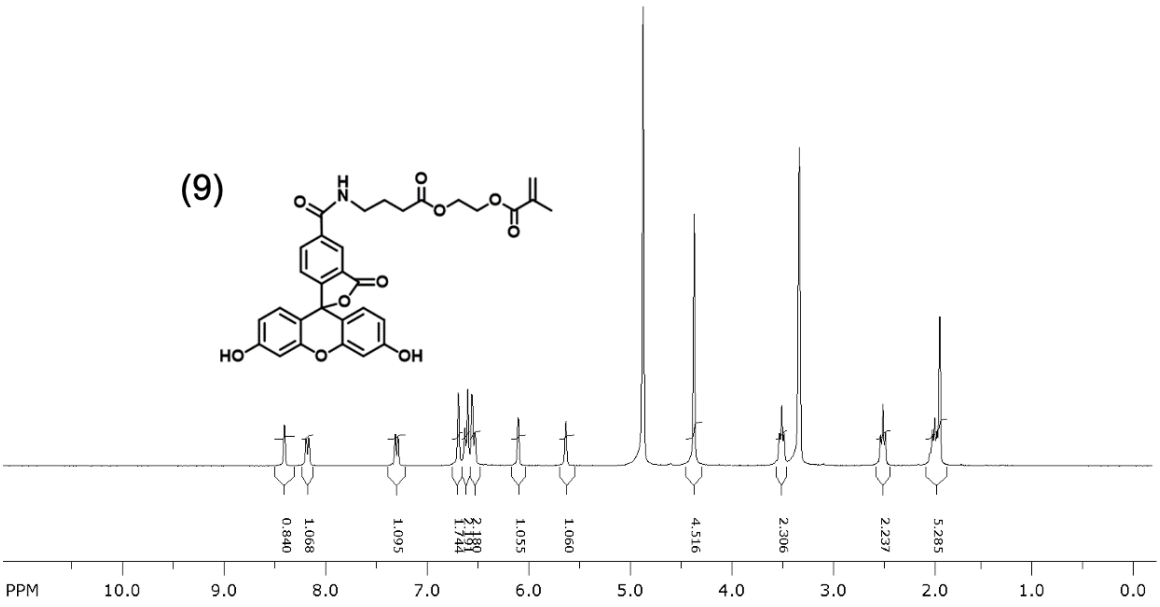
(9)
0.840
1.068
1.095
2.180
1.744
1.055
1.060
4.516
2.306
2.237
5.285
PPM
10.0
9.0
8.0
7.0
6.0
5.0
4.0
3.0
2.0
1.0
0.0

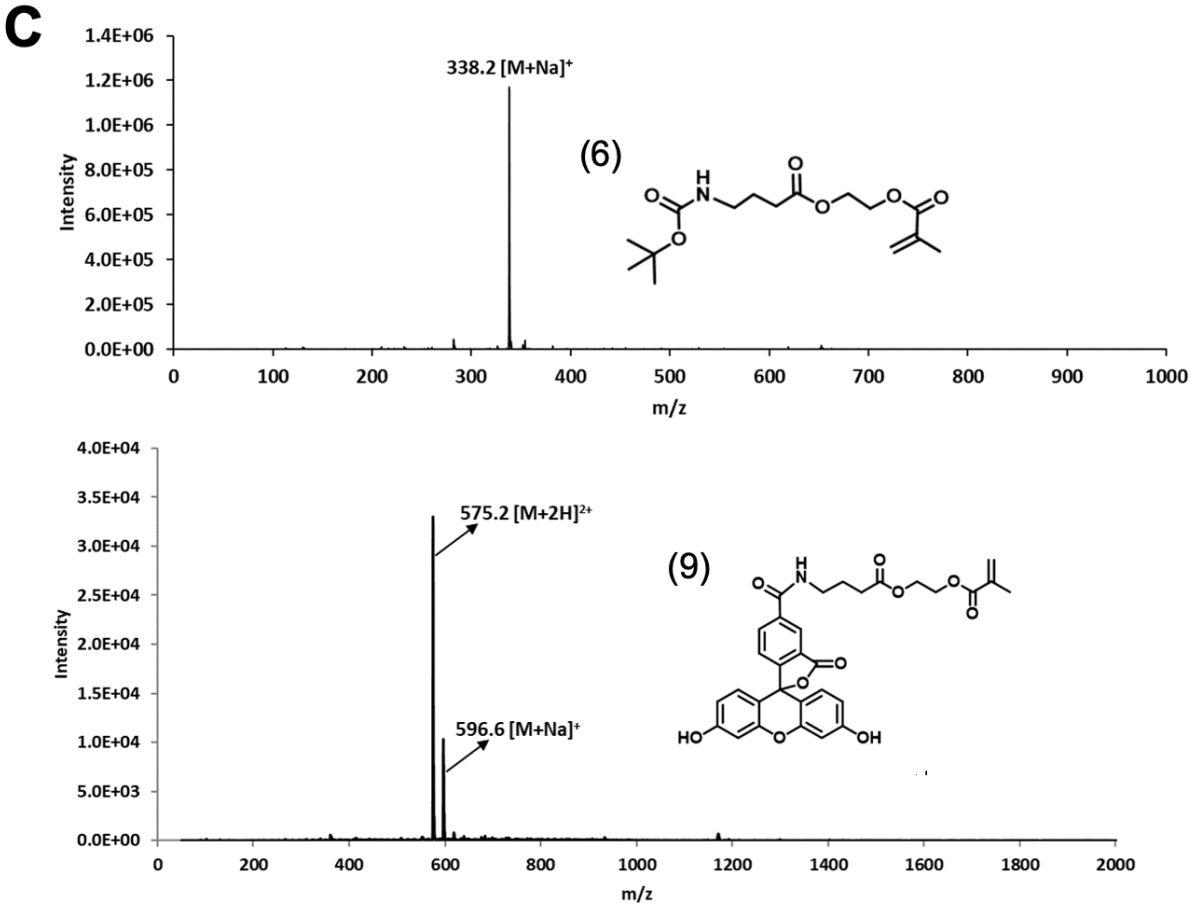
C
338.2 [M+Na]+
(6)
Intensity
m/z
575.2 [M+2H]2+
596.6 [M+Na]+
(9)
Intensity
m/z

Figure S4.3. PI-103 Drugamer Synthesis and Characterization. (A) Table of PI-103 drugamer polymerization stoichiometry and results (B) ^{1}H-NMR spectrum of purified PI-103 drugamer in DMSO-d_6 (C) ^{1}H-NMR spectrum of PI-103 drugamer using a Fasudil HCl internal standard in DMSO-d_6 for drug weight percentage of drugamer calculation (D) Gel permeation chromatography of PI-103 Drugamer using differential refractive index detector (E) HPLC PI-103 standard curve used for quantification of drug release kinetics from drugamer (mean ± SD, n = 3) (F) ^{1}H-NMR spectrum of purified control drugamer in $CDCl_3$. MW, molecular weight; DP, degree of polymerization; HPLC, high performance liquid chromatography; AUC, area under the curve.

A PI-103 Drugamer Polymerization Stoichiometry and Results

Monomer	MW [g mol^{-1}]	Target DP	Mol %	Wt %	Calculated DP[a]
PEGMA 950	950	16.25	65	76	15
PI-103-SMA	560.56	6.25	25	17	6
FIMA	573.55	1.5	6	4	1.4
REMA	591.15	1	4	3	1
[M]:[CTA]:[I]	Total monomer conversion[a] [%]		Total MW [g mol^{-1}][a]		Drug loading [wt%]
25:1:0.25	92		19,000		13.25

[a]based on monomer conversion determined by ^{1}H-NMR

B

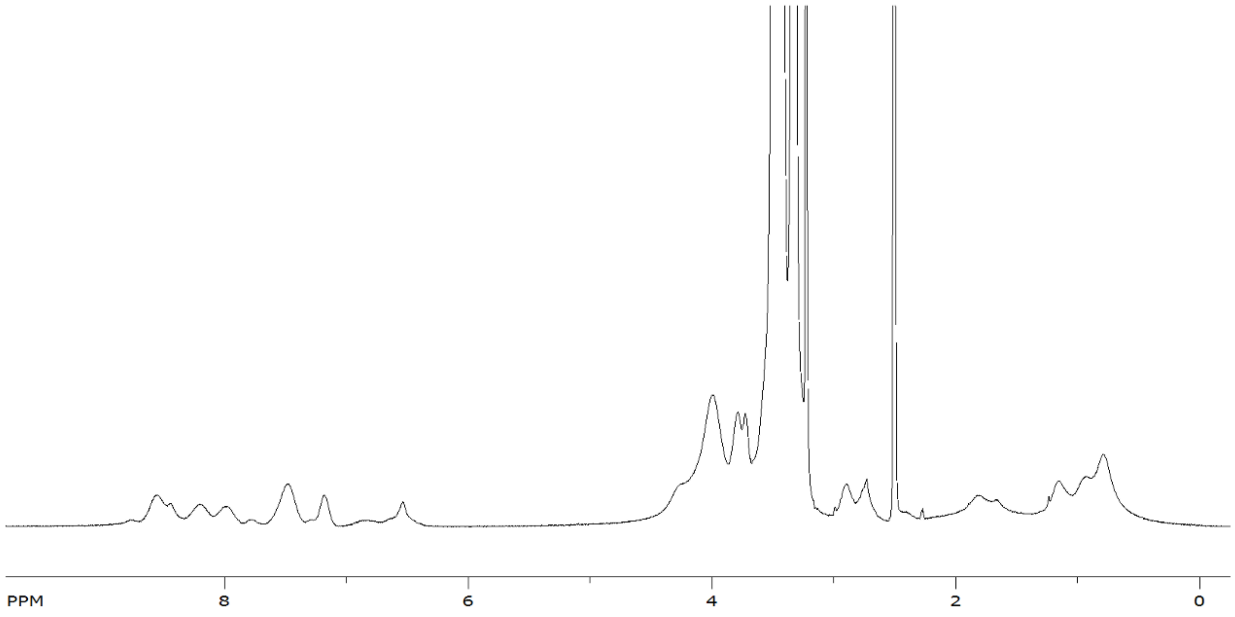

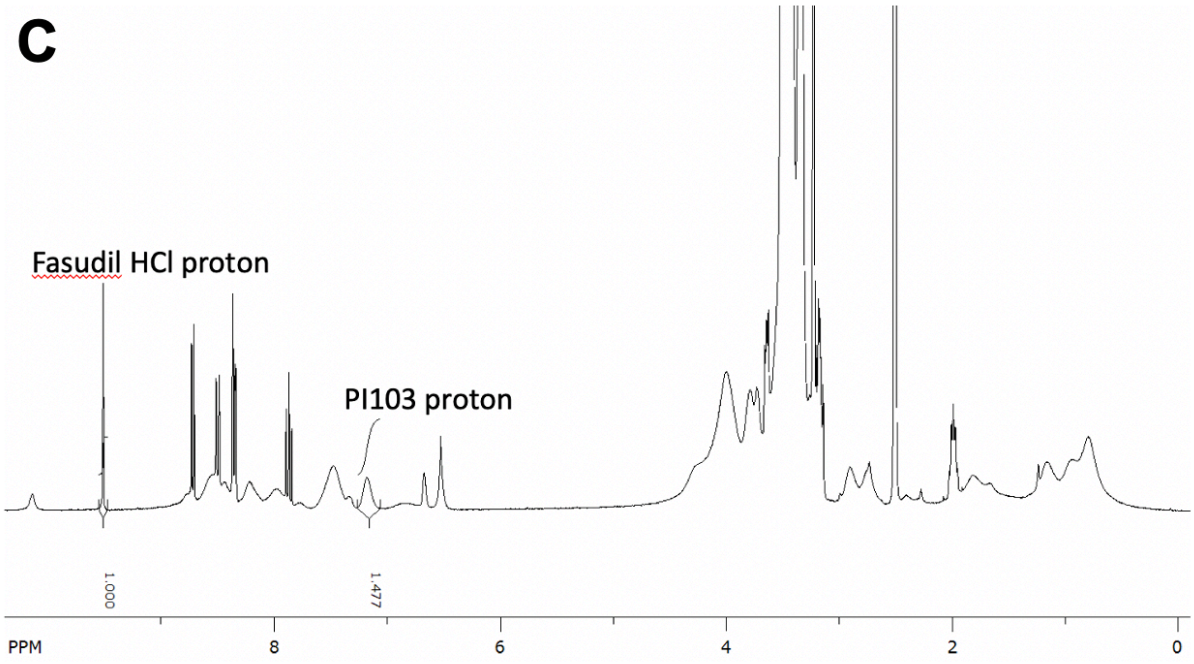
C
Fasudil HCl proton
PI103 proton
1.000
1.477
PPM
8
6
4
2
0

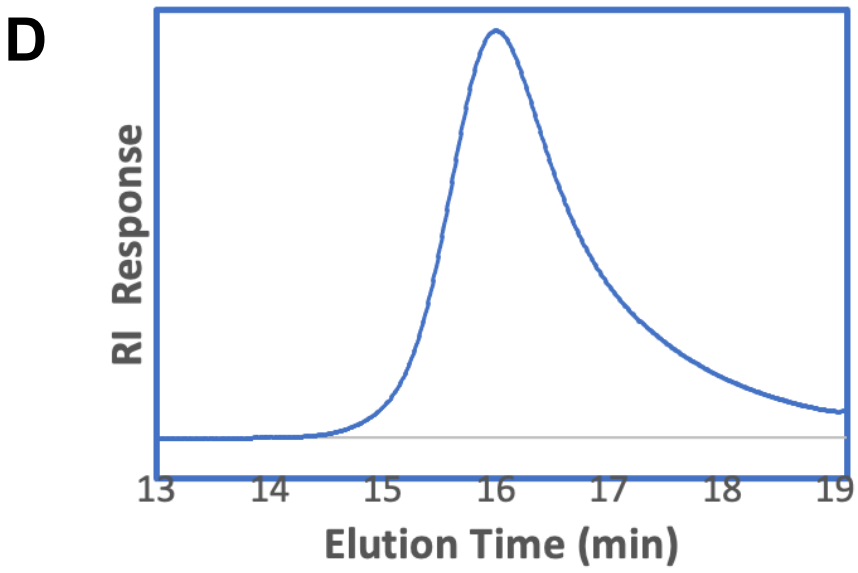
D
RI Response
13
14
15
16
17
18
19
Elution Time (min)

E

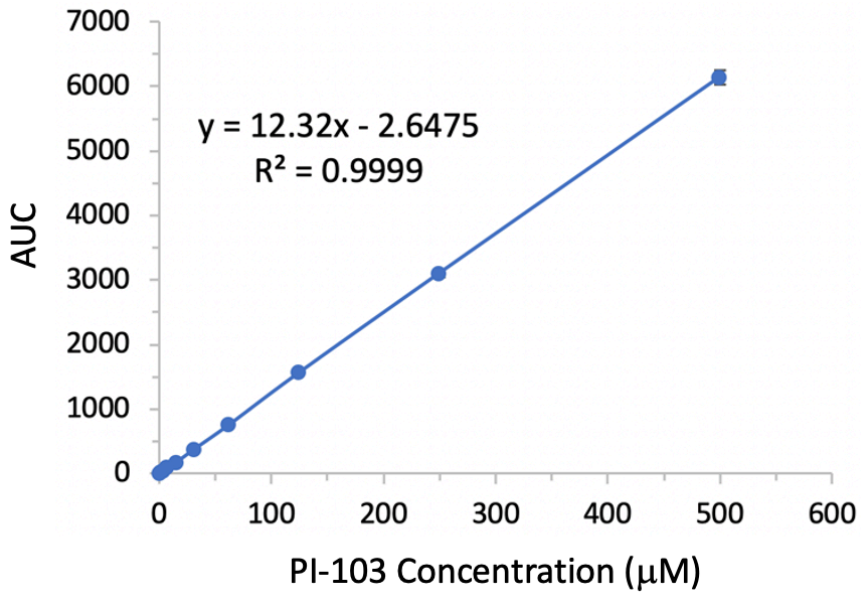

F

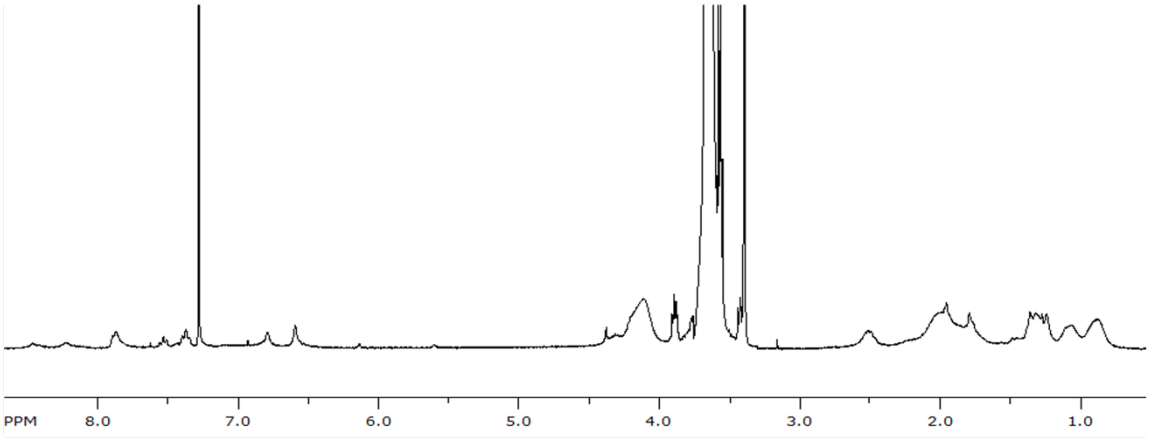

^{1}H-NMR spectrum of control drugamer in $CDCl_3$

Figure S4.4. AntiFl lentiviral construct design and validation. (A) Six constructs were transduced in macrophages and assessed for the surface expression of FITC-E2. AntiFl- β, γ, *δ*, and ***ζ*** exhibited successful FITC-E2 surface expression as indicated by fluorescent detection. (B) AntiFl- γ, *δ*, and ***ζ*** transduced GEMs were then compared to controls (antiFl-*α* and WT) for their ability to load drugamer. 500nM PI-103 drugamer was incubated with GEMs for 15 minutes, followed by a 2X PBS wash. Of the constructs tested, AntiFl-***ζ*** had highest drugamer loading and was selected for subsequent experiments. AntiFl- β, γ, and *δ* proved to be functional receptors as well. (C) AntiFl construct designs and validation. MFI values correspond to histograms (A) and (B) to quantify FITC-E2 expression and drugamer binding, respectively, for each construct and compared against CD19t and WT controls. GEMs, genetically engineered macrophages; AntiFl, Anti-fluorescein receptor; CD19t, truncated CD19; MFI, median fluorescence intensity; fluor, fluorescence.

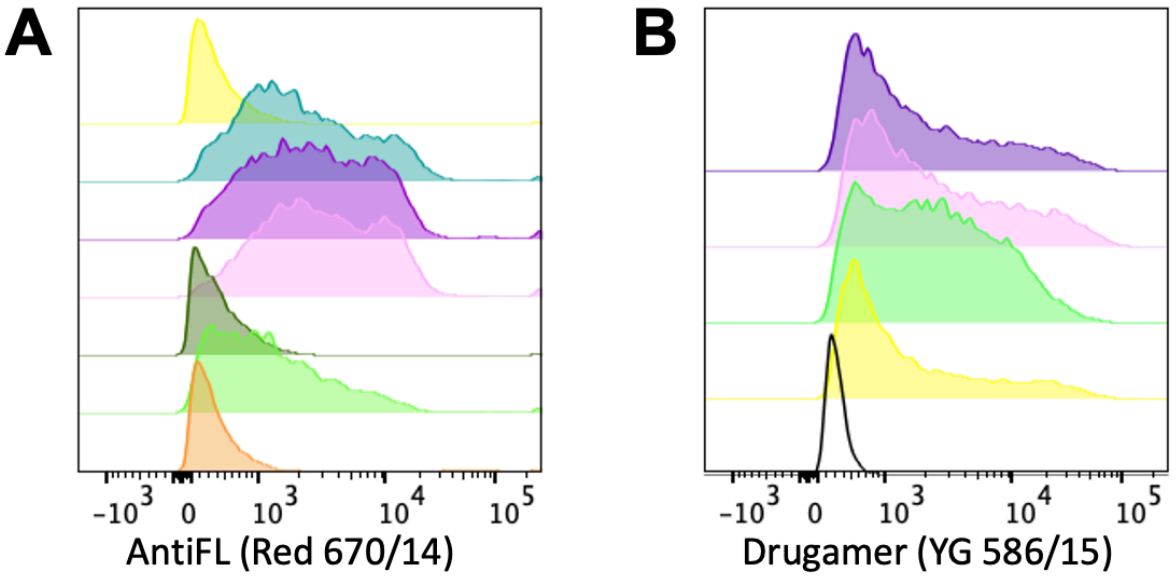

C

Anti-fluorescein receptor construct designs and validation[a].

Shorthand name	Construct design details	FITC-E2 expression [Yes/No]	FITC-E2 fluor [Red 670/14 MFI]	PI-103 Drugamer binding [Yes/No]	PI-103 Drugamer fluor [Red 670/14 MFI]
AntiFl-*α*	FITC-E2-GGGS-CD19t	No	318	Yes	945
AntiFl-β	FITC-E2-IgG4 Hinge-GGGS-CD19t	Yes	1846	--	--
AntiFl-γ	FITC-E2-GGGS-Her2tG	Yes	2457	Yes	1209
AntiFl-*δ*	FITC-E2-IgG4 Hinge-GGGS-Her2tG	Yes	28044	Yes	1633

AntiFl-ε	FITC-E2-IgG4 Hinge-CD28tm-T2A-Her2tG	No	350	--	--
AntiFl-ζ	FITC-E2-GGGS-EGFRt	Yes	1065	Yes	2044
Controls					
CD19t	Truncated CD19 (no scFv)	No	298	--	--
Wild Type	N/A	--	--	--	301

[a]n = 1 - 3

Figure S4.5. PI-103 drugamer binding to AntiFl-ζ and control GEMs (A) AntiFl-ζ GEMs which express an anti-fluorescein single chain variable fragment (scFv) and control truncated (CD19t) GEMs (no scFv) were bound with 0 – 1600 nM PI-103 drugamer, followed by PBS washes and a rest overnight. Flow cytometry histograms show the drugamer-bound GEM populations distribution as a function of drugamer fluorescence (based on rhodamine tag on drugamer). (B) Confocal imaging of untransduced macrophages and AntiFl-ζ GEMs on day 1 after binding with 500 nM PI-103 drugamer (rhodamine, pink). Total scans confirmed the increased co-localization of drugamers to AntiFL-ζ GEMs compared to untransduced control macrophages at a 63X objective and 1.5x digital zoom. Z-slices at different cell depths were used to determine drugamer location (surface-bound or internalized) with respect to the cell nucleus (DAPI, blue) and the cytoskeleton (WGA, green). GEMs, genetically engineered macrophages; DAPI, 6-diamidino-2-phenylindole; WGA, wheat germ agglutinin.

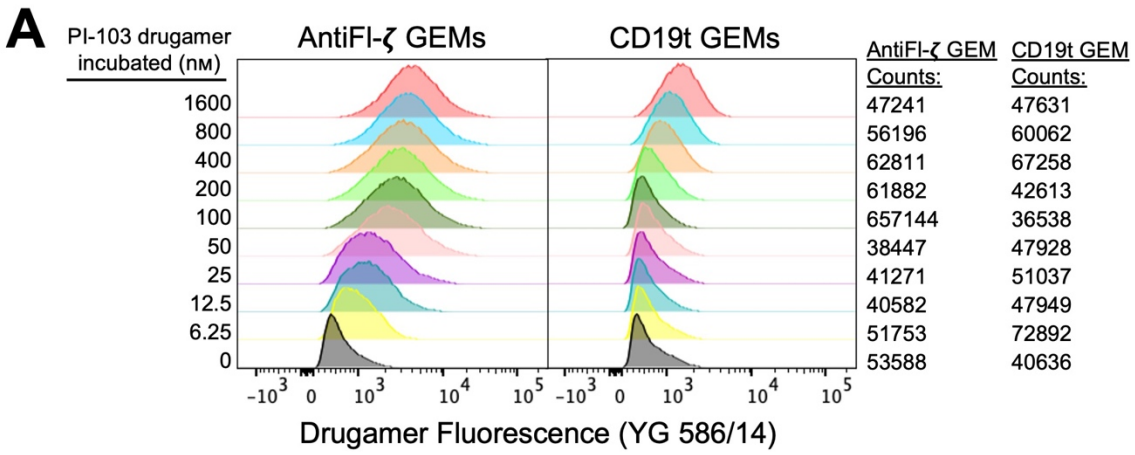
A
PI-103 drugamer incubated (nM)
AntiFl-ζ GEMs
CD19t GEMs
1600
800
400
200
100
50
25
12.5
6.25
0
-10^3 0 10^3 10^4 10^5
Drugamer Fluorescence (YG 586/14)
AntiFl-ζ GEM Counts:
47241
56196
62811
61882
657144
38447
41271
40582
51753
53588
CD19t GEM Counts:
47631
60062
67258
42613
36538
47928
51037
47949
72892
40636

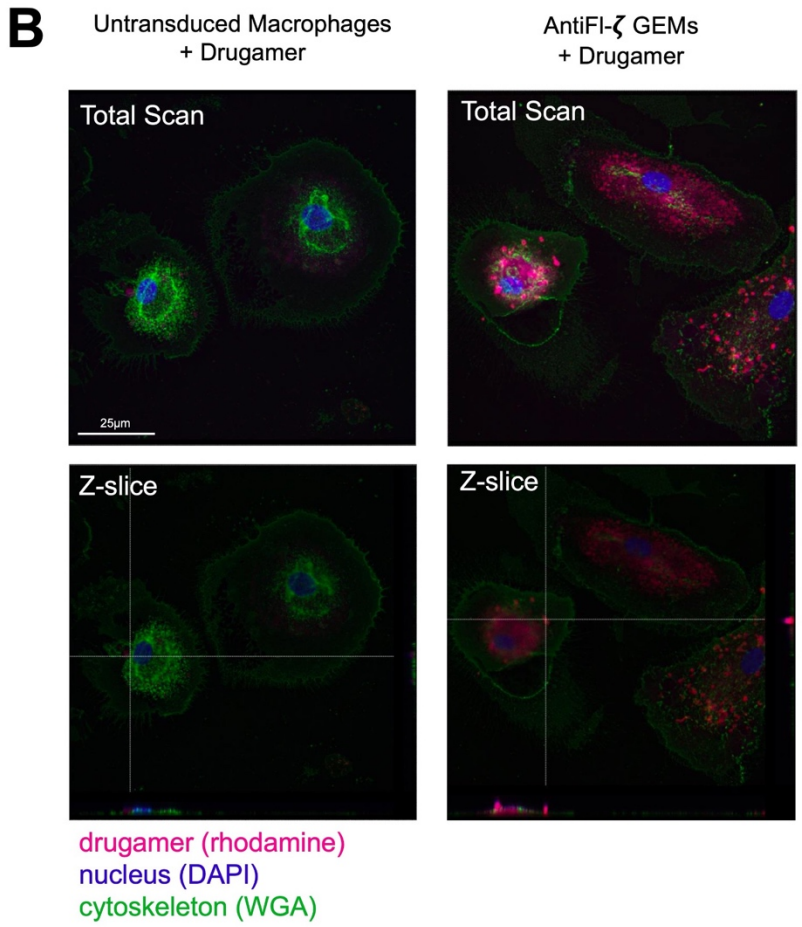
B
Untransduced Macrophages + Drugamer
AntiFl-ζ GEMs + Drugamer
Total Scan
Total Scan
25μm
Z-slice
Z-slice
drugamer (rhodamine)
nucleus (DAPI)
cytoskeleton (WGA)

Figure S4.6. CMP8-SMA monomer synthesis. (A) CMP8-SMA monomer (**11**) was synthesized via HBTU coupling chemistry. To a solution of mono-2-(methacryloyloxy)ethyl succinate (**2**) 345 mg (1.5 mmol) in 300 mL CH_2Cl_2 at 0 ºC, was added *N,N,N′,N′*-tetramethyl-O-(1*H*-benzotriazol-1-yl)uronium hexafluorophosphate (HBTU) 682 mg (1.8 mmol) and *N*,*N*-diisopropylethylamine (DIEA) 525 µL (3 mmol). After stirring at 0 ºC for 10 min, the reaction mixture was stirred at RT for 20 min. DMAP 31 mg (0.25 mmol) and 9a-[(4-chlorophenyl)methyl]-7-hydroxy-4-[4-(2-piperidin-1-ylethoxy)phenyl]-2,9-dihydro-1H-fluoren-3-one (**10**, CMP8) (660 mg, 1.25 mmol) were added as solids and the stirring was continued at room temperature for 3 h. Solvent was concentrated under reduced pressure and the resulting oily crude residue was purified by silica gel column chromatography using 10 % methanol in chloroform to obtain CMP8-SMA (**11**). Yield = 740 mg (80 %). ^{1}H NMR spectrum accounted for all the protons of the monomer. ESI-MS calculated for $C_{43}H_{46}ClNO_8$ (M): 740.3, found: 741.3 $[M+1]^+$. (B) ^{1}H-NMR spectrum of CMP8-SMA monomer (**11**) (C) ESI-Mass spectrum of CMP8-SMA monomer (**11**)

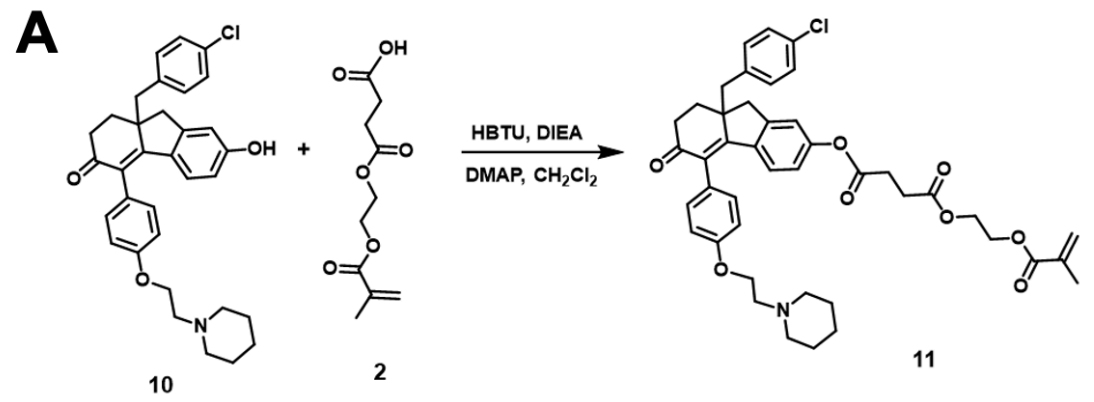
A
Cl
OH
OH
+
HBTU, DIEA
DMAP, CH2Cl2
Cl
10
2
11

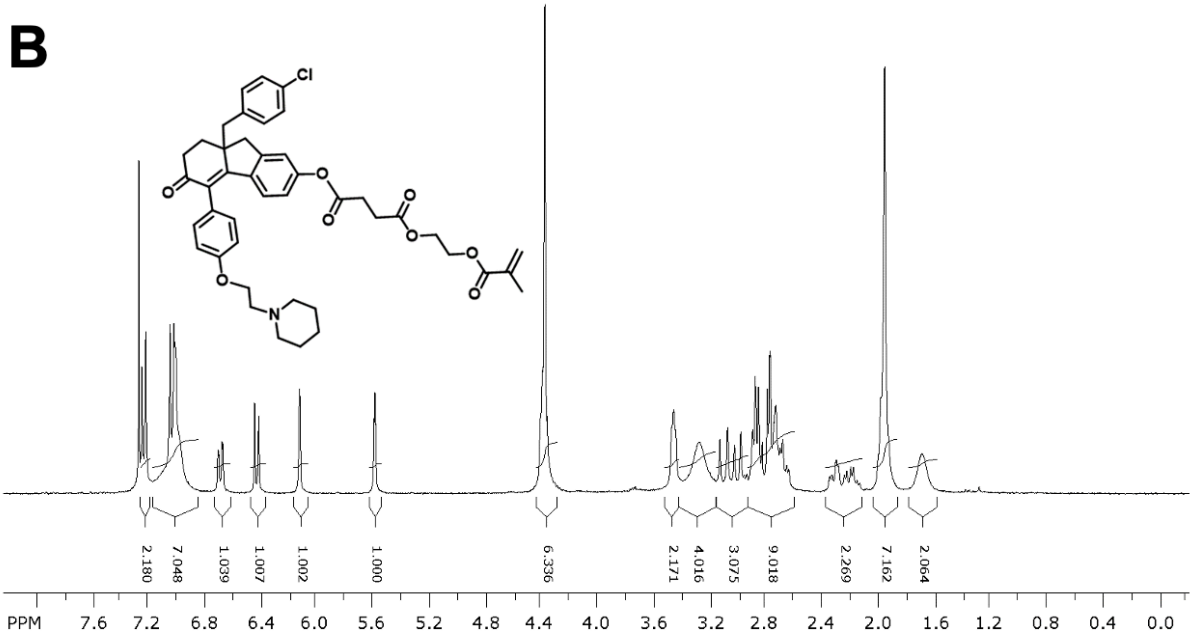
B
Cl
2.180
7.048
1.039
1.007
1.002
1.000
6.336
2.171
4.016
3.075
9.018
2.269
7.162
2.064
PPM
7.6
7.2
6.8
6.4
6.0
5.6
5.2
4.8
4.4
4.0
3.6
3.2
2.8
2.4
2.0
1.6
1.2
0.8
0.4
0.0

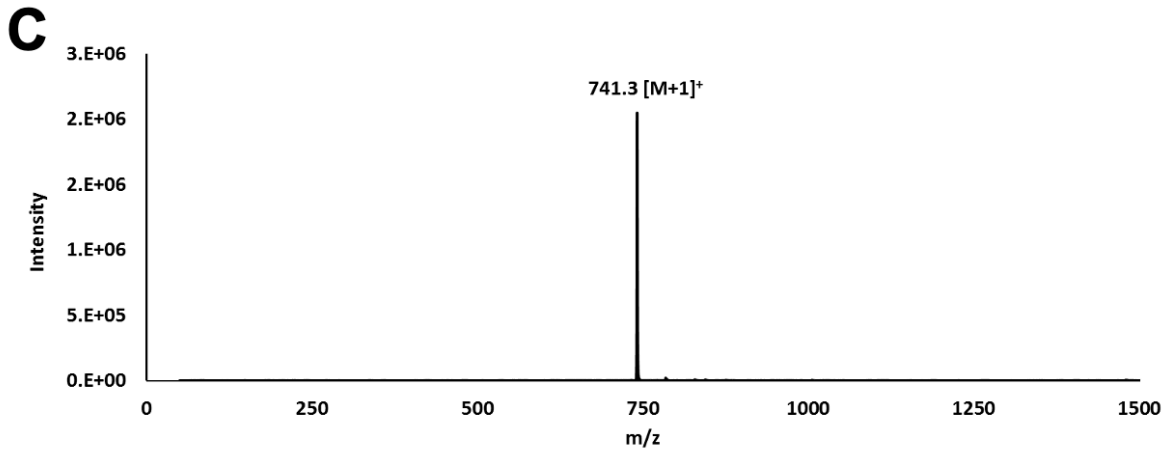
C
741.3 [M+1]+
Intensity
3.E+06
2.E+06
2.E+06
1.E+06
5.E+05
0.E+00
0
250
500
750
1000
1250
1500
m/z

Figure S4.7. CMP8 drugamer synthesis. (A) **Synthesis of poly(tquat-*co*-CMP8SMA-*co*-FIMA):** CMP8-SMA (100 mg, 1.3×10^{-1} mmol), tquat[2, 3] (317 mg, 9.0×10^{-1} mmol), FIMA (52 mg, 9.0×10^{-2} mmol) and 4-cyano-4-(phenylcarbonothioylthio)-pentanoic acid (CTP, 6.3 mg, 2.3×10^{-2} mmol) were dissolved in 1.4 mL anhydrous DMSO in a 5 mL round bottom flask. Finally, 20 µL DMSO solution (65mg/mL concentration) of 4,4'-azobis(4-cyanovaleric acid) (ABCVA, 1.3 mg, 4.5×10^{-3} mmol) was added. The molar ratio of **monomer to chain transfer agent to initiator ratio** ($[M]_0$:$[CTA]_0$:$[I]_0$) was 50:1:0.2. The flask was then sealed with a rubber septum and degassed by purging the solution with nitrogen for 30 min. The flask was then placed in a pre-heated oil bath at 70 °C for 18 h. The solution was cooled to room temperature and precipitated in diethyl ether and centrifuged. The supernatant was decanted, and the polymer was re-dissolved in DMSO (2 mL) and again subjected to ether precipitation (2 times). Yield = 374 mg. **Synthesis of poly(CB-*co*-CMP8SMA-*co*-FIMA):** Poly(tquat-*co*-CMP8SMA-*co*-FIMA) 300 mg was treated with 6 mL trifluoroacetic acid at 4 ºC. After 5 minutes at 4 ºC, the reaction mixture was stirred at room temperature for 4.5 hours. Polymer solution was precipitated in diethyl ether, and centrifuged. The precipitated polymer was washed with ether and dried under high vacuum for 2 h. The polymer was further purified by PD10 desalting columns and lyophilized for 2 days. Yield = 147 mg. Target DP: 50 (B) ^{1}H-NMR spectrum of poly(CB-*co*-CMP8SMA-*co*-FIMA) in deuterated trifluoroacetic acid (C) CMP8 drugamer composition as determined by ^{1}H-NMR.

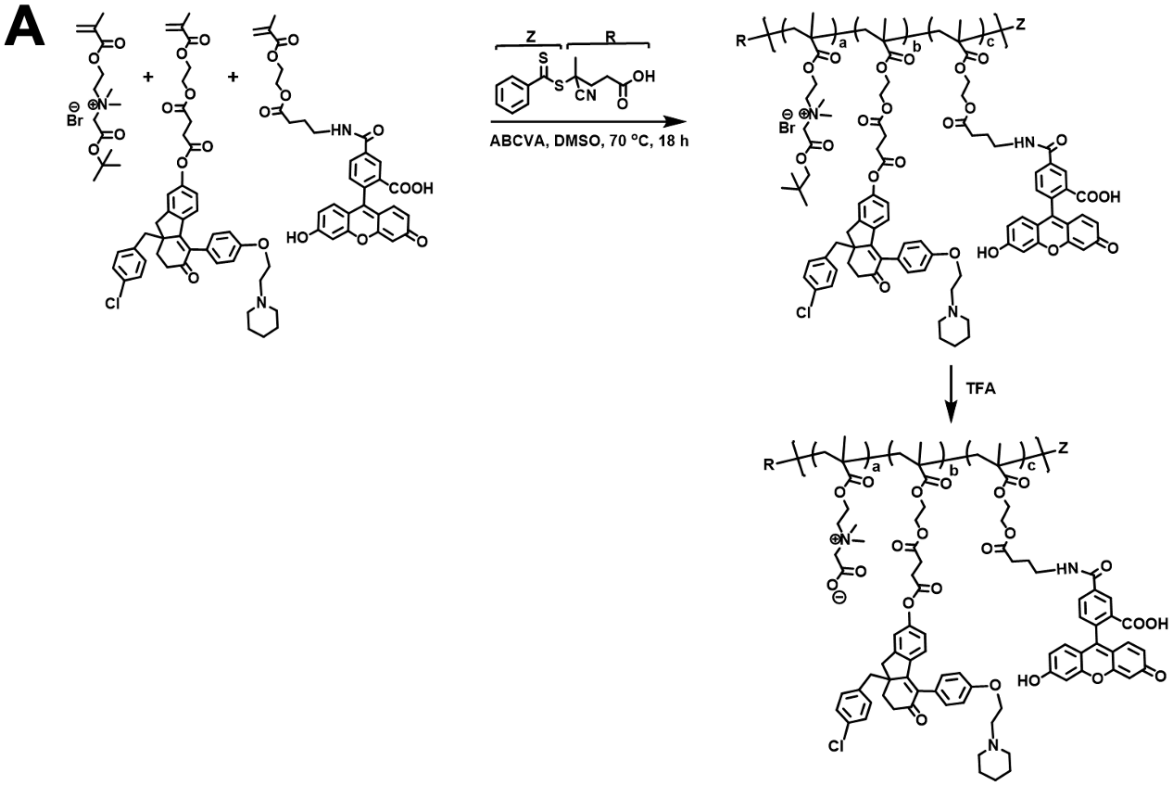
A
ABCVA, DMSO, 70 °C, 18 h
TFA
B
PPM
11.5
10.5
9.5
8.5
7.5
6.5
5.5
4.5
3.5
2.5
1.5
0.5
-0.5
9.2
8.8
8.4
8.0
7.6
7.2
6.8
1.129
1.229
1.228
16.20
1.002
1.039
225.11
66.83

C

CMP8 Drugamer composition as determined by ^{1}H-NMR

Monomer	MW [g mol^{-1}]	Mol %	Wt % of monomer	Wt % of drug
CB	215	83	62	--
CMP8-SMA	740	8	20	14.6
FIMA	574	9	18	11.3

Figure S4.8. Jurkat AntiFl-**ζ** expression and CMP8 drugamer binding. Jurkat cells were co-transduced with AntiFl-**ζ** and eBFP2-ERdd. Anti-fluorescein scFv (FITC-E2) expression in AntiFl.BFP Jurkats was high compared to wildtype and unstained controls. AntiFl.BFP Jurkats incubated with CMP8 drugamer had decreased scFv fluorescence intensity, indicating that CMP8 drugamer loading was successful and that scFv was no longer available for anti-fluorescein antibody binding.

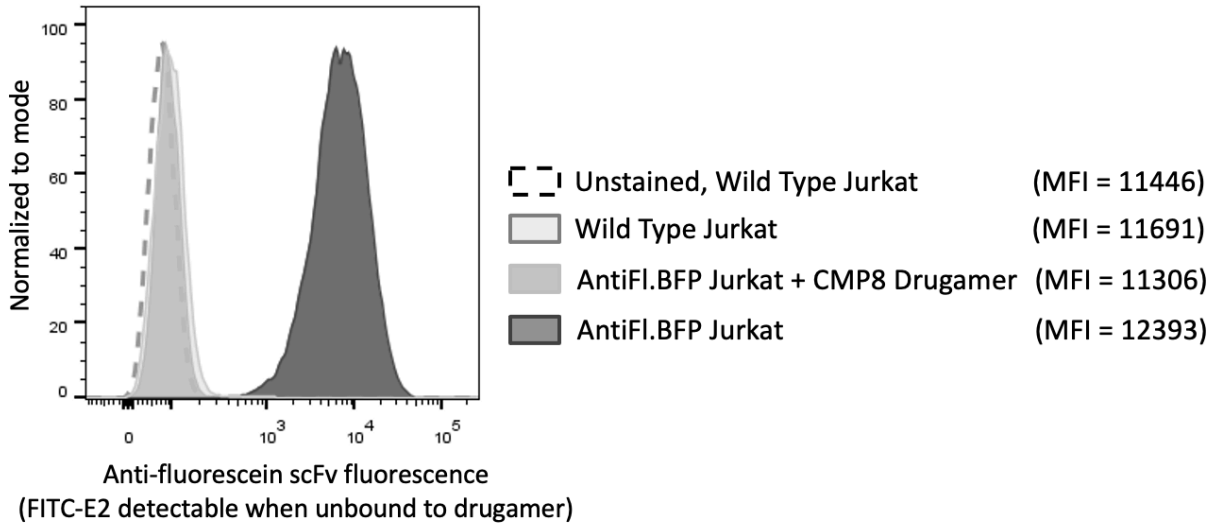

[1] S. Buchini, A. Buschiazzo, S.G. Withers, A New Generation of Specific Trypanosoma cruzi trans-Sialidase Inhibitors, Angewandte Chemie International Edition, 47 (2008) 2700-2703.
[2] Z. Cao, Q. Yu, H. Xue, G. Cheng, S. Jiang, Nanoparticles for Drug Delivery Prepared from Amphiphilic PLGA Zwitterionic Block Copolymers with Sharp Contrast in Polarity between Two Blocks, Angewandte Chemie International Edition, 49 (2010) 3771-3776.
[3] H. Freeman, S. Srinivasan, D. Das, P. Stayton, A. Convertine, Fully synthetic macromolecular prodrug chemotherapeutics with EGFR targeting and controlled camptothecin release kinetics, Polymer Chemistry, 9 (2018) 5224-5233.

Chapter 5. CONCLUSIONS AND FUTURE DIRECTIONS

Ciana L López

5.1 SUMMARY

The investigations presented herein expand on previous work that validate the incredible versatility of drugamers in a variety of disease contexts with improved targeting, controlled drug release properties, and straight-forward synthetic schemes. In each application, incorporation of functional monomers at precisely tuned ratios facilitated design of soluble drugamers with targeting ligands and fine-tuned drug release. We also present the first investigations combining drugamers with virus-like particles and cell-based therapeutics and demonstrate that their modular design allows for efficient co-delivery and small molecule drug activity to complement biologic mechanisms.

First, the use of inhalable antibiotic drugamers, which were initially designed to treat intracellular pulmonary infections, was expanded for the treatment of extracellular pulmonary infections caused by *Klebsiella pneumoniae* (Kp). These drugamers are linear random copolymers composed of ciprofloxacin prodrug and mannose comonomers. The incorporation of multiple units of mannose allows for effective targeting of the mannose receptor on alveolar macrophages. Once the polymer is taken into the endolysosomal compartment, the release of the drug cargo is triggered by cleavage of a peptide linker creating local drug reservoirs that lead to enhanced whole lung pharmacokinetic properties. Drugamer treatment significantly improved survival compared to an equivalent dose of parent ciprofloxacin. Drugamer treatment also decreased bacterial burdens, lung

injury, and neutrophilic inflammation, suggesting that the improved delivery of antibiotic was able to improve homeostasis and prevent the excessive host response associated with Kp infections.

Next, we showed that radiant star drugamers could reformulate the TLR7/8 agonist resiquimod and be encapsulated within self-assembling I53-50-V5 ("V5") protein nanoparticles for a vaccine application. This polymer was synthesized from a hyperbranched core and incorporated a random distribution of resiquimod prodrug, anionic mono-2-(methacryloyloxy)ethyl succinate (SMA), and a small amount of rhodamine fluorescent tag comonomers. The SMA imparted a negative charge on the polymer, which allowed for association with the inner luminal surface of the self-assembling protein nanoparticle. The degree of polymerization of the drugamer was also optimized to allow for efficient packaging of the dense polymer material. *In vitro* release studies showed that packaging of the drugamer did not inhibit drug release, which was hydrolysis-mediated and sustained over a week. Co-delivery of the nanoparticle-packaged drugamer *in vivo* resulted in more potent humoral immune responses against V5 compared to V5 mixed with a 55-fold higher dose of parent resiquimod, while also minimizing systemic toxicity.

Lastly, we demonstrated that fluorescein-tagged drugamers could be loaded onto immune cell therapeutics via a genetically encoded anti-fluorescein receptor. Loading on Genetically Engineered Macrophages (GEMs) was primarily surface-displayed and stable over the course of 10 days. Drugamers containing phosphoinositide-3-kinase (PI3K) inhibitor drugamers were loaded onto Genetically Engineered Macrophages (GEMs) for delivery to cancer cells. Estrogen receptor analog drugamers were loaded onto T cells to activate intracellular protein activity.

5.2 FUTURE DIRECTIONS

5.2.1 Inhalable drugamers to treat pulmonary infection

In Chapter 2 we showed that inhalable antibiotic drugamers significantly improved survival in mice with bacterial Kp pneumonia compared to treatment with an equivalent dose of parent drug. In our studies the fluoroquinolone antibiotic, ciprofloxacin, was used in our drugamer formulation because it is a frontline approach to treatment of susceptable Kp infections. However, the drugamer platform is widely adaptable to other classes of antibiotics as well as other drug classes. Combination therapy against Kp infections is fairly common (53% compared to 47% monotherapy in one meta-analysis) and have been more effective in respiratory infections (29% failure vs. 67% failure for monotherapy).[1] It might be possible to enhance survival and bacterial clearance further by co-delivery of carbapenem (e.g. meropenem or ertapenem) drugamers.[2, 3] Our lab has successfully synthesized meropenem monomers that could easily be incorporated into a mannose-targeted, VC-linker drugamer (Figure 5.1A). Initial safety and tolerability studies following intratracheal administration of the parent drug, meropenem, up to 50 mg/kg showed no significant effect on weight or % neutrophil influx indicating meropenem drugamers would be a viable option.

Another exciting direction would be to stimulate an immunomodulatory defense mechanism to compliment antibiotic drugamer treatment. Extracellular pathogens such as *Streptococcus pneumoniae* have been shown to activate type I IFN cascades in the lungs to promote eradication of infection, indicating that STING agonists could have therapeutic benefits against Kp.[4] While there are challenges associated with the timing of treatment with immunostimulatory drugs that would need to be carefully optimized, there is potential to enhance infection clearance and gain understanding of underlying immune responses to inflammatory pneumonia. Our drugamer platform supports all-in-one combination therapy that could allow for

spatial and temporal control to enhance respective drug efficacy. We've shown that RAFT-based drugamers can be synthesized with different classes of drugs (e.g. Resiquimod-co-Galunisertib drugamer for anti-cancer therapy, Figure 5.1B) and are confident that well-defined combination drugamers could be reproducibly synthesized for infection therapeutics as well.[5]

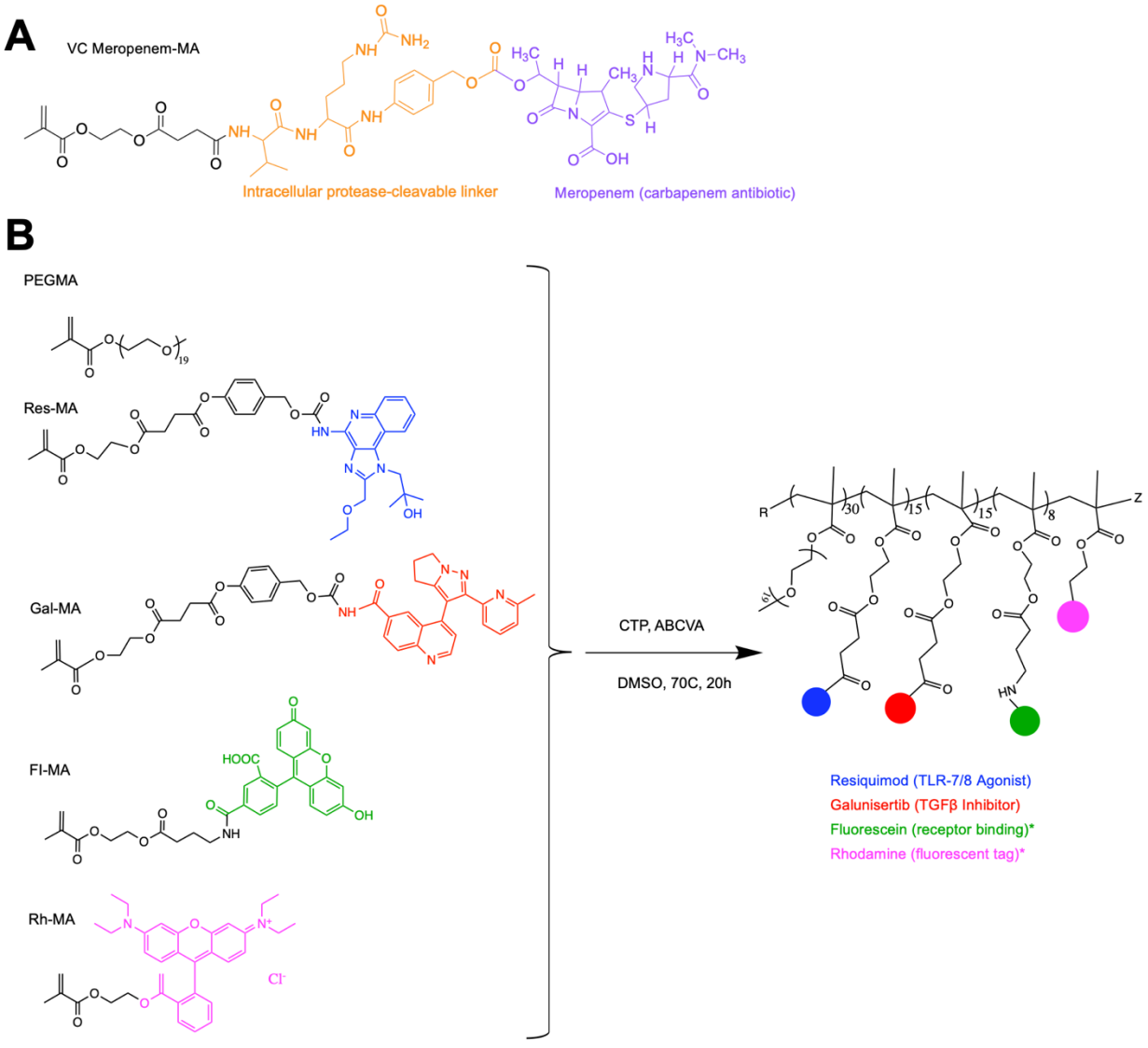

Figure 5.1 Alternative synthetic approaches to improve therapeutic efficacy of drugamer against *Klebsiella pneomoniae* infections. (A) A VC-Meropenem monomer could be co-polymerized with mannose-MA. (B) Combination drugamers have been successfully synthesized using RAFT, including this tert-co-polymer containing

TLR-agonist, Resiquimod and TGFβ-inhibitor, Galunisertib. *Fluorescein and rhodamine methacrylates were also included for successful binding to GEMs (as described in Chapter 4).

5.2.2 Protein vaccines

While the antigen used for this initial study here was the protein nanoparticle itself, it is also worth exploring modalities for delivery of different types of antigens. Since we have demonstrated encapsulation of both adjuvant drugamer and nucleic acid cargos with VLPs separately, the possibility of dual encapsulation should be investigated to develop a potent mRNA-based vaccine. Acid-degradable (e.g., hydrazone) conjugation of genetic cargos to radiant star polymers could facilitate co-encapsulation within VLPs to facilitate protection from enzymatic degradation prior to delivery to a cellular target.[6] If dual encapsulation is difficult, alternatively, SpyCatcher-tagged antigens have been attached to SpyTag-decorated VLPs.[7] By a similar mechanism targeting ligands could be used to deliver vaccines to specific immune cell types as a means of controlling immune response elicited.[8, 9] While it could be impactful to co-delivery antigen and adjuvant within our VLP system, others have shown that packaging of antigen and adjuvant in separate VLPs may also lead to effective vaccination, due to efficient lymphatic trafficking.[10]

Encapsulation of the TLR7/8 agonist resiquimod was able to elicit a potent humoral immune response by co-delivery of radiant star drugamer within a protein nanoparticle. Such a response indicates vaccination by antigen processing via the MHC II pathway. Depending on the disease target for the vaccine and whether applied as a prophylactic or therapeutic agent, it may be desired to elicit an adaptive immune response. Vaccines achieve such a response by successful presentation of an antigen via MHC class I pathway. The drugamer platform could be used to

incorporate other types of small molecule adjuvants, such as STING agonists, that are known to activate type-I interferon responses, upregulate antigen cross-presentation, and induce CD8+ T cell immune responses.[11]

5.2.3 Biologic-secreting GEMs for treatment of pulmonary infections

Macrophages are an emerging class of cell therapeutics because they can rapidly traffic and become tissue-resident within key sites of disease and inflammation.[12-14] Beyond their investigation for cancer therapies as described in Chapter 4, their use has been investigated in other disease settings. Trapnell et al. showed that pulmonary transplantation of macrophages was safe, well-tolerated, and corrected murine models of hereditary pulmonary alveolar proteinosis (hPAP) lung disease for 9 months – 1 year following just one intratracheal administration.[13, 15-17] Transplanted cells became tissue resident AMs. The striking long-term localization of these therapeutic macrophages in such lung disease contexts indicates their potential for treatment of LRIs like Kp.

Macrophages are key to host defense at every stage of Kp infection. Upon initial exposure, detection of Kp-associated endotoxins induces the expression of interleukin-1 (IL-1) and tumor necrosis factor alpha (TNFα) within one hour and a subsequent neutrophilic exudate at 6 – 12 hours.[18] Circulating monocytes are also recruited to the lungs around 24 hours. Phagocytic neutrophils and macrophages (both resident and recruited) clear bacteria and apoptotic cells.[14, 19, 20] Around 48 hours macrophages secrete interferon gamma (IFNγ), granulocyte colony stimulating factor (GCSF), and interleukin-12 (IL-12) to recruit and activate leukocytes. Antimicrobial peptides (AMPs) such as cathelicidin-related AMP (CRAMP) are also secreted by as important mediators of host defense against Kp.[21-27]

Given the endogenous roles of both IL-12 and AMPs in pulmonary infection clearance, others have investigated the use of oral, parateral and intranasal treatment with such recombinant proteins.[19, 22, 26] Unfortunately, protease degradations, poor pulmonary biodistribution, and off-target toxicity have prevented sustained therapeutic efficacy. **We hypothesized that transplantation of biologic-secreting GEMs could facilitate local, extended delivery of therapeutic proteins such as antimicrobial peptides and immunomodulatory cytokines (i.e., IL-12 and CRAMP) to resolve Kp infections.** We have conducted preliminary studies as described below towards the goal of validating this hypothesis:

AIM 1. Determine murine GEM trafficking to K. pneumoniae pulmonary infection niches

To study pulmonary trafficking of GEMs, we use GEMs that express eGFP:ffluc, a common gene construct that contains a fluorescent tag (enhanced green fluorescent protein, eGFP), and a light-emitting enzyme firefly luciferase (ffluc) that catalyzes oxidation of D-luciferin substrate.[13] Using IVIS bioluminescent imaging, we visualized GEMs in live mice over time.

Preliminary studies were conducted in healthy mice. Following both intratracheal and IV administration routes, eGFP:ffluc GEMs were detected in murine lungs as shown by 1 hour IVIS images (Figure S1A and Figure 5.2, respectively). Initial characterization of both administration routes importantly suggests that therapeutic GEMs could ultimately be administered by either route, however for simplicity, subsequent experiments will focus on intratracheal administration. A data analysis tool called InVivoPLOT was used to quantitatively determine GEM distributions in mice using defined spatial geometry and organ probability maps based on a statistical mouse atlas (Figure S1B).[28] Intratracheal studies showed that there was good distribution of GEMs

between the left and right lungs, with slightly more in the larger right lung (62%, Figure S1C). GEMs were well-tolerated after both intratracheal and IV administration, with no significant changes in mouse weight and temperature (Figure S1E). For both routes, GEMs were undetectable via IVIS in healthy mouse lungs by 24 hours. Flow cytometry analysis of BALs collected from mice on day 7 after intratracheal administration indicated that 5% of BAL cells were GFP+, indicating that a small number of GEMs remained 7 days later (Figure S1D); we expect that GEM lung residence time and amount will be prolonged in our Kp infection model and plan to evaluate this hypothesis next.

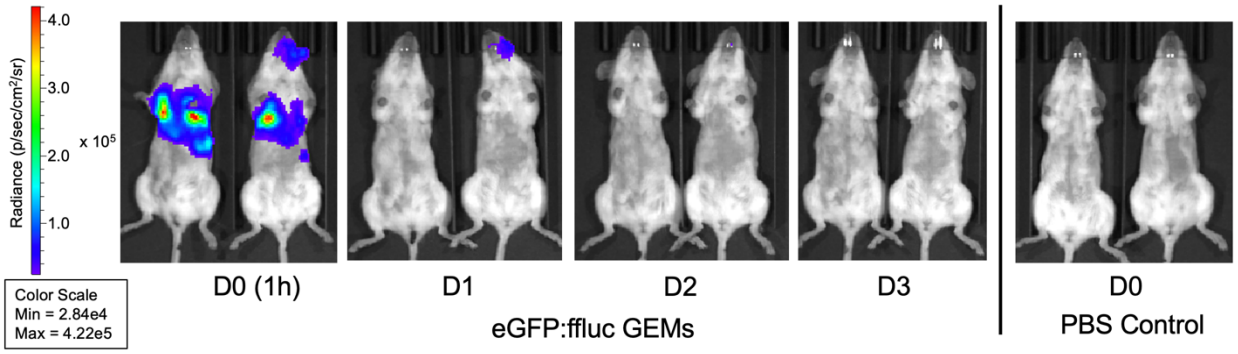

Figure 5.2 IVIS imaging of eGFP:ffluc GEMs in healthy mice following retroorbital administration. 250,000 eGFP:ffluc GEMs were administered to healthy albino C57BL/6 mice and showed rapid delivery to mouse lungs by 1 hour as detected by IVIS bioluminescent imaging. The GEMs are no longer detectable in the lungs by 24 hours. All images scaled to D0 optimal radiance settings (min = 2.48e4, max – 4.22e5).

AIM 2. Generation and validation of biologic-secreting GEM therapeutics

Our preliminary studies have shown that murine GEMs can be transduced with lentivirus encoding for secretion of murine IL-12 (Figure 5.2A). Transduction is titratable, as shown in Figure 5.2B. With increasing lentiviral particles per cell there is increased production of IL-12.

This may be advantageous in determining an optimal dose of IL-12 GEMs to elicit therapeutic efficacy in Kp models.

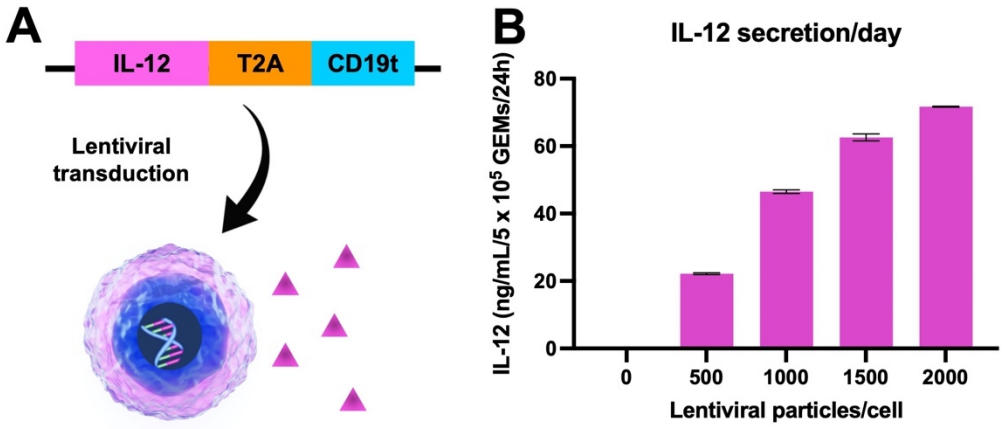

Figure 5.2 Generation of IL-12 secreting GEMs as pulmonary infection therapeutics. (A) plasmid construct used for constitutive secretion of murine IL-12 from GEMs. (B) Expression of IL-12 from GEM was quantified six days after transduction and shows titratable dosage of IL-12 dependent on amount of lentiviral particles/cell.

Towards the goal of generating mCRAMP GEMs, we evaluated the microbicidal activity of murine CRAMP and found it to inhibit the growth of Kp in a dose-dependent manner (Figure 5.3A). Generation of a plasmid construct as shown in Figure 5.3B will allow us to determine the antimicrobial activity of mCRAMP secreting GEMs *in vitro* with relative ease.

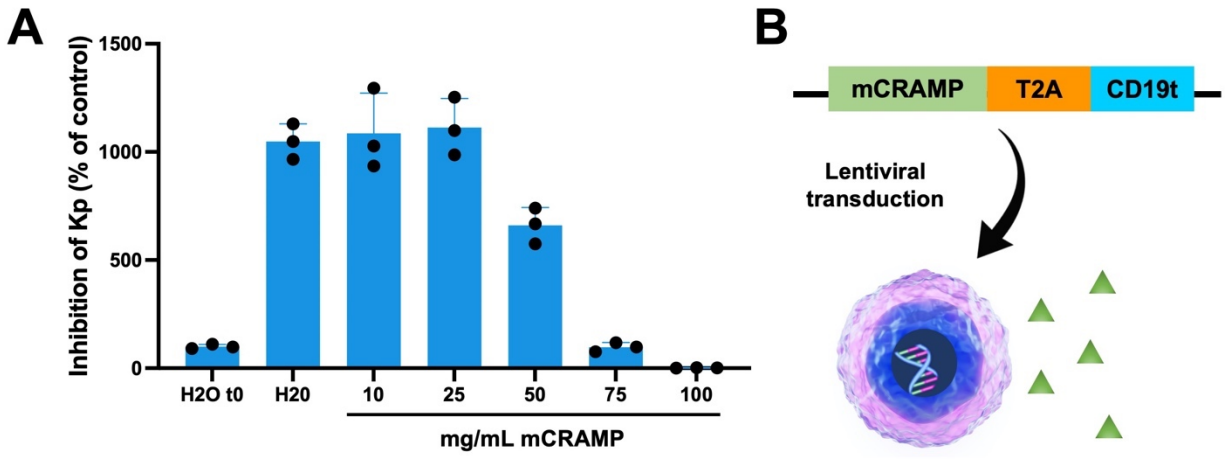

Figure 5.3 Validation of AMP activity against Kp prior to design of AMP-secreting GEMs (A) *In vitro* assay demonstrated inhibition of Kp at increased concentrations of murine

CRAMP (mCRAMP) (B) Proposed plasmid design for lentiviral transduction of macrophages to achieve constitutive expression of mCRAMP.

AIM 3. Evaluation of therapeutic GEM efficacy in vitro and in vivo

As a final step, the therapeutic efficacy of IL-12 and CRAMP GEMs will be assessed in a murine model of Kp compared to free recombinant protein. A survival study will be conducted as a primary read out for therapeutic efficacy. Bacterial burden and host response will be evaluated to elucidate the mechanisms and dynamics of these therapeutic cell product.

5.3 LIST OF PUBLICATIONS AND PRESENTATIONS

Peer-reviewed publications

1. **Ciana L López**, Guilhem Rerolle, Sarah Snyder, Simbarashe Jokonya, Abdullah Abasham, Brian Lee, Jessica Snyder, T Eoin West, Shawn Skerrett, Patrick Stayton. Alveolar macrophage-targeted drugamers improve survival against extracellular *Klebsiella pneumoniae* infections. *[in prep]*
    - Chapter 2
2. Karla-Luise Herpoldt, **Ciana L López,** Isaac Sappington, Selvi Srinivasan, Minh Pham, Jason Netland, Kate Montgomery, Anthony J Convertine, Marion Pepper, Patrick S Stayton, Neil P King (2024). Macromolecular cargo encapsulation via in vitro assembly of engineered two-component protein nanoparticles. *Advanced Healthcare Materials*, doi: 10.1002/adhm.202303910
    - Chapter 3

3. **Ciana L López**, Katherine J Brempelis, James F Matthaei, Kate S Montgomery, Selvi Srinivasan, Debashish Roy, Fei Huang, Shannon A Kreuser, Jennifer L Gardell, Ian Blumenthal, John Chiefari, Michael C Jensen, Courtney A Crane, Patrick S Stayton (2021). Arming Immune Cell Therapeutics with Polymeric Prodrugs. *Advanced Healthcare Materials*, doi: 10.1002/adhm.202101944
    - Chapter 4
4. Duy-Khiet Ho, Clare LeGuyader, Selvi Srinivasan, Debashish Roy, Vladimir Vlaskin, Thomas EJ Chavas, **Ciana L Lopez**, Jessica M Snyder, Almar Postma, John Chiefari, Patrick S Stayton (2020). Fully synthetic injectable depots with high drug content and tunable pharmacokinetics for long-acting drug delivery. *Journal of Controlled Release*, doi: 10.1016/j.jconrel.2020.11.030
5. Nicole AP Lieberman, Shannon Kreuser, **Ciana Lopez**, Katherine Brempelis, Harrison Chinn, Courtney A Crane (2019). Current state of genetically engineered macrophages for anti-cancer therapy. Cell & Gene Therapy Insights, doi: 10.18609/cgti.2019.063
6. Sarah Snyder, Guilhem Rerolle, Simbarashe Jokonye, Dinh Chuong Nguyen, **Ciana L López**, Shawn Skerrett, T Eoin West, Patrick Stayton. Host-directed immune therapy with combination STING agonist and antibiotic polymeric prodrugs against intracellular bacterial infections. Experiments in progress.
7. **C. L. López**, G. Rerolle, O. Arias, A. Bashmail, G. Gonzalez, P. S. Stayton, S. Skerrett, T. E. West. “Host-directed macrophage therapeutics deliver IL-12 locally to treat pulmonary infection.” Experiments in progress.

Presentations at national and international conferences

1. Oral Presentation at the 2023 Biomedical Engineering Society (BMES) Annual Meeting in Seattle, WA "*Arming Immune Cells with Polymeric Prodrugs via a Genetically-encoded Anti-fluorescein Receptor"*
2. Oral Presentation at the 2023 LatinXinBMES Symposium in Seattle, WA "*Alveolar macrophage-targeted drugamers improve survival against extracellular Klebsiella pneumoniae infections"*
3. Poster Presentation at the 21st Annual Nanomedicine and Drug Delivery Symposium in Cambridge, MA *"Alveolar macrophage-targeted polymer prodrugs improve survival against Klebsiella pneumoniae infections"*
4. Oral Presentation at the Materials Research Society Spring Virtual Meeting 2021 *"A Platform for Macrophage-Mediated Delivery of Polymeric Prodrugs to Solid Tumors"*
5. Oral Presentation at the Society for Biomaterials (SFB) Virtual Conference 2021 *"Arming Genetically Engineered Macrophages with Pathway Inhibitor Drugs for Sustained Release"*
6. Poster Presentation at the Biomedical Engineering Society (BMES) Virtual Conference 2021 *"A Platform for Macrophage-mediated Delivery of Polymeric Drugs to Solid Tumors"*

REFERENCES

[1] G.C. Lee, D.S. Burgess, Treatment of Klebsiella Pneumoniae Carbapenemase (KPC) infections: a review of published case series and case reports, Annals of Clinical Microbiology and Antimicrobials, 11 (2012) 32.
[2] C.A. DeRyke, M.A. Banevicius, H.W. Fan, D.P. Nicolau, Bactericidal activities of meropenem and ertapenem against extended-spectrum-beta-lactamase-producing Escherichia coli and Klebsiella pneumoniae in a neutropenic mouse thigh model, Antimicrobial agents and chemotherapy, 51 (2007) 1481-1486.
[3] E.S. Wiener, E.L. Heil, L.M. Hynicka, J.K. Johnson, Are Fluoroquinolones Appropriate for the Treatment of Extended-Spectrum β-Lactamase-Producing Gram-Negative Bacilli?, J Pharm Technol, 32 (2016) 16-21.
[4] D. Parker, F.J. Martin, G. Soong, B.S. Harfenist, J.L. Aguilar, A.J. Ratner, K.A. Fitzgerald, C. Schindler, A. Prince, Streptococcus pneumoniae DNA initiates type I interferon signaling in the respiratory tract, mBio, 2 (2011) e00016-00011.
[5] H.N. Son, S. Srinivasan, J.Y. Yhee, D. Das, B.K. Daugherty, G.Y. Berguig, V.G. Oehle, S.H. Kim, K. Kim, I.C. Kwon, P.S. Stayton, A.J. Convertine, Chemotherapeutic copolymers prepared via the RAFT polymerization of prodrug monomers, Polymer Chemistry, 7 (2016) 4494-4505.
[6] I. Dovydenko, I. Tarassov, A. Venyaminova, N. Entelis, Method of carrier-free delivery of therapeutic RNA importable into human mitochondria: Lipophilic conjugates with cleavable bonds, Biomaterials, 76 (2016) 408-417.
[7] A. Marini, Y. Zhou, Y. Li, I.J. Taylor, D.B. Leneghan, J. Jin, M. Zaric, D. Mekhaiel, C.A. Long, K. Miura, S. Biswas, A Universal Plug-and-Display Vaccine Carrier Based on HBsAg VLP to Maximize Effective Antibody Response, Frontiers in Immunology, 10 (2019).
[8] T. Ung, N.S. Rutledge, A.M. Weiss, A.P. Esser-Kahn, P. Deak, Cell-targeted vaccines: implications for adaptive immunity, Frontiers in Immunology, 14 (2023).
[9] S. Bhagchandani, J.A. Johnson, D.J. Irvine, Evolution of Toll-like receptor 7/8 agonist therapeutics and their delivery approaches: From antiviral formulations to vaccine adjuvants, Adv Drug Deliv Rev, 175 (2021) 113803.
[10] M.O. Mohsen, A.C. Gomes, G. Cabral-Miranda, C.C. Krueger, F.M.S. Leoratti, J.V. Stein, M.F. Bachmann, Delivering adjuvants and antigens in separate nanoparticles eliminates the need of physical linkage for effective vaccination, Journal of Controlled Release, 251 (2017) 92-100.
[11] J.M. Ramanjulu, G.S. Pesiridis, J. Yang, N. Concha, R. Singhaus, S.-Y. Zhang, J.-L. Tran, P. Moore, S. Lehmann, H.C. Eberl, M. Muelbaier, J.L. Schneck, J. Clemens, M. Adam, J. Mehlmann, J. Romano, A. Morales, J. Kang, L. Leister, T.L. Graybill, A.K. Charnley, G. Ye, N. Nevins, K. Behnia, A.I. Wolf, V. Kasparcova, K. Nurse, L. Wang, A.C. Puhl, Y. Li, M. Klein, C.B. Hopson, J. Guss, M. Bantscheff, G. Bergamini, M.A. Reilly, Y. Lian, K.J. Duffy, J. Adams, K.P. Foley, P.J. Gough, R.W. Marquis, J. Smothers, A. Hoos, J. Bertin, Design of amidobenzimidazole STING receptor agonists with systemic activity, Nature, 564 (2018) 439-443.
[12] K.B. Long, G.L. Beatty, Harnessing the antitumor potential of macrophages for cancer immunotherapy, Oncoimmunology, 2 (2013) e26860.
[13] K.J. Brempelis, C.M. Cowan, S.A. Kreuser, K.P. Labadie, B.M. Prieskorn, N.A.P. Lieberman, C.I. Ene, K.W. Moyes, H. Chinn, K.R. DeGolier, L.R. Matsumoto, S.K. Daniel, J.K. Yokoyama, A.D. Davis, V.J. Hoglund, K.S. Smythe, S.D. Balcaitis, M.C. Jensen, R.G. Ellenbogen, J.S. Campbell, R.H. Pierce, E.C. Holland, V.G. Pillarisetty, C.A. Crane, Genetically

engineered macrophages persist in solid tumors and locally deliver therapeutic proteins to activate immune responses, J Immunother Cancer, 8 (2020).
[14] H. Xiong, James W. Keith, Dane W. Samilo, Rebecca A. Carter, Ingrid M. Leiner, Eric G. Pamer, Innate Lymphocyte/Ly6Chi Monocyte Crosstalk Promotes Klebsiella Pneumoniae Clearance, Cell, 165 (2016) 679-689.
[15] K.W. Moyes, N.A. Lieberman, S.A. Kreuser, H. Chinn, C. Winter, G. Deutsch, V. Hoglund, R. Watson, C.A. Crane, Genetically Engineered Macrophages: A Potential Platform for Cancer Immunotherapy, Hum Gene Ther, 28 (2017) 200-215.
[16] T. Suzuki, P. Arumugam, T. Sakagami, N. Lachmann, C. Chalk, A. Sallese, S. Abe, C. Trapnell, B. Carey, T. Moritz, P. Malik, C. Lutzko, R.E. Wood, B.C. Trapnell, Pulmonary macrophage transplantation therapy, Nature, 514 (2014) 450-454.
[17] C. Happle, N. Lachmann, J. Škuljec, M. Wetzke, M. Ackermann, S. Brennig, A. Mucci, A.C. Jirmo, S. Groos, A. Mirenska, C. Hennig, T. Rodt, J.P. Bankstahl, N. Schwerk, T. Moritz, G. Hansen, Pulmonary transplantation of macrophage progenitors as effective and long-lasting therapy for hereditary pulmonary alveolar proteinosis, Sci Transl Med, 6 (2014) 250ra113.
[18] T.R. Ulich, L.R. Watson, S.M. Yin, K.Z. Guo, P. Wang, H. Thang, J. del Castillo, The intratracheal administration of endotoxin and cytokines. I. Characterization of LPS-induced IL-1 and TNF mRNA expression and the LPS-, IL-1-, and TNF-induced inflammatory infiltrate, Am J Pathol, 138 (1991) 1485-1496.
[19] M.J. Greenberger, S.L. Kunkel, R.M. Strieter, N.W. Lukacs, J. Bramson, J. Gauldie, F.L. Graham, M. Hitt, J.M. Danforth, T.J. Standiford, IL-12 gene therapy protects mice in lethal Klebsiella pneumonia, J Immunol, 157 (1996) 3006-3012.
[20] H. Xiong, R.A. Carter, I.M. Leiner, Y.W. Tang, L. Chen, B.N. Kreiswirth, E.G. Pamer, Distinct Contributions of Neutrophils and CCR2+ Monocytes to Pulmonary Clearance of Different Klebsiella pneumoniae Strains, Infect Immun, 83 (2015) 3418-3427.
[21] A.M. van der Does, P. Bergman, B. Agerberth, L. Lindbom, Induction of the human cathelicidin LL-37 as a novel treatment against bacterial infections, Journal of Leukocyte Biology, 92 (2012) 735-742.
[22] M.D. Seo, H.S. Won, J.H. Kim, T. Mishig-Ochir, B.J. Lee, Antimicrobial peptides for therapeutic applications: a review, Molecules, 17 (2012) 12276-12286.
[23] K.E. Ridyard, J. Overhage, The Potential of Human Peptide LL-37 as an Antimicrobial and Anti-Biofilm Agent, Antibiotics (Basel), 10 (2021).
[24] B. Rivas-Santiago, C.E. Rivas Santiago, J.E. Castañeda-Delgado, J.C. León–Contreras, R.E.W. Hancock, R. Hernandez-Pando, Activity of LL-37, CRAMP and antimicrobial peptide-derived compounds E2, E6 and CP26 against Mycobacterium tuberculosis, International Journal of Antimicrobial Agents, 41 (2013) 143-148.
[25] M.A. Kovach, M.N. Ballinger, M.W. Newstead, X. Zeng, U. Bhan, F.S. Yu, B.B. Moore, R.L. Gallo, T.J. Standiford, Cathelicidin-related antimicrobial peptide is required for effective lung mucosal immunity in Gram-negative bacterial pneumonia, J Immunol, 189 (2012) 304-311.
[26] H.C. Flick-Smith, M.A. Fox, K.A. Hamblin, M.I. Richards, D.C. Jenner, T.R. Laws, A.L. Phelps, C. Taylor, S.V. Harding, D.O. Ulaeto, H.S. Atkins, Assessment of antimicrobial peptide LL-37 as a post-exposure therapy to protect against respiratory tularemia in mice, Peptides, 43 (2013) 96-101.
[27] J. Schauber, R.A. Dorschner, K. Yamasaki, B. Brouha, R.L. Gallo, Control of the innate epithelial antimicrobial response is cell-type specific and dependent on relevant microenvironmental stimuli, Immunology, 118 (2006) 509-519.

[28] A.D. Klose, N. Paragas, Automated quantification of bioluminescence images, Nature Communications, 9 (2018) 4262.

SUPPORTING INFORMATION

Supplemental Methods

Macrophage/GEM Culture: BMDMs were generated by bone marrow isolation from Albino B6 mice as described previously.[1, 2] Briefly, the bone marrow was flushed from mouse femurs and tibias and cultured in Roswell Park Memorial Institute buffer (RPMI; Gibco) supplemented with 10% FBS (RP10) and 1% penicillin-streptomycin (P/S; Gibco). Macrophage differentiation was facilitated by supplementation with 50 ng/mL recombinant murine (rm) macrophage CSF (rm-CSF; Peprotech) every 3-4 days. On day 6, differentiated BMDMs were replated in RP10 with mM-CSF. On day 7, transduction with 1500 lentiviral particles (LPs) per initially plated BMDMs occurred in the presence of 2 μg/mL polybrene (Sigma). One week after transduction, GEMs were ready for use and were lifted with TrypLE (Gibco) following by scraping of culture dishes and washing cells in PBS.

Lentiviral vectors and virus production: mIL12:CD19t and eGFP:ffluc fusion construct plasmids were a gift from Dr. Courtney Crane. Lentivirus production was accomplished by co-transfection of plasmid into 293T cells along with Vpx, reverse transcriptase (Rev), gag polyprotein (Gag-pol), and vesicular stomatitis virus G glycoprotein envelope (vsv-g) as previously described.[3] LPs were harvested from the 293T supernatant, purified and concentrated by ultracentrifugation (90 min, 24 500 rpm, 4 °C), and titered for p24 using the QuickTiter Lentivirus Titer kit (Cell Biolabs).

Live imaging analysis: Bioluminescent imaging (IVIS Spectrum, Caliper Life Sciences) was conducted following subcutaneous administration of D-luciferin. Image analysis was conducted using Living Image Software (Caliper Life Sciences). For 3D imaging analysis of GEMs following intratracheal administration, mice were imaged within a body conforming animal mold placed within a mirror gantry accessory that was compatible with the IVIS instrument.[96] InVivoPLOT analysis was conducted using InVivo Analytics Software.

mIL-12 ELISA analysis: ELISA was conducted using a Mouse IL-12 ELISA kit from Fisher (catalog # SM1270) and according to the manufacturer protocols.

In vitro mCRAMP inhibition of Kp assay: mCRAMP (0.1 mg/mL in H_2O) was diluted as appropriate for the following treatment groups (0.01, 0.1, 1, 10, 100 µg/mL). Kp at $5x10^4$ CFU in 100 µL of TSB is added to a 96-well plate. Control group includes Kp with H_2O. 10 µL of mCRAMP at various concentrations are added to the treatment groups. Total volume per well remained constant at either 110 µL (100 µL Kp + 10 µL mCRAMP) or 200 µL (100 µL Kp + 100 µL mCRAMP). All controls and treatment groups were done in triplicate. The 96-well plate was incubated for 2 hours at 37 C. After incubation, each well was plated in duplicate on TSB agar plates at 10^{-1} and 10^{-2} -fold dilutions. Plates were incubated overnight and Kp quantified the next day.

Supplemental Figures

Figure S5.1 Res-Gal-FITC-Rh drugamer synthesis. (A) ^{1}H-NMR spectrum in MeOD. (B) Molecular weight distribution curve determined by gel permeation chromatography.

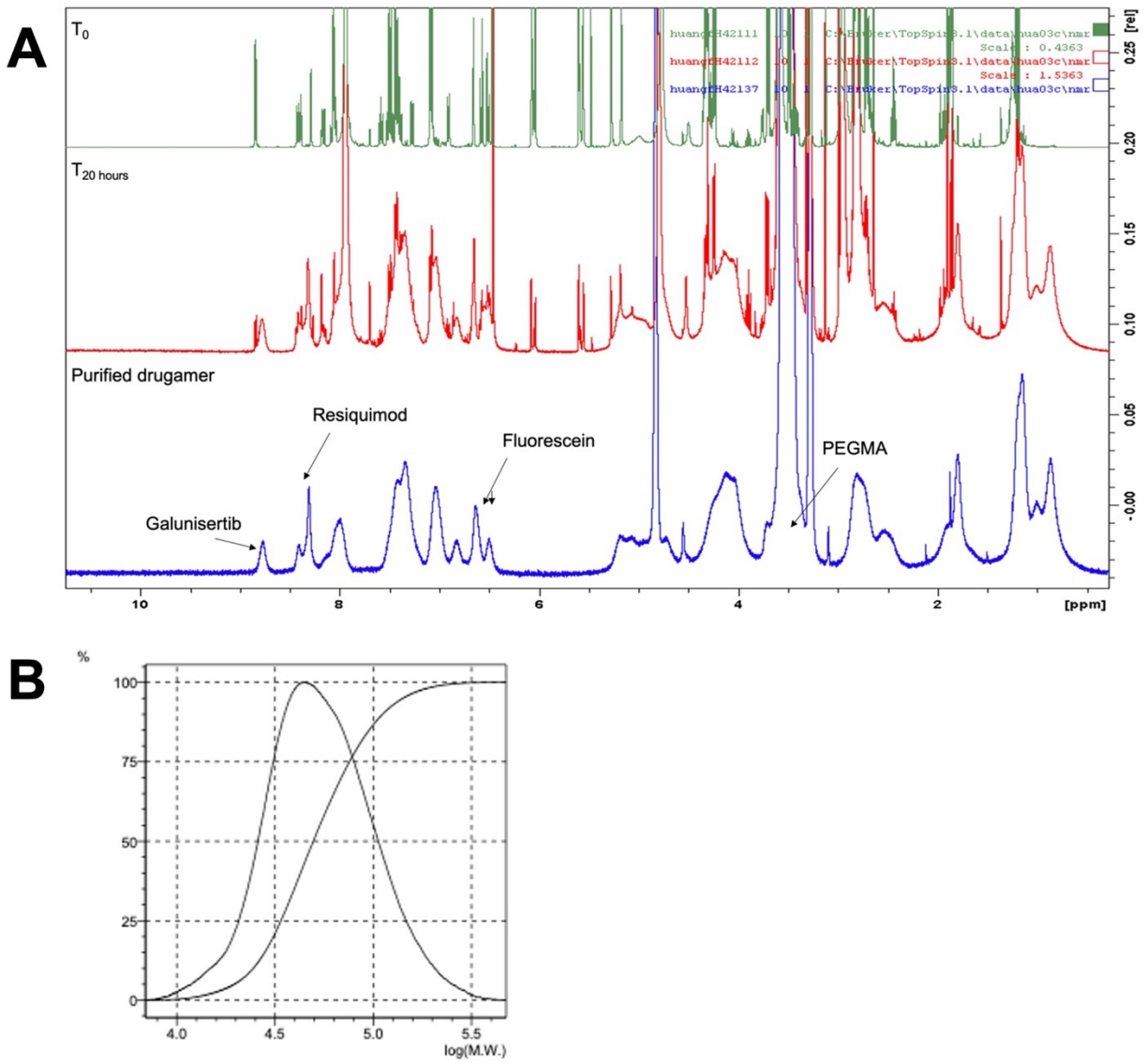

Figure S5.2 Pulmonary residence time of 2 x 10^6 eGFP:ffluc GEMs following intratracheal administration into healthy balb/c mice. (A) 2D IVIS imaging of representative mouse within body conforming animal mold in mirror gantry to visualize GEM luminescence with dorsal, ventral, left, and right views shows that GEMs are detected in mouse lungs as shown at 1-hour IVIS image but the majority were cleared by 24 hours (B) Invivoplot 3D reconstruction of eGFP:ffluc GEMs within left and right lungs for 5 mice (C) eGFP:ffluc GEM distribution to left and right lungs following intratracheal administration, imaged at 1 hour (D) Percent eGFP+ cells detected from bronchoalveolar lavage of whole mouse lungs on day 7 (E) Weight and temperature health monitoring indicate intratracheal delivery of GEMs is well-tolerated. n = 5 for GEMs, n = 3 for PBS controls.

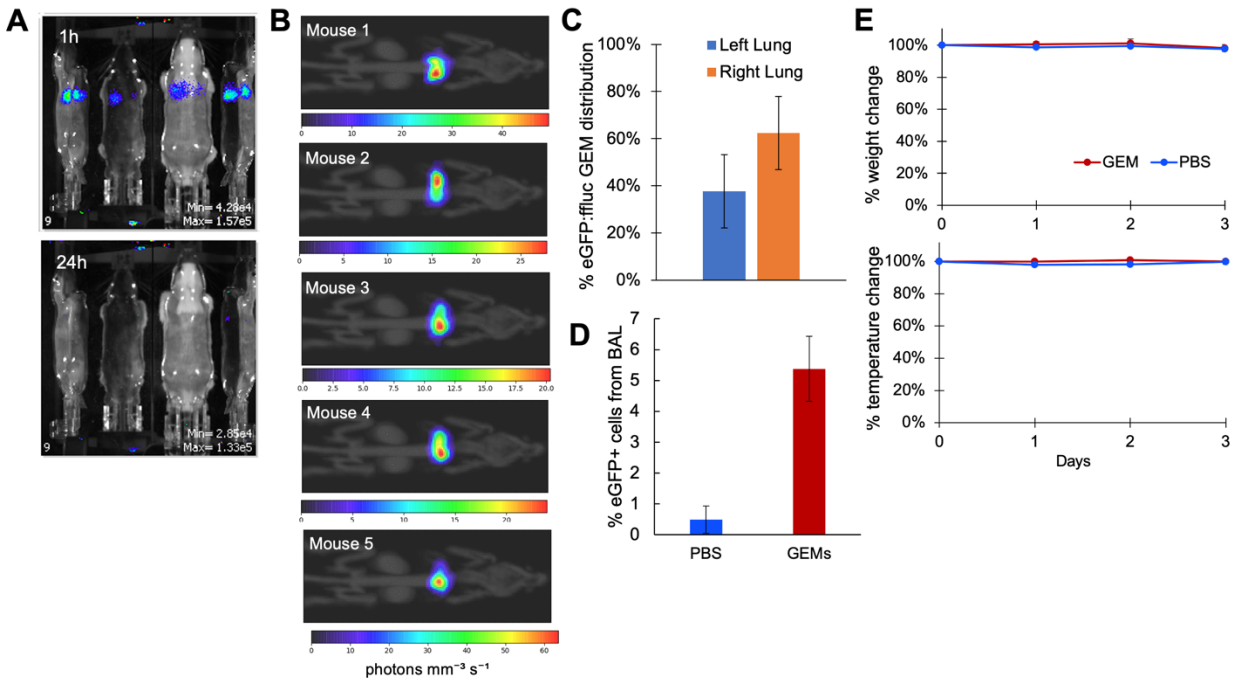

[1] K.J. Brempelis, C.M. Cowan, S.A. Kreuser, K.P. Labadie, B.M. Prieskorn, N.A.P. Lieberman, C.I. Ene, K.W. Moyes, H. Chinn, K.R. DeGolier, L.R. Matsumoto, S.K. Daniel, J.K. Yokoyama, A.D. Davis, V.J. Hoglund, K.S. Smythe, S.D. Balcaitis, M.C. Jensen, R.G. Ellenbogen, J.S. Campbell, R.H. Pierce, E.C. Holland, V.G. Pillarisetty, C.A. Crane, Genetically engineered macrophages persist in solid tumors and locally deliver therapeutic proteins to activate immune responses, J Immunother Cancer, 8 (2020).
[2] A. Madaan, R. Verma, A.T. Singh, S.K. Jain, M. Jaggi, A stepwise procedure for isolation of murine bone marrow and generation of dendritic cells, Journal of Biological Methods, 1 (2014) e1.
[3] K.W. Moyes, N.A. Lieberman, S.A. Kreuser, H. Chinn, C. Winter, G. Deutsch, V. Hoglund, R. Watson, C.A. Crane, Genetically Engineered Macrophages: A Potential Platform for Cancer Immunotherapy, Hum Gene Ther, 28 (2017) 200-215.